3D TOMOGRAPHIC IMAGING USING AD HOC AND MOBILE SENSORS

A thesis submitted to The University of Manchester for the degree of

Doctor of Philosophy

in the Faculty of Engineering and Physical Sciences

2010

RENEE KA YIN CHIN

SCHOOL OF ELECTRICAL AND ELECTRONIC ENGINEERING

Table of Contents

List of Tables

List of Figures

List of Abbreviations

ADC	Analog-to-digital converter
AET	Augmented Electrical Tomography
AHET	Ad Hoc Electrical Tomography
BEM	Boundary Element Method
CEM	Complete Electrode Model
CFD	Computational Fluid Dynamics
CT	Computed Tomography
DAQ	Data acquisition card
DMM	Digital multi-meter
DPC	Discrete Picard Condition
ECT	Electrical Capacitance Tomography
EEG	Electroencephalography
EET	Extended Electrical Tomography
EIDORS	Electrical Impedance and Diffuse Optical Reconstruction Software
EIT	Electrical Impedance Tomography
EMT	Electromagnetic Tomography
ERT	Electrical Resistance Tomography
ET	Electrical Tomography
FC	Fourier Coefficients
fEITER	Functional Electrical Impedance Tomography of Evoked Responses
FEM	Finite Element Method
FDM	Finite Difference Method
FOM	Figures-of-merits
fsp	Frames per Second
FWHM	Full-Width Half-Maximum
GSVD	Generalized Singular Value Decomposition
IPT	Industrial Process Tomography
ITS	Industrial Tomography System
LCT	Low Cost Tomography
LGN	Linear Gauss-Newton
MEMS	Micro-Electro-Mechanical Systems
MRI	Magnetic Resonance Imaging

NLGN	Non-Linear Gauss Newton
OS	Operating system
PC	Personal Computer
PIC	Peripheral Interface Controller
PLD	Programmable logic device
psf	Point-spread-function
RF	Radio Frequency
RIDAM	Reduced Internal-Drive Adjacent Measurement
RMS	Root mean square
SNR	Signal-to-Noise Ratio
SVD	Singular Value Decomposition
SVMS	Standalone Voltage Measurement System
TSVD	Truncated Singular Value Decomposition
UCT	University of Cape Town
UMIST	University of Manchester Institute of Science and Technology
USB	Universal Serial Bus
UWB	Ultra Wide-Band
VM	Virtual machine
WSN	Wireless Sensor Network
WSN4IP	Wireless Sensor Network for Industrial Process

Nomenclatures

α	Regularization parameter
α_k	Limiting factor as determined by noise level of measurement
ε	Electrical permittivity
ϕ	Piecewise linear basis function
λ	Singular values
σ	Electrical conductivity
σ_α	Tikhonov regularized solution
σ_o	Initial estimate of conductivity
σ_k	Known solution, localized conductivity measurement
σ_{ref}	Reference conductivity
σ_{MP}	Moore-Penrose generalized solution
γ	Complex admittivity
Ω	Domain of the imaged space
Ω_k	Elements/voxels/tetrahedral
$\partial\Omega$	Boundary of the domain Ω
b	Boundary data
l	Electrode index
q	Integer selected for a single crossing-point through 1 in the DPC plot
u	Scalar potential
u_i	Image space vector, left singular vector
v	Outward unit vector
x	Solution, conductivity vector
z_i	Data space vector, right singular vector
z_l	Contact impedance on the l^{th} electrode
A	Global conductance matrix
E_l	Surface area of the l^{th} electrode
I_l	Current injected on the surface of the l^{th} electrode
I^d	Current pattern
J	Jacobian matrix
L	Regularization Matrix
M	Number of measurements, number of voxels

N	Number of electrodes
R	Resolution matrix
U	Nodal potential distribution
V_{meas}	Measurement vector
V_l	Potential measured on the l^{th} electrode
V_L	Potential values on the boundary electrodes

Abstract

The aim of this research is to explore the integration of ad hoc and mobile sensors into a conventional Electrical Resistance Tomography (ERT) system. This is motivated by the desire to improve the spatial resolution of 3D reconstructed images that are produced using ERT. The feasibility of two approaches, referred to as the Extended Electrical Tomography (EET) and Augmented Electrical Tomography (AET) are considered. The approaches are characterized according to the functionality of the sensors on the ad hoc 'pills'.

This thesis utilizes spectral and numerical analysis techniques, with the goal of providing a better understanding of reconstruction limitations, including quality of measurements, sensitivity levels and spatial resolution. These techniques are applied such that an objective evaluation can be made, without having to depend heavily on visual inspection of a selection of reconstructed images when evaluating the performance of different set-ups.

In EET, the sensors on the pills are used as part of the ERT electrode system. Localized voltage differences are measured on a pair of electrodes that are located on an ad hoc pill. This extends the number of measurements per data set and provides information that was previously unobtainable using conventional electrode arrangements. A standalone voltage measurement system is used to acquire measurements that are taken using the internal electrodes. The system mimics the situation that is envisaged for a wireless pill, specifically that it has a floating ground and is battery-powered. For the present exploratory purposes, the electronic hardware is located remotely and the measured signal is transmitted to the PC through a cable. The instrumentation and data acquisition circuits are separated through opto-isolators which essentially isolates both systems. Using a single pill located in the centre of a vessel furnished with 16 electrodes arranged in a single plane, spectral analysis indicates that 15 of the 16 extended measurements acquired using the adjacent current injection strategy are unique. Improvement is observed for both the sensitivity and spatial resolution for the voxels in the vicinity of the ad hoc pill when comparing the EET approach with the conventional ERT approach. This shows the benefit of the EET approach. However, visual inspection of reconstructed images reveals no apparent difference between images produced using a regular and extended dataset. Similar studies are conducted for cases considering the opposite strategy, different position and orientation of the pill, and the effect of using multiple pills.

In AET, the sensors on the ad hoc pills are used as conductivity probes. Localized conductivity measurements provide conductivity values of the voxels in a discretized mesh of the vessel, which reduces the number of unknowns to be solved during reconstruction. The measurements are incorporated into the inverse solver as prior information. The Gauss-Newton algorithm is chosen for implementation of this approach because of its non-linear nature. Little improvement is seen with the inclusion of one localized conductivity measurement. The effect on the neighbouring voxels is insignificant and there is a lack of control over how the augmented measurement influences the solution of its neighbouring voxels.

This is the first time that measurements using ad hoc and 'wireless' sensors within the region of interest have been incorporated into an electrical tomography system.

Declaration

No portion of the work referred to in the thesis has been submitted in support of an application for another degree or qualification of this or any other university or other institute of learning.

Copyright Statement

i. The author of this thesis (including any appendices and/or schedules to this thesis) owns certain copyright or related rights in it (the "Copyright") and s/he has given The University of Manchester certain rights to use such Copyright, including for administrative purposes.

ii. Copies of this thesis, either in full or in extracts and whether in hard or electronic copy, may be made **only** in accordance with the Copyright, Designs and Patents Act 1988 (as amended) and regulations issued under it or, where appropriate, in accordance with licensing agreements which the University has from time to time. This page must form part of any such copies made.

iii. The ownership of certain Copyright, patents, designs, trade marks and other intellectual property (the "Intellectual Property") and any reproductions of copyright works in the thesis, for example graphs and tables ("Reproductions"), which may be described in this thesis, may not be owned by the author and may be owned by third parties. Such Intellectual Property and Reproductions cannot and must not be made available for use without the prior written permission of the owner(s) of the relevant Intellectual Property and/or Reproductions.

iv. Further information on the conditions under which disclosure, publication and commercialisation of this thesis, the Copyright and any Intellectual Property and/or Reproductions described in it may take place is available in the University IP Policy (see http://www.campus.manchester.ac.uk/medialibrary/policies/intellectual-property.pdf), in any relevant Thesis restriction declarations deposited in the University Library, the University Library's regulations (see http://www.manchester.ac.uk/library/aboutus/regulations) and in The University's policy on presentation of Theses.

Acknowledgement

I would like to take this opportunity to express my gratitude and appreciation to all those who have provided me a tremendous amount of help, love and support throughout my Ph.D studies.

This wouldn't be possible without the opportunity provided by my supervisor, Professor Trevor York. I am deeply grateful for this opportunity and the financial support, so I could make this bold move which took me halfway across the world to Manchester to further my studies. It has been a real pleasure to learn from you, through all the challenges and questions that I may not have always enjoyed, but that ultimately pushed me to become a better student and researcher. Thank you for the encouragement, the support and trying to get me to be less quiet.

I am very grateful to my many friends and colleagues in the Sensing, Imaging and Signal Processing group, both past and present. I would like to thank especially Dr. Stephen Murphy for his continuous support and constantly available for all the questions I have from time to time. I will always cherish the numerous musings and ramblings on ERT. My apologies for still not having all the issues in tomography fixed. Also, to all those who had generously given their time to me. I would also like to express my deepest gratitude to Dr. Paul Wright, Dr. John Davidson and Dr. David Stephenson, as well as a special thank you to Tom Rodgers, who provided me help when I was starting out.

I would also like to thank my colleagues and friends in the WSN4IP project team, in particular to Mr. Peter R. Green, Dr. Peter N. Green, Mathew Boon and Dominic Crutchley for their help and support.

I'd like to extend a special thank you to Professor Bill Lionheart and Dr. Oliver Dorn from the School of Mathematics. They generously provided their time to me, so I could better understand inverse problems and pushed me to think like a mathematician at times.

I would like to thank all the supporting staff of the School of Electrical and Electronic Engineering, especially to the following: Derrick, for agreeing to take up the challenges of all my absurd PCB projects; the lovely people at the Mechanical Workshop and Electrical Workshop, especially John and Chris, who spent a lot of time being patient with me, manufacturing a vessel which has made the experimental testing for the work of this thesis possible; Steve at the stores; and Ms. Marie Davies at the administration office.

My heartfelt gratitude to Rebecca Robinson, Will Carr and Dr. Eugenio Constantino, who have become dear friends to me during my time in Manchester. I will always cherish the silliness, the laughs, and most important of all, the love that you've shown me. A very special thank you to Mark Pottinger for being a constant presence in my life during these last 3 years. I will miss our struggle with the heater every winter and our highly insightful conversations, in particular those that involves solving the England National Team problem or football in general. We shall always have to agree to disagree on one thing (i.e. which is the best football team in the country), but you'll always be a great friend to me. Also, to "my girls", Debra Black (thanks for doing all the 'impromptu' proof-reading I tend to spring onto you), Renata Mussi and Kate Zsiray. Thanks for being my epically awesome friends over these past few years. Unfortunately, I don't think there's much of my sanity left to salvage despite your best efforts.

Last but not least, to my mom and dad, and my dear sister, whom I love more than anyone or anything in this world; thank you for being so supportive and being the anchor that you are in my life. You are my constant and I'm forever grateful for that.

List of Publications

Murphy S.C., Chin R.K.Y. and York T.A. (2008) 'Design of an impeller-mounted electrode array for EIT imaging,' *Meas. Sci. Technol.,* **19** (9)

Chin R.K.Y., Wright P. and York T.A. (2010) 'Electrical Tomography Using Ad Hoc Wireless Sensors,' *6th World Congress on Industrial Process Tomography, Beijing, China.*

Chin R.K.Y., Murphy S.C. and York T.A. (2010) 'Reconstruction Limitations for Electrical Resistance Tomography,' *6th World Congress on Industrial Process Tomography, Beijing, China.*

CHAPTER 1
INTRODUCTION

Electrical Resistance Tomography (ERT) is an imaging technique which is used to investigate the resistivity distribution of materials within a volume. Conventionally, cross-sectional images of resistivity distribution within the imaged space is generated but recent efforts have progressed to reconstruction of 3D images that exploit the "soft field" nature of the ERT (Warsito et. al., 2007), taking advantage of the fact that the current do not travel in straight lines but follow the path of least resistance. In reality, the ERT problem is three-dimensional even though older applications of ERT performed image reconstruction assuming 2D space (Lionheart, 2004). This was mainly influenced by factors which include speed of producing results and computational limitations.

ERT is gaining popularity in industrial process applications. Examples of recent successful applications include monitoring a liquid-liquid mixing process (Kourunen et. al., 2007), solid suspension in liquid (Murphy et. al., 2007) and liquid-liquid dispersion (Kaminoyama et. al., 2007), characterization of physical stability of solutions (York et. al., 2007), control and monitoring in milk powder processing (Sharifi and Young, 2010), multiphase flow measurement for gas-liquid in a bubble column (Jin et. al., 2007; Normi et. al., 2010), boiling bubble column reactors (Sudhakaran et. al., 2010) and a horizontal pipeline (Ramskill and Wang, 2010), measurement of flow velocities (Lee and Bennington, 2007), classifying hydrocyclone behaviour (Brennan et. al., 2007), water infiltration through soil (Gnecchi et. al., 2007), and wood characterization

(Steele et. al., 2007). A selection of applications relevant to the work of this thesis is discussed in Chapter 2.

One of the attractive aspects of ERT is that it is non-intrusive such that although the electrodes penetrate the wall of the vessel they do not enter into and therefore do not disturb the contained materials that are under consideration. However, this limits the location of electrodes to positions that are typically around the periphery and consequently this restricts the number of useful measurements that can be used to inform the computation of reconstructed images. Therefore reconstructed images using electrical tomography suffer from low spatial resolution compared to techniques based on, for instance, X-ray attenuation or magnetic resonance. Efforts are continually seeking to improve spatial resolution and one example aims to increase the stability of measurements (Murphy 2008). This thesis explores the possibility of integrating ad hoc and mobile wireless sensors with conventional tomographic techniques to determine the conductivity distribution of materials in a process vessel through 3D tomograms. This approach represents a radical departure from conventional practice involving peripheral electrodes and aims to provide extra information, particularly in the normally inaccessible central region of the process vessel.

This chapter provides a brief preview of the work presented in this thesis. Section 1.1 describes the aim of this project. Section 1.2 provides background information about this project. This project is part of the Wireless Sensor Network for Industrial Process (WSN4IP) project, which is briefly described in this section.

Section 1.3 describes the motivation which prompted the idea of using ad hoc pills with a conventional ERT system. The main motivation of this work is to improve tomograms, which typically have poor spatial resolution especially in regions further away from the electrodes. Section 1.4 provides a summary of previous related work, reviewing efforts to use internal electrodes to extend the number of electrodes in an ERT system.

Section 1.5 provides an outline of the work in this thesis, detailing the anticipated challenges. This chapter concludes with Section 1.6, which outlines the structure of this thesis.

1.1 Aim of Project

The aim of this project is to explore the use of ad hoc and wireless sensors to acquire localized measurements which are integrated with a conventional set of measurements obtained using an ERT system. This is done in effort of improving the spatial resolution of reconstructed images obtained using a conventional ERT technique. This thesis investigates different approaches of integrating the localized measurements. The performance of the novel approaches are compared to a conventional ERT system using analysis techniques where numerical results in regard of sensitivity level and spatial resolution, as well as the stability of measurements can be acquired and compared.

1.2 Project Background

This research work is part of an on-going project, Wireless Sensor Network for Industrial Process (WSN4IP), funded by the UK Engineering and Physical Sciences Research Council (EPSRC grant EP/D076900/1). The aim of WSN4IP is to utilise an array of ad hoc wireless sensors, referred to here as "pills", given the freedom of mobility to assume any location within a process vessel, to acquire measurements throughout the volume of the vessel and hence furnish information for control and monitoring purposes. Properties of interest, such as temperature, pressure, pH level and conductivity in different locations of the process vessel can be measured using sensors located on the pills.

The pills are designed to be as small as possible in order to intrude as little as possible on the process initially. It is envisaged that the pills will be spheres that are several centimetres in dimension. Each pill is equipped with a microcontroller with flash memory for 'store and dump' of data, a 868MHz radio interface, four antennas, a battery power source with a high efficiency switched-mode regulator and integrated sensors for measurements. The embedded system is responsible for localisation, networking and sensor measurements.

The WSN4IP project aims to deliver a demonstrator to provide information regarding storage and granular flow in hoppers (Figure 1.1). The system is targeted to map flow patterns of granular solids and to provide information about thermal gradients and moisture content within storage hoppers. This application provides a suitable platform to address generic issues related to wireless sensor network development. Challenges include: RF propagation in grain in a confined space with rich multipath; localisation of the pills; establishing an ad hoc network of pills to provide transmission of data from the pills within a limited power budget; measurements of process parameters using small, low power, low cost sensors; power reduction to allow extended measurement campaigns.

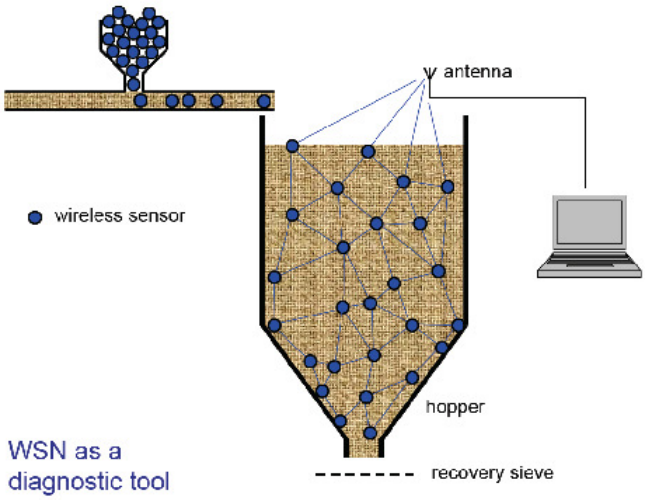

Figure 1.1 Schematic diagram of the demonstrator for the WSN4IP

The research work presented in this thesis is independent of the main part of the WSN4IP project. It focuses on utilising the ad hoc and wireless sensors within an otherwise conventional ERT system to provide enhanced reconstructed images. Importantly it is assumed that positional information regarding the location of the pills is already provided by the data acquisition system. Consequently the development of communication and data transfer protocols is not of concern for the present project.

To avoid complicating and distracting factors that may arise in working with materials such as grain, the present project considers ad hoc sensors in water, a relatively well understood medium. Experiments are targeted at a laboratory-sized vessel. This research aims to tackle the generic issues and findings can subsequently be migrated to other applications.

1.3 Motivation

Reconstructed images that are produced using ERT techniques often suffer from having low spatial resolution and contrast. Consequently, the reconstructed images misrepresent the imaged conductivity distribution. This is rooted in the ill-posed nature of the ERT problem (Lionheart et. al. 2005).

The problem of recovering unknown conductivities from boundary data is severely ill-posed as the solution depends continuously on the data. (Lionheart et. al. 2005). This means that, for any given measurement precision, there are arbitrarily large changes in the conductivity distribution which are undetectable by the boundary measurements at that precision. This problem is often addressed by introducing *a priori* information to constrain the solution such that large perturbations causing instability can be discarded. Another issue is the sufficiency of the data. It is important that the data are consistent with a conductivity distribution, as small errors in the measurements can violate consistency conditions. There are also a limited amount of measurements obtainable from a fixed system of electrodes. Electrodes typically cover only a portion of the surface of the vessel and in many cases, electrodes driving currents are excluded from being used for measurements. In practice, the ability of an EIT system to recover the parameterized conductivity distribution is limited by the number of independent measurements obtained and the precision of the measurements.

In an effort to improve the spatial resolution of tomograms, a commonly employed approach is to increase the quality of measurements. This is achievable through several methods. The first is to provide better quality measurements by improving accuracy and precision of the instrumentation and sensor system. Difference imaging is often employed to reduce the effect of noise. Using difference imaging, a measurement frame for a distribution with inhomogeneities is subtracted from a reference measurement frame, which is typically acquired for a homogeneous distribution. It is safely assumed that the system noise does not vary within the reasonably short period of time when both frames of measurements are taken. The second approach is to improve the accuracy of modelling. The quality of reconstruction ultimately relies on the quality of a model to relate electrical properties of the imaged space. It has been shown that the quality of the mesh and the accuracy of the modelling of details have an effect on the

quality of the reconstructed images (Woo et. al. 1994). Another method that can be employed is to improve the application of inverse algorithms. There is a lot of ambiguity regarding the choice of a suitable algorithm and associated parameters. Consequently, inversion techniques are often not optimized. The final method is to maximise the amount and quality of information of a measured dataset. This can be achieved by adopting unconventional data acquisition methods to increase the amount of unique information to inform the reconstruction. This method includes exploring unconventional measurement strategies, electrode arrangements and location of electrodes.

This thesis considers all of the fore-mentioned approaches, putting a heavier emphasis on the last approach through employing an unconventional electrode arrangement. Typically electrodes in an ERT system are confined to the walls of the vessel. This limits the areas where information is obtained. This research explores the utilisation of sensors on ad hoc pills to break away from this restriction. Through ad hoc positioning of the electrodes, localised measurements can be obtained within the process vessel. The localized measurements potentially contain unique information acquired in areas located further away from wall-mounted electrodes, which may help improve the spatial resolution of reconstructed images.

1.4 Previous Related Work

There are a number of published works which consider unconventional electrode arrangements. Huang et. al. (2008) explored the possibility of increasing the number of measurements without increasing the number of electrodes, through rotating the fixed number of electrodes attached to the periphery of the vessel and data acquisition is repeated when the set of electrodes are shifted. However, the desirable information in the central region of the vessel remains elusive through these methods. The increase in information obtained remains limited to the vicinity of the wall of the vessel and any obtainable advantage in spatial resolution is ultimately limited by the uniqueness of measurements and sensitivity (Polydorides and McCann, 2002).

Several studies have been conducted to investigate the possibility of integrating electrodes into internal structures of a process vessel, such that the electrode system remains non-intrusive. Examples include Lyon and Oakley (1993), Heikkinen et. al. (2001a) and Kim et. al. (2002), who explored the use of internal electrodes on a stationary fixture within the process vessel and it is claimed that improvements to sensitivity or resolution can be observed. Murphy (2008) explored the use of electrodes mounted on a rotating impeller to further extend the number of measurements. Advantages of this approach are that the electrodes are located centrally within the vessel, hence increasing the sensitivity in its vicinity, and the rotation of the impeller also increases the number of measurements that are possible. A new strategy, the Reduced Internal-Drive Adjacent-Measurement (RIDAM) was introduced to accommodate the internal electrodes (Murphy and York, 2006). The internal electrodes are used as a current sink that is paired with a current driving electrode and are excluded from voltage difference measurements. A mesh-mapping method is used to map Jacobian matrices obtained using different forward models according to the orientation of the impellers onto a generic model used for inverse solving. Using the generic model for inverse solving, measurements acquired with various impeller orientations can be combined and used to increase the number of measurements. Spectral analysis indicates that there is an increase in the amount of unique information that is obtained using the RIDAM strategy in comparison to a regular dataset, and there is an improvement in sensitivity throughout the domain. Additional measurement sets are obtainable through rotating the impeller, and measurement sets can be combined to expand the number of measurements. Spectral analysis suggests that there is an increase in unique information for combined datasets, indicating that there are potential benefits from the different sets of measurements. However, the amount of redundant information increases at a faster rate than unique information, which indicates that the RIDAM strategy is not optimised. While the number of unique measurements acquired is increased significantly, there is no substantial improvement seen through statistical and visual analysis.

1.5 Challenges

The primary challenge of this research is to formulate and evaluate methods to integrate the ad hoc and wireless sensors into a conventional ERT system. It is assumed that the

embedded system within the pill can furnish the necessary measurements. In this case, the sensors can be used as either conductivity probes or part of the ERT electrode system, to acquire conductivity or voltage difference measurements respectively. These measurements can then be incorporated into an ERT system.

The main question that this thesis is concerned with is whether the localized measurements obtained using the ad hoc and wireless pills could influence or enhance the inverse solution, as well as to what extent and how they can influence the reconstructed image. The work in this thesis intends to devise approaches to incorporate the localized measurements into inverse solving with the aim to improve the quality of reconstructed images. To incorporate the new information into the ERT system, the modifications necessary to the hardware, model and simulation need to be identified and considered. Another important issue that this thesis seeks to address is methods to evaluate the performance of the new approaches to integrate ad hoc measurements with a conventional ERT dataset. These analysis techniques, ideally, should produce unbiased results and provide more information on reconstruction properties that will help improve the quality of inverse solving or image reconstruction, including sensitivity and spatial resolution.

When utilising the ad hoc pills, one of the main concerns is how this would affect the ERT system. It is important that effects of the intrusion of the ad hoc pills are as minimal as possible. This begs the question of how many pills can be deployed into a vessel before the effect of the intrusiveness due to the ad hoc pills starts to have a negative impact on the quality of reconstructed images, as well as degradation of the quality of a regular ERT measurement dataset. Another interesting question is whether the presence of the ad hoc pills will affect the current paths using conventional current injection strategies. This may mean that some strategies are better suited for this purpose compared to others.

A suitable size of the ad hoc pills is an important consideration. Instinctively, the pills should be small so that multiple pills can be employed in the process vessel to obtain localized measurements. From a practical standpoint, this is limited by the minimum size required to ensure a measurement and communication system can fit in the internal volume of the pill. When considering the size of the pill, this also determines the size of

electrodes and separation between electrodes on the pill and affects whether a measurable voltage difference can be obtained with the available instrument.

During the development stage of this work, when considering the experimental set-up, suitable hardware is required to evaluate the practical implementation of the approaches that are used. An important aspect is that the measurement system should mimic the system that is contained within the ad hoc pills. In other words, the system should be battery-powered and have a floating reference point. This is likely to have an effect on the measurements, especially when the sensors on the ad hoc pills are used as part of the electrode system. The effect of the inconsistency of grounding between two instruments used should be investigated.

In terms of image reconstruction and the availability of localized conductivity measurements, modifications to inverse solving algorithms are anticipated. The considerations to implement the modifications include the choice of reconstruction algorithm and what kinds of modifications are necessary in order to include the information acquired.

1.6 Thesis Structure

This thesis presents the results from investigations using ad hoc and mobile sensors in addition to conventional electrode arrangements for an ERT system. The work considers a novel approach to utilise measurements from any location within the process vessel to further inform the reconstruction of 3D tomograms. The construction and evaluation of the system that has been developed is presented using analysis techniques which inspect factors that relate to the quality of reconstructed images.

Chapter 2 reviews published work related to ERT and its application in industrial processes. This chapter provides an overview of measurement strategies, modelling and image reconstruction using conventional set-ups, as well as recent developments that provide alternatives to traditional practices.

Chapter 3 discusses nalysis techniques which provide impartial and conclusive methods to evaluate the performance of an ERT system are also described. This is intended to help understand the reconstruction limiting factors through evaluation of the performance of different measurement strategies and analysis techniques. The analysis techniques discussed are used to evaluate the performance of the ERT systems explored in this thesis.

Chapter 4 explores methods of improving spatial resolution of reconstructed images through increasing the number of measurements. Two methods were explored in this chapter. The first is through varying measurement strategies, and the second is through increasing the number of electrodes. The aim of these studies is to improve understanding of the factors which influence the changes of spatial resolution before adopting more complex systems to improve spatial resolution.

Chapter 5 discusses wireless pills. A brief review focusing on recent development in wireless sensor networks is presented. The chapter discusses novel strategies developed to incorporate the ad hoc and wireless sensors into a conventional ERT system. Augmented Electrical Tomography and Extended Electrical Tomography are described in the context of such sensors together with consideration of practical issues for implementation and challenges for each approach are discussed.

Chapter 6 describes the Extended Electrical Tomography strategy in further detail. A feasibility study through simulation is presented. The performance of this approach, measured against the conventional ERT technique is evaluated using the analysis techniques discussed in Chapter 3. Practical factors such as suitable dimension of the pill and the effect of different orientation and positioning of ad hoc internal electrodes are investigated. From a practical perspective the size of the pill should be chosen to be small such that it is as non-intrusive as possible. The effect of the location of ad hoc electrodes is also investigated. Chapter 5 also describes the laboratory set-up used, including the standalone voltage measurement system that is used to acquire voltage difference measurements from the ad hoc internal electrodes. Experimental results are presented.

Chapter 7 reports the conclusions and considers possible future directions.

CHAPTER 2
ELECTRICAL RESISTANCE TOMOGRAPHY

This chapter aims to provide an overview of the topics in Electrical Resistance Tomography (ERT) which are relevant to the interest of this thesis. This chapter is divided into six subsections. Section 2.1 provides an introduction to Electrical Tomography and Electrical Impedance Tomography. Section 2.2 provides an overview of applications of ERT in industrial processes. A selection of applications in this area of interest to this thesis are discussed, including mixing processes and flow monitoring, with special interest in applications which involve particle-sized materials. This specific interest is related to targeted applications for the Wireless Sensor Network for Industrial Process (WSN4IP) project, in which the primary demonstrator is grain storage monitoring.

Section 2.3 discusses the technical implementation of ERT relevant to this thesis, and is further divided into three subsections. The first subsection discusses electrode systems, including electrode design and typical electrode arrangements. Secondly, conventional measurement strategies are reviewed, including the adjacent and opposite strategies. Finally, the instrumentation used is detailed, primarily considering the Low Cost Tomography 2 (LCT2) instrument. Literature reviewed in Section 2.3 aims to provide relevant background information as a precursor to the primary interests of this thesis. This work is concerned with improving spatial resolution of reconstructed images using ad hoc sensors which inevitably requires modifications of conventional set-ups to accommodate the ad hoc sensors or electrodes.

Section 2.4 discusses different aspects of the image reconstruction in three subsections. Subsection 2.4.1 provides an overview on forward solving. The requirements to produce a discretized model, including the Finite Element Method and Complete Electrode Model, which was used throughout this thesis, are also briefly provided. Subsection 2.4.2 discusses the sensitivity matrix and the Jacobian matrix calculation. Subsection 2.4.3 discusses inverse solving, in particular the Gauss-Newton algorithm and Singular Value Decomposition (SVD) algorithm, which are used extensively throughout this thesis. The mathematical model discussed is based on the Electrical Impedance and Diffuse Optical Reconstruction Software (EIDORS) (Polydorides and Lioneart, 2002) used throughout this work.

Section 2.5 discusses the quality of reconstructed images and aims to provide a better understanding on contributing factors which define the quality of a reconstructed image. Brief descriptions of the properties which contribute to the quality of reconstructed images are given in subsection 2.5.1, while subsection 2.5.2. provides an overview on the different types of analysis techniques which can be used to evaluate the selected properties of a reconstructed image. Further details are provided in the following subsections describing spectral analysis using SVD, numerical analysis using sensitivity visualization and numerical analysis using resolution matrices. The analysis techniques described are applied in subsequent chapters to analyse the different properties of reconstructed images.

2.1 Electrical Impedance Tomography

Electrical Impedance Tomography (EIT) is one of the earliest process imaging techniques developed. Much of the early developments were initiated at the University of Manchester Institute of Science and Technology (UMIST) in the early 1990s. EIT has emerged as a preferred method in comparison with more well-established techniques such as X-Ray Computed Tomography (X-Ray CT) and Magnetic Resonance Imaging (MRI) because of its relative ease of implementation at a lower cost. EIT tends to be capable of a good temporal resolution, adequately capturing data for applications with demanding temporal variation. The disadvantage of EIT is its

relatively weak spatial resolution, hindered by the soft-field and ill-posed nature of the modality.

EIT determines the internal admittivity of an imaged space by injecting low frequency (typically <1MHz) current and acquiring voltage difference measurements on the periphery of the volume. EIT belongs to the Electrical Tomography (ET) family, which also includes Electrical Capacitance Tomography (ECT) and Electromagnetic Tomography (EMT). EIT is sometimes referred to as Electrical Resistance Tomography (ERT), and is done so throughout this thesis. The usage of both terms is deemed interchangeable within the research field. To better distinguish the differences between both terms, from a mathematical aspect, the usage of the term ERT is only valid when the phase angle of the measured signals is zero. EIT, however, takes into consideration both the amplitude and phase angle of measurements during image reconstruction. In practice, phase angle does exist and most instruments employ a phase sensitive demodulator to measure the amplitude of the measured signal accurately. However, most instruments only produce the magnitude of the measured signal and a majority of algorithms used for image reconstruction only consider the real component (conductivity) of the admittivity distribution.

2.2 Applications of ERT in Industrial Processes

ERT is applied in three main areas of applications, namely medical, industrial processes and geophysics. Imaging using ERT in medical applications is perhaps the most developed area, primarily in instrumentations and image reconstruction. Many of the developed techniques in medical applications are transferred and adopted for applications in industrial processes. ERT is applied in industrial processes to validate the design and investigate the performance of a process, as well as for monitoring and control purposes, offering insights to the reaction and dynamics of the process in a process vessel or pipeline. There are many reviews and published work on various implementation of ERT in industrial processes such as Dickin et. al. (1992), Williams and Beck (1995), Dickin and Wang (1996) and York (2005). Beyond these reviews, recent successful implementations also include applications on bubble columns, flows and suspensions. There are also applications of ERT for wood characterisation, soil-

water infiltration, and hydrocyclone classifiers. The work presented in this thesis is targeted for various applications, including mixing processes, flow, and monitoring changes in storage units (such as the demonstrator chosen for the WSN4IP project, grain storage in a silo).

ERT is applied extensively in mixing processes across a wide range of industries including chemical, food, and pharmaceutical. ERT can be applied to provide information and understand the dynamics of the process such that its design can be optimised. The requirement of mixing processes may vary from one application to another, but all ultimately aim to reduce inhomogeneity. The applications may involve multi-phase (gas, liquid and solids). ERT is better suited for applications of liquid phase as it tends to be more conducting in comparison with solids and gas. There are a large amount of publications detailing implementations of ERT/EIT in monitoring mixing-flow. The majority of literature focused on monitoring flow or distribution of solid materials in liquid, in applications such as monitoring mixing processes, hydraulic conveying and multi-phase flow in fluidized beds. A selection of the literature includes Butler and Bonnecaze (1999) looked into using EIT for multiphase imaging, quantifying shear-induced particle migration in a suspension undergoing pressure-driven flow through a tube. It was shown that the particle migration measured using EIT was in good agreement with those obtained using magnetic resonance imaging (MRI). This paper showed that it is feasible to use EIT, a relatively inexpensive imaging technique, to measure conductivity distribution of particle-sized material suspended in fluid.

Lucas et. al. (1999) used a dual-plane ERT system to study vertical and inclined upward flows, intended for flow meters to monitor oil well drilling operations. A local, intrusive conductivity probe system was also used to obtain reference measurements. The conductivity probe was designed to be as small and streamlined to reduce the intrusiveness of the probe. Experiments were conducted using plastic beads suspended in water. Results were compared from measurements using the dual-plane ERT system and the local intrusive conductivity probe, and the qualitative results were in good agreement between the profiles obtained using the two techniques.

Kaminoyama et. al. (2005) presented a study on dispersion states of floating and settling particles in a stirred vessel using ERT. The authors used a conventional three-plane electrode system, each plane with 16 electrodes. Tomograms were produced to represent the different stages of the mixing process, and compared with dispersion index and average of the change in electrical resistance within the measured volume. Both sets of results were found to be in good agreement. The authors also used the tomography measurements to estimate the rotational speed of the impeller required to achieve a homogeneous dispersion state.

Ricard et. al. (2005) looked into applying ERT in monitoring multiphase pharmaceutical processes such as dispersion, phase inversion and settling processes using a linear sensor array of electrodes. Experiments were setup for solid-liquid mixing process and liquid-liquid mixing process in laboratory scale vessels. The solid suspension study was performed with sand particles, representative of those particle sizes in the pharmaceutical industry. The results showed that the visual observation matches well with those obtained through Computational Fluid Dynamics (CFD) modelling.

Murphy et. al. (2007) suggested using unconventional measurement strategy using multiple linear EIT probes to monitor solid-liquid suspension in metallic vessels. The measurement strategy aimed to maximize the separation of the current driving electrodes and measuring electrodes in order to minimize the sensitivity gradient error to increase reconstruction accuracy. The conductivity profiles were obtained using reconstructed data to study the trend during the sedimentation process to provide a better understanding of the characteristics of the process and the quality of suspension at different stages of the process.

The above literatures are a small portion of the vast publications which describe application of EIT/ERT which involves solid-liquid multiphase industrial processes. The literatures suggest that the presence of liquid is essential in applications of ERT if solid materials are present during the process to create a conducting medium for current flow.

There are no works published which describe the implementation of ERT in monitoring changes in storage units, specifically for moisture content measurements in solid

particle which is of special interest to this work in conjunction with the WSN4IP project. Published work focused on using microwave and capacitance techniques as the primary modalities. The basis of both techniques is to relate measurements acquired to the dielectric of the measured material, which in these materials relates to the water content in the materials. There are reported works which use ECT technique to monitor changes in particles. Among the literatures are Shao and Liu (2006) described using ECT to monitor moisture distribution in grain storage area in a simulation-based study. The published results indicate that ECT can be applied efficiently for this purpose.

Chaniecki et. al. (2007) suggested using ECT to provide a graphical representation of the flow of particles through a hopper or silo. Using a conventional two-plane sensor set-up with 12 electrodes in each plane, the paper presented 2D tomograms to study the characteristics of the flow of material through a silo, including the porosity distribution. With the series of tomograms obtained, the continuous characteristics could be deduced and allowed studies to be made in relation to the different factors that affect the flow of particles through the silo.

Romanowski et. al. (2007) also described using ECT to monitor hopper flow with 12 electrodes placed around a section of a pipe in three planes. The gravitational hopper flow was measured by monitoring the capacitance changes in time, which correspond to the material concentration change. The paper also provided 3D visualization of the propagation of powder flow within the hopper.

The lack of publications implementing ERT for applications described above indicates the unfeasibility of using this modality in this specific application. As the demonstrator is not a crucial aspect of the work presented in this thesis, this work presented is based on a liquid-based process.

2.3 Technical Implementation of ERT

An ERT setup generally comprises of a set of electrodes connected via cables to a data acquisition system or tomograph where measurements are captured based on a predetermined measurement strategy. Measurements captured are stored and transferred

to a PC where measurements will be used for image reconstruction (Figure 2.1). This section describes the main components which are relevant to this thesis.

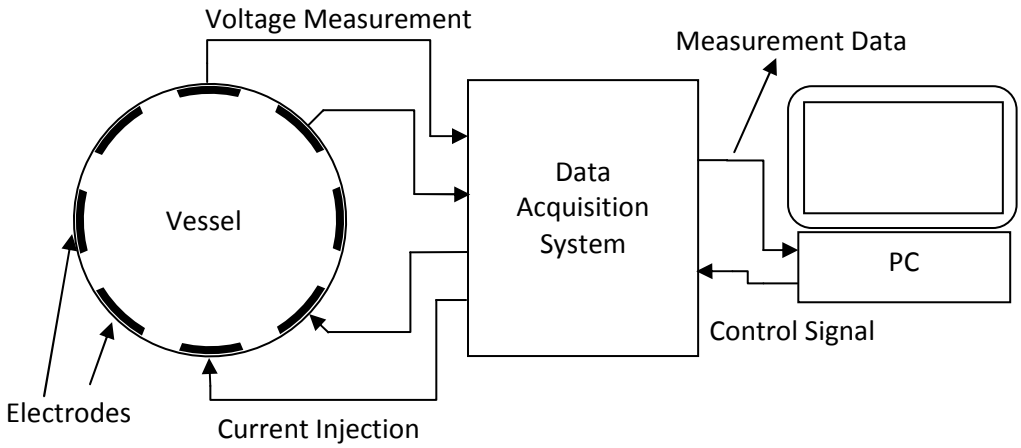

Figure 2.1: A typical ERT set-up for industrial process applications

2.3.1 Electrode System

Electrodes for an ERT system for industrial process applications are traditionally mounted on the inside of the wall of the process vessel, such that the electrodes are in contact with the material. The electrode system is invasive, but non-intrusive. Careful consideration needs to be made when choosing the make of electrodes. Typically, electrodes are made of metallic material such that they are more conductive than the conducting materials measured to ensure more reliable measurements. As electrodes are in contact with the material, relatively passive materials are preferred, such as stainless steel, platinum, gold, silver palladium or other materials with the same properties (Dickin and Wang, 1996), to avoid corrosion and large amount of electrochemical reactions.

Electrodes in IPT applications are often rectangular in shape. This is far from ideal, as narrow angles on the electrode corners result in higher current densities in these areas. Circular electrodes are ideal for this purpose and preferred for modelling purposes (Cheng et al. 1989). However, forward solving for ERT requires discretizing the model using Finite Element Methods (FEM) into tetrahedral elements and accurate modelling of circular electrodes requires a large amount of small elements, resulting in increased computational requirements. A coarser mesh structure results in inaccurate

representation of the shape of the electrode, leading to errors in forward and inverse solving. While rectangular shaped electrodes eliminate this issue, the accuracy of the electric field calculation is compromised due to the high current densities in the corners, and the larger sizes of tetrahedral elements representing the electrodes areas. A good compromise is to use hexagonal shaped electrodes. However, such electrode design is cost inefficient. In medical ERT applications, circular electrodes are used based around existing electroencephalography (EEG) sensors. The electrodes are commonly modelled as point source (1D), hence eliminating the discretization issue.

Most ERT systems use the four-terminal measuring protocol. This requires two electrodes to be used for current injection and current sinking. Although there are no strict guides for the design of current sourcing electrodes, several studies were carried out to investigate different options, including Hua et. al. (1993), Paulson et al (1992), Pinheiro et. al. (1998) and Isaacson (1986), which suggested that the size of the current injecting electrodes should be maximized.

Although there are no strict rules when choosing the dimensions of electrodes, it is important to note that the size of electrodes influences the amount of current injected through the imaged space. Given a large enough amount of current injected through the imaged space, measurements with better quality (higher Signal-to-Noise Ratio (SNR)) can be acquired. The limiting factor which requires consideration is contact impedance. Consider the typical arrangement where electrodes are in contact with a conducting medium: when electrically charged, a thin impedance layer is formed on the electrodes due to electrochemistry, which is referred to as contact impedance. Contact impedance is a function of the electrolyte as well as the electrode material (Cheng, et. al. 1989). Contact impedance is difficult to predict and measure due to variations across the surface of the electrode. One of the commonly used methods to tackle this issue is through ‘difference imaging’. Difference imaging produces images of conductivity change from a reference conductivity state. The reference state is usually known and measured. Since contact impedance does not vary with time, this method is more robust in comparison with a static imaging technique (Boone and Holder, 1996a).

When considering the ideal dimension for electrodes used for voltage measurements, the electrodes should be as small as possible (Dickin and Wang, 1996). This prevents

averaging of different equi-potentials and increases the resolution of measurements. Using small electrodes covering the boundary of the imaged space, the probability of detecting conductivity changes in material is increased. In practice, however, electrodes shares functionality. Electrodes not involved in current injection and current sinking are used for voltage measurements. Therefore, it is common that the size of electrodes is kept uniform. While this arrangement reduces the resolution of measurements, the dimensions of electrodes are commonly considerably large as it is more advantageous to have larger current sourcing electrodes than voltage measurement electrodes to maintain a good level of SNR, and increase recoverability of information.

There is no 'one-fit-all' solution when deciding an electrode configuration system. A suitable configuration depends highly on vessel size. The objective is to configure an electrode system which is capable of providing good sensitivity and resolution across the imaged space. Amongst the criteria which needs to be taken into consideration includes the number of electrodes per plane, the number of electrode planes and size of electrodes (considering uniform dimensions for all electrodes) and positions of electrodes. The configuration should be able to provide good sensitivity across the image space, as well as good resolution when using a particular measurement strategy. However, this is difficult to achieve due to various limiting factors such as positioning of the electrodes and the ill-posedness nature of the ERT problem. A commonly employed configuration is the planar arrangement, where electrodes are placed equi-spaced on the perimeter of the process vessel and the centre of the electrodes are aligned on a defined plane, as shown in Figure 2.2. A single planar arrangement is typically used in 2D imaging, while 3D imaging extrapolates information from multiple planes of electrodes.

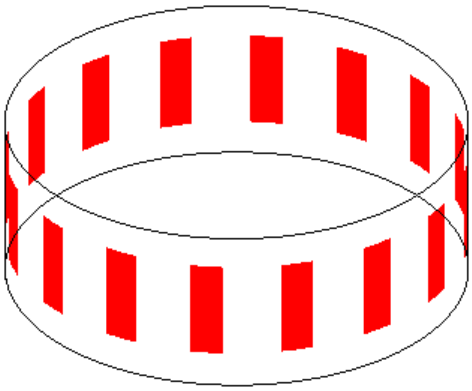

Figure 2.2: Single planar arrangement with 16 equi-spaced electrodes on the wall of the vessel

Unconventional Electrode Arrangement

There are unconventional electrode arrangements, such as linear arrays, where electrodes are placed on the same plane. By adopting this method of electrode placement, installation of an ERT electrode system is simplified as it requires minimal access to the process vessel. Linear arrays have been applied in industrial process applications for process monitoring (LaBrecque et. al. 1996; Bolton 2006; Meng et. al. 2006). Several publications explore multiple linear arrays of electrodes for spatial interrogation (Cullivan et. al. 2005; Schlaberg et. al. 2007) where diametrically opposed linear arrays are used, while Murphy et. al. (2007) demonstrated using three linear arrays on the points of a triangle.

Ismail et. al. (2010), and Fan and Wang (2010) described using multi-planar electrode arrangements where the top electrode plane is arranged at an offset from the bottom electrode plane. In other words, the electrodes are not aligned vertically. Ismail et. al. (2010), who referred to this electrode arrangement as the 'Zigzag' arrangement, reasoned that arrangement would allow equal spacing in all directions for all electrodes in either electrode plane, resulting in a more uniform electric field over the 3D domain.

As noted in Section 1.4, publications were also found where electrodes are fitted on internal structures of a process vessel, aimed to improve the sensitivity in regions towards the centre of the vessel. Amongst the publications include electrodes mounted on impeller shafts (Lyon 1997; Heikkinen et. al. 2001b; Kim et. al. 2002), impeller blades (Murphy and York 2007), and rod bundles (Ijaz et. al. 2006).

2.3.2 Measurement Strategy

For any electrodes arrangement, there are different combinations of source and measurement strategies that can be employed. The different combinations form a measurement strategy. In ERT, measurement strategies are concerned with acquiring resistance measurements in order to compute the conductivity of the material. A resistance measurement is obtained through measuring the voltage drop across the material with a current passing through the material. A minimum of two terminals is required to acquire the measurements. A two electrode (or terminal) system uses the

current source and sink electrodes for voltage differential measurements. It is worth noting that the system is easily affected by contact impedance which may result in erroneous measurements, therefore a four electrodes system is preferred to tackle this issue. A constant current is applied between a pair of electrodes and resultant voltage difference is measured between a pair of electrodes not used as current source (Barber and Brown, 1984). This method is widely adopted in various ERT systems. A three electrodes system is used when a conductive boundary is involved (Wang et. al., 1994). The strategy employs two electrodes at a time, coupled with the conducting boundary (metallic wall of a vessel or a pipeline, for example) as the third electrode used as ground. The conducting boundary also acts as a shield, reducing the effects of electromagnetic interference. The main drawback of this system is the requirement for high dynamic ranges for instrumentation circuitry and the decrease in resolution (Sasaki, 1992).

Measurements can also be acquired using a multiple-drive or optimum-current strategy (Isaacson, 1986), where current sources originate from more than one pair of electrodes. This strategy is often used to create a custom electric field distribution, targeting specific regions within the imaged space (Gisser et al., 1987). Measurements are acquired on electrodes referenced to a single independent electrode potential (Gisser et. al. 1988). Some instruments allow measurements to be obtained simultaneously, using parallel channels to acquire measurements for each current injection.

For the interest of this research, the four-electrode strategy is used. All four-electrode strategies are derived from a minimum dataset (Dines and Lytle, 1981; Barber and Brown, 1984).

Adjacent strategy

The adjacent strategy (Seager et al, 1987) is considered as the standard measurement strategy. In the adjacent strategy, current is injected and sunk on neighbouring electrodes. Voltage measurements are taken on adjacent electrode pairs for all remaining electrodes, except for the pair of electrodes used for current injection. The current injection and sink electrode pair is then moved to the next pair of electrodes and similarly, measurements are taken for the remaining electrodes, as shown in Figure 2.3.

This is repeated until the current injection electrode pairs have been switched for all electrodes on the plane.

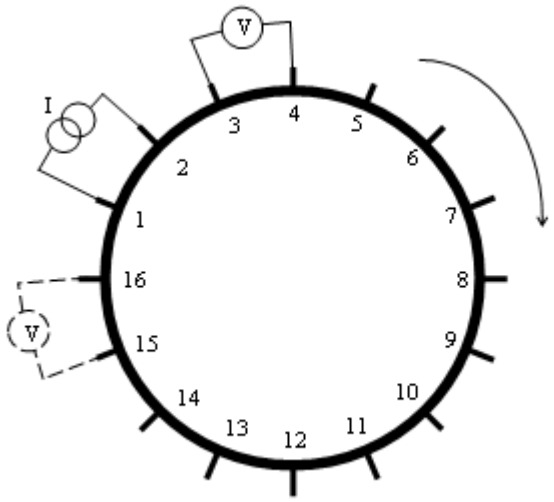

Figure 2.3: The adjacent measurement protocol

This strategy yields *N(N-3)* measurements, where *N* is the number of electrodes. However, only *N(N-3)/2* measurements are independent. The main drawback of the adjacent strategy is the non-uniform current distribution within the imaged space as the current path travels near the boundary electrodes, resulting in relatively low current density and therefore sensitivity in the centre of the imaged space. Consequently, measurements are also sensitive to measurement noise and errors (Hua et al, 1993).

Opposite strategy

Another commonly employed strategy is the opposite strategy (Webster 1990), where current is applied through diametrically opposed electrodes. Voltage differences are measured on adjacent pairs of electrodes for all electrodes not used for current injection, as shown in Figure 2.4. The current injection pair is switched to the next pair and measurements are repeated. The frame of measurements is complete when current injection is applied on all diametrically opposite pairs of electrodes.

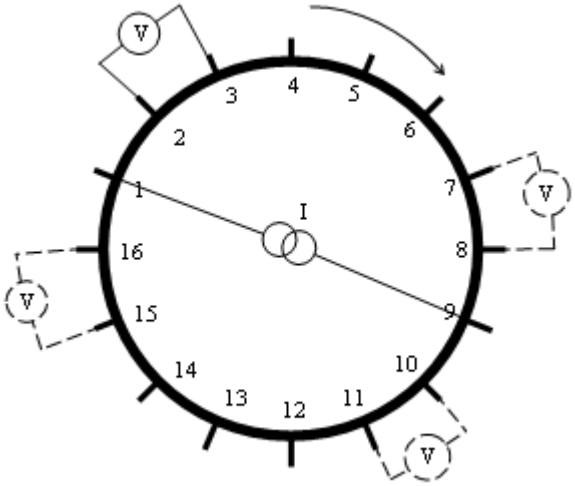

Figure 2.4: The opposite measurement strategy

The opposite strategy yields *N(N-4)* measurements per data frame. Considering the function of current injection and current sink electrodes are reversed for half of the 'cycle', only half of the measurements are unique. This reduces the total number of unique measurements to *N(N-4)/2*. The opposite strategy is less sensitive to changes near the boundary as current flows across the imaged space. However, the current distribution is more uniform across the centre region of the imaged space, therefore the strategy is more likely to detect changes in the centre region (Hua et al 1993). The disadvantage of the opposite strategy is the significant reduction in number of unique measurements obtained compared to the adjacent strategy, which results in decrease of resolution.

Other strategies

There are other variations of measurement strategies. Shi et. al. (2006) suggested the pseudo-opposite strategy. Instead of using the electrode diametrically opposite of the current injection electrode as a current sink, the electrode previous to the direct opposite electrode is used, as shown in Figure 2.5(a). This retains the number measurements to *N(N-4)*. The same publication also described the cross-drive strategy which uses electrodes that are 90^{o} apart as current driving electrode pairs (Figure 2.5(b)). Voltage difference measurements are taken on all adjacent pairs of electrodes not used for current injection. This measurement strategy also yields *N(N-4)* measurements.

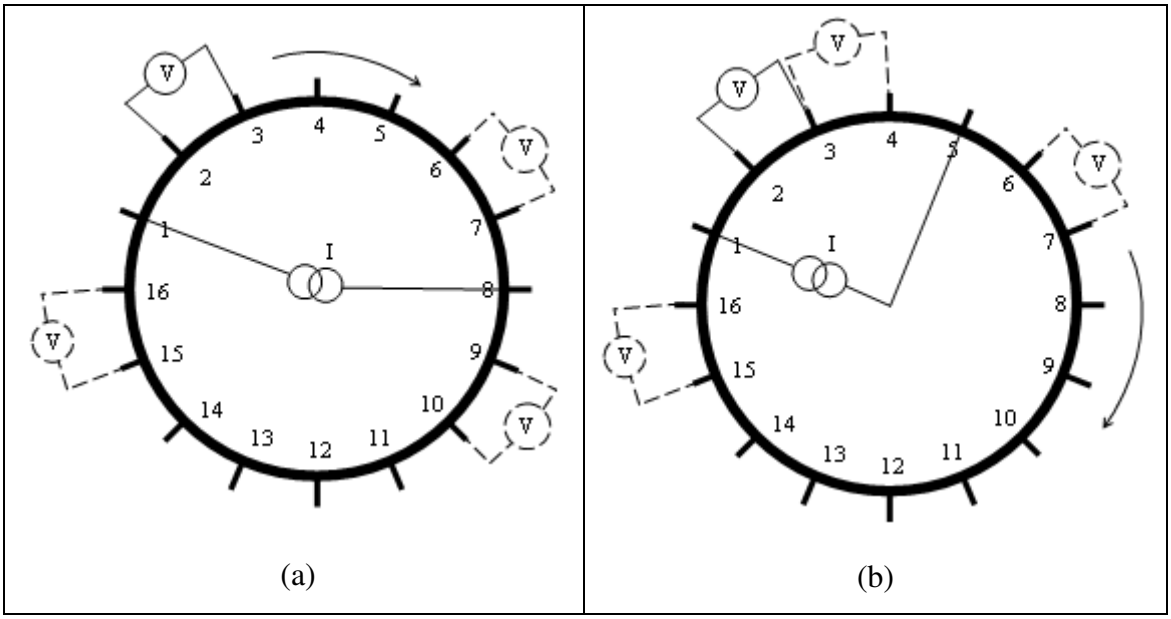

Figure 2.5: (a) The pseudo-opposite and (b) the cross-drive measurement strategy

Typically, for multi-planar electrode arrangement, each electrode plane is treated independently, resulting in a quasi-3D measurement strategy. Current injection strategies can be expanded through using electrode pairs located on different electrode planes. For example, vertically adjacent electrode pairs can be used for current injection, as well as electrodes located diametrically opposite on different electrode planes. Fan and Wang (2010) described using electrodes located on different electrode planes. The paper described the 'W-type' current drive strategy, where current are injected through electrode pairs located on different electrode planes for vertically and diagonally adjacent electrode pairs.

2.3.3 Instrumentation

The hardware architecture for ERT instrumentations is relatively simple. The basic building blocks consist of an impedance analyser and a switching network to enable customized sets of measurements to be acquired. A typical ERT hardware architecture consists of an output stage, an input stage, and a multiplexing system. The output stage consists of a current source designed to have high output impedance such that the magnitude of the current does not affect the load. Current sources can be either constant-current or constant-voltage. A constant-voltage source is sometimes preferred instead of a constant-current source as the latter is more complex and costly to design. The constant-voltage current source is also capable of performing well with a wide

range of loads, provided that the output impedance is significantly lower. The constant-voltage source is typically designed to have very low output impedance such that the amount of current delivered is only dependent on the load impedance. Consequently, the current delivered is measured. With a constant-voltage source, current magnitudes and measured signals are not guaranteed, resulting in sensitivities and noise levels dependent on the load.

The input stage functions as a filter and gain for the differential voltage inputs prior to digitization of the signals. A typical input stage consists of an instrumentation amplifier and programmable gain stage to adjust the signal to full-scale input to match the digitizer, which is dependent on the dynamic range of the inputs. The maximum and minimum measurements may vary for a measurement strategy, therefore the amplification levels are selected per measurement basis.

Recent development of ERT instruments focuses on higher performance in terms of data acquisition rate, accuracy and precision. The demand for high acquisition rate is of particular concern for IPT applications for imaging dynamic subjects, typically acquiring thousands of frames (measurement sets) per second. Therefore, instruments designed for IPT applications tend to compromise flexibility in switching protocols and precision in favour of higher data acquisition rate.

There are various reviews on available tomographs (Boone and Holder, 1996b; York, 2005; Murphy 2008). Stephenson (2008) compared the performance of three instruments – the ITS P2000 system (Primrose and Qiu, 1999), the Low Cost Tomography Instrument 2 (LCT2) tomograph (York et. al., 2005) and the University of Cape Town (UCT) EIT instrument (Wilkinson et. al., 2006). The criteria evaluated were data acquisition rate, conductivity operating range, linearity of response, and measurement strategy flexibility.

The Low Cost Tomography Instrument 2 (LCT2)

The LCT2 is used primarily throughout this work. The tomograph is designed to provide a constant voltage current source which can be varied to provide an output source between 10mV and 12V, and frequencies between 10Hz and 1MHz. Differential voltage measurements are obtained through a high input impedance operational

amplifier (>1TOhms). The multiplexing system consists of mercury-wetted relays in a crossbar switch configuration, which allows flexibility when configuring four-terminal measurement strategies, allowing any of the four terminals to be connected to any electrode. Settling time for the relays ranges between 3ms and 15ms, and this ultimately dictates the data acquisition rate. The LCT2 is capable of providing up to approximately 70 measurements per second, which is relatively modest in comparison with other available instruments.

Data is transmitted through a high-speed USB2.0 serial link to a customised software package. The raw data are saved and are accessible for image reconstruction. One of the main issues with the LCT2 is the hardware implementation for the USB. The design is not optimised, resulting in various problems stemming from failure of communication between the LCT2 and the corresponding software. A redesign should be implemented or sourcing a different transfer protocol which is better-suited for data transfer.

An important aspect which is of interest to this work is the noise level of the instruments, which is used as an indicator of the precision of measurements. The overall noise levels of an ERT system vary with factors including the phantom used and electrodes arrangements even though the intrinsic instrument noise may be much lower. To serve the purpose of evaluating the precision of measurements, the signal-to-noise ratio (SNR) is calculated by taking the ratio of the mean to standard deviation, for each measurement in the data set, for certain number of repeat frames of measurements. Stephenson (2008) presented a study using this method. The result presented indicates that the SNR for the LCT2 varies from a maximum of 59 dB at 0.59 frame per second (fps) to 54dB at 0.35fps. This is comparable with other available instruments. For example, the ITS P2000 is capable of maximum SNRs which vary between 64dB at 2fps to 24dB at 75fps. The author noted that the excitation frequency of the ITS P2000 was set above the recommended maximum frequency of 19.6 kHz in order to achieve data acquisition rate exceeding 50fps. The UCT instrument is capable of achieving a maximum SNR of 65dB at 1fps to 45dB at 285fps. All the SNRs were calculated using the same experimental set-up described in Stephenson (2008), for 100 frames of measurements. One of the newest EIT instruments developed, the Functional Electrical Impedance Tomography of Evoked Responses (fEITER) is reported to achieve approximately 80dB precision for 100fps (Davidson et. al., 2010).

2.4 Image Reconstruction

The purpose of image reconstruction using ERT is to ultimately obtain visualization of the conductivity distribution within the imaged space. This is achieved through the impedance measurements acquired on the boundary of the imaged space. The ERT image reconstruction problem involves two stages, namely the forward solution and the inverse solution. To solve the inverse problem, the forward problem needs to be solved for an initial estimated conductivity such that the predicted voltages can be compared with the measured data. The forward problem solves for the internal voltage and subsequently the current density distribution (Jacobian) given the resistivity distribution with boundary current density and voltage distribution. The inverse problem solves for the resistivity distribution given the voltage and current density distributions. Numerical methods for general geometry and arbitrary conductivity require the discretization of both the domain and the conductivity (Lionheart, 2004).

Throughout this research EIDORS, a toolkit based in Matlab, is used. The toolkit was originally developed for 2D EIT imaging (Vauhkonen et. al. 2001) and was later further developed for 3D imaging (Polydorides and Lioneart, 2002). The EIDORS toolkit consists of a collection of functions to setup parameters for forward solving and calculation of the Jacobian matrix, for a Finite Element mesh structure imported into the workspace. With parameters such as electrode surface area, current patterns and current injection level defined and interior fields and subsequently the Jacobian matrix calculated, the inverse solution can be computed with various inverse solving algorithms included in the EIDORS toolkit. The inverse solution can be visualized using functions included in the toolkit. Full details of the mathematical models and formulation can be found in Tarantola (1987), Vogel (2001), Hansen (1998) and Engl et. al. (1996), Vauhkonen et. al. (1999), Borcea (2002), Borsic (2002), Polydorides (2002) and Lionheart et. al. (2005). The following section describes some of the important topics in image reconstruction for completeness.

2.4.1 The ERT Forward Problem

The forward problem includes setting up the interior electric fields based on current patterns used. Solving the forward problem requires an electric field solver and a model

of the imaged space with sources of current. After computing the interior potentials, the voltages at certain locations on the boundary of the imaged space Ω, corresponding to electrode locations can be determined. Based on this information, a simulated dataset corresponding to a measurement strategy can be computed for the defined conductivity distribution. This protocol is later reversed for image reconstruction to compute a conductivity distribution based on a given measurement set.

To solve the ERT problem, we first consider the complex admittivity form. The admittivity distribution within the imaged space is given by:

$$\gamma = \sigma + i\omega\varepsilon \tag{2.1}$$

where σ is the electrical conductivity, ε the electrical permittivity, and γ the complex admittivity of the medium at the angular frequency of the applied current. The relationship between electromagnetic fields and admittivity are described by Maxwell's equations (Feynman et. al. 1977). EIT is concerned with low frequency signals and quasi-static electric fields which allow the magnetic field component to be neglected (Lionheart et. al., 2005). Providing there are no internal current sources within the imaged space, Maxwell's equations simplify to the continuum Kirchoff's law connecting admittivity and potential according to:

$$\nabla \cdot (\gamma \nabla u) = 0 \text{ in } \Omega \tag{2.2}$$

For low frequency current injections, the phase angles of the measured voltages will be small and so only the real component of the voltage is measured. Under these conditions, the electrical conductivity can be reconstructed and the complex admittivity can be replaced with electrical conductivity and EIT is transformed into ERT.

Discretization of the Model Using Finite Element Method

Before calculating the Jacobian matrix the model needs to be discretized, an important factor which requires careful consideration. The density of the mesh must be fine enough such that the electric field in the interior given the conductivity can be predicted close to the accuracy of the measurements. The Finite Element Method (FEM) is chosen as the heterogeneous imaged conductivity distributions are often on an irregular

domain. Lionheart (2004) summarizes various other methods that have been used to discretize the model, including the Finite Difference Method (FDM) and the Boundary Element Method (BEM).

In the FEM, the 3D domain (Ω) is decomposed into polyhedral known as 'elements' (Ω_k), preferably irregular, such as tetrahedral, prisms, etc. The elements represent unknown potentials in a polynomial of fixed orders. The elements intersect only in whole faces or edges or at the vertices and potentials are assumed continuous across the faces. The FEM converges to a solution (or a close approximation) of the partial differential equation it represents, as the elements become more numerous (provided their interior angles remain bounded) or as the order of the polynomial is increased. Netgen (Schoberl 2008) , used as the primary mesh generator throughout this research, creates meshes by performing a combination of advancing front surface meshing and Delaunay tessellation, followed by mesh optimization. The software allows meshing criteria to be customized, such as mesh granularity, maximum number of elements and maximum edge size.

There are alternative meshing methods applied, namely multi-grid and adaptive meshing. In multi-grid method, a course grid is first used to obtain the rough features of a solution, which is then extrapolated to a finer grid for a more accurate solution. The adaptive meshing method (Molinari et. al., 2001) is used to reduce solution time. The mesh density is increased where the high field strengths are found and decreased where the potential is only slightly varying. This results in a more accurate solution than using a regular mesh. The complexity of this method is determining whether to use the same mesh for all current patterns or to use a different mesh for every current drive configuration. The mesh-mapping technique (Murphy and York, 2006) is suggested to map the properties of the elements calculated for a mesh onto another mesh with different density level. This technique allows forward solution to be calculated on a finer mesh and inverse solve on a coarser mesh but retaining most of the information calculated during forward solving which will be used for inverse solving.

Complete Electrode Model

Reliable discretization typically imposes some form of restrictions on the structure of the mesh near the boundary and the outer surface of the mesh. It is important that the

elements near the boundary, especially near electrodes, are discretized such that they are small enough to preserve the accuracy of the measurements. For industrial applications of EIT, the modelling of the phantom includes details such as locations and geometrical characteristics of the electrodes. It is necessary that the structure of the boundary accommodates the areas the electrodes occupy such that the appropriate areas where the electrodes occupy can be assigned.

To ensure a unique solution, boundary conditions are required. In this case, a combination of Neumann (boundary current density) and Dirichlet (boundary potentials) conditions (Lionheart et. al. 2005) are used. The Complete Electrode Model (CEM) (Cheng et. al. 1989) is used for as boundary conditions in ERT, where the discrete current injection on the surface of the volume ($\partial\Omega$) exists via a set of electrodes. For the l'th electrode, the integral of the current density over the electrode is equal to the current flowing to the electrode:

$$\int_{e_l} \sigma \frac{\partial u}{\partial \nu} = I_l \text{ on electrode } e_l \tag{2.3}$$

$$u + z_l \sigma \frac{\partial u}{\partial \nu} = V_l \text{ on electrode } e_l \tag{2.4}$$

where I_l is the current on the surface of the l'th electrode, V_l is the potential measured by the l'th electrode, z_l the contact impedance of the l'th electrode and v the outward unit vector, normal on the boundary of the domain. On surfaces that are not occupied by electrodes:

$$\sigma \frac{\partial u}{\partial v} = 0 \tag{2.5}$$

The stability and uniqueness of the forward solution is preserved by enforcing the conditions:

$$\sum_{l=1}^{L} I_l = 0 ; \sum_{l=1}^{L} V_l = 0 \tag{2.6}$$

where L is the total number of electrodes attached to the boundary. The CEM is known to be well-posed and has a unique solution (Somersalo et al. 1992). The drawback of CEM is the difficult in accurately predicting the contact impedance. Some efforts (Vilhunen et. al. 2002; Heikkinen et. al. 2002) have been made to address this issue, however, it is not possible to correctly predict the contact impedance on a consistent basis considering contact impedance may vary with time.

Computing the Electric Field

The global conductance matrix A is assembled starting from building the local matrices $A_{M,}A_z$ and $A_{V,}$ which are defined as (Polydorides 2002): .

$$A_M = \sigma \iiint_\Omega \left(\frac{\partial \phi_i}{\partial x}\frac{\partial \phi_j}{\partial x} + \frac{\partial \phi_i}{\partial y}\frac{\partial \phi_j}{\partial y} + \frac{\partial \phi_i}{\partial z}\frac{\partial \phi_j}{\partial z} \right) dxdydz \tag{2.7}$$

$$A_Z = \sum_{l=1}^{L} \frac{1}{z_l} \int_{el} \phi_i \phi_j dS \tag{2.8}$$

$$A_V = -\frac{1}{(z_l)_j} \int_{el} \phi_i dS \tag{2.9}$$

where ϕ_i and ϕ_j are piecewise linear basis functions which describe the independence of the potentials on each vertex, taking the natural form of (Polydorides and McCann 2002):

$$\phi = \begin{cases} 1, \text{ on vertex k} \\ 0, \text{ otherwise} \end{cases} \tag{2.10}$$

A_D is the estimate of the normalized contact impedance for each electrode, expressed as:

$$A_D = diag\left(\frac{|E_l|}{z_l} \right) \tag{2.11}$$

for i,j = 1, 2,...K, with K as the number of boundary electrodes. $|E_l|$ represents the surface area of the l'th electrode and

The global conductance matrix A is assembled starting from the local matrix A_M, on top of which the A_Z elements are superimposed. The A_V and A^*_V are assembled in a similar manner and patched along with the diagonal A_D to form the CEM based FEM operator for forward solving. For a specific current pattern I^d, the forward problem can be written as (Polydorides 2002):

$$\begin{bmatrix} A_M + A_Z & A_V \\ A_V^* & A_D \end{bmatrix} \begin{bmatrix} U \\ V_L \end{bmatrix} = \begin{bmatrix} 0 \\ I^d \end{bmatrix} \tag{2.12}$$

where U is the nodal potential distribution and V_L is the potential values on the boundary electrodes in the form of $Ax=b$.

In order to preserve the existence and uniqueness of the solution, additional conditions need to be included. Each current pattern must be set-up such that the sum of discrete current pattern vectors should be zero, ensuring that the amount of current injected into the imaged space equals the amount of current sunk for each current pattern. This should be true regardless of measurement strategy applied.

The uniqueness of the forward solution is only guaranteed when the system matrix is full-rank, meaning that the matrix should have a rank as large as possible. However, the block matrix in Eq. (2.12) is bound to be rank deficient by one. In order to bring it to full-rank state, a ground selection should be made, or equivalently the boundary measurements must be gathered in a way such that $\sum_{l=1}^{L} V_l = 0$ is fulfilled. A ground can be made by either choosing an arbitrary vertex on the model or incorporating a ground electrode. In practical terms, a 0V reference point is necessary to provide a reference for extracting the electrodes potentials before computing the pair differences.

2.4.2 Jacobian Matrix

Using optimization-based inverse solvers, it is necessary to calculate the derivative of the voltage measurements with respect to a conductivity parameter. The complete matrix of the partial derivatives is the Jacobian (sensitivity) matrix, relating a

conductivity distribution and a distributed set of impedance measurements. The Jacobian matrix contains all first-order partial derivatives of a vector-valued function and represents a linear approximation to a differentiable function near a given point. Given a set of non-linear equations:

$$\begin{aligned} y_1 &= f_1(x_1,...,x_n) \\ &\vdots \\ y_n &= f_n(x_1,...,x_n) \end{aligned} \tag{2.13}$$

the Jacobian matrix $J \in \mathbb{R}^{mxk}$ takes the form (Polydorides 2002):

$$J = \begin{bmatrix} \frac{\partial y_1}{\partial x_1} & \cdots & \frac{\partial y_1}{\partial x_n} \\ \vdots & \ddots & \vdots \\ \frac{\partial y_n}{\partial x_1} & \cdots & \frac{\partial y_n}{\partial x_n} \end{bmatrix} \tag{2.14}$$

Calculation of the Jacobian matrix in EIDORS is done by calculating the Fréchet derivative of the measured voltages on the electrodes with respect to the perturbations of the conductivity, which is detailed in Polydorides (2002). For the *d*'th current pattern in a measurement strategy and *m*'th voltage difference measurement, the Jacobian of the element Ω_k can be calculated through:

$$J_{d,m}^{(k)} = -\int_{\Omega^k} \nabla u(I^d) \cdot \nabla u(I^m) dxdydz \tag{2.15}$$

In ERT, the rows of the Jacobian matrix represent the sensitivity map relating a particular boundary voltage measurement to a conductivity distribution. The conditioning of a Jacobian matrix is closely related to the numerical accuracy of an inverse solution. Therefore, information on the effectiveness of ERT related parameters and accuracy of the inverse solution can be extracted through analysis of the Jacobian matrix.

2.4.3 The ERT Inverse Problem

The inverse problem in ERT is concerned with computing the unknown conductivity distribution of the discretized model from the inverse of the Jacobian matrix with the measurement vector. Consider complex vectors $x \in \mathbb{C}^n$ and $b \in \mathbb{C}^m$ and complex matrix $A \in \mathbb{C}^{mxn}$, the inverse problem sets out to find *x*, given *b* and *A*, for $Ax = b$. In ERT, *b* is the measurement vector (V_{meas}), *x* is the conductivity vector (σ) and *A* is the Jacobian matrix (*J*). Ideally, in order to determine the solution σ, an inverse of the *J* is necessary. However, due to its compact nature, matrix *J* has an unbounded (discontinuous) inverse. This means J^{-1} is unstable against variations in data, violating Hadamard's third criterion for well-posedness. In practice, the number of measurements and unknowns are often varied. It is normal that the number of measurements exceeds the number of unknowns. However, the opposite is true for the ERT problem, where there are more unknowns to be solved far exceeds the number of measurements. If this is the only problem, an obvious choice would be the popular Moore-Penrose least squares method (Lionheart et. al. 2005) which provides the generalised inverse in the form of:

$$\sigma_{MP} = J^{\dagger}V = (J^T J)^{-1} J^T V \tag{2.16}$$

with the least squares solution given as:

$$\sigma_{MP} = \arg\min_{\sigma} \left\| J\sigma - V \right\| \tag{2.17}$$

This can also be expressed as the minimum of the sum of squares of the errors between the measured and predicted voltages:

$$\sigma_{MP} = \arg\min \left\| V - F(\sigma) \right\|^2 \tag{2.18}$$

where $F(\sigma)$ is the forward operator. However, the approach is not suited for the badly conditioned Jacobian matrix, whose inverse does not exist.

Regularization

The Tikhonov regularisation method (Phillips 1962; Tikhonov 1963), which was extended by Hoerl (1962) for finite dimensional problems, is used instead. As the least squares approach fails for a badly conditioned *J*, the strategy is to replace the least squares solution with:

$$\sigma_\alpha = \arg\min_\sigma \left\|J\sigma - V\right\|^2 + \alpha^2 \left\|\sigma\right\|^2 \tag{2.19}$$

where a trade-off is made to obtain a solution for $J\sigma = V$ and not let the term $\left\|\sigma\right\|$ get too large. The scalar α controls the trade-off and is termed as the 'regularisation parameter'. The minimum for Eq. (2.19) can be written as:

$$\sigma_\alpha = (J^T J + \alpha^2 I)^{-1} J^T V \tag{2.20}$$

It is worth noting that for a big α, the matrix $(J^T J + \alpha^2 I)$ which is inversed is well conditioned, and even if *J* does not have full rank, $(J^T J + \alpha^2 I)$ does. Eq. (2.18) is modified to include the regularisation terms as:

$$\sigma_\alpha = \arg\min \left\{ \left\|V - F(\sigma)\right\|^2 + \alpha^2 \left\|L(\sigma - \sigma_{ref}\right\|^2 \right\} \tag{2.21}$$

where *L* is known as the 'regularization matrix', a matrix approximation to some partial differential operator, and σ_{ref} is the 'reference conductivity', an initial estimate introduced as a form of *a priori* information. This minimization includes a trade-off between an exact fitting of the data and not making the derivatives of the conductivity too large, controlled by the regularization parameter, α which determines the level of damping imposed.

The selection of the regularization parameter α has an implication on the inverse solution. As mentioned previously, the Jacobian matrix *J* is ill-conditioned, whereby the condition number (the ratio of its largest singular value to its smallest) is large (Polydorides 2002). This is because of the solution's high frequency, and the lack of precision in the measurements to retain all details of the distribution components,

resulting in the non-continuous dependency between the measured voltages and the solution. Regularization adds a restraining element which essentially 'irons out' the discrepancies, stabilising the inverse problem and controls any amplification of errors. Therefore, optimum choice of regularization parameter requires careful consideration such that the regularized solution matches the exact solution as closely as possible. A large value for α limits any amplification of the high oscillatory components of the solution. When smooth regularization operators are applied in ERT, solution errors due to regularization is visible as distortions in the distributions, typically expanding the solution contours, and the quantitative results tend to saturate at a lower value. A smaller value for α reduces the influence of regularization applied.

Inverse Solving Algorithms

A linear approximation is often adopted to solve $F(\sigma)$ with:

$$F(\sigma) \approx F(\sigma_o) + J(\sigma - \sigma_o) \tag{2.22}$$

where σ_o is the initial estimate, which may differ from σ_{ref} and F is the forward operator that gives $V = F(\sigma)$, the measured voltages on the electrodes for a conductivity distribution. J is calculated at an initial conductivity estimate σ_o. Eq. (2.21) can then be expressed in its quadratic minimisation form (Lionheart et. al. 2005):

$$\sigma = (J^T J + \alpha^2 L^T L)^{-1} (J^T (V_{meas} - F(\sigma_o)) + \alpha^2 L^T L(\sigma_{ref} - \sigma_o)) \tag{2.23}$$

$F(\sigma_o)$ is commonly replaced with reference measurement, often taken at a homogeneous or stable state of the process. This approach reduces the effect of system errors and is referred to as 'difference imaging' (Vauhkonen et al 1999). Eq. (2.23) is only valid for small conductivity changes from the initial estimate due to the approximation. In such cases, a non-linear iterative algorithm should be used instead.

There are various algorithms developed to inverse solve or produce reconstructed images. Algorithms can be linear, non-linear, single-step, and iterative. Linear algorithms compute the inverse solution in a single-step. Non-linear algorithms update the Jacobian matrix based on the updated solution calculations, hence iterative. In

quantitative terms, difference algorithms produce solutions which reflect conductivity change from the reference state, which is a prior information and stable state, while absolute reconstruction algorithms compute numerically accurate conductivity values of the image space. Even with the vast amount of algorithms available, there is no one algorithm which is able to produce a reconstructed image to a high degree of accuracy. It is difficult to establish the limiting factor, be it the weakness of the algorithm, accuracy of the Jacobian matrix, modelling errors to measurement accuracy. Reconstruction properties and limitations are discussed in Section 2.5.

The two algorithms that are predominantly used throughout this thesis are discussed in brief below.

Gauss-Newton Algorithm

For the Linear Gauss-Newton (LGN) (sometimes known as Linear Newton-Raphson) algorithm, a Gauss-Newton approximation is applied to the calculation that neglects the second derivatives of the function which is minimized. Applying the approximation, Eq. (2.23) becomes:

$$\tilde{\sigma} = (J^T J + \alpha^2 (L^T L))^{-1} (J^T (V_{meas} - F(\sigma_o))) \tag{2.24}$$

where the initial estimate σ_o is typically chosen to be the reference value σ_{ref}. The level of smoothness applied is determined by the $(\alpha^2 (L^T L))$ term. α^2 is selected based on the confidence we have on the accuracy of the measurement. *L* is usually a Gaussian smoothing operator, although there are other alternatives. The LGN algorithm is only suitable to reconstruct small conductivity changes from a reference state as the Jacobian is a linear operator. Therefore, the LGN algorithm is suited for difference imaging where $F(\sigma_o)$ is substituted with measured voltages of a conductivity distribution similar to that used to calculate the Jacobian.

The NLGN is an iterative version of the LGN. The Jacobian matrix is updated after every iteration of the solution with *k* as the current iteration, resulting in a longer and therefore more costly computation. The next solution update is calculated by:

$$\tilde{\sigma}_{k+1} = \tilde{\sigma}_k + (J_k^T J_k + \alpha^2 (L^T L))^{-1} (J_k^T (V_{meas} - F(\sigma_k))) \quad (2.25)$$

As the linearization of the Jacobian matrix is updated after each iteration of the solution update, NLGN is able to break free from the restriction imposed on the LGN algorithm. The quality of the reconstructed images, however, is subjected to similar limitations as its counterpart. Further details about this algorithm can be found in Lionheart et. al. (2005).

Singular Value Decomposition

The Singular Value Decomposition (SVD) reduces the elements in a matrix into singular components to calculate the regularized inverse, and provides a means to study the ill-conditioning of the matrix. Comprehensive details and derivations of SVD can be found in Hansen (1998), but is briefly described here for completeness. Considering a set of orthonormal vectors in the image space u_i and in the data space z_i such that $Ju_i = \lambda_i z_i$ where λ_i are scalar values arranged in descending form ($\lambda_1 \geq \lambda_2 \geq \ldots \geq 0$). It should be noted that it can be taken to mean that the component of the image corresponding to u_i is attenuated by λ_i. This can be expressed in matrix form as:

$$J = Z\Sigma U^T = \sum_{i=1}^{n} z_i \lambda_i u_i \quad (2.26)$$

where $\Sigma = diag(\lambda_i)$ padded with zeros such that it has the same dimension as *J*. It should be noted that the standard notations used in SVD derivations are slightly modified to avoid confusion with other parameters with similar notations in this section. The pseudo-inverse of *J*, which is later used to compute the least squares solution can be written as:

$$J^{MP} = \sum_{i=1}^{N} z_i \lambda_i^{-1} u_i^T \quad (2.27)$$

In order to use the SVD for image reconstruction, the SVD is calculated for the pre-calculated *J*. Although this is computationally costly, especially for a relatively large model, the matrices are only required to be calculated once for the same geometry and

initial background set-up. The singular components can be seen as the discrete frequency spectrum of a solution. Most of the properties of the image, or low frequency components, will be contained in singular values with higher magnitudes as the system of equations containing a large amount of information with the properties. The finer details, however, may only be available in a small proportion of the equations. Therefore, the corresponding singular values have very small magnitudes. This observation is reflected when considering the least squares solution to $J\sigma = V$:

$$\sigma_{LS} = J^{MP}V = \sum_{i=1}^{N} \frac{u_i^T V}{\lambda_i} z_i \tag{2.28}$$

It has been shown that for a discrete ill-posed problem, the singular vectors become increasingly oscillatory when λ_i decreases as the index of the components increases (Hansen 1998). Consider the case where the measurement vector is ideal, the high frequency components will be well-represented in the solution. However, in practice, the data in the measurement vector is likely to contain noise or unwanted perturbations. This may result in ($u_i^T V$) becoming large and for singular components of higher index, the error is amplified with the lower singular value magnitudes λ_i, which ultimately dominates the solution, as shown in Eq. (2.28)

This condition can be stabilised by applying some form of regularization. The Truncated Singular Value Decomposition (TSVD) method is the simplest form of regularization, where the unstable singular components are filtered and excluded in the summation. For a user defined truncation point, *k*, the solution becomes:

$$\sigma_k = \sum_{i=1}^{k} \frac{u_i^T V}{\lambda_i} z_i \tag{2.29}$$

The choice of truncation point is often chosen by applying the Discrete Picard Condition (DPC) (Hansen 1998). According to the DPC, in order for the singular values to be considered stable, the absolute Fourier coefficients ($u_i^T V$) must decay to zero at a faster rate than its corresponding singular values (λ_i).

A better form of regularization is to apply a damping factor to the unstable components, reducing the contribution of these components rather than eliminating it. A commonly used method is introducing the properties of the regularization matrix, generalizing the SVD. Details and derivatives of the Generalized Singular Value Decomposition (GSVD) can be found in Hansen (1998).

2.5 Summary for Electrical Resistance Tomography

This chapter aims to provide background information on some of the related aspects of ERT relevant to this thesis. Applications of ERT in industrial process engineering relevant to this work were discussed. Applications involving particle-sized materials are included specifically due to the relevance to the chosen demonstrator for the WSN4IP project, which is monitoring changes in grain storage or silo. The initial intention of this project is to share a common demonstrator with the WSN4IP project. The idea was to implement ERT to monitor moisture content change in grain storage. There are no publications found for the application of ERT to monitor moisture content change in grain or other particle-sized material. As provided in the review in Section 2.2, applications of ERT in particle-sized materials usually involve liquid in order to provide a sufficiently conducting medium for current flow. In grain storage, presence of water is limited to moisture in grain, which is insufficient to provide a conducting medium for sensible ERT measurements to be acquired. Publications describing moisture measurement techniques typically use modalities such as microwave and capacitance. These modalities are capable of deducing information of the monitored properties through the changes in the dielectric of materials. This suggests that ERT may not be suited for this application. As sharing a common demonstrator between this project and the WSN4IP is not a critical aspect of this thesis, it was decided that this thesis would focus on tackling the generic issue, which is to improve the spatial resolution of reconstructed images using ad hoc sensors. The demonstrator is chosen to be a liquid-based medium.

Background information on the technical implementation of ERT was also reviewed. Special emphases are put on relevant aspects to this work, including electrode arrangements and measurement strategies. Conventional arrangements and strategies in

industrial process applications are discussed, providing background information to set-up the modifications necessary to accommodate the ad hoc sensors with conventional ERT set-ups in later chapters of this thesis. A review of related work done using unconventional electrode arrangements is included to provide a review of related work.

Relevant topics to this thesis on modelling and image reconstruction aspect of ERT are also discussed. The Gauss-Newton and Singular Value Decomposition algorithms are included as these are the main algorithms used throughout this thesis. The Gauss-Newton algorithm was chosen for its iterative nature, as it is suitable for one of the approaches considered to incorporate measurements from ad hoc sensors into inverse solving. Singular Value Decomposition and the truncated variation of the algorithm were chosen for the simplicity of choosing a filtration parameter methodically.

CHAPTER 3
UNDERSTANDING RECONSTRUCTED IMAGES

Before undertaking efforts to improve the quality of reconstructed images, it is essential to understand the properties that are associated to the images. This chapter aims to provide an overview on the image properties and the factors that contribute to them. Seager et. al. (1987) provided the first comprehensive analysis to assess properties and limitations of reconstructed images in tomography. The same publication suggested three properties of reconstructed images that define the capabilities of a tomographic technique or set-up, namely spatial resolution, accuracy and stability. Murphy (2008) provided an extension to this study and provides a more comprehensive analysis on the different attributes which contribute to the quality of a reconstructed image. This chapter also describes analysis techniques which aid in further understanding of image properties such as quality or stability of measurements, sensitivity and spatial resolution. These analysis techniques are robust and more scientific in comparison to a more commonly adopted practice within the tomography community, which is through visual inspection of a number of reconstructed images.

Section 3.1 discusses the image properties and the inter-dependency of the properties is briefly discussed. Among the properties discussed include sensitivity, stability of measurements and spatial resolution. Section 3.2 discusses the types of analysis which can be applied to further understand the influencing factors which lead to changes in the properties of interest.

Section 3.3 focuses on spectral analysis using Singular Value Decomposition (SVD). In this subsection, SVD is applied to extract information about the quality of the measurements obtained. Using SVD and applying the Discrete Picard Condition (DPC), the amount of unique information that can be obtained and the amount of content that can be recovered for image reconstruction can be extracted. This information is useful when comparing different measurement strategies, as well as evaluating different noise levels of measurements acquired.

Section 3.4 discusses numerical analysis for sensitivity visualization. Sensitivity provides information on the detectability of changes in the imaged space and provides initial information the potential reconstruction quality of images. Section 3.5 discusses numerical analysis for spatial resolution using resolution matrices. In this section, resolution matrices is described and used to acquire information regarding the point contrast or spatial resolution of the discretized model and the correlation between elements.

3.1 Image Properties

In order to consider the analysis of reconstructed images, it is necessary to define associated properties. Seager et. al. (1987) provided the first complete analysis in attempting to assess the limitations of a tomographic modality. It was suggested that the properties of reconstructed images that define the capabilities of a tomographics are spatial resolution, accuracy and stability. Image properties can be grouped into three main categories, namely reconstruction, sensor and application. The properties are inter-related with each other, as illustrated in Figure 3.1. Reconstruction parameters are linked to the choice and implementation of algorithm. Sensor parameters are linked to instrumentation performance, electrode arrangement and measurement strategy. Application parameters include any additional information that can be provided to simplify the calculation, for example material properties. Therefore, when considering making changes to one property, the effect of this change on other aspects should be taken into consideration as well.

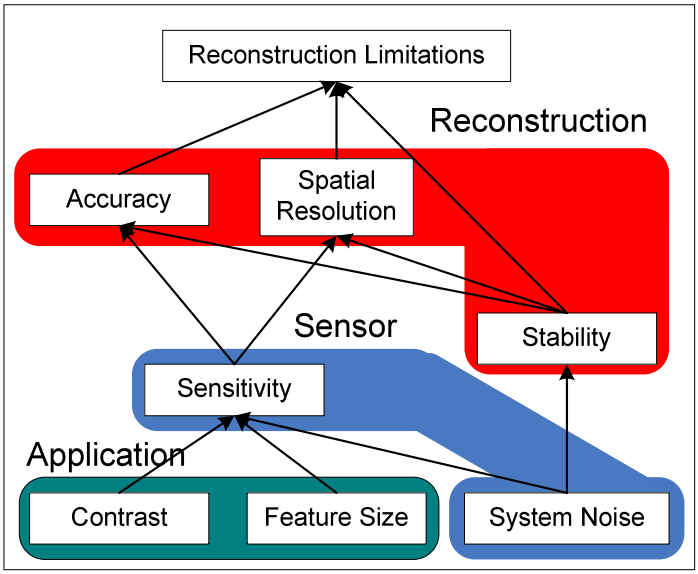

Figure 3.1: Relationship between properties of reconstructed images (Murphy 2008)

Reconstruction parameters include spatial resolution, accuracy and stability. In ERT, spatial resolution in reconstructed images indicates the smallest region which can be resolved and shown (visible) on the image. Accuracy refers to the smallest conductivity contrast that can be distinguished by the set-up and reconstruction, providing an indication of the ability to solve for accurate quantitative information. Spatial resolution and accuracy can be viewed in the same vein as the ability to reconstruct or resolve is dependent on the size of the area. Stability provides information on how susceptible a reconstruction algorithm is to system noise and non-systematic errors. Stability varies between measurement strategies and is sensitive to system noise. Modelling errors are less influential on the stability, as even the most precise model will contain numerical errors due to machine precision round-offs that are non-systematic and could influence the reconstruction stability. Essentially, stability is a measure of the repeatability of reconstruction.

Sensor related parameters include system noise and sensitivity. System noise refers to exterior factors which influence the precision of measurements, usually originating from instrumentation and environmental effects. The quality of calibration and modelling have an effect on the accuracy of a measurement set, which subsequently influences the associated reconstruction properties. A detectable conductivity perturbation is the minimum requirement in order to invoke measurement change above system noise. It is worth noting that a detectable perturbation does not translate into visibility on the reconstructed image. Sensitivity is influenced by factors such as electrode arrangements,

electrode geometry and dimensions, and measurement strategy. It is also dependent on spatial position within the image space. When analysing the sensitivity of the tomography system, associated parameters such as feature size, contrast and system noise should be included into the analysis.

Application parameters include feature size and contrast. Feature size refers to the dimensions that are required to represent the geometry of the model, for instance electrode size, to a specified accuracy. In ERT, this is defined by the density of the mesh when the model is discretized using the FEM algorithm. This directly influences any calculation of reconstruction limitations. Contrast is defined as the relative difference between the conductivities in different regions. In ERT, it is used to describe the conductivity difference between an inclusion in an otherwise homogeneous solution space. Feature size is used together with contrast to help define ideal reconstruction features specific to the application's requirement. Subsequent calculation of reconstruction limitations can be used to suggest whether these ideals can be met or otherwise.

3.2 Types of Analysis

There are two main reasons for analysing tomographic characteristics. The first is for feasibility studies or confidence testing of results when using a reconstruction algorithm, sensor configuration and instrument for a specific application. The second is as a comparative study for choosing settings and parameters. Ideally, analysis techniques to evaluate the quality of a reconstructed image should be robust and provide numerical evidence. A common practice is to evaluate the performance of an ERT setup through visual inspection of reconstructed images. The conclusions reached are easily biased, based on personal preference and are highly dependent on users having prior knowledge of the test distribution used, resulting in lack of confidence when evaluating different ERT setups. Seager et. al. (1987) provided a generalized overview on analysis techniques that can be applied to analyse the parameters described in Section 2.4.1. Murphy (2008) provided a more comprehensive insight into several methods targeting analysis on stability, sensitivity and spatial resolution, as well as a compilation of relevant statistical figures-of-merits which can be used when comparing reconstructed

images. Analysis can be categorized into four groups with members of each group sharing similar restrictions, namely comparative analysis, analytical analysis, spectral analysis and numerical analysis.

3.2.1 Comparative Analysis

Comparative analysis is used for comparing reconstructed images. Users are often obliged to attach numerical value when post analysing the reconstructed images obtained for comparison between different ERT set-ups or algorithm parameters.

Statistical figures-of-merits (FOM) are used, comparing the inverse solutions to the expected results or actual distribution. Cheney et. al. (1999) provided physical comparisons where the actual distribution used is carefully controlled and characterized. Although comparative analysis is easily applicable, the results provided can be highly subjective as they are often based on visual inspection with little scientific justification. Statistical errors may lead to conflicting conclusions depending on the chosen statistical FOM used. As there are no definitive FOM used within the tomographic community, this often leads to debatable conclusions.

Comparative studies can be useful when choosing or optimizing algorithms, however the need to have a controlled target distribution is restrictive. The results may also be skewed due to certain reconstruction algorithm favouring specific test distributions. Some algorithms perform better with soft-boundary distributions (gradual change between regions of different conductivity) while others favour abrupt changes. For completeness, it is necessary to conduct a comprehensive study, exploring a wide range of conditions and possibilities. This becomes difficult and time-consuming. Another disadvantage of comparative studies is that results can be influenced by the mesh that is used in the finite element model. Importantly, no actual information regarding the reconstruction properties (i.e. resolution, accuracy, stability and sensitivity) can be extracted from the results of a comparative study as the statistical FOMs are relative to a specific test distribution.

3.2.2 Analytical Analysis

Analytical techniques involve solving for the inverse problem without requirement for discretization. In principle, analytical studies are very accurate. However, the formulations are complex and simplifications through various assumptions are required (for example, circular boundaries, two-dimensional geometry). The assumptions, in turn, limit the flexibility and applicability of the studies. There is no published work for analytical techniques for 3D geometries. The highly detailed modelling that is required for utilizing unconventional electrode arrangements means that analytical analysis is intractable.

3.2.3 Spectral analysis

Spectral analysis requires the conversion of a numerical formulation from spatial to spectral domain prior to analysis and is particularly useful for determining information regarding stability. In ERT, the spectral form is the transformation of the tomographic operator, otherwise known as the sensitivity matrix, as well as the regularization matrix, into a diagonalized form. The image is separated into multiple components with varying levels of detail or spatial frequency.

Spectral methods include some novel and complex mathematical techniques in addition to well-defined and well-practised numerical techniques such as the Singular Value Decomposition (SVD) method, described in Section 2.3.3. Extracting spatial parameters such as resolution and accuracy, from the spectral information is mathematically challenging and requires a good command of how a reconstruction algorithm reconstitutes the spectral components when forming the image. As each spectral component within the image is affected by the system noise on various degrees, each of these separate components allows the impact of the system noise to influence the image or content to be assessed. Spectral analysis using SVD is often used to compare system noise and stability of measurements.

3.2.4 Numerical Analysis

Numerical analysis involves computing for the inverse solution using a discretized model before extracting the relevant information. Most reconstruction algorithms use a numerical formulation from which the main reconstruction properties are derived. One of the advantages of using numerical methods is that it is highly flexible and provides robust results. However, the veracity of the results is debatable as it depends on the discretization level of the model. For example, the FEM assumes that the field gradient is constant within each element when calculating the electric field. The assumption is especially true for a very dense mesh. Therefore, the best results can be obtained by choosing the highest mesh density, which is limited by available computing resources.

It has been shown that the accuracy of numerical field solvers can approach that of analytical solvers provided that a high mesh density is employed. Alternatively adaptive meshing can be employed (Woo et. al. 1994; Molinari et. al. 2001). The relative simplicity of numerical methods in comparison with analytical method when modelling complex 3D geometries provides a more favourable platform for exploring various parameters such as the effect of electrode arrangements and geometries, and measurement strategies.

3.3 Spectral Analysis using Singular Value Decomposition

SVD and its derivates are powerful analysis tools when studying ill-conditioned problems. SVD is sensitivity to measurement strategy, reconstruction algorithm and algorithm settings. Importantly, in terms of reconstruction parameters, SVD can provide information on system noise and stability without requiring any knowledge of the target application or material distribution.

An important application of SVD is to analyse the quality and recoverability of the content of a particular measurement set (Hansen 1998). Each individual singular value, together with the corresponding singular vector, is a partial solution to the discretized problem. Each partial solution contains a value for the unknowns although the value can be zero. The summation of all the partial components provide a complete solution and

the singular value can be seen as a control on the influence each component has on the final solution. All measurements that contribute to a solution must be unique and the number of singular vectors that contributes to the solution cannot exceed the number of unique measurements that define the problem. If a singular value is zero, this implies that the corresponding singular vector does not contribute to the final solution, as the associated measurement is likely to be redundant, which also indicates that the system is rank deficient. Rank deficiency in ERT indicates that measurement strategy is not optimized.

All measurements that contribute to a solution must be unique. Figure 3.2 shows a typical example of a set of singular values calculated by applying the adjacent strategy to a single plane of 16 electrodes model. The figure shows that after the 104th singular value, the rest of the singular values have magnitudes which are effectively zero to machine precision. This shows that although the strategy is capable of producing 208 measurements, only 104 measurements are unique. This also shows that the number of singular vectors which can be used to compute a solution cannot exceed the number of unique measurements to solve a problem.

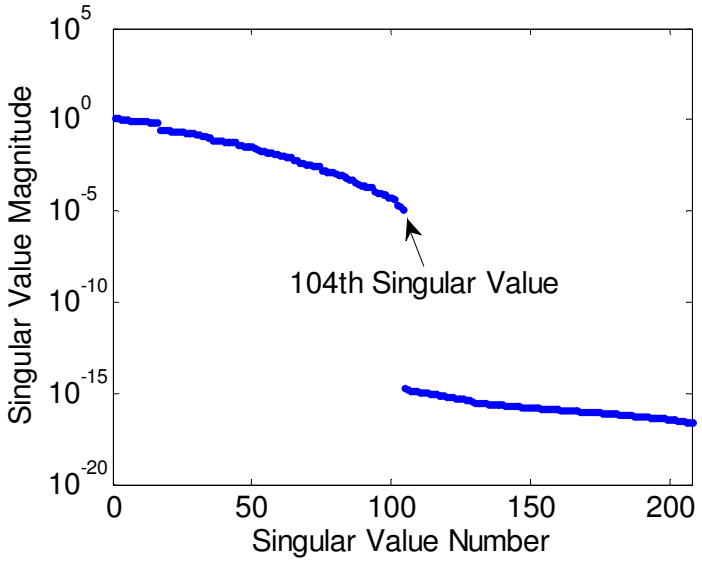

Figure 3.2 Logarithmic plot of singular values as ordered in ∑ for the adjacent without reciprocity (208 measurements) strategy using a single plane of 16 electrodes model

The Discrete Picard Condition (DPC) is used as an indicator of the stability of a solution. To ensure that a solution converges, unstable singular components should be excluded. The required filtration level depends predominantly on the measurement

precision as associated perturbations (noise in measurements, for example) are amplified for low values of the singular values λ.

The DPC (Hansen, 1998; Wu, 2003) is a requirement for stability and is satisfied if the absolute Fourier coefficients (FCs), $|u_i^T b|$ decay faster to zero, on average, than the corresponding singular values (SVs). If the singular value decay to zero faster than the Fourier coefficients, then the ratio $\frac{(u_i^T b)}{\lambda_i}$ becomes large and will dominate the solution. This definition can be misleading in some cases. A more robust numerical definition based on a moving geometrical mean is suggested in place of a regular averaging technique (Hansen, 1998):

$$DPC_i = \lambda_i^{-1}\left(\prod_{i-q}^{i+q}\left|u_i^T b\right|\right)^{\frac{1}{(2q+1)}},\ i = 1+q,\ldots,M-q \tag{3.1}$$

where M is the number of measurements or number of voxels, depending on which is larger, and q is a small integer which is selected to ensure that there is only a single crossing-point through unity. If $DPC_i<1$, the component i is deemed stable, satisfying the Picard condition.

The DPC is an essential tool when evaluating the noise level on measurements and influence due to modelling errors, providing insight to the necessary level of regularization required when choosing suitable regularization or smoothing parameters. An example is shown in Figure 3.3. q is chosen to be 2 for the DPC analysis shown in Figure 3.3(b), which is obtained by applying Eq. (3.1). Figure 3.3(a) is obtained by applying the adjacent with reciprocity strategy for a single plane of 16 electrodes model. Artificial noise is imposed onto the simulated voltages and is indicated using the Signal-to-Noise Ratio (SNR) in decibels. In practice, measurements contain noise. If a singular component relies on information from noisy measurements, that information may be unstable and unrecoverable. Therefore, in reality, it may not be possible to utilize or recover all independent information regarding a solution.

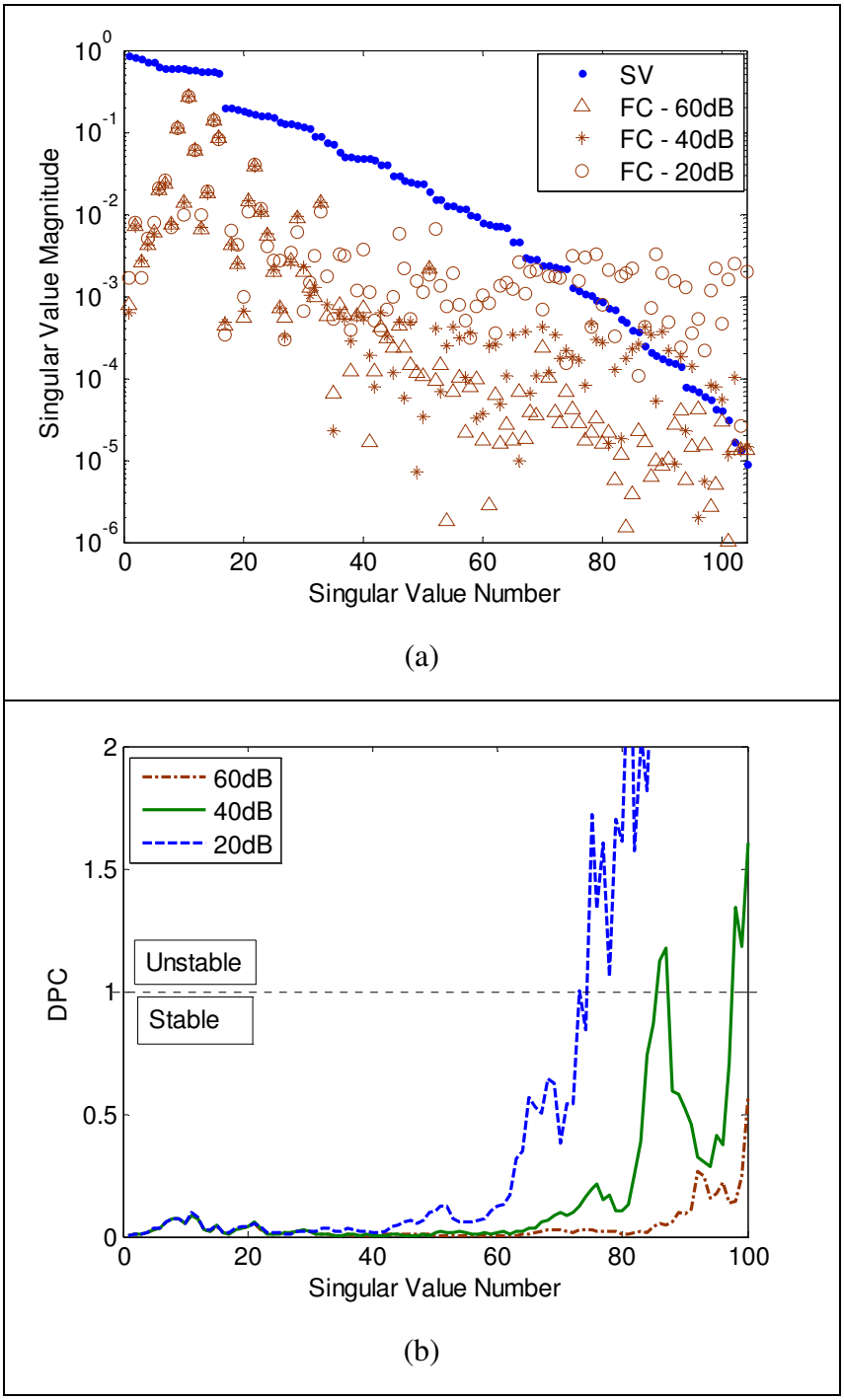

Figure 3.3: (a) SVD plot comparing Fourier Coefficients for varying levels of measurement noise, and (b) the corresponding DPC analysis for a single plane of 16 electrodes model using the adjacent with reciprocity strategy, using measurements with various SNRs

Figure 3.3 shows how SVD plots and DPC can be used to evaluate the stability for measurements with different noise levels. The SVD plot in Figure 3.3(a) compares the number of stable components with varying noise in the measurements. As one would expect, as measurement noise increases less singular values satisfy the DPC as suggested by the reduced gradient of the Fourier components in the graph. In other

words the problem becomes less stable as reflected in the plots in Figure 3.3(b). As the noise level increases the number of stable singular values decreases. As the noise level increases, the DPC value exceeds unity at a lower singular value number, meaning the number of stable singular value decreases.

3.4 Numerical Analysis using Sensitivity Visualization

Sensitivity is an indicator of the potential success of a reconstruction algorithm. Analysis of the sensitivity of a measurement system provides direct information on the potential success of any reconstruction algorithm. A detectable sensitivity is the minimum requirement for the solution for the element to be resolved. If a feature is undetectable, it is impossible to resolve or visualize it. For a discretized model, each voxel has a sensitivity value for any particular measurement. The sensitivity for each measurement can be visualized using standard visualization techniques such as slice plots. Sensitivity visualization provides a way to identify regions with detectable and undetectable sensitivities. However, it is more efficient and beneficial to judge the collective performance of a particular measurement strategy. With the information obtained, users can optimize electrode placements or measurement strategies, equipped with the knowledge of which measurements offer better coverage of detectable sensitivity across the image space.

In ERT, the Jacobian (sensitivity) matrix is the forward operator which relates the conductivity distribution to a set of measurements. Visualizing the properties of the Jacobian matrix requires a single value which represents each voxel. One approach is to sum the columns of the Jacobian matrix. This approach perhaps provides the most complete information regarding the overall sensitivity distribution. However, some of the measurements in a particular strategy, corresponding to the rows in the Jacobian matrix, may be redundant, hence the measurements are not contributing to the reconstructed image. This provides a misrepresentation of the capability of the measurement strategy.

A different approach is to visualize the maximum sensitivity distribution. A conductivity change, which induces a relatively small change in the measured voltages

is susceptible to measurement noise and becomes unrecoverable during reconstruction. A regularized reconstruction algorithm selects the information contained in the measurement data set depending on the associated sensitivities and the regularization level applied, based on the user's knowledge of the noise level. Assuming the reconstruction algorithm will only retain image components that are supported by measurements with high sensitivities, a good indicator of the reconstructability of the dataset is given by the maximum sensitivities of each voxel of the discretized model. An absolute maximum taken as a contrast can induce either a positive or negative change in a dataset.

Sensitivity values are dependent on several factors, namely reference conductivity, level of current injection and the voxel volumes. A typical cylindrical ERT mesh structure tends to have smaller voxels on the boundaries in comparison with the centre, due to the finer geometric details of electrodes, for example. Therefore, when visualizing the maximum sensitivity distribution directly on a mesh structure, central voxels appear to have similar sensitivities as the boundary voxels, due to the relative volumes. Mesh dependency can be reduced by normalizing each voxel's maximum sensitivity value to its volume.

3.5 Numerical Analysis using Resolution Matrix

Resolution matrix is a diagnostic tool which can be used to extract information about the correlation between voxels in a discretized model. Although resolution matrix has been used in other imaging modalities and applications such as geophysics, little work has been done for ERT applications for industrial process. Murphy (2008) adapted the technique for this purpose. A comprehensive review and derivatives of the resolution matrix method can be found in Menke (1989). The technique is briefly described in this section for completeness.

As described in earlier sections, due to the ill-conditioned nature of ERT, the Jacobian matrix is not invertible or squared. This leads to difficulties when determining the distribution of conductivities from the voltage measurements. A generalized inverse of

the Jacobian matrix A^{-g} is required to provide an estimate of conductivities x^{est}. The generalized inverse is not a full inverse, but an estimate. Therefore, the accuracy with which the generalized inverse represents the true inverse provides an indication of the exactness of the estimated solution. The estimated model can be obtained through:

$$Ax^{est} = b \tag{3.2}$$

$$x^{est} = A^{-g}b \tag{3.3}$$

$$x^{est} = A^{-g}[Ax^{exact}] \cong Rx^{exact} \tag{3.4}$$

where R is termed the model resolution matrix (Menke 1989). In an ideal case, R is an identical matrix, such that $x^{est} = x^{exact}$. Any deviation of R from the identity matrix defines the degree of inaccuracy that is present in each component of the solution.

Each row of the resolution matrix indicates the extent to which properties of the voxel can be independently resolved. Since R is not ideal, the i^{th} parameter is correlated with other parameters and cannot be independently resolved. Therefore, x^{est} is a weighted sum of a number of the other exact model parameters. The information obtained from the resolution matrix can be used to determine the spatial resolution in the image, which is influenced by the Jacobian (sensitivity) matrix and the choice of inverse algorithm. This information reflects on the electrode arrangement and measurement strategy, and is not directly dependent on any particular conductivity distribution.

The columns of the resolution matrix are directly proportional to the reconstructed image of a point contrast of a voxel, termed as the point-spread-function (psf). The psf described the spread of a point contrast throughout the image. Similar information can be obtained by reconstructing simulated data. However, a single resolution matrix calculation provides the psf of all locations within the image space, whereas multiple reconstructions of various distributions are required. Murphy and York (2006) showed that a point contrast may not be visible (cannot be reconstructed) in some cases, depending on the size and location of the contrast. As a result, this may lead to error in analysis. The visibility of a contrast is dependent on both its magnitude and dimensions. It is unclear which property must be increased to provide a reliable reconstructed image

for further analysis. Analysis using resolution matrix, on the other hand, is independent of contrast magnitude and is therefore more robust and efficient.

A measure of spatial resolution can be obtained using the Full-Width Half-Maximum (FWHM) technique, similar to that described in Wheeler et. al. (2002), with the exception that the psfs are not determined from a reconstruction. This measure is analogous to determining the size of the smallest object or the minimum distance between two point sources that an optical lense can resolve in optical imaging by applying Rayleigh criterion is applied (Vigoureux and Courjon 1992).

Since a psf represents the reconstruction of the smallest visible contrast, the resultant spread of the contrast is the minimum feature size that can be reconstructed. FWHM is a measure of the distance between two locations in an image that share a solution value that is half the peak value. Referring to Figure 3.4(a), the peak is measured from the highest psf value to zero, ignoring the negative overshoots which is a common characteristic of ERT inverse solutions. The reconstructed conductivity contrast is spread in 3D and is not necessarily symmetrical (a distorted sphere). Therefore, the FWHM is measured between the closest half-maximum and furthest half-maximum from the peak location.

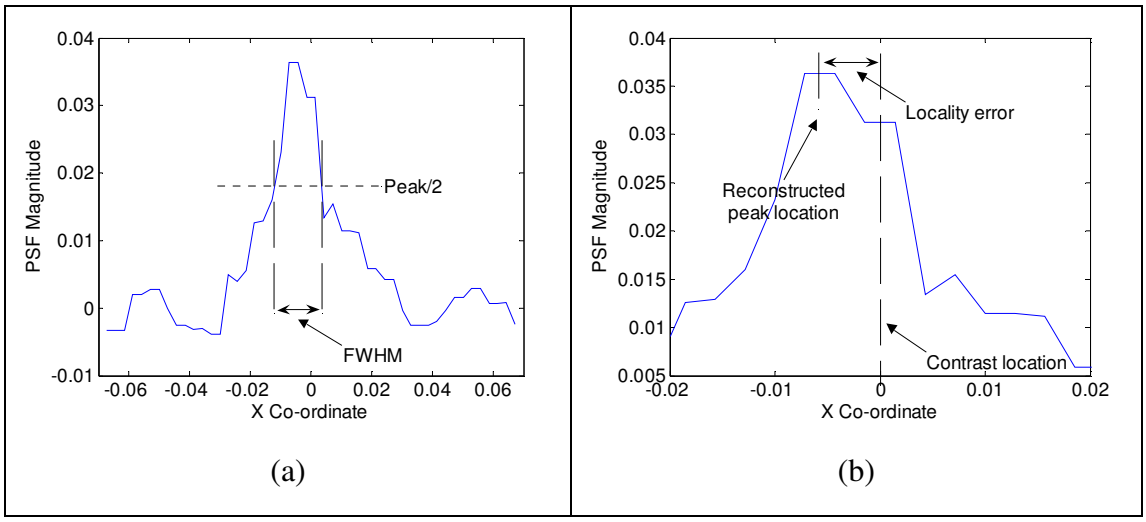

Figure 3.4: Line plots along the x-axis of a psf demonstrating the approach for measuring (a) FWHM and (b) locality error (Murphy 2008)

Another property of psfs is the location of the peak that does not correspond to location of the point contrast. The difference between the peak location and the location of the

contrast is known as the locality error (Figure 3.4(b)). Low locality error implies a capability of accurately locating features in an ERT application.

Since both the FWHM and locality error are dependent on the mesh structure, the size and positioning of elements must be taken into consideration when analysing spatial resolution between different meshes. If the reconstruction of a contrast results in a peak in a neighbouring element, the locality error will depend on the size of the elements. From a reconstruction perspective, the effect of the mesh structure on reconstruction properties is a tangible problem. Therefore, any analysis of these properties should include it. The fact that spatial resolution may degrade if a coarser mesh structure is used is an important observation.

Spatial resolution analysis can be applied when analysing different measurement strategies, electrode arrangements, and reconstruction algorithm. The relative simplicity of calculating resolution matrices allows a rapid method of evaluating spatial resolution. Resolution matrix can be used to demonstrate the capabilities of a reconstruction algorithm. Spatial resolution can be visualized by plotting the FWHMs of fixed intervals along a fixed axis to demonstrate the variation of the spatial resolution at different locations. Through spatial resolution analysis, regions of poor spatial resolution can be identified, which is useful when evaluating unconventional electrode arrangements or strategies.

3.6 Summary for Understanding Image Properties

This chapter provides an overview of reconstructed image properties to provide an appreciation to the work described. It is important to have a good understanding on influencing factors which dictates changes in reconstruction properties of interest, including stability of measurements, sensitivity and spatial resolution. Through this understanding, better-informed decisions can be made in effort to improve the quality of reconstructed images.

Choices of inverse solving algorithms are often ambiguous, therefore producing debatable results. It is a common practice within the tomography community to evaluate the performance of an ERT system by doing a comparative study based on an array of reconstructed images. Analysis techniques to evaluate selected image properties, namely stability of measurements, sensitivity and spatial resolution, are also discussed as an introduction to the analysis and results described in later chapters. Stability of measurements provides information on noise level of the ERT system, and the number of unique and usable measurements which can be used for inverse solving. Sensitivity level indicates the detectability of changes induced by change in conductivity in measurements. Spatial resolution analysis produces results which indicate the ability to visualize the changes in reconstructed images.

The analysis techniques described in this chapter aims to produce analysis results which are unbiased towards particular conductivity distribution or inverse solving algorithm. Importantly, these techniques are independent of having prior knowledge of any test distributions and choices of inverse solving algorithms, and numerical justification can be obtained to further understand reconstruction properties. Each technique provides information on one aspect of image properties. Therefore, it is essential to take into consideration the relative merits of the different aspects of the ERT systems evaluated before deriving conclusions on the performances of these systems.

CHAPTER 4
IMPROVING SPATIAL RESOLUTION THROUGH INCREASING INFORMATION

This chapter aims to provide a preliminary look into improving spatial resolution through increasing information using a conventional ERT set-up. Two commonly employed methods are considered. The first is through increasing the number of electrodes and the second through extending conventional measurement strategies. These methods are considered as they are most relevant to the work presented in this thesis, which is to improve spatial resolution through utilising ad hoc sensors.

This chapter is divided into three sections. Section 4.1 provides an overview of the different methods to improve spatial resolution for reconstructed images. Subsequent sections focus on the methods relevant to this thesis. Section 4.2 focuses on increasing the number of measurements through varying or expanding conventional measurement strategies. This section is further divided into two subsections. The first subsection compares commonly used measurement strategies in industrial and medical applications, such as the adjacent and opposite strategies. The comparative study in this subsection considers a planar electrode arrangement and pseudo-3D measurement strategies when multiple electrode plane models are used. The second subsection considers full-3D measurement strategies. Section 4.3 explores the effect of using different number of electrodes in a single plane. For simplicity, a single planar arrangement is used for the comparative studies in this section. Different electrode

width is also taken into consideration (electrode height is kept constant) to explore the effect of electrode width on resolution, as well as other reconstructed image properties.

The effect of the increase of measurements in both subsections 4.2 and 4.3 is analysed and compared using analysis tools described in Chapter 3. Image properties, including stability of measurements and sensitivity are taken into consideration, such that a more informed conclusion can be made.

4.1 Improving Spatial Resolution

Reconstructed images produced using ERT are known to have poor spatial resolution, especially towards the centre of the vessel, away from the electrodes. This is largely due to the ill-posed nature of the ERT problem. Typically, the problem is stabilised through applying some form of regularisation, based on prior knowledge of the system. Although the nature of the problem cannot be altered, there are means to improve the stability.

In terms of modelling and inverse solving, several approaches can be taken. The first is through improving the accuracy of modelling. Woo et. al. (1994) showed that the quality of the mesh structure and the accuracy of modelling play an important role on the quality of reconstructed images. The accuracy of modelling determines how closely-matched the initial predictions of electrical properties are to those of the actual imaged space. This means a densely discretized model is likely to perform better with the image space broken into smaller elements, and the properties of the image space are better represented by the smaller-sized elements. However, this method has its limitations. One of the issues is computational limitation. It is also worth considering that when setting up a discretized model, it should consist of a sensible number of elements, such that there are sufficient to represent the discretized image space, but not too many to further complicate the problem for inverse solving. The number of elements also represents the number of unknowns which need to be solved. The ERT inverse problem is an under-determined case, which means the number of unknowns to be solved exceeds the number of data. If the model is discretized into fine elements, the solution of the problem suffers from the insufficiency of data, resulting in inaccurate solutions.

Another method is through better application of inverse algorithms. There are a lot of ambiguities when applying inverse algorithms as there is no 'one-fits-all' solution. There is also a lack of scientific methods when selecting appropriate parameters. Decisions made are often based on personal preferences and past experience. Consequently, the accuracy of the resulting reconstructed images is often questionable.

A more direct approach is by improving the quality of measurements. This can be achieved by increasing the accuracy and precision of measurements through the instrumentation and electrode system. Difference imaging (Vauhkonen et. al. 2001) is often used to reduce the effect of noise with the assumption that the noise level of the system varies little over a short period of time.

Another method is to obtain more information. With the development and transition from 2D to 3D tomography, more measurements can be obtained to better inform the inversion problem either through expanding the number of electrodes or through measurement strategies. Spatial resolution is closely related with the amount of data which can be used to inform the reconstruction process. Therefore emphasis has been placed on acquiring more data, which would potentially result in more recoverable and usable information used for image reconstruction. This method of improving spatial resolution forms the focus of this thesis which is based on utilising ad hoc sensors in an effort to improve spatial resolution through obtaining more information.

4.2 Obtaining More Information through Measurement Strategies

When devising a measurement strategy, several factors are taken into consideration. This includes measurement stability (including noise level, number of usable measurement), number of unique measurements, current injection pattern providing sufficient sensitivity (detectability) across the plane, overall spatial resolution and overall data acquisition time (temporal resolution).

This section compares the relative merits of typically used measurement strategies, with special interest in spatial resolution. Spatial resolution is strongly influenced by the

amount of information that can be used for inverse solving. Therefore, measurement stability analysis is also an important aspect of this comparative study.

Although a combination of all possible measurements can be taken for a four-terminal measurement protocol, it is established that some measurements are likely to be redundant and offer no unique information for inverse solving. This also comes at the expense of longer data acquisition time, compromising the temporal resolution. Depending on the requirement of the applications, strategies other than the adjacent strategy (discussed in Section 2.3.2) may be adopted. Strategies such as the opposite strategy, which is well-established to provide better sensitivity across the current injection plane Stephenson (2008), may be more appropriate for applications where measurement noise is relatively higher, as the current injection path penetrates the image space.

4.2.1 Measurement Strategies for Single Electrode Plane Arrangement

This subsection compares measurement strategies for a single planar electrode arrangement. Some well-established comparisons are included for completeness. A planar electrode arrangement refers to electrodes arranged around the periphery of the wall of the vessel at the same height. This electrode arrangement is commonly used in industrial process applications. A single plane of 16 electrodes model is used as shown in Figure 4.1. The electrodes are of equal size and equi-spaced on the circumference of the model. A homogeneous distribution of 0.01S/m, the approximate conductivity of tap water, is used. Measurements are simulated using the EIDORS toolkit (Polydorides and Lioneart, 2002). 60dB Gaussian noise, the approximate noise level of the LCT2 instrument (York et. al., 2005), is imposed on the measurements for more practical measurements.

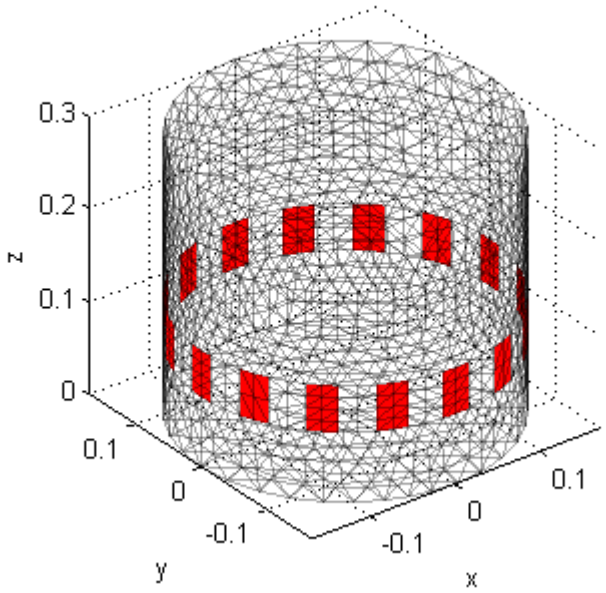

Figure 4.1 Discretized model of a 16 electrodes model arranged in a single plane. Electrodes are marked in red.

It is well-established that the full planar adjacent strategy (without reciprocity) produces *N(N-3)* measurements (208 measurements for single planar arrangement of 16 electrodes) with half of the measurements deemed redundant, therefore containing no unique measurements. Therefore, the reciprocity theorem can be applied to discard redundant measurements, whereby if two pairs of adjacent electrodes used for a particular measurement are interchangeable, the measurements are deemed redundant. It is, however, worth comparing the benefits of each strategy and the analysis is included for completeness.

Figure 4.2 shows the spectral analysis using SVD to compare the stability of the measurements simulated using the adjacent strategy with reciprocity (104 measurements) and adjacent without reciprocity (208 measurements). The non-unique measurements, with magnitudes effectively zero to machine precision, for the latter strategy are excluded from the plot for clarity. From Figure 3.2, it is shown that the magnitudes of the singular values are higher for the adjacent without reciprocity strategy. When analysing the stability of measurements, higher magnitudes of the singular components indicates that the measurements are more stable and therefore less susceptible to noise. Therefore, although half of the measurements acquired using the adjacent without reciprocity strategy are redundant, the usable measurements are shown

to be slightly more stable in comparison to those obtained using the adjacent with reciprocity strategy, although the difference is insignificant. This means the adjacent without reciprocity strategy is able to produce measurements with better SNR. The adjacent without reciprocity strategy can be seen as taking two frames of adjacent with reciprocity measurements. Therefore, the noise level for the adjacent without reciprocity measurements is reduced through averaging over twice as many measurements obtained using the adjacent with reciprocity measurement.

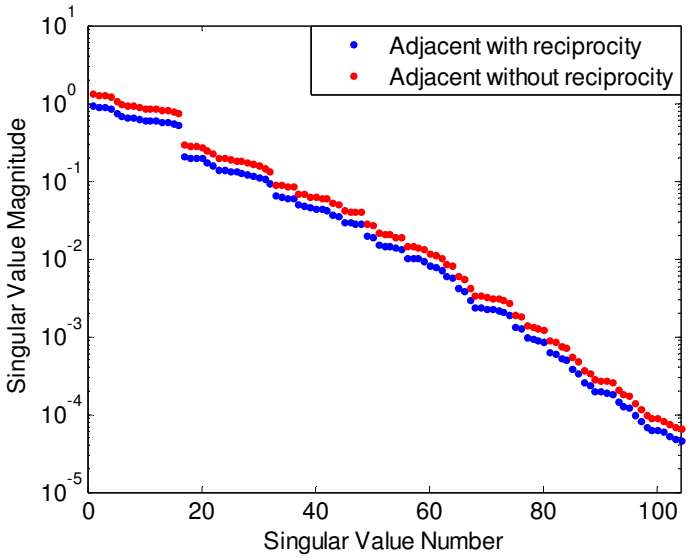

Figure 4.2 Spectral Analysis comparing Planar Adjacent Strategies

Sensitivity analysis is used to evaluate the detectability of any changes in the image space in the voltage difference measurements. The plot in Figure 4.3(a) shows the maximum sensitivity magnitude normalized to the volume of the voxels variation for a line on the electrode plane, for the adjacent with reciprocity (blue plot) and adjacent without reciprocity (red dots) strategies. It can be observed in the plots that for both cases, the sensitivities are the highest in the regions near the wall of the vessel. In both cases, the sensitivities decrease towards the central region of the vessel. The plot suggests that both strategies produce the same level of sensitivity, as the magnitudes calculated for the selected points for both strategies are the same. This is expected as the current injection protocol is the same and sensitivity is predominantly dependent on current injection patterns.

Spatial resolution analysis using resolution matrices in Figure 4.3(b) shows that both strategies produce the same spatial resolution across the plane for the adjacent with

reciprocity (blue plot) and adjacent without reciprocity (red dot) strategies, as the FWHM calculated for selected points along the horizontal axis on the electrode planes are shown to have the same values. Spatial resolution represents the visibility in reconstructed images, indicating that the changes in conductivity that were detected can be shown. The number of usable measurements is similar for both measurement sets. As a result, the resolution matrices are computed using a similar number of singular values.

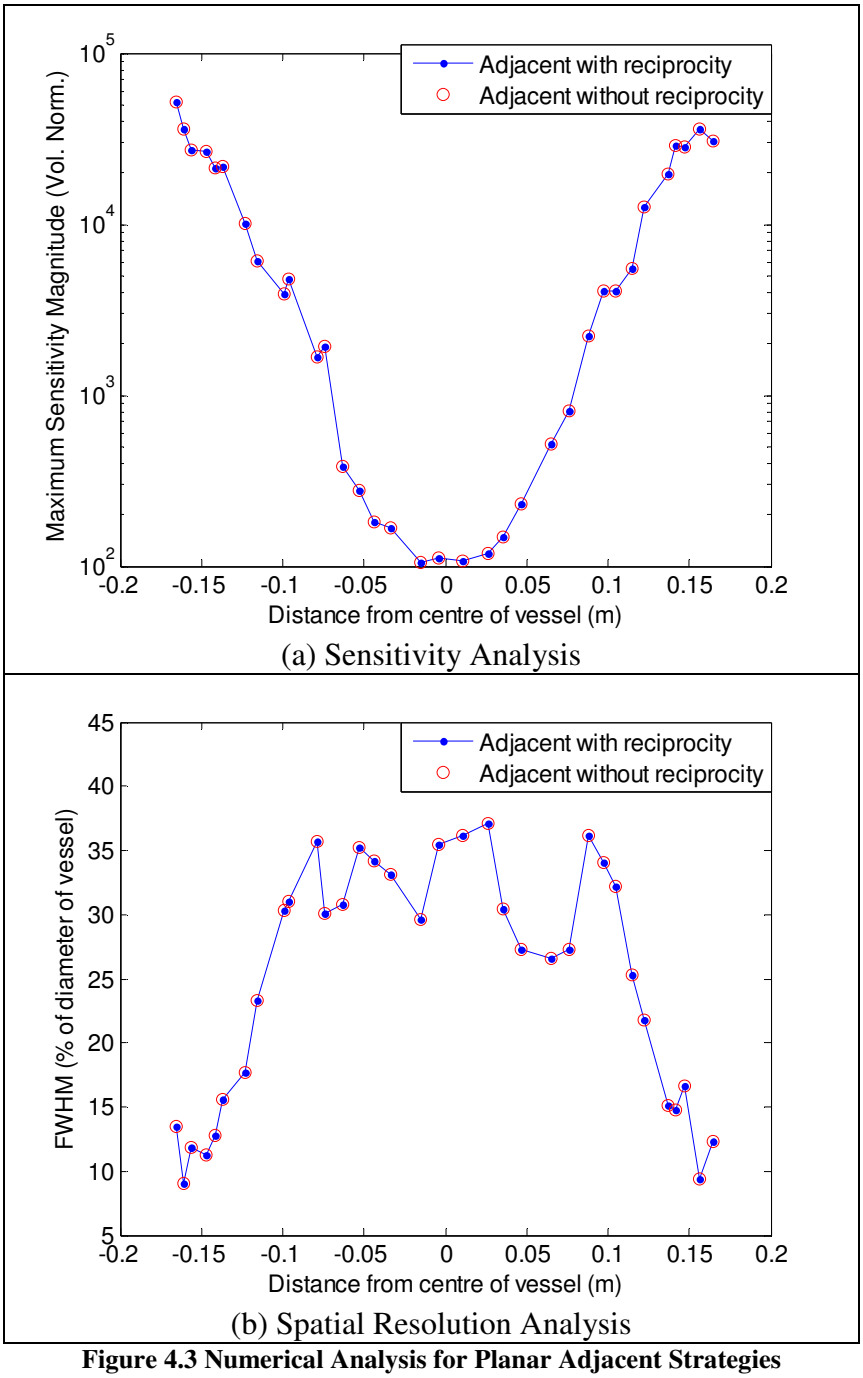

Figure 4.3 Numerical Analysis for Planar Adjacent Strategies

It is shown in Figure 4.3(b) that the regions near the wall of the vessel have better resolution (low FWHM) in comparison with regions in the centre of the vessel (higher FWHM). This is consistent with the sensitivity analysis which shows that the sensitivity is low in the centre region. This means the likelihood of detecting a change in conductivity is low, and therefore the possibility of reconstructing the change is low. In conclusion, the adjacent without reciprocity strategy does not provide advantage over the adjacent with reciprocity in terms of sensitivity and spatial resolution. This justifies reducing a full adjacent strategy to adjacent with reciprocity as the analysis shows that there are no benefits in acquiring the redundant information.

A full planar opposite strategy yields *N(N-4)* measurements (192 measurements for single planar arrangement of 16 electrodes). Typically, only half a cycle of the current injection protocol is carried out as the latter half only inverts the function of current source and current sink electrodes. This means the measurements taken are redundant and do not contain unique information. Therefore, the number of measurements acquired is reduced to *N(N-4)/2* (96 measurements for single planar arrangement of 16 electrodes). From spectral analysis, it is shown that even with the reduced measurement set (reciprocity principle applied), only 76 out of 96 measurements are unique. This indicates that the measurement strategy is not optimized, suggesting a disadvantage in comparison with the adjacent strategy. As shown above, redundant measurements do not provide any contribution to improving the sensitivity and spatial resolution.

Figure 4.4 shows the sensitivity analysis and spatial resolution analysis comparing the adjacent and opposite strategy. The opposite strategy is expected to produce higher sensitivity levels in comparison with the adjacent strategy in the centre of the region, as the current pattern penetrates across the image space. This is reflected in Figure 4.4(a).

The spatial resolution analysis in Figure 4.4(b) shows that the overall resolution is evenly matched for both strategies. Instinctively, this was not anticipated as the opposite strategy gives better sensitivity in comparison to the adjacent strategy. However, both the adjacent and opposite strategies result in a similar amount of usable information for image reconstruction, despite of the advantage in better detectability for the opposite strategy. As spatial resolution is largely influenced by the amount of usable content

which is available for image reconstruction it is, perhaps, unsurprising that the spatial resolutions for both strategies are evenly matched across the plane.

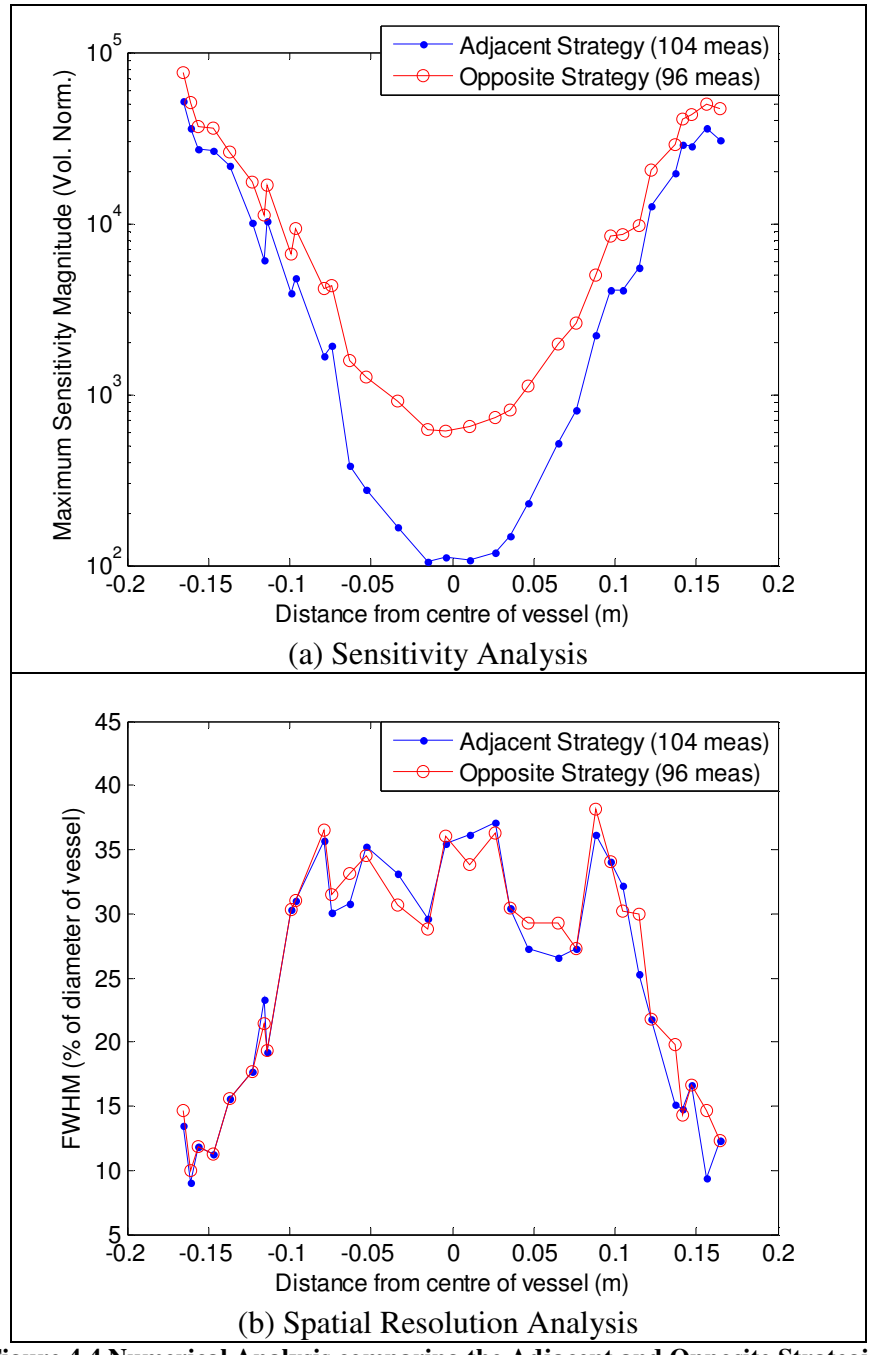

Figure 4.4 Numerical Analysis comparing the Adjacent and Opposite Strategies

As an alternative to the opposite strategy, a pseudo-opposite strategy was proposed in Shi et. al. (2006). The pseudo-opposite strategy produces *N(N-4)* measurements (192 measurements for a single planar arrangement of 16 electrodes), anticipating more unique information in comparison with the conventional opposite strategy. Spectral analysis shows that only 104 measurements out of 192 measurements are unique which,

similarly, indicates that the pseudo-opposite strategy is not optimized. Figure 4.5 compares the magnitude of the singular values for the adjacent strategy, the opposite strategy and the pseudo-opposite strategy, showing only the unique components (first 104 measurements for this electrode set-up). It can be seen that the magnitude of a majority of the singular values for the pseudo-opposite strategy are higher in comparison than those of the adjacent strategy, indicating that the singular components are more stable. The magnitude of singular values for the pseudo-opposite strategy is also slightly higher in comparison to those of the opposite strategy.

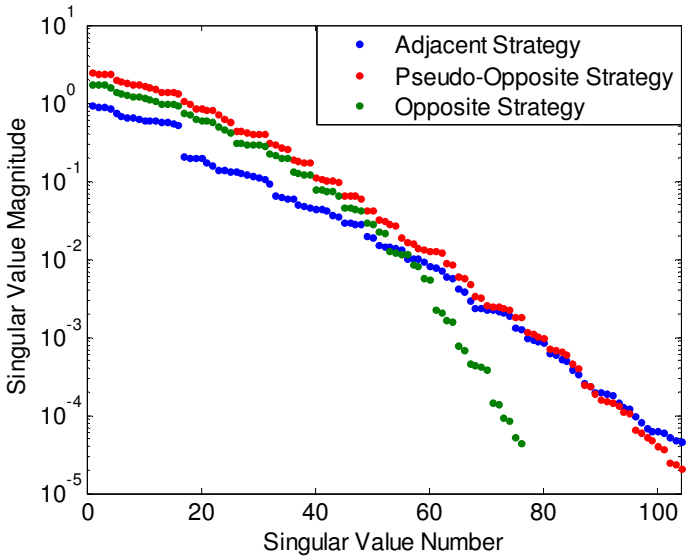

Figure 4.5 Spectral Analysis for the Adjacent, Opposite and Pseudo-Opposite strategies

Figure 4.6 compares the sensitivity level and spatial resolution between the adjacent, opposite and pseudo-opposite strategy. As shown in Figure 4.6(a), the sensitivity level for the opposite and pseudo-opposite strategies are similar, indicating that the pseudo-opposite current injection strategy provides similar current pattern as the opposite strategy and that the signal penetrating across the image space is similar in strength. In terms of spatial resolution (Figure 4.6(b)), the pseudo-opposite strategy does not provide an advantage over the adjacent or the opposite strategy. Similarly, as the number of unique and stable measurements which are available for image reconstruction is similar for all three strategies, the spatial resolution remains similar across the space.

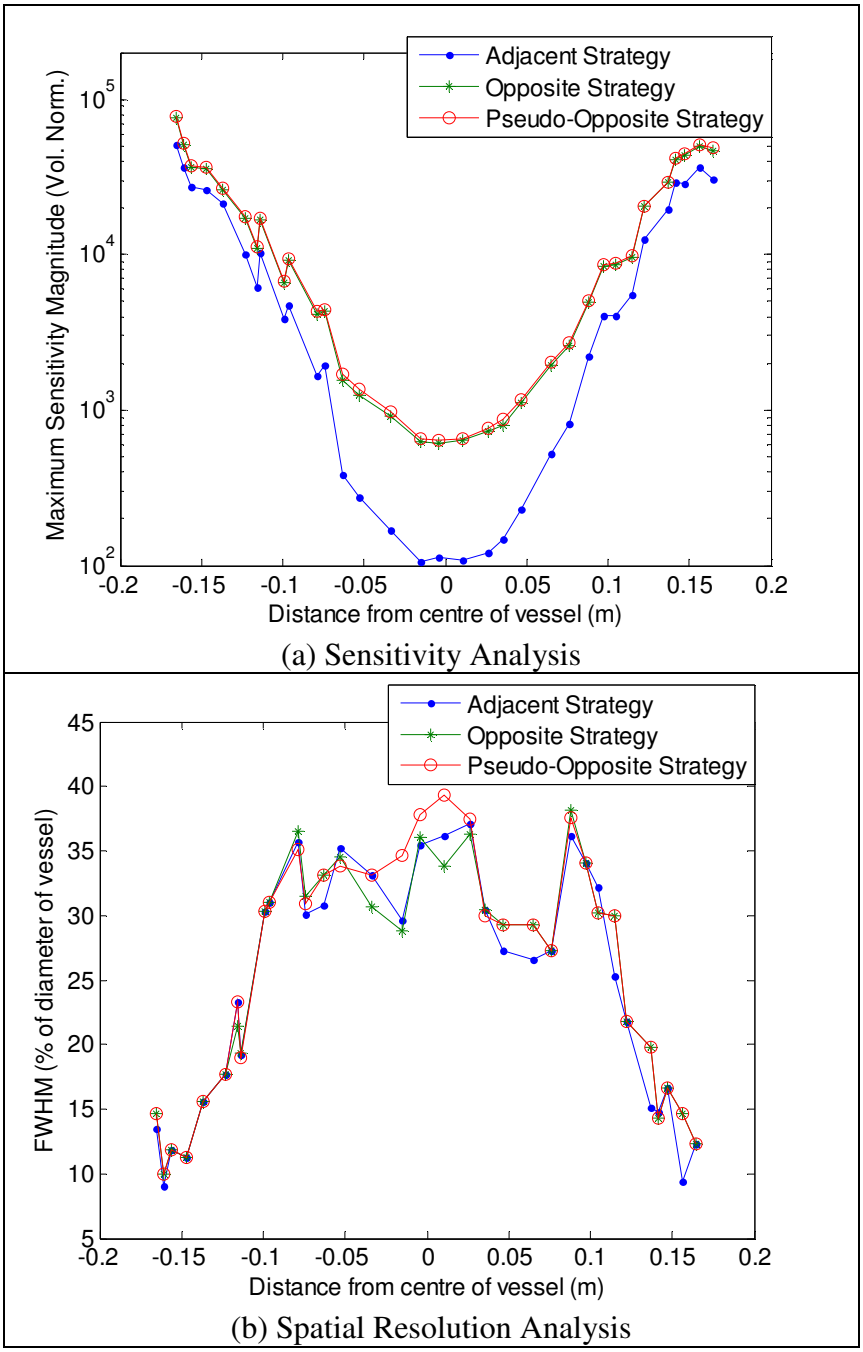

Figure 4.6 Numerical Analysis comparing the Adjacent, Opposite and Pseudo-Opposite Strategies

Although the sensitivity analysis gives the initial expectation that opposite strategy is capable of improving spatial resolution due to the superior detectability in the centre region of the image space, the spatial resolution analysis suggests otherwise. The lack of additional unique information that can be acquired means that the spatial resolution across the plane remains fairly similar to that using the adjacent strategy. This shows that a high level of detectability does not necessarily translate into a good level of visibility and the amount of information usable for image reconstruction plays a bigger role in improving spatial resolution of images.

The pseudo-opposite strategy provides an alternative to the conventional opposite strategy through a small modification, resulting in more measurements without compromising the sensitivity levels and spatial resolution. Analysis shows that the number of unique measurements acquired is the same as that of the adjacent considering reciprocity strategy although the pseudo-opposite strategy is capable of acquiring more measurements per frame of measurement. This begs the question whether there is a limit to the number of unique measurements obtainable for a planar electrode arrangement. Murphy (2008) shows that the combination of the adjacent and opposite strategy only yields 104 unique measurements although the adjacent strategy considering reciprocity produces 104 unique measurements on its own, and the opposite strategy gives 76 unique measurements. It was concluded that for a single planar electrode arrangement, the number of unique measurements obtainable is $N(N-3)/2$. This is a limitation which should be noted when considering extending a planar measurement strategy to improve spatial resolution.

In conclusion, the opposite strategies offer better immunity to noise in comparison with the adjacent strategy, as shown in the stability analysis. The sensitivity analysis also shows that the opposite strategy gives higher detectability than the adjacent strategy. However, the number of unique measurements is reduced using the opposite strategy. This could be resolved using the pseudo-opposite strategy to regain the same amount unique measurements. For applications with higher noise level, the pseudo-opposite strategy is preferred over the adjacent strategy.

4.2.2 Measurement Strategies for Two Electrode Planes Arrangement

Typically, measurements are taken on the same plane as the current injecting electrodes are located, even for a model which consists of multiple planes of electrodes. In other words, each plane of electrodes is treated independently when developing measurement strategies. This practice does not take advantage of utilizing available electrodes on other planes. As shown earlier in Section 4.2.1, the number of unique measurements obtainable saturates after a point when considering planar measurement strategies, resulting in saturation in sensitivity and spatial resolution.

Little work has been done to investigate multi-planar strategies. Metherall et. al. (1996) report that resolution between planes improves when current injection and voltage measurements are taken between horizontally and vertically adjacent electrodes. Heikkinen et. al. (2005) described using the cross-planar current injection protocol for 3D tomography. Stephenson et. al. (2005) concluded that visible improvements on reconstructed images can be seen for multi-planar current injection protocols, but negligible differences were observed for strategies where voltage measurements are acquired on all planes of electrodes. This subsection investigates the possibility of acquiring more unique information using multi-planar electrode arrangement.

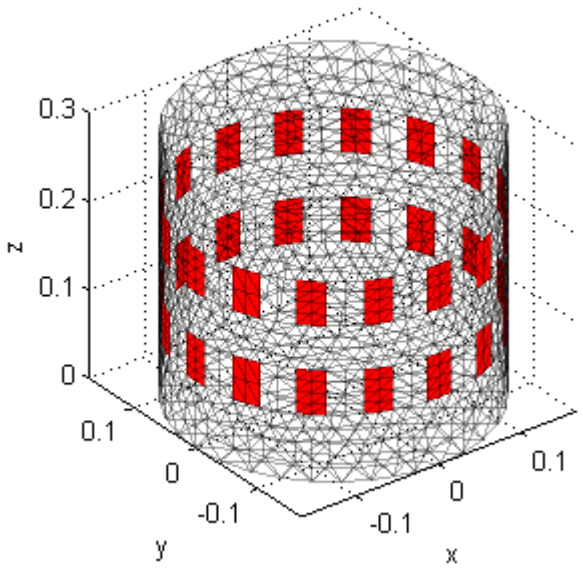

Figure 4.7 Discretized model of a 32 electrodes model arranged in two planes. Electrodes are marked in red.

The first case considered is expanding the adjacent strategy. Typically, the adjacent planar strategy for a 32-electrodes model, arranged evenly in two planes, as shown in Figure 4.7, yields 208 measurements (with reciprocity) when the electrode planes are treated independently (planar arrangement). The model used is 34cm in diameter and 30cm in height. The centre of the bottom electrode plane is located 10cm from the base of the vessel, and the centres of each electrode plane are 10cm apart. The electrodes are 5cm by 3cm and are equispaced on the wall of the vessel. A summary of the horizontal strategies is given in Table 4.1, including the number of measurements. Names of strategies are selected to be informative.

Table 4.1 Summary of Multi-Planar Adjacent Strategies

Strategy	Current Injection	Voltage Measurement	Number of Measurements
HaHa	Horizontally adjacent	Horizontally Adjacent	928
HaVa		Vertically Adjacent	448
HaHVa		All Adjacent	1376
VaHa	Vertically adjacent	Horizontally Adjacent	448
VaVa		Vertically Adjacent	240
VaHVa		All Adjacent	688
HVaHa	All adjacent	Horizontally Adjacent	1376
HVaVa		Vertically Adjacent	688
HVaHVa		All Adjacent	2064

Table 4.2 provides a summary of the number of unique measurements acquirable and the number of stable measurements obtained from spectral analysis as described in Section 3.3, with examples of obtaining the number of unique measurements and number of stable measurements illustrated in Figures 3.2 and 3.3 respectively. The number of stable measurements is computed for simulated voltage measurements with 60dB Gaussian noise, using the DPC analysis (Hansen, 1998). The spectral analysis shows that 3D measurements taken between planes provide additional unique measurements. However, the low percentage of unique measurements indicates that the measurement strategies are not optimized. Comparing the HaHVA and HVaHVa strategies, only one additional unique measurement is obtainable, while twice as many measurements are acquired for the latter case. This indicates that careful consideration should be taken when planning for a measurement strategy, as more acquired measurements do not necessarily mean more unique measurements.

Table 4.2 Summary of Uniqueness and Stability of Measurements for Various Multi-Planar Adjacent Strategies

Strategy	Total Number of Measurements	Number of Unique Measurements	Number of Stable Measurements
HaHa	928	433 (47%)	398 (43%)
HaVa	448	343 (77%)	313 (70%)
HaHVa	1376	463 (34%)	437 (32%)
VaHa	448	343 (77%)	315 (70%)
VaVa	240	120 (50%)	107 (45%)
VaHVa	688	344 (50%)	298 (43%)
HVaHa	1376	463 (34%)	444 (32%)
HVaVa	688	344 (50%)	305 (44%)
HVaHVa	2064	464 (22%)	435 (21%)

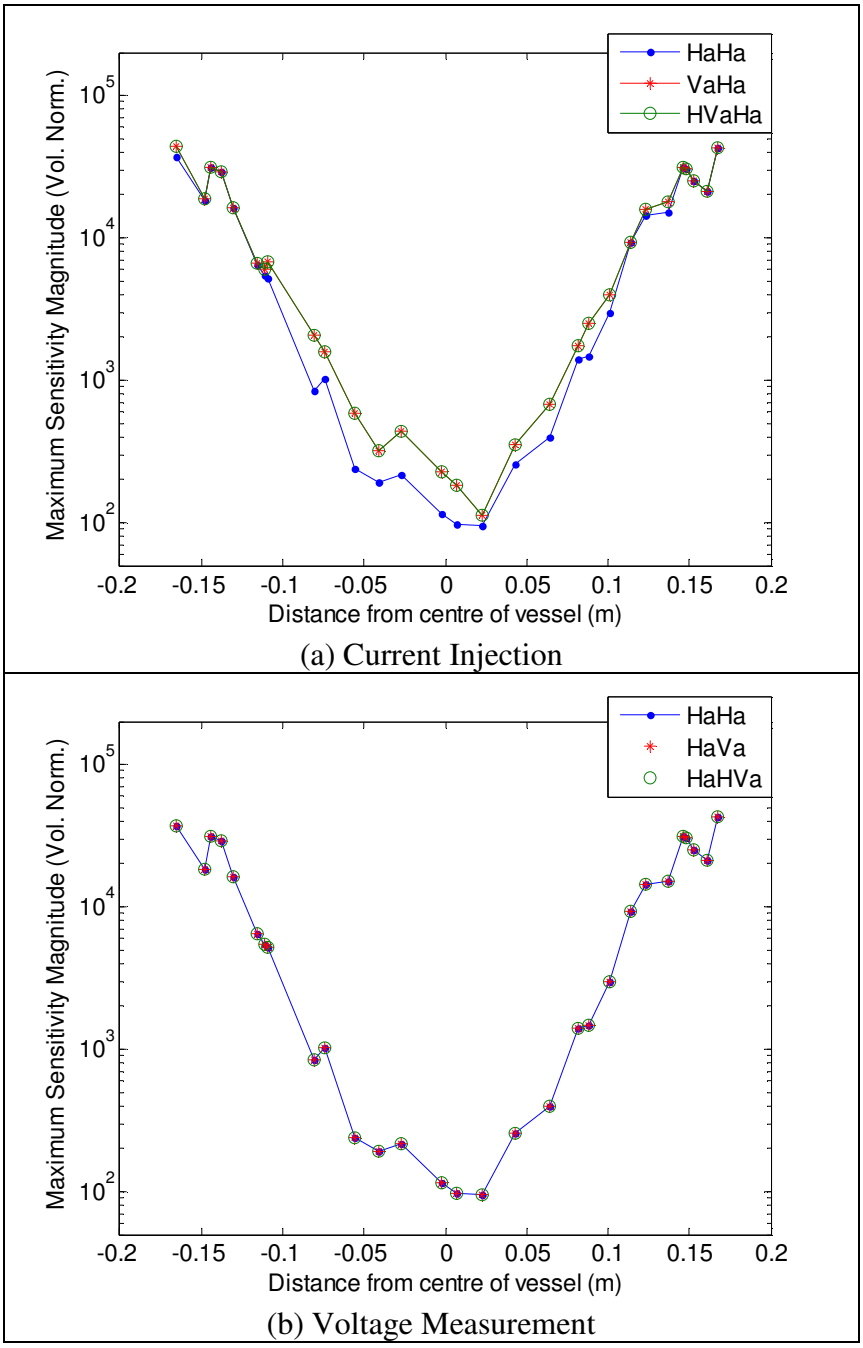

Figure 4.8 Sensitivity Analysis for Multi-Planar Adjacent Strategies at Electrode Plane (height = 0.10m from base of vessel)

Figure 4.8 compares the sensitivity levels for multi-planar strategies. Figure 4.8(a) compares the horizontal adjacent, vertical adjacent and all adjacent current injection strategies. The sensitivity level is improved slightly in the centre region when vertical pairs of electrodes are used (VaHa and HVaHa strategies). Figure 4.8(b) compares the horizontal adjacent, vertical adjacent and all adjacent voltage measurement strategies. In contrast to Figure 4.8(a), the multi-planar voltage measurement strategies do not improve the sensitivity levels. This is expected as the current injection pattern remains

the same. This also indicates that the detectability of changes is predominantly influenced by the current pattern and not the voltage measurement protocol.

Figure 4.8 shows the sensitivity in the electrode plane for the adjacent strategies. An interesting comparison is to observe the changes in sensitivity levels on an off-electrode plane. Figure 4.9 shows the variation of sensitivities in a plane located equidistant between the two centres of electrodes planes (at 0.15m from the base of the vessel for the model shown in Figure 4.7) for the HaHa, VaHa and HVaHa strategies (comparing current injection protocols). The plots in Figure 4.9 show that there are no significant differences in the sensitivities. Comparing the magnitudes of the sensitivity for on- and off-electrode planes, there is also no significance decrease in sensitivity for the off-electrode plane in comparison with the sensitivities located directly along the electrode plane (refer to Figure 4.8(a)). This is unexpected because current injection in the electrode plane is stronger than for an off-electrode plane. Therefore, the sensitivity levels are expected to be different.

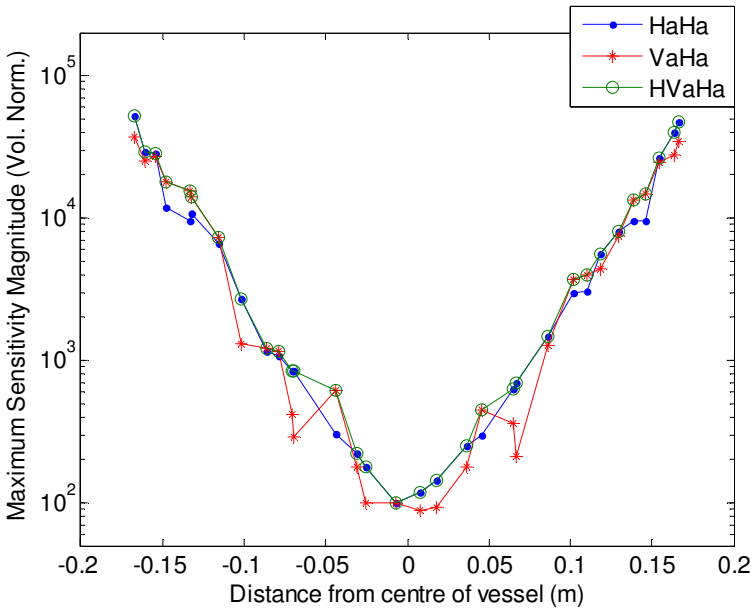

Figure 4.9 Sensitivity Analysis for Multi-Planar Adjacent Strategy at an Off-Electrode Plane (height = 0.15m from base of vessel)

Figure 4.10 compares the spatial resolution across the electrode plane for the adjacent strategies. Figure 4.10(a) compares the spatial resolution for various adjacent current injection strategies. The vertical adjacent (VaHa) strategy resulted in the worst spatial resolution in general, while the all adjacent (HVaHa) generally produced better spatial resolution, in spite of the irregularity. The VaHa strategy produces the least amount of

usable data for image reconstruction in comparison with HaHa and HVaHa. This explains why the VaHa strategy produces the worst spatial resolution across the plane in comparison with the other two strategies. Figure 4.10(b) compares the spatial resolution for various adjacent voltage measurement strategies. The plots indicate that the HaHVa strategy resulted in the best spatial resolution in general. The improvement can be attributed to the number of extra unique measurements which can be used for image reconstruction.

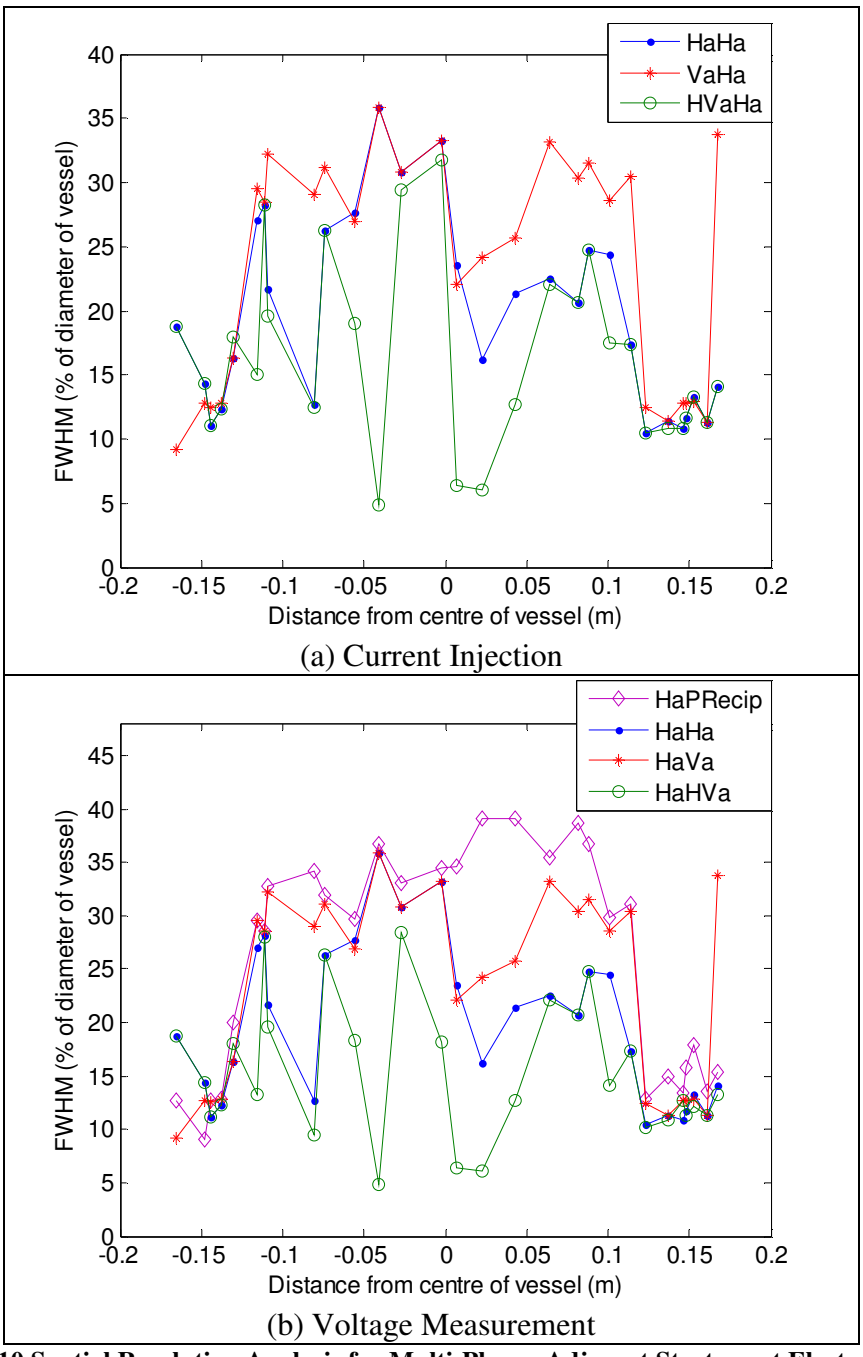

Figure 4.10 Spatial Resolution Analysis for Multi-Planar Adjacent Strategy at Electrode Plane (height = 0.10m from base of vessel)

'HaPRecip' in Figure 4.10(b), represents adjacent considering reciprocity with the electrode planes treated independently (208 measurements for 2 planes of 16 electrodes per plane arrangement, all measurements are unique). The planar strategy is included in this comparison study to highlight the improvement in spatial resolution when using multi-planar strategies. Comparing the spatial resolution for HaPRecip and HaHa strategies, a noticeable improvement is suggested in the centre region of the vessel.

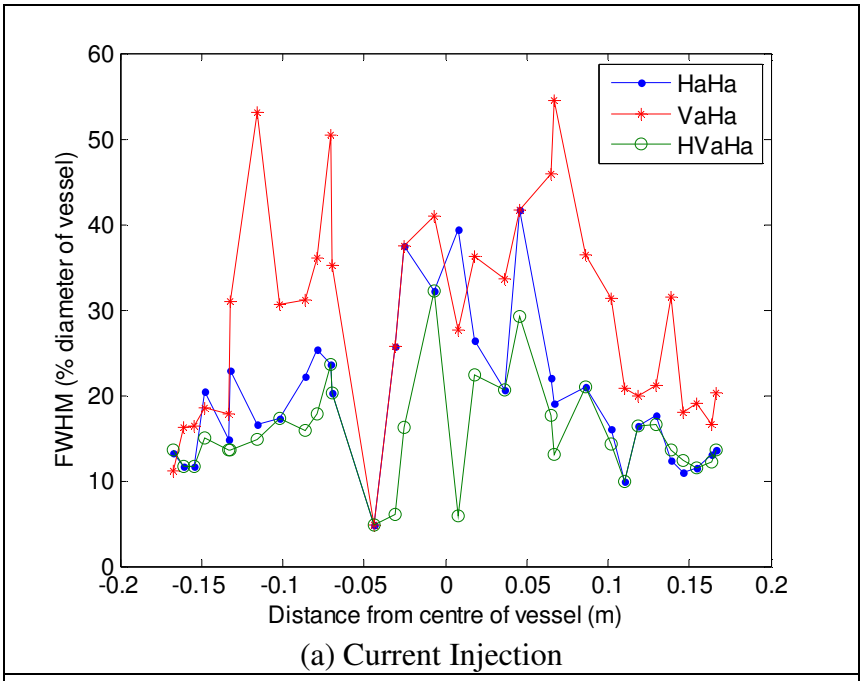

Figure 4.11 Spatial Resolution Analysis for Multi-Planar Adjacent Strategy at an Off-Electrode Plane (height = 0.15m from base of vessel)

Figure 4.11 compares the spatial resolution on an off-electrode plane located equidistant between the centre of the two electrode planes, for the adjacent strategies. Figure 4.11(a) shows that the VaHa strategy provides the worst spatial resolution overall, especially in the central region. A similar trend is observed in Figure 4.11(b) for the HaVa strategy. This highlights the disadvantage of the strategies which struggle to capture changes with a lack of number of unique data acquirable. The advantage of acquiring more measurements is more prominently shown in Figure 4.11(b). Comparing the plots for HaPRecip, HaHa and HaHVa, it is evident that the HaHVa produces the more superior resolution with the relatively larger amount of usable information for image reconstruction. This shows that the multi-planar measurements acquired prove to be beneficial to improve the spatial resolution with a significant increase of unique and usable measurements, as shown in Table 3.2, especially on an off-electrode plane.

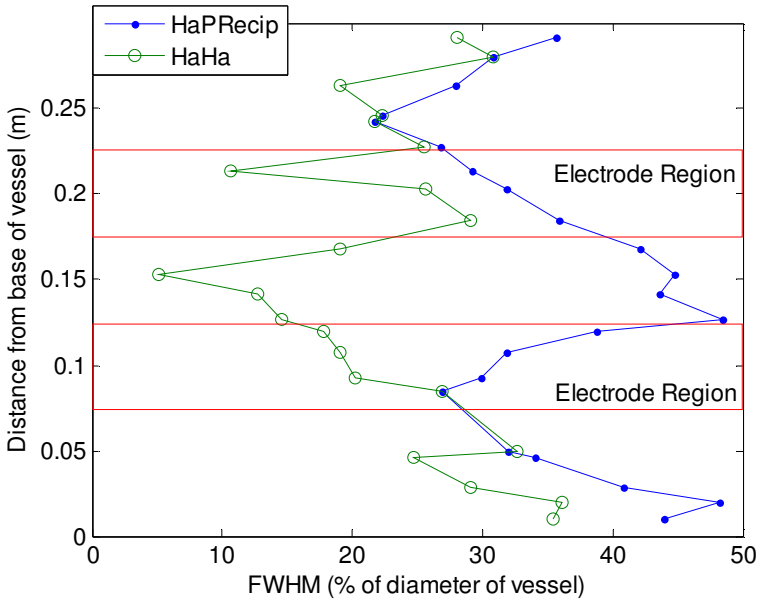

Figure 4.12 Spatial Resolution Analysis for Multi-Planar Adjacent Strategy at various heights along the z-axis located equidistance between the wall and centre of vessel

Another way to better illustrate the advantage of acquiring multi-planar measurements is by comparing the spatial resolution at various points along a vertical axis. Figure 4.12 compares the spatial resolution at different points along a vertical axis located equidistant between the wall and centre of the vessel, for the HaPRecip and HaHa strategies. It can be seen clearly that the HaHa performs better in comparison, benefiting from the extra measurements acquired on the non-current injecting electrode plane. The difference is especially significant for the off-electrode regions between the two

electrode regions. An interesting observation worth noting is that the spatial resolution is not necessarily the best within the electrode regions.

As shown in Figures 4.11(b) and 4.12, there are benefits in acquiring full 3D measurements to maximize the resources available, especially with the improvement in spatial resolution shown on an off-electrode plane. Although negligible difference is observed when comparing sensitivity levels, the increase in unique and usable information prove to be more important in improving the spatial resolution of reconstructed images. It can be concluded that spatial resolution is predominantly influenced by the amount of unique and usable information that can be used for image reconstruction.

4.3 Obtaining More Information by Increasing the Number of Electrodes

Another direct way to increase the number of measurements is by increasing the number of electrodes. With any measurement strategy, the more electrodes that are available, the more measurements can be acquired. Theoretically, this also translates into more unique information, which can benefit the quality of reconstructed images. Typically, in industrial process applications, electrodes are mounted on the wall of the process vessel such that the electrodes are non-intrusive to the on-going process. As there are no strict rules for electrode configurations and electrode designs, electrode systems are usually designed based on previously known working arrangements which leads to some inertia in exploring further possibilities.

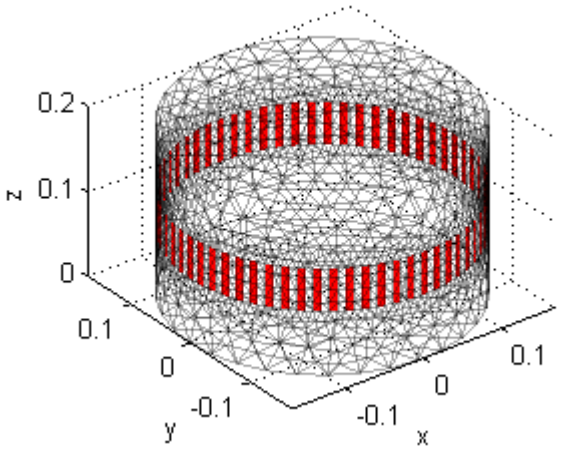

Figure 4.13 Discretized model of a single model with the circumference of electrode divided into 128 equal sections. Alternate sections are highlighted in red.

In this section, comparative studies are reported to compare the effect of different number of electrodes on the stability of measurements, sensitivity and spatial resolution of the image space. A cylindrical model 0.34m in diameter and 0.20m in height is used. The electrode plane is 0.05m in height with the centre of the electrode plane located at 0.10m from the base of the model. A single model is created with the electrode region divided into 128 equal rectangles of approximately equal areas (alternate segments are highlights in red as shown in Figure 4.13). Electrode areas are defined manually using the EIDORS toolkit. Voltages are simulated using the adjacent considering reciprocity strategy. Each model is normalized such that the current injecting electrodes are held at a constant voltage of 1V. This is consistent with the constant-voltage source used on the LCT2 tomograph (York et. al., 2005) used throughout this thesis. This results in different current magnitudes for each model. These are normalized when forward solving using the EIDORS toolkit as the solver assumes constant-current source.

The first comparative study compares the effect of different number of electrodes on stability of measurements, sensitivity and spatial resolution. The models compared, as shown in Figure 4.14, are of 16, 32 and 64 electrodes arranged in a planar arrangement. Electrode width is kept constant at 0.008m. The current injection magnitudes are 0.33mA for the 64 electrodes system, 0.29mA for the 32 electrodes system and 0.28mA for the 16 electrodes system. These are normalized according to a constant 1V voltage-source output stage, consistent with the LCT2 instrument used. The increase in current injection magnitudes with the increase in number of electrodes are due to the

compactness of the electrode arrangement as the number of electrodes increases. This leads to shorter current paths between electrodes and higher current magnitude.

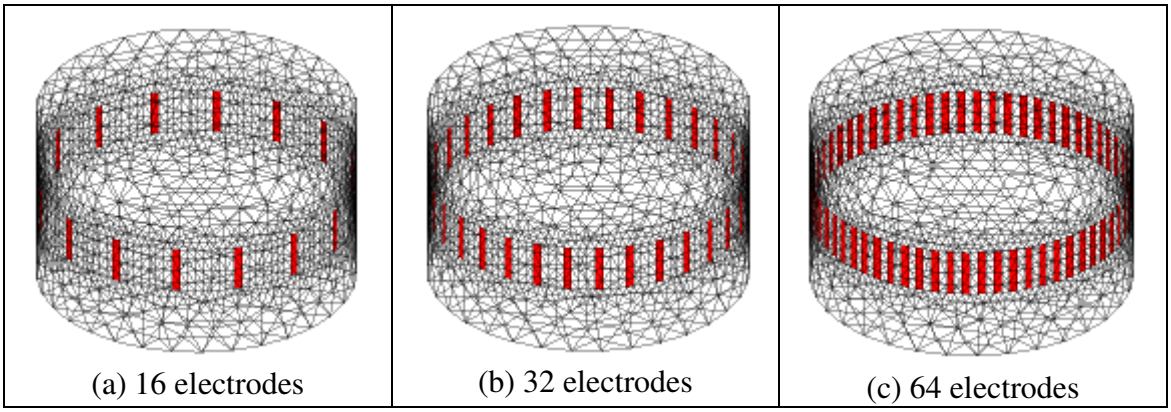

(a) 16 electrodes (b) 32 electrodes (c) 64 electrodes

Figure 4.14 Discretized models with different number of electrodes (highlighted in red) with constant electrode size

Using the adjacent strategy with reciprocity, the number of measurements increases with the increase in number of electrodes. This results in 464 measurements for the 32 electrode model and 1952 measurements for the 64 electrode model, from 104 measurements for the 16 electrode model. The stability and quality of the measurements is analysed using SVD.

SVD plots in Figure 4.15 show that all measurements are unique. The stability of measurements is compared for simulated voltages imposed with 60dB Gaussian noise for all three models. It can be seen that the percentage of stable measurements decrease significantly. For the 16 electrodes model, approximately 55 out of 104 measurements are stable (~52%). For the 32 electrode model, the percentage decreases to ~37%, where approximately 170 out of 464 measurements are stable, and to ~18%, where approximately 360 out of 1952 measurements are stable for the 64 electrodes model. It is worth noting that as the number of electrodes increase, the magnitudes of the singular values are higher, as highlighted in Figure 4.16. This suggests that the spectral components become more stable as the number of electrodes increase.

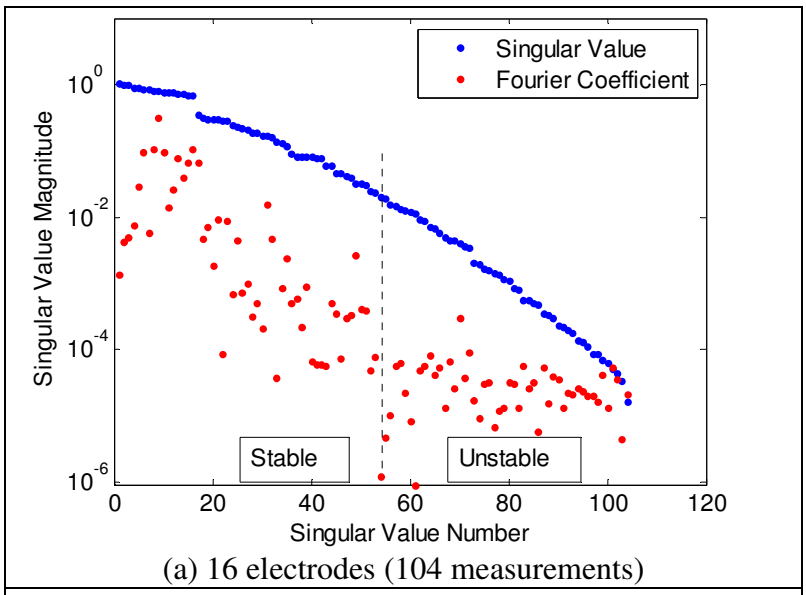

(a) 16 electrodes (104 measurements)

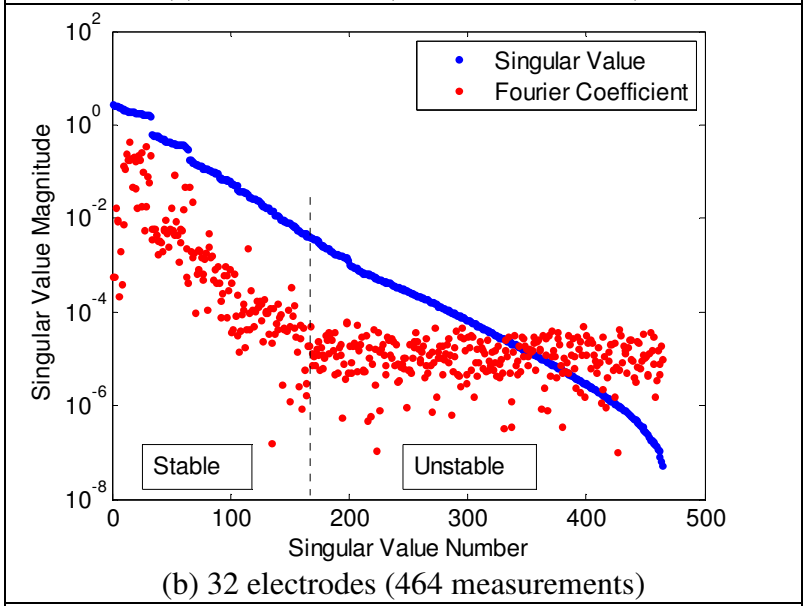

(b) 32 electrodes (464 measurements)

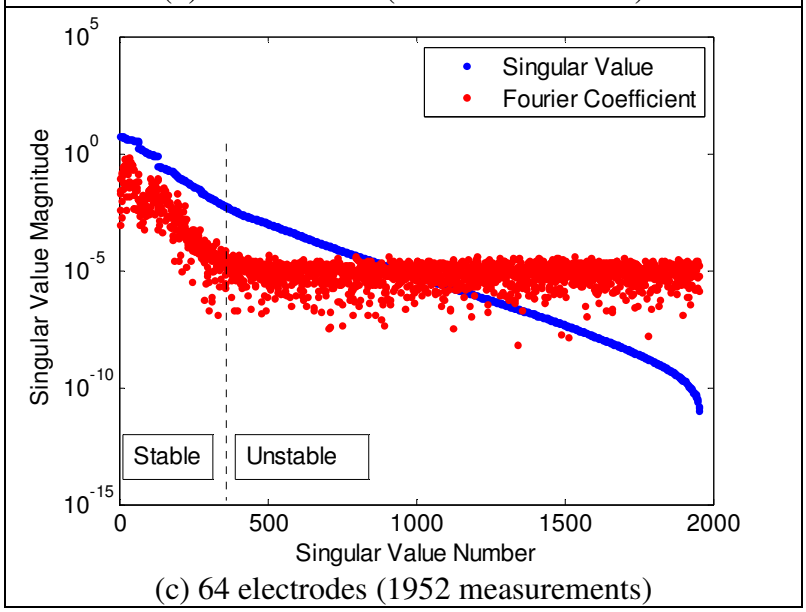

(c) 64 electrodes (1952 measurements)

Figure 4.15 Spectral Analysis to compare stability of measurements using the adjacent strategy for models with different number of electrodes of the same size

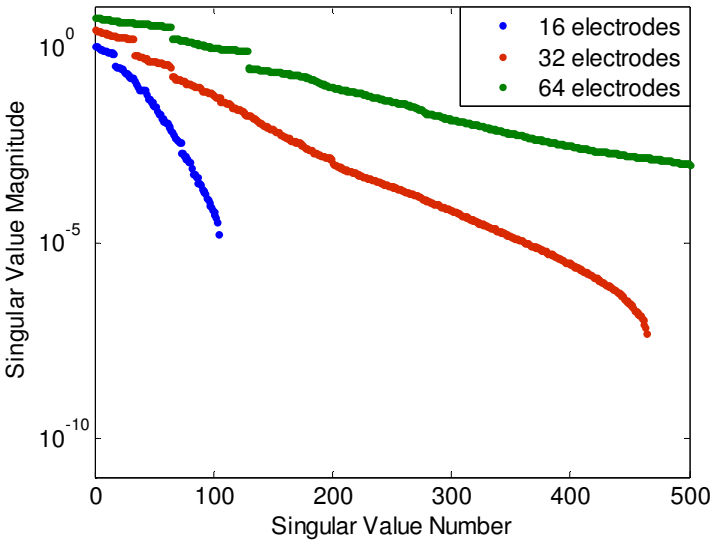

Figure 4.16 Spectral Analysis to compare the magnitude of the singular values for models with 16, 32 and 64 electrodes of the same size

Figure 4.17 compares the maximum sensitivity across the electrode plane. In the near-wall regions, the magnitude of the maximum sensitivities shows that the 64 electrodes model provides the highest detectability in comparison with the 32 and 16 electrodes models. This is attributed to the lower current injection level for models with lower number of electrodes. It is worth noting that the decrease in sensitivity magnitude for the 64 electrodes model begins rapidly and continues to drop to the lowest approaching the centre of the vessel, in comparison to the other models. In contrast, the highest magnitude of maximum sensitivity for the 16 electrodes model is the lowest nearer the electrodes but decreases relatively slower towards the centre of the vessel. Overall, the 16 electrodes model provides a more evenly distributed maximum sensitivity across the plane, where the decline in maximum sensitivity begins further away from the wall of the vessel. With the compactness of the 64 electrodes system, the current distribution is more confined near the wall of the vessel as the path is much shorter between current injecting and current sink electrodes. This may be the reason why the sensitivity levels drop rapidly for the 64 electrodes model, and is the lowest in the centre region in comparison with models with less electrodes.

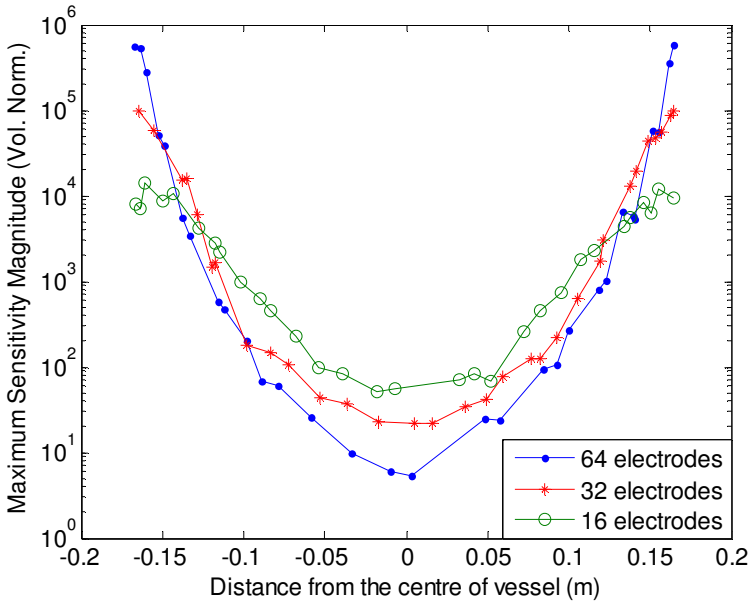

Figure 4.17 Sensitivity Analysis for 16, 32 and 64 electrodes models with constant electrode size

Figure 4.18 compares the spatial resolution across the electrode plane. The spatial resolution is fairly similar for different number of electrodes. This result is not expected as the 64 electrodes model provides a significant increase in the number of unique measurements, therefore an improvement in spatial resolution is expected. As shown in Section 3.2, the amount of unique and usable information which can be used for image reconstruction proved to be a predominant factor to improve resolution of reconstructed images.

A plausible reason is the location of the electrodes. With the electrodes arranged in a single planar arrangement, the information acquired is restricted to the same area. Despite the spectral analysis results indicating that the measurements acquired are all unique, there reaches a saturation point where the data acquired are on similar information. The detectability is also lower, as shown in Figure 4.17. Therefore changes in conductivity towards the centre of the vessel are likely to be undetected for models with a larger number of electrodes.

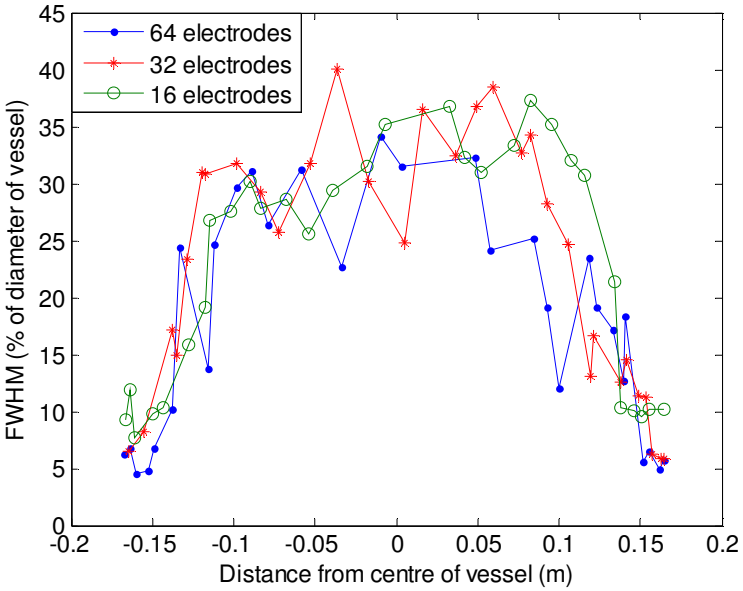

Figure 4.18 Spatial resolution analysis for 16, 32 and 64 electrodes models with constant electrode size

Considering electrode set-ups for 16 and 32 electrodes used in the first comparative study in this section, it is worth considering whether the usage of the available space on the wall of the electrode should be maximized. Even though there are no strict rules for the design of electrodes in terms of suitable dimensions, some of the literatures conclude that bigger electrodes are favourable for current injection but compromise the resolution achievable (Isaacson, 1986; Paulson et. al., 1992).

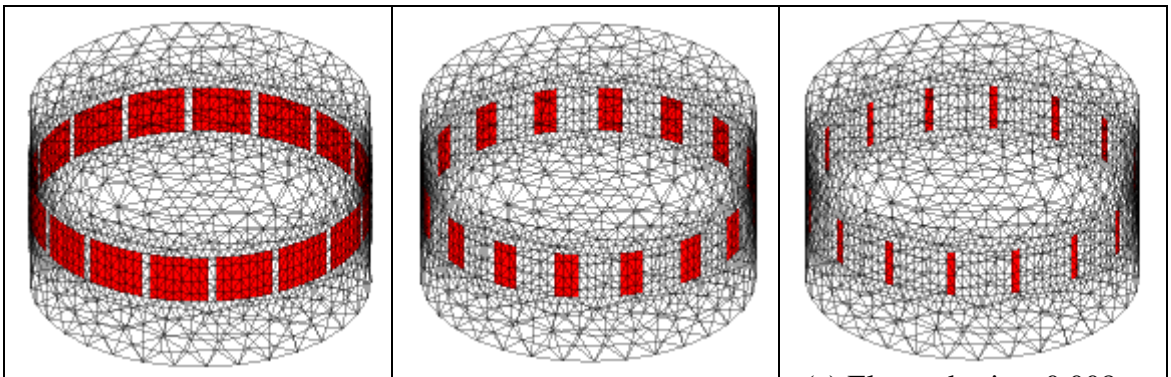

(a) Electrode size: 0.058m (b) Electrode size: 0.025m (c) Electrode size: 0.008m

Figure 4.19 Discretized models with 16 electrodes (highlighted in red) with varying electrode sizes

To further examine the effect of the size of electrodes on the sensitivity and spatial resolution, a comparison study is done with 16 electrodes models with varying electrode widths. Similarly, a single model, as shown in Figure 4.13, is used. The width of the electrodes is varied by manually defining the surfaces in EIDORS. The widths of

electrodes are selected to be 0.008m, 0.025m and 0.058m, as shown in Figure 4.19. Similarly, voltages are simulated using the adjacent considering reciprocity strategy, with the current injection magnitude normalized to a constant voltage-source of 1V.

Using the adjacent considering reciprocity strategy (104 measurements), stability analysis indicates that all 104 measurements are unique. With 60dB random noise imposed on the simulated voltage measurements, stability analysis indicates that the measurements acquired using the larger electrodes are more stable with the singular values having higher magnitudes in general, as shown in Figure 4.20. As mentioned earlier, the larger size electrodes are capable of injecting a higher magnitude of current into the system when normalized to a 1V constant voltage-source. For the 16 electrodes model with electrode width of 0.008m, the current injection magnitude is 0.28mA. The current injection magnitude increases to 0.59mA for the model with electrode width of 0.025m and 1.18mA for the model with electrode width 0.058m. The higher current results in better quality voltage measurements acquired, as they are less susceptible to noise.

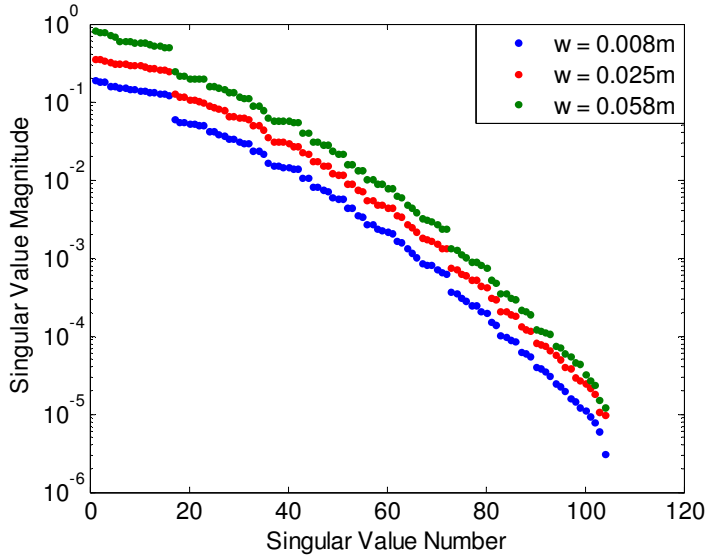

Figure 4.20 Spectral Analysis to compare the magnitude of the singular values for 16 electrode models with varying electrode sizes

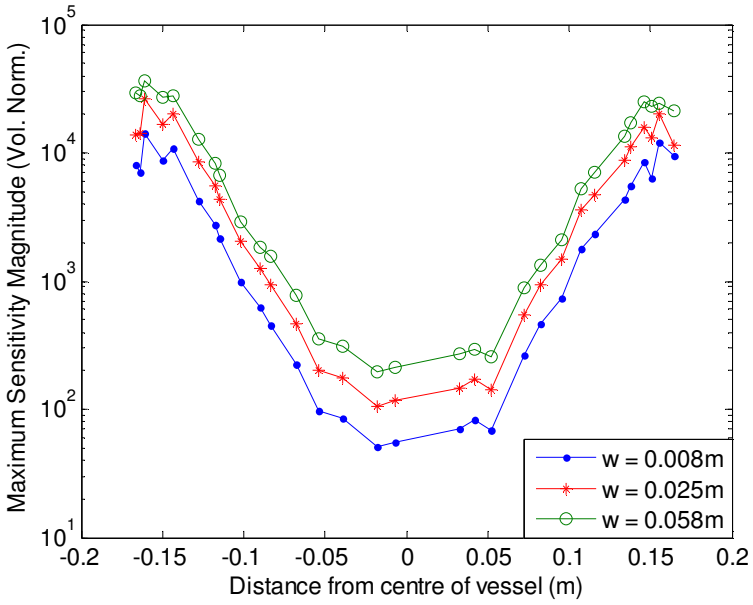

Figure 4.21 Sensitivity Analysis for 16 electrodes models with varying electrode sizes

Sensitivity analysis, as shown in Figure 4.21, indicates that the sensitivity levels increase as the width (and size) of the electrodes decrease, although not substantially. Figure 4.22 shows the spatial resolution comparison for the 16 electrodes models with varying electrode sizes. It can be seen that the model with the widest electrode produced the worst resolutions in the near-wall regions, most noticeably with the high spikes on either side of the plot.

The other two models produced fairly similar spatial resolution across the plane. This observation is consistent with the findings in previously published literature, such as Pinheiro et. al. (1998), where the spatial resolution degrades when the width of electrodes increases. The occurrence of the high spikes is likely to be an anomaly due to large locality error when computing the FWHM.

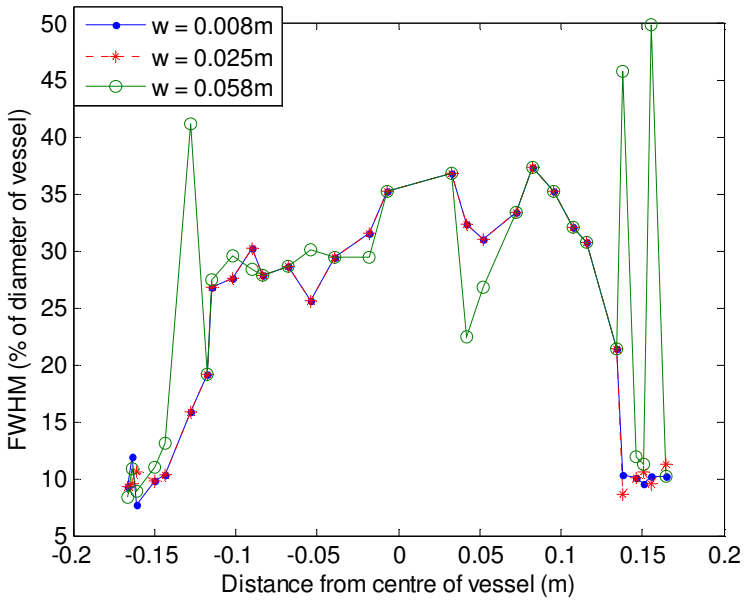

Figure 4.22 Spatial Resolution Analysis for 16 electrode models with varying electrode sizes

The next comparative study compares different models with the intention of maximizing the usage of the available space on the periphery of the vessel for models with different number of electrodes. The width of the electrodes is increased to utilize the available space on the periphery of the vessel. In this comparative study, the gap between electrodes is kept constant. A single model, as shown in Figure 4.13 is used with the circumference of the model divided into 128 equal rectangles of approximately similar area. Similarly, electrodes are defined manually using the EIDORS toolkit. In this comparison study, the gap between electrodes is kept constant at 0.008m. Three models are compared. The first is a 64 electrode model with 0.008m electrode width (50% coverage); the second is a 32 electrode model with 0.025m electrode width (75% coverage); and the third is a 16 electrode model with 0.058m electrode width (87% coverage), as shown in Figure 4.23. Similar to the previous comparative study, voltages are simulated using the adjacent considering reciprocity strategy, with the current injection magnitude normalized to a constant voltage-source of 1V. The performances of these models are compared in terms of stability analysis, sensitivity analysis and spatial resolution analysis.

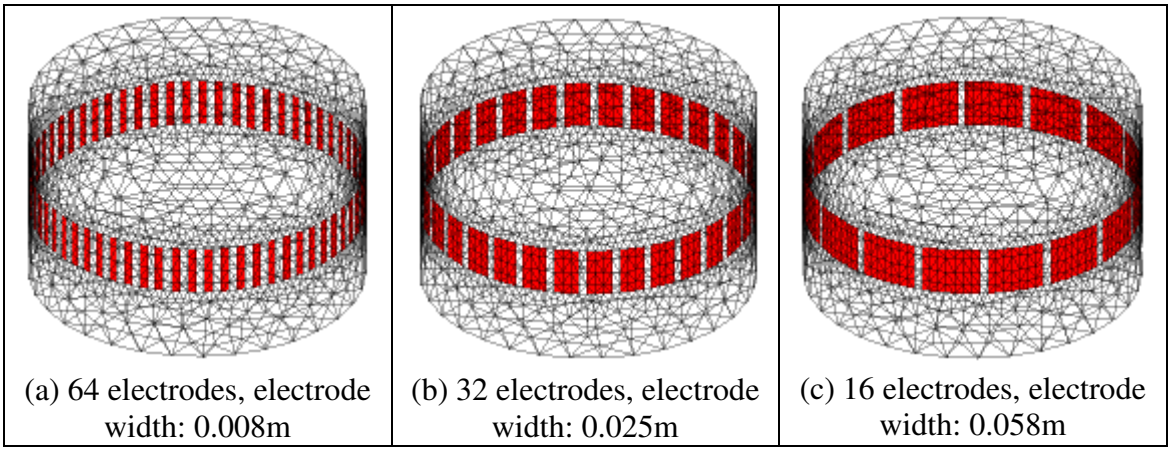

(a) 64 electrodes, electrode width: 0.008m | (b) 32 electrodes, electrode width: 0.025m | (c) 16 electrodes, electrode width: 0.058m

Figure 4.23 Discretized models with different number of electrodes (highlighted in red) with varying electrode sizes

The spectral analysis of the measurements is similar to Figure 4.15, which indicates that the stability of the measurements do not decrease due the increase in width (or area) of electrodes. Figure 4.24 shows the sensitivity analysis comparing the detectability across an electrode plane. The increase in electrode area shows an improvement in the magnitude of the maximum sensitivities detectable, comparing Figure 4.24 with Figure 4.17. This is likely to be associated with the increase in current injection magnitude. For example, for the 32 electrodes system, the current magnitude injected is 0.69mA for when the width of the electrode is 0.025m, while the current magnitude is 0.29mA for electrode width 0.008m. Similarly for the 16 electrodes system, the current injection magnitudes are 0.28mA for 0.008m electrode width and 1.18mA for 0.058m electrode width. Therefore, the sensitivity level increases as the current magnitude increases.

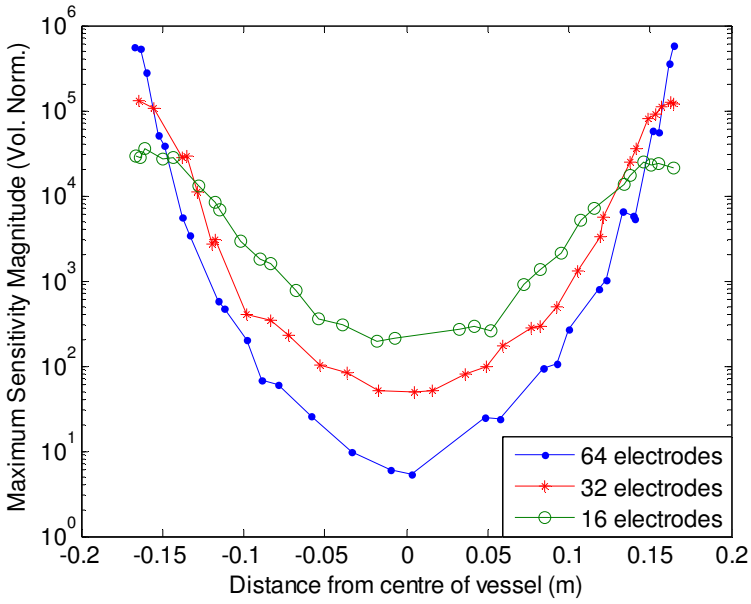

Figure 4.24 Sensitivity Analysis for 16, 32 and 64 electrodes models with varying electrode sizes

Spatial resolution analysis using resolution matrix, as shown in Figure 4.25, shows that the increase in electrode size does not result in visible improvement in resolution. While there is no difference for the 32 electrodes systems, the spatial resolution for the 16 electrodes system looks worse. This is especially evident on the far ends from the centre of the vessel with the spikes. This is likely to be due to the decrease in spatial resolution with the large electrode surface which makes it difficult to differentiate the location where the changes happened based on the voltage measurements acquired.

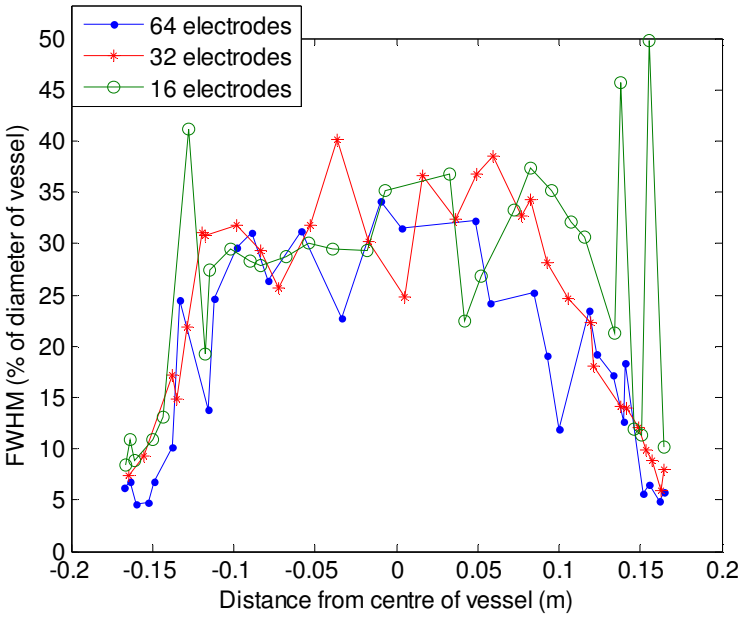

Figure 4.25 Spatial Resolution Analysis for 16, 32 and 64 electrodes models with varying electrode sizes

In summary, the impact on spatial resolution from increasing the amount of unique measurements through increasing the number of electrodes is negligible. Although spectral analysis indicates that there is a significant increase in the number of unique measurements obtainable, the spatial resolution analysis indicates that there are negligible differences across the image space. The likely reason for this is the restriction on where measurements are obtained. With the electrodes placed on a planar arrangement, the data acquired are constrained to the same area, even though the spectral analysis shows that all measurements acquired are unique. There is a lack of improvement in spatial resolution shown in the analysis although the measurements are shown to be unique through spectral analysis. Another factor which requires consideration is the size of electrodes. Analysis shows that the increase in sensitivity or

detectability which is obtained by using electrodes of larger size, compromises the spatial resolution.

4.4 Summary for Improving Spatial Resolution through Increasing Information

The analysis in this chapter has shown that several factors need to be considered when searching for means to improve spatial resolution of reconstructed images. Through spatial resolution analysis, it is shown that the improvement in spatial resolution is predominantly influenced by the amount of usable information which can be used for image reconstruction. The amount of usable information is limited by the number of unique measurements obtainable. The number of unique measurements obtainable can be acquired through varying measurement strategies or increasing the number of electrodes.

Section 4.2 shows that while measurement strategies are capable of increasing the number of measurements from a fixed set of electrodes, the measurements acquired may not all be unique. In other words, the measurement strategy is not optimized. Redundant measurements do not contribute to the image reconstruction process, and are likely to be filtered and excluded. The comparative study between the adjacent and opposite strategies shows that an improvement in detectability (sensitivity analysis) does not necessarily translate into an improvement in visibility (spatial resolution analysis). Sensitivity or detectability is primarily influenced by current pattern, while spatial resolution or visibility is predominantly affected by the number of usable measurements for image reconstruction. Even though the opposite strategy is capable of improving the detectability especially towards the central region of the model, the number of usable measurements for image reconstruction is similar to those produced using the adjacent strategy. This results in similar spatial resolution across the image plane for both strategies. Analysis also indicates that full-3D measurements for a multiple-plane electrode set-up, where measurements between planes are acquired, offers benefits for improving the spatial resolution. The benefits of this approach are highlighted when comparing the resolution across an off-electrode plane. However, full-3D measurement

strategies suffer from a longer data acquisition time and the measurement strategies are not optimized, resulting in a relatively large percentage of redundant measurements.

The results shown in Section 4.3 indicate that by increasing the number of electrodes on a single plane, the impact on spatial resolution is negligible. It is shown that for a planar arrangement, there is a saturation point whereby the increase of measurements obtained either through measurement strategy or increasing the number of electrodes has no impact on the spatial resolution. The decline in visibility is also backed-up by the sensitivity analysis, where the detectability decreases in the central region of the model (further away from the electrodes) with the increase of electrodes. Referring to full-3D measurement strategies in Section 4.2, the improvement in spatial resolution when using multi-planar measurements hints that the locations of electrodes are an important factor when considering improving spatial resolution.

The studies conducted in this chapter indicate that in order to improve spatial resolution, considerations should be made on measurement strategies and electrode arrangement. In order to avoid redundancy and saturation of information, it is important to consider the locations of electrodes, as this dictates where the measurements are taken. Spatial resolution analysis also indicates that the resolution is better nearer to the wall of the vessel, where the electrodes are mounted. This hints at potential improvement in resolution in regions further away from the wall of the vessel with the presence of electrodes inside the vessel. This, however, means the electrodes intrude the space within the vessel. The following chapters explore the possibility of improving spatial resolution through positioning electrodes for voltage difference measurements in different locations within a process vessel and evaluate its effect on spatial resolution.

CHAPTER 5
WIRELESS 'PILLS' AND ELECTRICAL RESISTANCE TOMOGRAPHY

The results presented in Chapter 4 indicate that increasing the amount of unique information by increasing the number of electrodes in a planar arrangement is effective. However, further analysis suggests that the additional unique information does not improve spatial resolution especially in the centre region, further away from the electrodes, of an imaged space, where resolution is typically poor. Knowing that additional electrodes are capable of improving resolution, the next logical step is to vary the location of electrodes. This approach enables 'localized measurements' to be obtained in different locations within the vessel, which may potentially improve the spatial resolution of reconstructed images. This chapter explores different methods of incorporating localized measurements acquired through ad hoc and wireless sensors with electrical resistance tomography (ERT).

This chapter is divided into 4 sections. Section 5.1 briefly introduces Wireless Sensor Networks (WSNs) through consideration of relevant published reviews. Section 5.2 relates wireless sensor network (WSN) to electrical resistance tomography (ERT). The system built for the WSN4IP project is briefly described in Section 5.2 for completeness. Possible ways of utilising the wireless sensors or 'pills' with a typical ERT system are explored and described. Given the freedom to determine the desired functionality of the sensors, these are chosen such that the measurements are suitable to be used with an ERT system. Three approaches are identified and briefly discussed,

namely the Augmented Electrical Tomography (AET) approach, the Extended Electrical Tomography (EET) approach and the Ad Hoc Electrical Tomography (AHET) approach.

Sections 5.3 and 5.4 explore two of the methods in more detail. Section 5.3 explores Augmented Electrical Tomography (AET), where the localized measurements are in the form of conductivity values. The localized conductivity values are equivalent to the solution values of the voxels of the discretized model in which the pills are located. Simulation results from a feasibility study are presented. Section 5.4 explores Extended Electrical Tomography (EET). In this case, the sensors on the pills are used as part of the ERT electrode system, hence extending the number of electrodes and measurements. The measurements acquired are in the form of voltage differences. Using this approach, an existing inverse solving technique can be used, with slight modification to accommodate the internal electrodes. The influence of the internal electrodes is evaluated through considering the quality of measurements, sensitivity and spatial resolution using analysis techniques described in Chapter 3. The chapter concludes by comparing the relative merits of the two approaches.

5.1 Recent Development in Wireless Sensor Networks

The development of Wireless Sensor Network (WSN) has attracted attention in recent times, largely due to the advancement of Micro-Electro-Mechanical Systems (MEMS) technology to further the development of smart sensors. The ‘pills’, also known as nodes or motes in the literatures are scattered in an environment of interest to capture data for monitoring. The pills are typically low power devices and each is usually furnished with sensors, a processor, power supply, communication system and actuators. The functionality of the sensors can be customized to measure properties of interest in the environment which the WSN is monitoring.

A selection of published literature which provides a broader review of areas of interest in development of WSN is given below. This serves as an introduction to WSN and details are not delved into as WSN is not the focus of this thesis.

Abd-El-Barr et. al. (2005a, 2005b) presents a two-part review with topics including topologies and design techniques, influencing factors, routing techniques and security issues. In Abd-El-Barr et. al. (2005a), a selection of topologies and design techniques are discussed. The paper also discusses influencing factors for the design of a WSN system, which includes power consumption, fault tolerance or reliability, and efficiency of communication protocol. Abd-El-Barr et. al. (2005b) reviews different routing techniques. The paper also discusses security requirements and available security routing protocols.

Kuorilehto et. al. (2005) focuses on four essential distribution aspects in WSNs, namely service discovery, task allocation, remote task communication and task migration. The review paper also evaluates a selection of proposed distribution protocols through considering different types of architectures including OS-based architectures, middleware architectures, VM-based architectures and standalone protocols. The different protocols are compared through evaluating characteristics including types of communication, scalability, fault tolerance, requirements, and relative merits of each technology, based on suitable applications identified.

Sun and He (2006) evaluates the requirements and constraints of a sensor network, identifying and discussing key management mechanism through evaluation metrics given, and security-related issue. Several limitations are discussed, including limited power/energy, low transmission range, limited data storage on the nodes and processing capacity, and unattended operations. The paper also reviews four main pre-distribution key management schemes, namely pure probabilistic key pre-distribution, polynomial-based, Blom's matrix-based and deterministic key pre-distribution schemes.

Dressler, et. al. (2007) is concerned with several WSN key distribution research issues including key management, performance and scalability, access control and authentication, security protocols, routing and clustering, and secure localization and intrusion detection. A key contains information which is required in order to establish communication between nodes.

Yick et. al. (2008) provides a comprehensive review of various aspects of WSNs. The paper provides an overview of key issues in WSNs, reviews different types of sensor

networks, suitable applications, and issues associated with internal sensor systems and communication protocol for the network.

The main interest of the review by Jiang et. al. (2006) is identifying issues related to reliability of WSN specifically for industrial process control applications. The reliability issues discussed include error in network addressing channels, communication disruptions, unexpected irregularity in traffic and operational environment and signal retransmission.

Johnson et. al. (2009) presents a comparative review of a selection of available WSN nodes or motes using criteria such as general parameters, processing and memory power, communication capabilities, sensor support and power consumption. The authors provided conclusions for the best technology from a selection of WSN technology based on the design requirements.

The selection of literature reviews provided in this section serves to highlight the general research interest in WSN. From the summaries of the papers provided, the research areas which generate the most interest are security-related issues, specifically designing reliable communication protocols. Another research area which has gathered momentum in recent times is localization for tracking the position of the ad hoc sensors.

Drawing for relevance to the work of this thesis, there is no published work at the time of writing which describes using WSN with tomography or to determine the distribution of materials. The papers found generally describe applications for WSN communications in air, while the work done in the WSN4IP project takes up the challenge for considering communication in grain. This poses different challenges in terms of the reflection of communication signals.

5.2 Incorporating Wireless Pills Into Electrical Resistance Tomography

This thesis explores the potential for using an ad hoc wireless network of sensors, or 'pills' to improve the images from electrical tomography. The idea is to scatter the pills within a process vessel. The pills have the freedom of mobility to acquire localized measurements which can be used together with measurements acquired using a conventional ERT setup, as shown in Figure 5.1. The deployment of ad hoc pills breaks away from conventional ERT set-ups, where the sensors are traditionally mounted on the wall of the vessel such that they do not intrude the on-going process. There are previous efforts which use internal electrodes. However, all published works describe an extended electrodes system which use internal electrodes mounted on internal structures such as baffles and impellers such that they remain non-intrusive to the on-going process within the vessel.

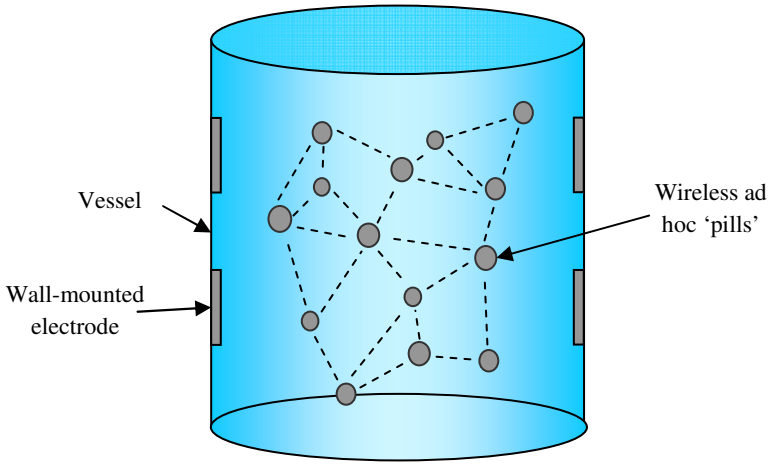

Figure 5.1: Ad hoc sensors with a conventional ERT set-up

For the purpose of this project, it is assumed that the position and orientation of a pill is provided. In the present case, this information is developed by the Wireless Sensor Network for Industrial Process (WSN4IP) project. The aim of the WSN4IP project is to establish a leading position for the United Kingdom in addressing the long term challenges in establishing WSN technology for interrogating industrial processes. Brief details of the proposed prototype of the ad hoc pill and the work-in-progress of developing the sensor node are described for completeness. Each sensor node, a sphere 14cm in diameter, is equipped with a system consisting of a microcontroller, memory,

an RF circuit for communication, transceiver and sensors, as shown in Figure 5.2. The system is powered by a lithium ion battery. The data communication system comprises of a Chipcon CC1101 transceiver interfaced with the PIC32 microcontroller through a high speed serial bus. Each node is furnished with four helical monopole antennas, connected to the transceiver using a microwave coupler. Each node functions as a router in the network where data is transmitted from node to node until the data is related to the destination, without assistance from the base station or the network infrastructure. This transmission protocol allows low transmission power while allowing all nodes to remain in contact with the base station. This type of network topology poses new challenges, as multiple nodes potentially undergo topology changes. Another challenge is to develop a strategy which takes into consideration the propagation of signals in wheat. Details of the communication protocol are described in Parkinson, et. al. 2010. Similar challenges are encountered for the localization protocol which combines the features of a Ultra Wide-Band (UWB) pulse edge-detection and time of flight tri-lateration as described in Parkinson, et. al. 2009.

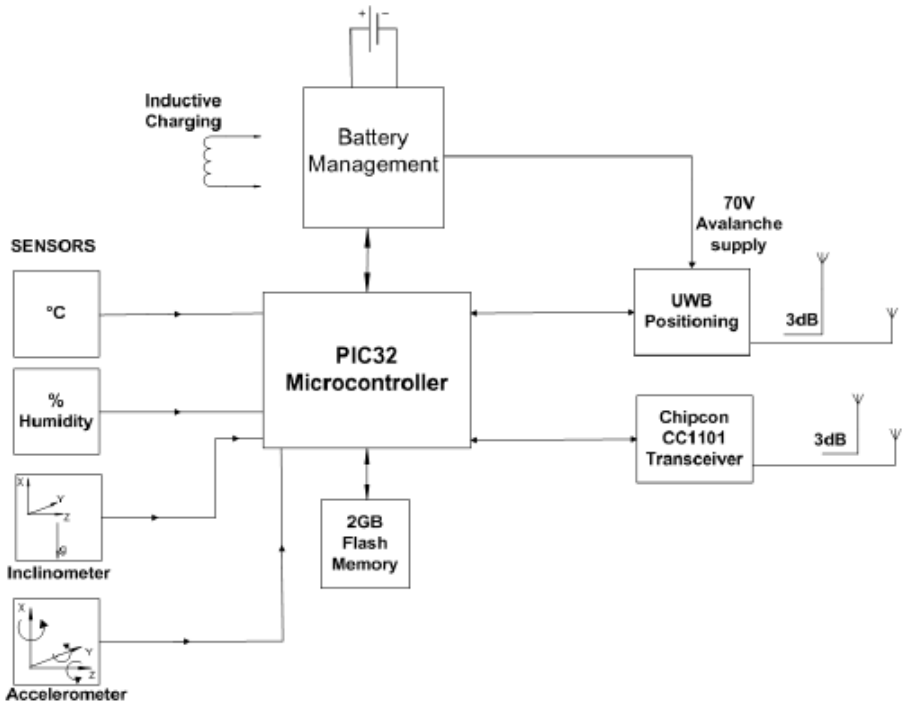

Figure 5.2 Major components for a Wireless Sensor Node (Parkinson et. al. 2010)

The aim of the present work is to consider incorporation of the localized measurements acquired from the ad hoc sensors into a set of typical ERT measurements. In other words, ad hoc sensors are used together with a typical electrode set-up for ERT

measurements. In ERT, voltage difference measurements are taken to estimate the conductivity distribution of the image space. Therefore, suitable functionality of sensors includes conductivity probes and as electrodes for acquiring voltage difference measurements. The measurements acquired have the potential to provide additional information to better inform the inverse problem of determining the distribution of materials.

The first approach considers the ad hoc sensors as conductivity probes to provide localised conductivity measurements. The localised measurements can be used to inform for a better initial prediction of the forward model, leading to a more accurate Jacobian matrix. Using this approach, the measurements will be incorporated into the inverse solving process and the additional information is likely to have an impact on the inverse solution. The localized conductivity acquired represents the conductivity of the voxels of the discretized model in which the ad hoc pill is located. In other words, the conductivity measurements become the solution of the corresponding voxels. Ideally, the measurements will influence and improve the estimated inverse solutions accordingly, especially in the vicinity of the ad hoc pill. This essentially augments the inverse solution, hence this approach is termed as 'Augmented Electrical Tomography' (AET).

The second approach is to use sensors on the ad hoc pills as electrodes in the tomography system. This effectively extends the number of electrodes available and the number of measurements, hence the approach is termed 'Extended Electrical Tomography' (EET). The simulation study in Chapter 4 suggests that measurements obtained in different locations could potentially improve the spatial resolution of reconstructed images. The simulations suggested that increasing the number of measurements through increasing the number of electrodes on the wall of the vessel does not necessarily translate into an improvement in spatial resolution in the image. Although the amount of unique information acquired increases, it reaches a saturation point when the unique information does not benefit the resolution. This prompts the need to vary the location of the electrodes. This approach explores the possibility of improving spatial resolution through invading the image space to interrogate the conductivity distribution of the image space. The ad hoc internal electrodes are primarily used for voltage measurements. There is an option to expand the functionality

of the ad hoc sensors to act as current source. However, this complicates the instrumentation requirement and is not considered further here.

A more ambitious approach is to only utilise the ad hoc sensors as electrode systems, eliminating the need for wall-mounted electrodes. Considering issues such as dynamic localization and positioning, configuring a feasible measurement strategy and maintaining the stability of the system, this approach, termed 'Ad Hoc Electrical Tomography', is challenging. Typically, in existing mathematical models used for ERT forward and inverse solving, like that adopted in the EIDORS toolkit, the model is set-up using boundary voltages. In other words, internal sources are excluded, as it may cause instability in the calculations leading to wrong prediction of the inverse solution.

5.3 Augmented Electrical Tomography

Augmented electrical tomography (AET) explores the idea of including known localized conductivity measurements into a set of ERT measurements. The sensors on the ad hoc, wireless pills are used as conductivity probes. Conductivity of the medium in the vicinity of the wireless pill is measured, termed as 'localized conductivity measurement'. The inclusion of the localized conductivity measurements translate into known solutions for the corresponding elements or voxels in the discretized model. This reduces the number of unknowns in the overall system. The concept is similar to that of substituting an unknown with the measured conductivity measurements, subsequently using the voltage measurements to solve for the other unknowns. Theoretically, this should improve the under-determined case of the ERT inverse problem.

The work published in Heikkinen et. al. (2001a) closely relates to this idea. The paper describes methods of including known structures and resistivity values into the inverse solution to help refine the quality of reconstructed images. Details of the structures of the process vessel were included in the model through exact modelling of all internal structures. This enables the exact parameterization of the resistivity distribution of the structures. The known resistivities of the structures were included by modifying the generalized Tikhonov regularization. Inverse solving was done using the Gauss-Newton method.

The paper considered different cases with the inclusion of internal structures. The first case included separated rods having high conductivity, the second had connected rod structures with high conductivity and the third with separated rods with low conductivity. The reconstruction targeted a low conducting region which occupied the same space as the internal rod structures. Data were simulated using the trigonometric current pattern (Kolehmainen et. al. 1997). Results were compared between reconstructed images without any inclusion of prior information and reconstructed images with the inclusion of information of the known internal structure and resistivity values. Comparing the reconstructed images, reconstruction with the inclusion of prior knowledge performed better when detecting the low conducting region for the case of separated rods with low conductivity. However, the inclusion of the prior knowledge failed to make any improvement on the reconstructed images for cases where the internal rods were highly conducting. The authors concluded that the inclusion of information of known internal structures is necessary, especially because large structures have the tendency to draw the estimated resistivity values towards the resistivities of the structures.

There are similarities between the work presented by Heikkinen et. al. (2001a) and the AET approach. Both aim to include prior information in the form of known resistivity or conductivity values into reconstruction in order to improve the estimated solution of the conductivity distribution the ERT system interrogates. The known values replace values of the voxels or elements which they occupy, reducing the number of unknowns that require solving during image reconstruction. However, there is an important difference between both works, in terms of the degree of influence the prior knowledge has on the solution of the neighbouring voxels. Heikkinen et. al. (2001a) aims to eliminate the effect of the structures by the inclusion, therefore the computation of the solution of the voxels should be minimal. The AET approach intends to influence the solution of the voxels in the vicinity of the voxel with known conductivity value. This assumes the surrounding voxels have similar conductivity values as the voxel with known conductivity. The work done by Heikkinen et. al. (2001a) provides ideas on how to incorporate known information into the inverse solution, although a direct implementation into the present work described was unsuitable due to the differences in

intended purpose for both works, as this works aims to utilise the known values to influence the inverse solutions while Heikkinen et. al. (2001a) aimed for the opposite.

The implementation of the AET approach requires several modifications to the inverse solving algorithm to include the localized conductivity measurements, with the aim to utilise these values to influence the solutions of the voxels in the vicinity of the voxel with known solution. Incorporating localized conductivity measurements acquired into the inverse solution is equivalent to substituting a solution into unknowns of the elements occupying the same space as the ad hoc sensors. With this information included into the inverse solution, this effectively reduces the amount of unknown conductivities in the measured vessel, which would improve the under-determined case of the ERT inverse problem. Subsequently, the algorithm should aim to minimize the errors between estimated and actual solutions of the voxels in the vicinity of the voxel with known solution.

An iterative algorithm is best suited for this approach. The Non-Linear Gauss Newton algorithm has been chosen for this purpose. The localised conductivity values are first substituted as solutions to the corresponding elements, where the solution for the corresponding element is $\sigma_k = x_k$ with σ_k as the localised conductivity value and x_k as the unknown for the corresponding element. The first iteration of the solution is calculated. In the following iterations, the inverse solving algorithm readjusts the estimated solution calculated from the previous iteration towards the measured localised conductivity value using Eq. (2.23). This assumes that the nearby elements have the same conductivity values as the elements which the localised conductivity values occupy. This approach requires an additional term to Eq. (2.21) to include the localized conductivity measurements into the minimization of the sum of squares error. The minimum of the sum of squares errors from Eq. (2.21) become:

$$\sigma = \arg\min\left\{\left\|V - F(\sigma)\right\|^2 + \alpha^2\left\|L(\sigma - \sigma_{ref})\right\|^2 + \alpha_k\left|x_k - \sigma_k\right|^2 + \ldots\right\} \tag{5.1}$$

where α is the regularisation parameter and α_k is a parameter that is determined by the noise level of the localized measurements. V is the measurement vector, σ is the

conductivity vector, σ_{ref} is the reference conductivity, and $F(\sigma)$ is the forward operator. L is the regularization matrix, set up in the form of a difference matrix which correlates elements sharing the same surfaces. This differs from the typical regularization matrix, where it is typically calculated to correlate elements sharing any point of a voxel, resulting in the highest degree of correlation between voxels. Throughout the iterations, the value of the known conductivity value is readjusted to the value obtained through the localized measurement prior to computing the inverse solution.

5.3.1 Feasibility Study for Augmented Electrical Tomography

The aim of the feasibility study is to investigate the effect of incorporating the localized conductivity measurements into the inverse solution for the reconstructed image. For this preliminary effort, it is assumed that a localized conductivity measurement occupies the space of a single element in the discretized model. It is also assumed that the localized conductivity value is noise free. These assumptions are made for simplicity. In practice, errors, for example localization of ad hoc sensors and measurement noise, should be taken into consideration.

A single plane model was used, with 16 electrodes arranged in planar arrangement. The model is 0.34m in diameter and 0.20m in height. The electrodes are 5cm in height and 3cm in width. Simulations were done using a homogeneous distribution, with conductivity 0.01S/m (conductivity of tap water). Voltages were simulated for the adjacent with reciprocity strategy, on a model with 26465 elements and imposed with 60dB Gaussian noise. This is a similar noise level that is delivered by the LCT2 instrument. The inverse solution was performed on a model with 5137 elements. This step is taken such that ‘inverse crime’ is avoided (Lionheart et. al. 2005). ‘Inverse crime’ refers to manipulation of the outcome of the inverse solution by performing forward and inverse solving on the same model, using noise free simulated voltages. This is likely to provide the wrong impression of the performance of the system.

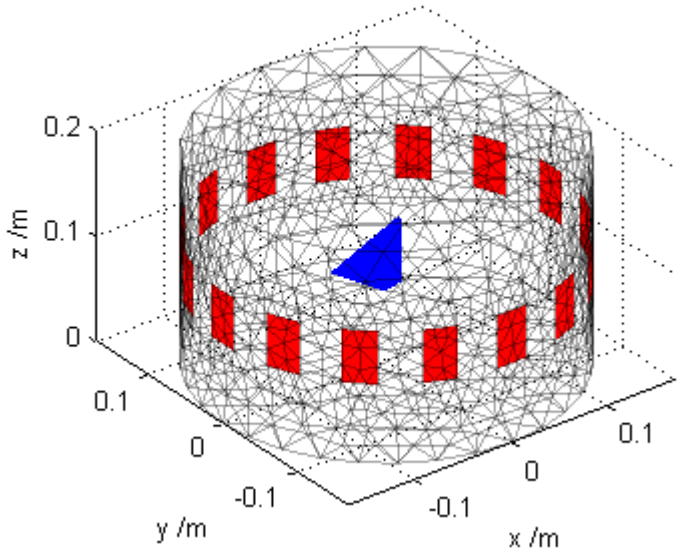

Figure 5.3: Discretized model for a single plane of 16 electrodes (highlighted in red) and an element with known conductivity (highlighted in blue)

An element located near the centre of the vessel is selected as the element with known conductivity value and is highlighted in blue in Figure 5.3. Results are compared between images reconstructed using conventional ERT measurements and those using the AET approach.

The comparison is shown in Figure 5.4. The results do not show any visible difference. Inspection of the estimated solution shows that there are slight changes. The estimated solutions of the neighbouring elements of the element with known conductivity value were driven closer to the value of the known conductivity. However, this was not true for elements further away from the known element. It was noted that some solutions for elements located further away from the element with known conductivity were in fact driven further away from the correct solution values.

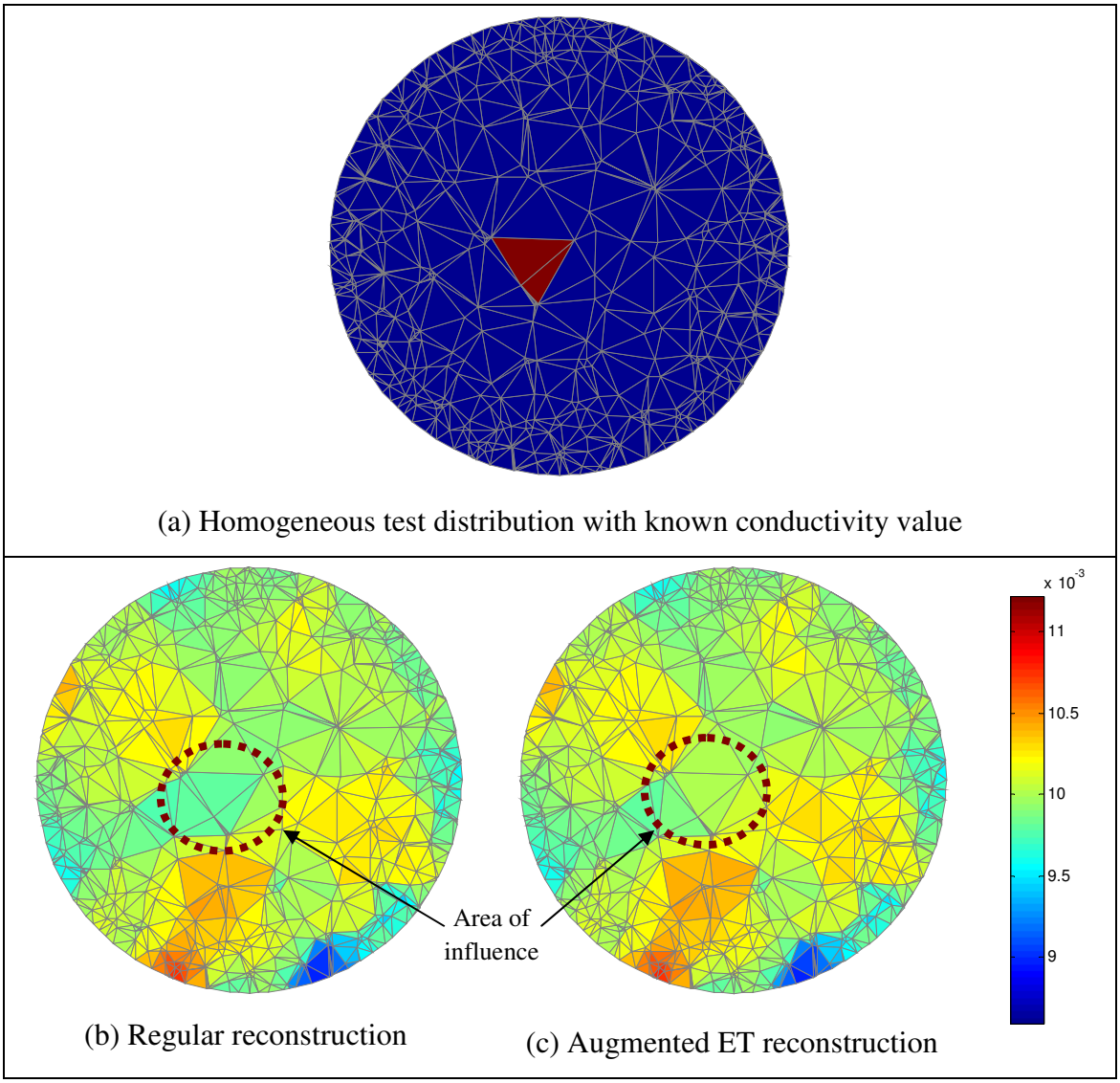

Figure 5.4: Images comparing reconstruction of a homogenous background resulting from regular ET and augmented ET. Images are shown at height 0.1m from the base of the vessel, and the colour-scale for (b) and (c) are the same.

Figure 5.5 maps the magnitude of changes of the estimated solution due to the inclusion of the localized conductivity value. It is clear that there is a distinctive 'area of influence' in the vicinity of the element representing where the known conductivity value is. The area of influence is dependent on the regularisation parameter that is set when computing the regularization matrix, as the parameter controls how much smoothing is applied.

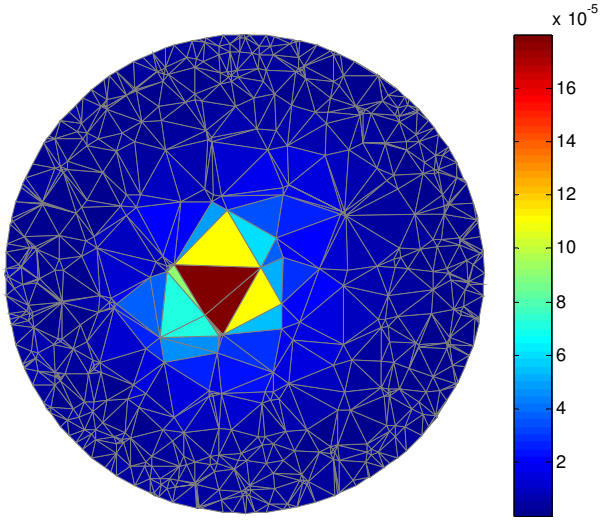

Figure 5.5: Slice plot showing the change in magnitude (absolute values) due to the inclusion of the known solution. The colour map shows the magnitude of changes of estimated solution.

Simulations were also done using inhomogeneous test distributions. The first example considers a test distribution as shown in Figure 5.6 with the known conductivity element strategically located away from the inhomogeneous area towards the centre of the vessel, such that the area of influence of the known element can be observed. The inhomogeneous region has a conductivity 0.02S/m against the background conductivity of 0.01S/m (tap water). The value of the inhomogeneous area is chosen arbitrarily for simulation purpose.

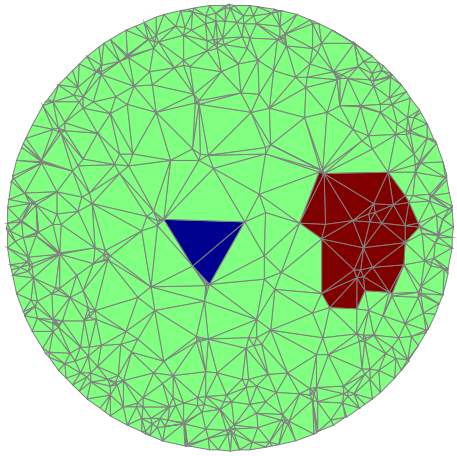

Figure 5.6: Test distribution used with inhomogeneous area highlighted in red and known conductivity element highlighted in blue located away from the inhomogeneous area

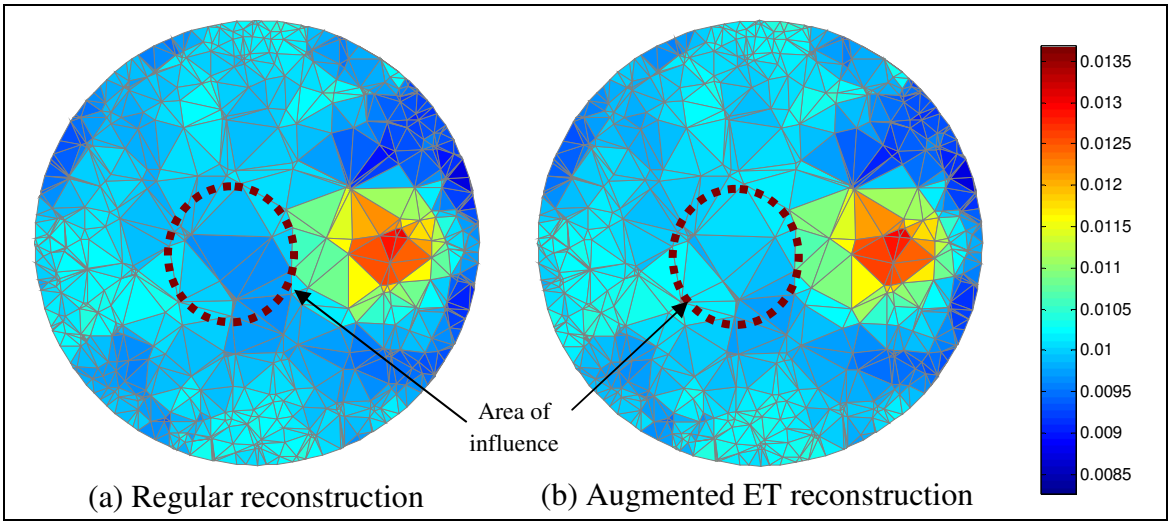

Figure 5.7: Images comparing reconstruction of a homogenous background resulting from regular ET and augmented ET for an inhomogeneous test distribution. Images are shown at height 0.1m from the base of the vessel, and the colour-scale for (b) and (c) are the same.

Typically, for a test distribution with a hard-boundary, edges of the objects are blurred and not well-defined in reconstructed images. This is due to the smoothing applied to stabilize the inverse problem. Figure 5.7 compares the reconstruction between conventional reconstruction and augmented method. The reconstructions look similar for both cases. The reconstructed shape of the inhomogeneous area was not improved by the inclusion of the known conductivity element. The area of influence is relatively constrained, as shown in Figure 5.5. Therefore it is unsurprising that the inclusion of the known conductivity element has no impact on improving the shape of the inhomogeneous area. At the location of the known conductivity element highlighted in Figure 5.7, the reconstructed value for the augmented reconstruction and elements in its vicinity are computed to be similar or near to the actual value.

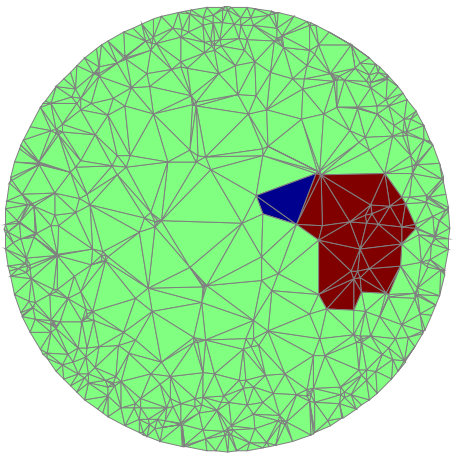

Figure 5.8: Test distribution used with inhomogeneous area (highlighted in red) and known conductivity element (highlighted in blue) located on the boundary of inhomogeneous area

The second case considers the same test distribution as described previously, with the known conductivity element located on the boundary between the inhomogeneous area and background as shown in Figure 5.8. The chosen location is to examine the effect that the known conductivity element has on reconstruction of the inhomogeneous area.

The reconstructions are compared between conventional and augmented approaches and are shown in Figure 5.9. From the reconstruction in Figure 5.9(b), it can be seen that the reconstructed value is readjusted to 0.01S/m for the element on the boundary, which is also selected as the known conductivity element. However, the value of the element located inside the inhomogeneous area is also readjusted to be lower, although the actual conductivity value is higher.

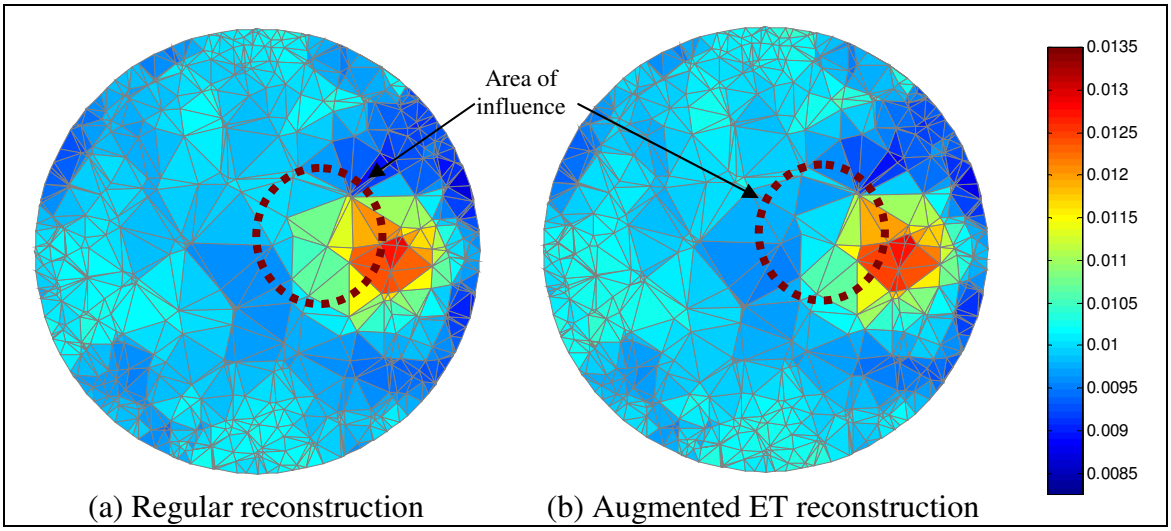

Figure 5.9: Images comparing reconstruction for test distribution (a) resulting from regular ET and augmented ET. Images are shown at height 0.1m from the base of the vessel, and the colour-scale for (b) and (c) are the same.

This is unsurprising considering the lack of control over how the adjustments are made using the Gauss-Newton algorithm. A closer inspection of the estimated solution indicates that the adjustments are not always made such that the readjusted solution is closer to the actual values. This is likely to be due to the Gauss-Newton algorithm attempting to minimize the sum squared function in Eq. (2.23). Ultimately, the solution calculated for each voxel is 'restricted' by the boundary measurements (i.e. the voltage difference measurements between electrode pairs). By substituting the solution of chosen voxels, the estimated solutions for other voxels are fitted by the algorithm such that all the solutions would fit the boundary measurements taken.

This is evident when the mean of all conductivity values was calculated and the value remains the same for both using a conventional ERT set-up and the AET approach. It was expected that the mean value of all conductivity would be drawn closer to the known conductivity value for a homogeneous case. However, it was not the case and there is no way through the algorithm to force adjustments to be made in the ideal manner.

In conclusion, the AET approach is feasible. The biggest challenge is to identify a suitable inverse solving algorithm which can provide users to have more control over how the values are readjusted based on the prior information provided through the known conductivity values. Gauss-Newton offers less control in terms of how the solutions are adjusted. Other commonly used inverse solving algorithms, such as the TSVD algorithm, were considered, but none were found to be suitable for this application. Further progress of this approach requires deeper mathematical consideration of the inverse problem.

5.4 Extended Electrical Tomography

Extended electrical tomography (EET) approach aims to utilise the ad hoc sensors as part of the electrodes system. With the ad hoc sensors located inside the vessel, localized voltage measurements can be acquired. This approach could potentially acquire unique information in regions that are less accessible using a conventional electrode set-up.

There is little published work available describing the use of internal electrodes, with the exception of Murphy (2008). Murphy (2008) described using electrodes attached to an impeller to extend the number of electrodes. The electrodes are used to pair with electrodes on the wall of the vessel for current injection. The Reduced Internal-Drive Adjacent measurement strategy (RIDAM) (Murphy and York, 2006) is introduced as a new measurement strategy to incorporate the internal electrodes. The internal electrode that is closest to the current injecting electrode on the wall of the vessel is used as the current sinking electrode. Voltage measurements were taken using the remaining electrodes mounted on the wall of the vessel on all adjacent pairs of electrodes. The

resulting reconstructed images are of comparable quality to those produced using a conventional ERT set-up.

The approach described by Murphy increases the sensitivity towards the centre region of the vessel. However, measurements are limited to be taken at the wall-mounted electrodes, similar to using a conventional ERT set-up. Although there is an increase in unique measurements acquired according to spectral analysis, which means more usable information is available for inverse solving, the information acquired are constrained to regions near the wall. It was shown in the previous chapter that even with the increase of electrodes mounted on the wall of the vessel to increase the number of measurements, the benefits of the increase in number of measurements reaches a saturation point in terms of improving the spatial resolution. It was also shown in Chapter 3 that the increase in sensitivity does not necessarily improve the spatial resolution of the reconstructed image.

The main differences between this thesis and Murphy's work are that, in this thesis, the internal electrodes are used for voltage measurements and the electrodes are not mounted on an internal structure which is part of the process vessel. This enables localized voltage difference measurements to be acquired, targeting to provide more measurements from different locations to improve the resolution of reconstructed images. This means unique information inside the vessel, which may not be accessible using a conventional ERT set-up, can be acquired. The internal electrodes are also given the freedom to assume any position and orientation within the vessel.

The implementation of the EET approach is more direct in terms of modelling, forward and inverse solving in comparison to the AET approach. The conventional measurement strategies used are required to be modified to include voltage measurements taken using the internal electrodes. In other words, for each current injection pattern, the measurement strategy is modified to include the extra voltage measurements which will be taken using the internal electrodes. The extra measurement is only taken on a pair of electrodes located on the same pill, referred to as the 'extended measurement'. The localized voltage measurements that are acquired are no different that are acquired using the conventional electrodes system. Therefore, modifications are only made to the inverse model, but no modification to the inverse solving algorithms is required. One of

the considerations that should be made is the inclusion of the body of the ad hoc pills into the model. This step is taken such that forward voltages and the Jacobian matrix can be calculated to a better accuracy, to accommodate the influence of the presence of the ad hoc pills.

One of the main challenges that has been identified is the sensing system on the ad hoc sensor does not share the same reference or earth as the tomograph. The anticipated instrumentation system contained in the wireless and ad hoc pilled is battery-powered. This means the measurement system and the current injection source have separate reference grounds. This could potentially pose an issue regarding the stability of measurements. This will be investigated using spectral analysis.

5.4.1 Feasibility Study for Extended Electrical Tomography

The aim for this study is to investigate the possibility of using voltage measurements from internal ad hoc electrodes to enhance electrical tomography images. For this preliminary effort, the pill is modelled as a cube for simplicity in terms of modelling. Each pill is furnished with two electrodes that are located on opposite sides of each other, as shown in Figure 5.10. Voltage difference measurements are acquired on an electrode pair located on the same pill, which is referred to as an 'internal electrode pair'. For the preliminary simulation, an ad hoc pill is used with the pill located in the central position of the electrode plane.

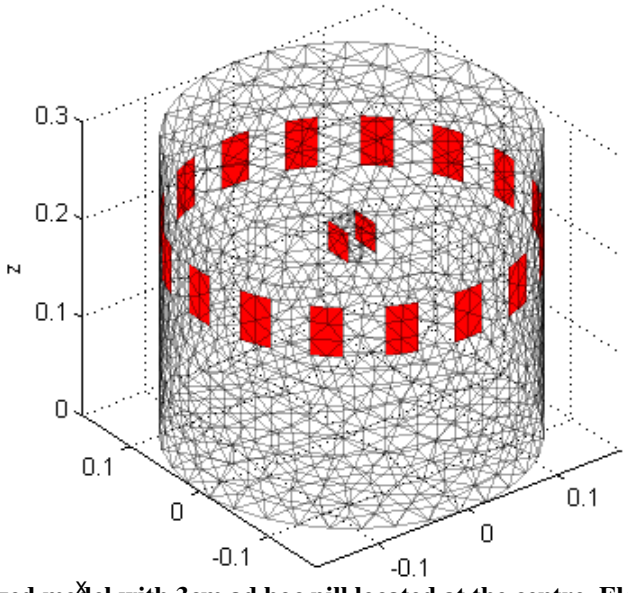

Figure 5.10 Discretized model with 3cm ad hoc pill located at the centre. Electrodes are highlighted in red. The scales are in metres.

Simulations were done using a cylindrical model which is 34cm in diameter and 30cm in height. The 16 wall electrodes are 5cm in height and 3cm in width. Dimensions are chosen according to the dimensions of the vessel which will be used for laboratory experiments in the latter stage of this work. A single plane of 16 electrodes, arranged in planar arrangement is used. The centre of the electrodes is 20cm from the base of the vessel and these are equispaced on the wall of the vessel, as shown in Figure 5.10.

Simulations for the conventional ET approach were done without the inclusion of the ad hoc pill. This is done to investigate the influence that the ad hoc pill has on the measurements. The model that is used for the extended ET (EET) approach is shown in Figure 5.10 and the electrodes arrangements is as shown in Figure 5.11. The ad hoc pill is modelled as a 3cm cube. This is approximately 9% of the diameter of the vessel. The size of the pill is chosen to be reasonably large for the purpose of this preliminary test, which is to evaluate the feasibility of the EET approach. Early simulations indicate that the size of electrodes and separation between electrodes are to be sufficiently large to produce measurable voltage difference. Simulations are done using the EIDORS toolkit (Polydorides and Lionheart, 2002). A homogeneous background with 0.01S/m is used (typical conductivity of tap water). Voltages are simulated using the adjacent strategy and are shown in Figure 5.12.

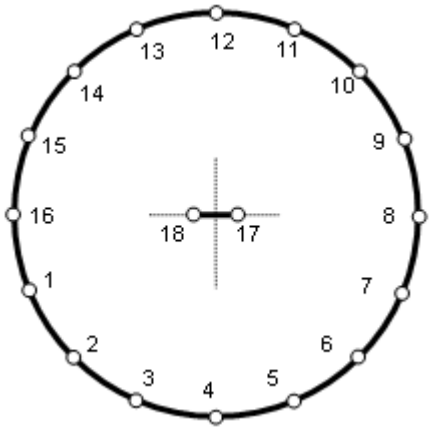

Figure 5.11 Electrodes arrangement showing a single 16-electrodes plane and a pair of internal electrodes

The measurement index in both plots in Figure 5.12 refers to the unique number in the data acquisition sequence. In Figure 5.12(a), the first 14 measurements are taken when electrodes 1 and 2 are used as current injection electrodes. Typically, when using the

adjacent with reciprocity strategy, 13 voltage difference measurements are acquired when electrodes 1 and 2 are used for current injection, with voltage difference measured at electrodes 3 and 4, followed by voltage difference measured at electrodes 4 and 5, and so on. Using the EET approach, each current injection results in an extra measurement. This results in the 14th voltage difference measurement obtained for the electrodes on the ad hoc pill, which are numbered electrodes 17 and 18 (referring to Figure 5.11). The extended measurements, acquired on the electrodes attached to the ad hoc pill are highlighted in red in Figure 5.12(a) and are isolated and shown in Figure 5.12(b). In figure in Figure 5.12(b), the measurement index refers to measurements taken at each current injection. For example, measurement 1 is taken when current injection electrodes 1 and 2 are used; measurement 2 is taken when current injection electrodes 2 and 3 are used, and so on. The simulated voltages indicate that measurable voltage difference can be acquired. According to Figure 5.12(b), the smallest magnitude of voltage difference is approximately 2.3mV peak-to-peak, which is measurable voltage difference for the instrument used.

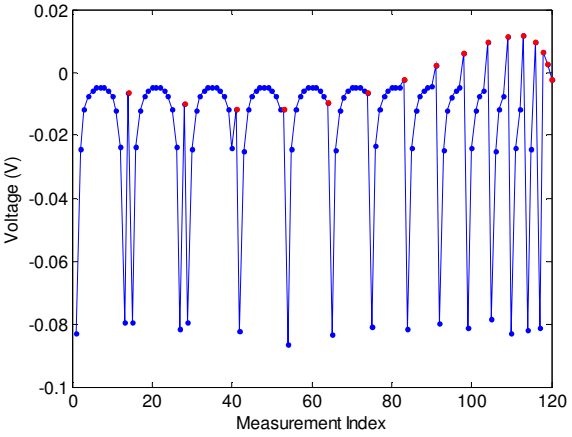

(a) full EET measurements (extended measurements highlighted in red)

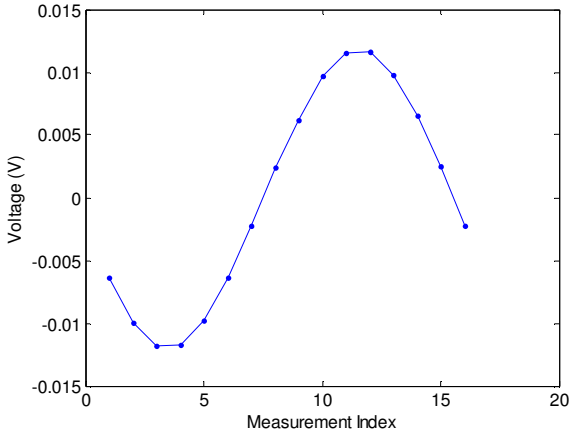

(b) only extended measurements

Figure 5.12 Simulated voltage difference measurements using the adjacent strategy for EET with a 3cm cube.

Isolating the extended measurements, shown in Figure 5.12(b), the plot takes the shape of a sinusoidal wave. Measurements are taken for each current injection rotating through each adjacent pair of wall-mounted electrodes. Therefore the orientation of the current injecting electrodes and the internal electrodes vary. Depending on the current path cutting through the internal electrodes, the measured magnitude of the voltage difference and its polarity varies. For example, with the position of the internal

electrodes in the central position and aligned parallel to the wall-mounted electrodes 8 and 16, the biggest measured magnitudes are taken when current injections are at electrode pairs 3 and 4, 4 and 5, 11 and 12, and 12 and 13. These measurements are acquired corresponding to current injection electrodes at 90^{o} to the internal electrodes, when the current paths cutting through the internal electrodes are greatest.

Figure 5.13 shows the SVD plot comparing measurements obtained using conventional ERT and the EET approach. The quality, in terms of uniqueness and stability of measurements is evaluated. For each current injection, each pair of internal electrodes produces an extended measurement. Therefore, for the adjacent current injection strategy for 16 electrodes in a planar arrangement, 16 extended voltage difference measurements are acquired. The SVD plot indicates that 119 out of 120 measurements are unique. Knowing that the adjacent with reciprocity strategy produces 104 unique measurements, it can be inferred that 15 out of the 16 extended measurements taken using the adjacent current injection strategy are unique. In terms of stability of the measurements, the magnitudes of both sets of singular values are similar. This indicates that the inclusion of the ad hoc pill does not degrade the stability of the conventional ERT measurements and the extended measurements are stable.

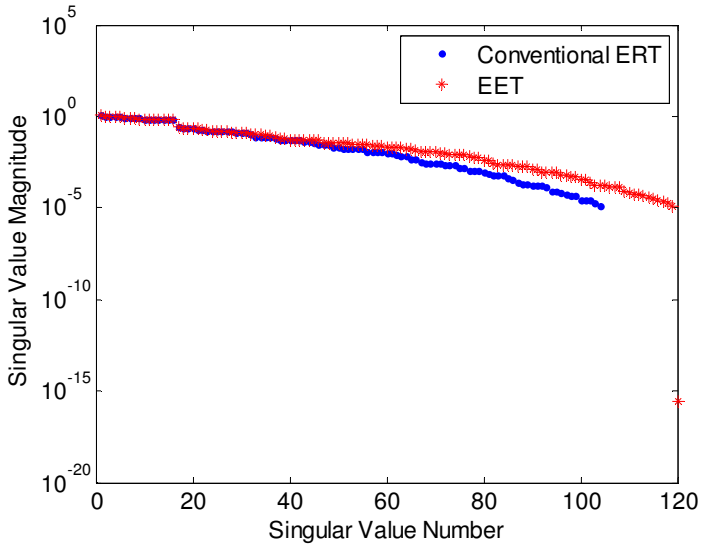

Figure 5.13 Spectral Analysis comparing conventional ERT and EET for the adjacent strategy

Figure 5.14 shows the variation of maximum sensitivity magnitudes across the electrode plane. It is interesting to observe that in the vicinity of the ad hoc pill (located at the centre of the vessel) the detectability increases. The internal electrodes allows localized measurements to be taken, which means that the effect of the changes in conductivity

can be measured, hence providing an improvement in detectability. This can be seen more clearly when comparing Figure 5.14(b) and Figure 5.14(c). In Figure 5.14(c), it can be seen that the sensitivity around the ad hoc pill is improved in general, while in Figure 5.14(b), the sensitivity is the lowest in the centre region.

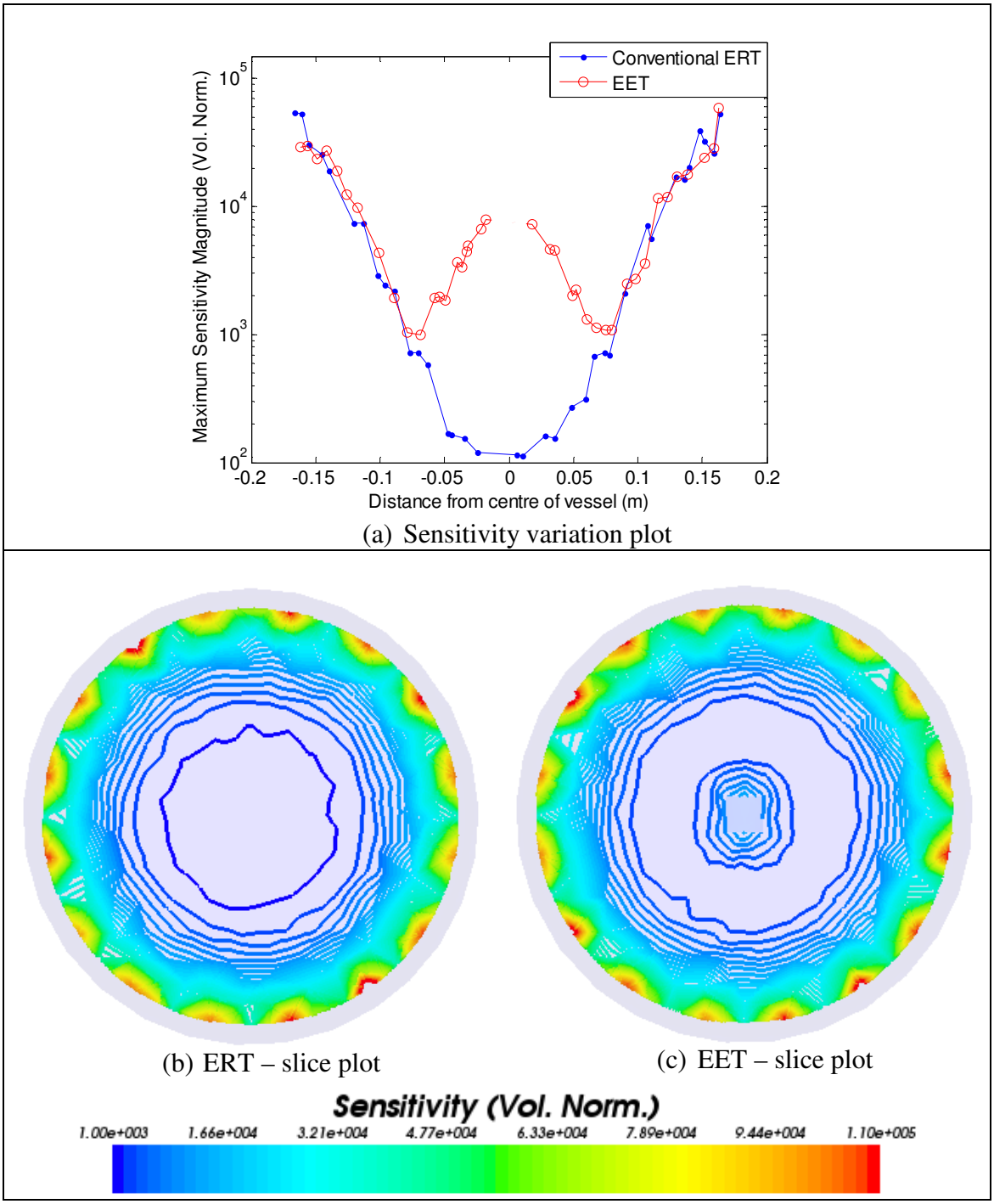

(a) Sensitivity variation plot

(b) ERT – slice plot

(c) EET – slice plot

Figure 5.14 Sensitivity Analysis comparing conventional ERT and EET for the adjacent strategy on the electrode plane

Figure 5.15 compares the spatial resolution across the electrode plane between conventional ERT and EET. The simulated voltages are imposed with 60dB Gaussian noise. This approximates system noise when using the LCT2 instrument. The resolution matrix is computed using 80 singular values for conventional ERT and 90 singular values for EET. The numbers of singular values are chosen based on the DPC (Hansen 1998) plots that are computed.

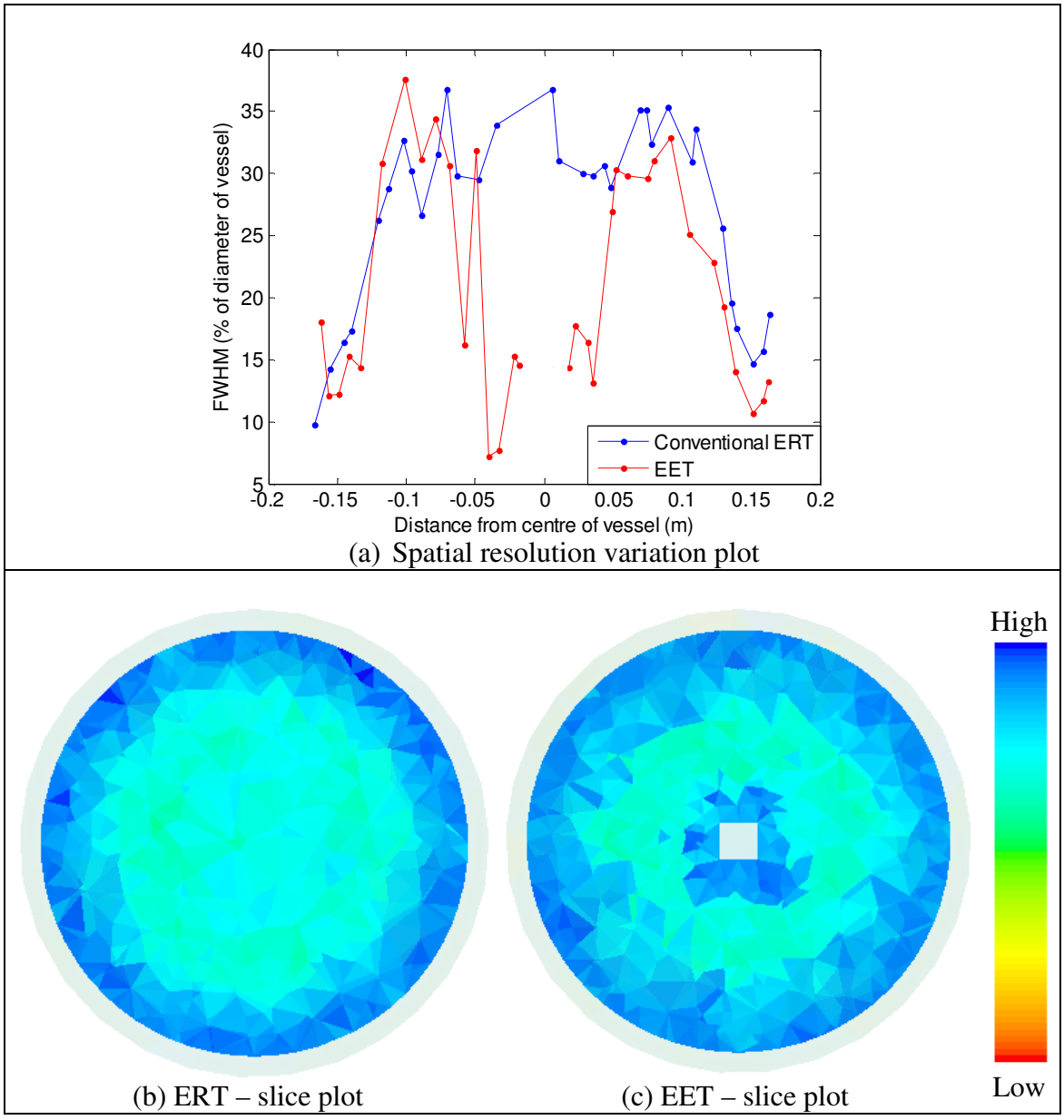

(a) Spatial resolution variation plot

(b) ERT – slice plot

(c) EET – slice plot

Figure 5.15 Spatial resolution analysis comparing conventional ERT and EET for the adjacent strategy on the electrode plane

It can be seen that there is an improvement in spatial resolution around the vicinity of the ad hoc pill in Figure 5.15(c). From the plots shown in Figure 5.15(a), the FWHMs calculated for the voxels near the vicinity of the ad hoc pill are close to those observed near the wall of the vessel. Better resolution is observed in a larger region comparing both approaches (Figure 5.15(b) and (c)).

Referring to the plots shown in Figure 5.15(a), it can be seen that there are small numerical mismatches in both plots, which is likely to be due to the differences in the discretized models. Although the meshing criteria are set to be as similar as possible to reduce the impact of the level of discretization on the computed resolution, the inclusion of the ad hoc pill as part of the structure in one of the models will have an impact on the voxel sizes.

Simulations were repeated for the opposite strategy. For a 16 electrode planar arrangement, eight extended measurements are acquired using the opposite strategy. Similarly, simulations were performed using the EIDORS toolkit. Voltages were simulated on a homogeneous background with 0.01S/m conductivity. The simulated voltages are as shown in Figure 5.16. The simulated voltages indicate that measurable voltage difference can be acquired.

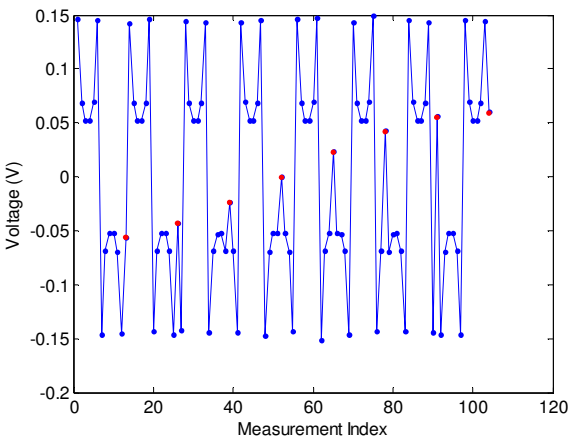

(a) full EET measurements (extended measurements highlighted in red)

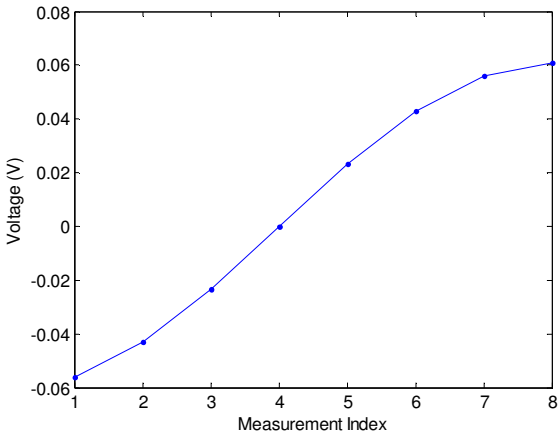

(b) Opposite strategy – only extended measurements

Figure 5.16 Simulated voltage difference measurements using the opposite strategy for EET with a 3cm cube.

Figure 5.17 shows the spectral analysis using SVD to compare the stability of measurements. The SVD plot for conventional ERT indicates that 76 out of 96 measurements are unique. In other words, 20 singular values have magnitudes which are zero to machine precision and are therefore deemed redundant. The SVD plot for EET indicates that 84 out of 104 measurements are unique. This means all eight of the extended measurements are unique. Similar to the adjacent strategy, the stability of measurements are similar to the measurements obtained using the EET approach.

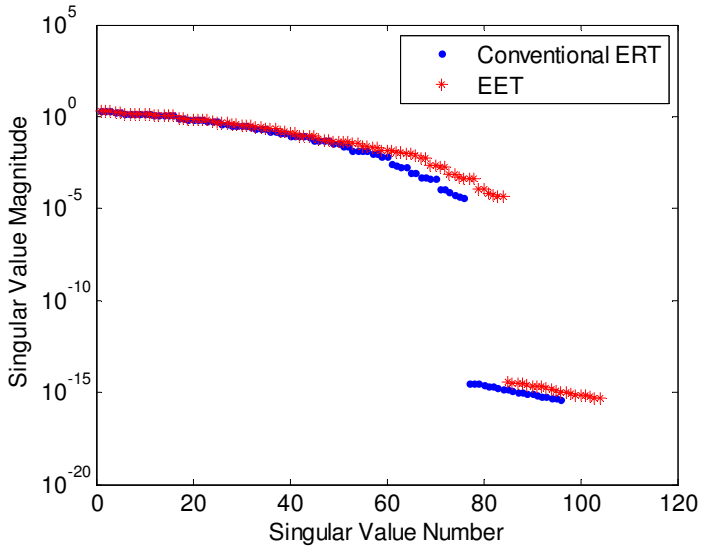

Figure 5.17 Spectral Analysis comparing conventional ERT and EET for the opposite strategy

The sensitivity analysis in Figure 5.18 shows the effect of the internal electrodes on the detectability. Similar to the sensitivity analysis for the adjacent strategy in Figure 5.15, there is an increase in detectability in the vicinity of the internal electrodes. The improvement is significantly higher in comparison with the improvement observed for the adjacent strategy. Near the wall, the magnitudes are almost similar to those for conventional ERT. This can be seen more clearly in Figure 5.18(c).

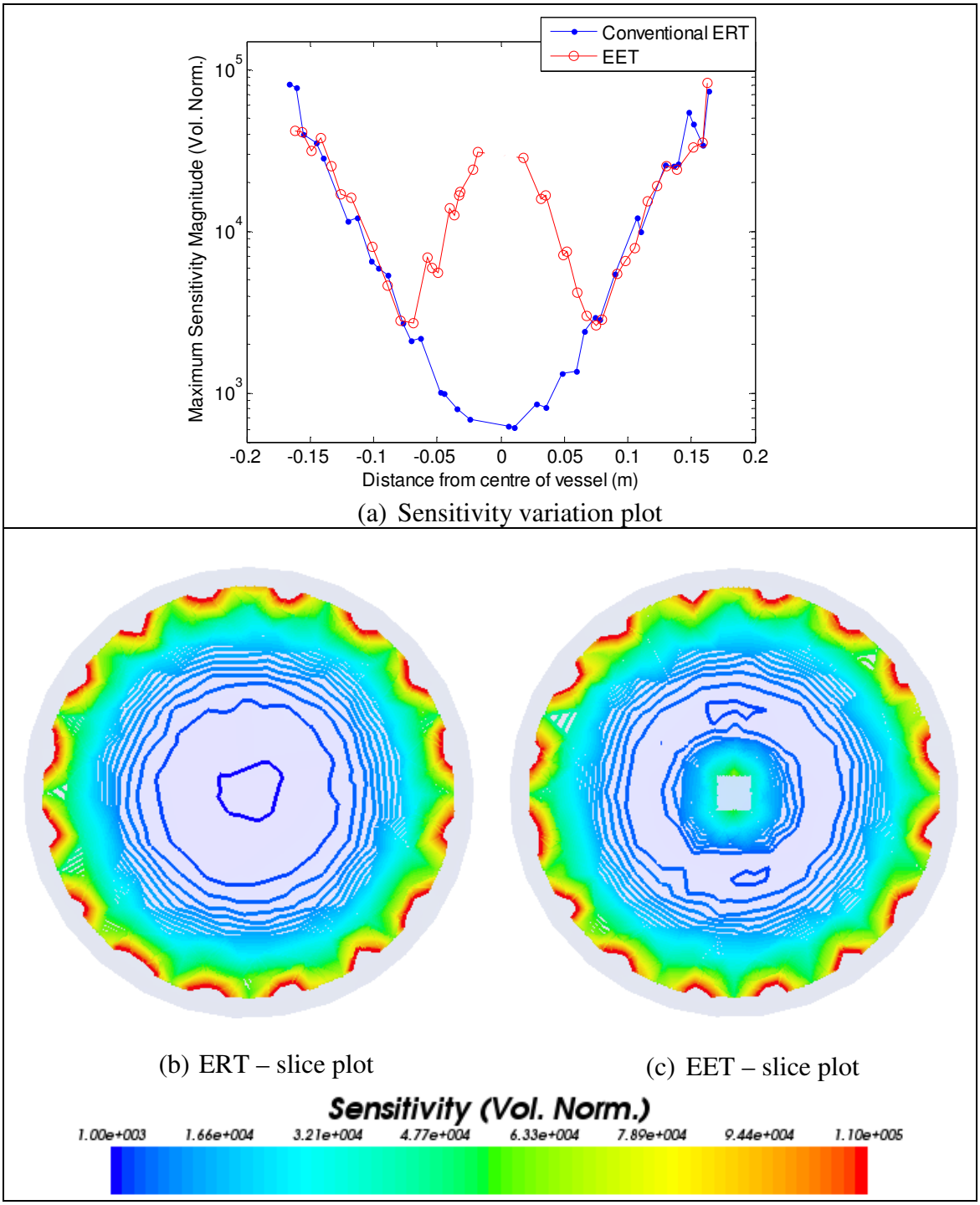

Figure 5.18 Sensitivity Analysis comparing conventional ERT and EET for the opposite strategy on the electrode plane

Figure 5.19 compares the spatial resolution across the electrode plane for conventional ERT and EET approach using the opposite strategy. The resolution matrices that are used to compute the spatial resolution for both the conventional ERT and EET uses 60 singular values. The number of singular values used is approximated by applying the DPC, using simulated voltages with 60dB Gaussian noise imposed. Although all eight extended measurements obtained using a single ad hoc pill are unique, the number of

additional usable measurements is insignificant in comparison to the overall number of usable measurements that can be used for inverse solving.

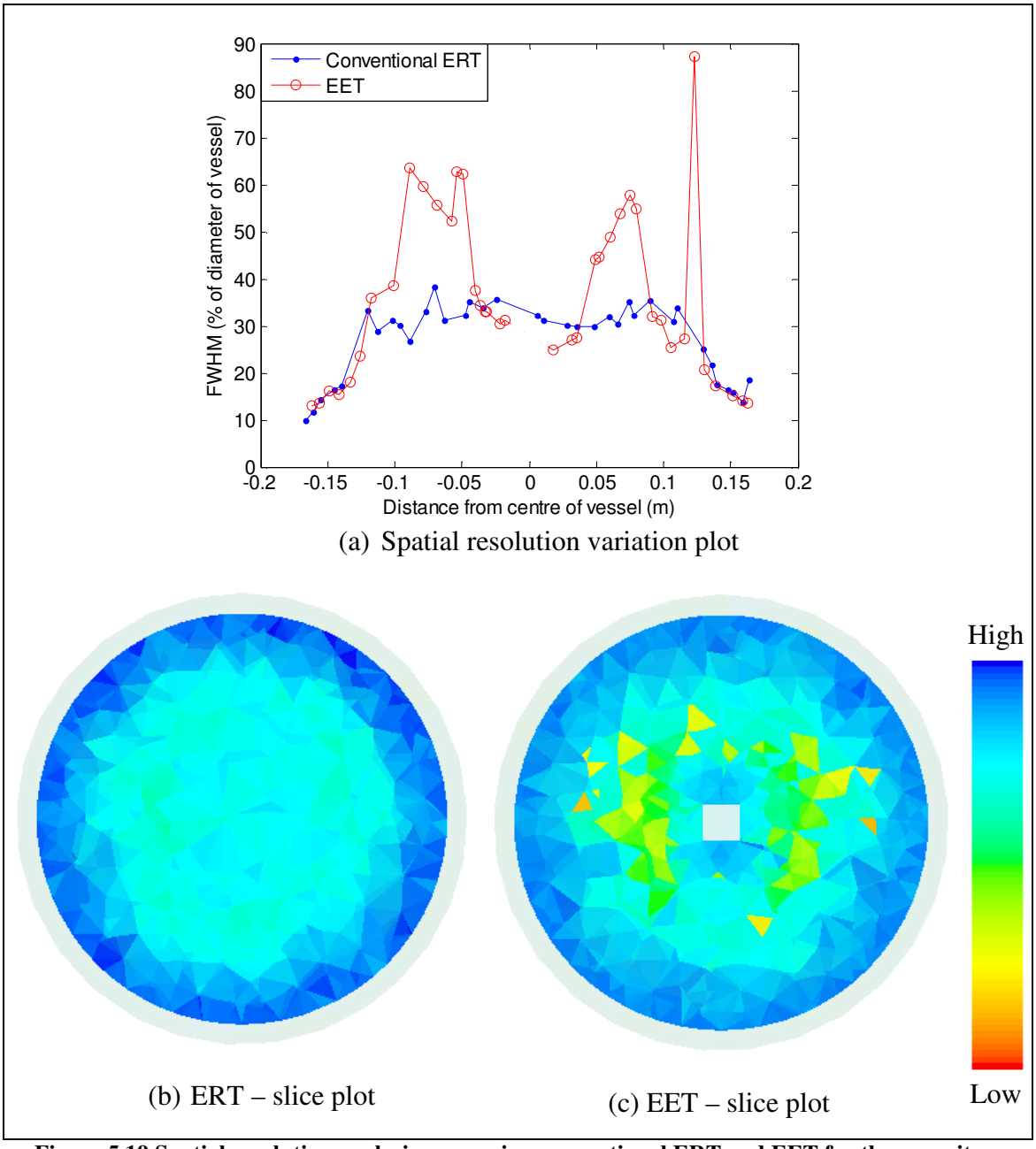

Figure 5.19 Spatial resolution analysis comparing conventional ERT and EET for the opposite strategy

It is shown in Figure 5.19 that using the opposite strategy, the inclusion of the ad hoc pill has a negative impact on the spatial resolution. The spatial resolution in the region between the wall of vessel and the ad hoc pill degrade when using the EET approach as shown in Figure 5.19(a). Similar degradation is observed at similar radius elsewhere on the plane as shown in Figure 5.19(c). The spatial resolutions for the elements in the

vicinity of the ad hoc pill are improved by an insignificant amount in comparison with the improvement seen for the adjacent strategy.

The degradation in resolution is a surprising result. The sensitivity analysis indicates no degradation in detectability due to the inclusion of the ad hoc pill. The reason for the degradation is likely to be due to the inclusion of the ad hoc pill, as the comparison shown in Figure 5.14 indicates that the influence due to the difference in meshing is unlikely. Using the opposite current injection strategy, the current path travelling across the plane and the presence of the ad hoc pill forces the current paths to divert. This is likely to disrupt the current field and the measurements acquired, and therefore degrading the spatial resolution.

In conclusion, based on the analysis shown in the feasibility studies, the EET approach is shown to be capable of improving the spatial resolution of images. There are factors that require consideration and further exploration. As the feasibility study suggested, the adjacent strategy is more appropriate and the application of the EET approach. The spatial resolution analysis suggests that the EET approach has a positive impact on the resolution for the adjacent strategy.

5.5 Summary for Wireless 'Pills' and Electrical Resistance Tomography

This chapter aims to investigate the possibility of utilising ad hoc sensors with a conventional ERT setup. Two approaches were investigated through feasibility studies, namely the augmented electrical tomography (AET) and the extended electrical tomography (EET) methods. The AET approach acquires localized conductivity measurements, while the EET approach acquires localized voltage difference measurements. Both methods showed that they can deliver measurable results. Through the feasibility studies, the merits and limitations for each approach were identified.

For the AET approach, the localized conductivity values are included into the inverse solving process. While the effect of the inclusion of the known conductivity values could be observed, the positive effect of the inclusion of the known conductivity on the solution of its neighbouring voxels is not guaranteed. The Non-Linear Gauss-Newton algorithm is chosen for this work, as the algorithm runs iteratively and the Jacobian matrix is recalculated for the following iteration of the solution after the estimated solution has been calculated and informed with the known conductivity.

However, there is a lack of control over how the known conductivity influence the estimated solutions of the voxels in the vicinity of the known element using this algorithm. This means the estimated solutions which are influenced by the known conductivity is not always adjusted to be closer to the actual solution. A more successful implementation of this approach is restricted by the inverse algorithm used. Further progress of this approach requires deeper mathematical consideration of the inverse problem.

The feasibility study for the EET approach indicates that the extended measurements using the adjacent strategy are capable of improving the spatial resolution, according to the spatial resolution analysis. Measurable voltage difference can be acquired and the extended measurements are unique, according to the spectral analysis. The feasibility study indicates that the adjacent strategy is more suitable for the application of the EET approach in comparison with the opposite strategy, as the spatial resolution analysis for the opposite strategy shows degradation in resolution when using the EET approach.

The extended measurements can be implemented directly into the inverse solving process as the measurements are used in the same way as conventional voltage measurements acquired using wall-mounted electrode pairs. One of the challenges to implementing the EET approach is to acquire the voltages under the constraints of a wireless pill. The system has to be battery-powered and will therefore have a different reference ground to the tomograph. The effect of difference in grounding on the stability of the measurement has to be investigated. Further explorations include varying the position and orientation of the ad hoc pill and effect on the stability of measurements, sensitivity and stability. Eventually, the effect of using multiple ad hoc pills should also be evaluated.

Comparing both approaches, EET provides more research interest from an engineering perspective. The next chapter further investigates issues of EET, including pill size, electrode size, effect of location and orientation of the internal electrodes and their effect on the stability of measurements, sensitivity and spatial resolution. Laboratory experimentation have been undertaken to evaluate the practical implementation of the approach.

CHAPTER 6
APPLICATION OF EXTENDED ELECTRICAL TOMOGRAPHY

Following the feasibility studies in Chapter 5, the extended electrical tomography (EET) approach is further explored in this thesis. The results from the feasibility study show that the extended measurements contain unique information, thus adding to the number of unique measurements from a conventional measurement dataset. The sensitivity and spatial resolution are predicted to improve in the vicinity of the ad hoc pill. This chapter takes a more in-depth look into the EET approach, including the hardware requirement for laboratory experiment, effect of varying position and orientation of the ad hoc pill, and using multiple ad hoc pills.

Section 6.1 describes the hardware requirement for implementing the EET approach to verify the simulation results. The overall experimental set-up is described and details are further discussed in three subsections. Subsection 6.1.1 describes the Standalone Voltage Measurement System (SVMS) which is used to acquire voltage measurements from the electrodes on the ad hoc pills. The system is designed to be battery-powered, such that it has a floating ground to mimic the system anticipated on a wireless pill. Subsection 6.1.2 describes the vessel used. The vessel is designed to be sufficiently large such that experiments to investigate the effect of ad hoc pills with a conventional ERT system can be carried out. The characterization of the vessel is detailed. Subsection 6.1.3 discusses the design of the 'pill' that is used for the experiments.

Section 6.2 discusses modelling aspects of the EET approach. Two aspects were investigated. The first is the effect of the inclusion of the ad hoc pill on the voltage difference measurements. The second aspect is the effect of measurements acquired from two instruments with different ground references. As measurements acquired using the SVMS has a floating reference, the stability of the measurements is investigated.

Section 6.3 investigates the effect of varying position and orientation of the ad hoc pill on the stability of measurements, sensitivity and resolution. In Subsection 6.3.1, the effect of moving the ad hoc pill along the horizontal and vertical axes is explored. The influence on the stability of measurements, sensitivity and resolution is investigated. Image reconstruction for selected cases is compared for conventional ERT and EET method. Subsection 6.3.2 investigates the effect of varying the orientation of the pill on the measurements. Similarly, the influence of the varying orientation of the pill on stability of measurements, sensitivity and resolution is compared. Selected cases of image reconstruction are compared.

Section 6.4 briefly discusses the effect of using multiple ad hoc pills. The effect on stability of measurements, sensitivity and resolution is investigated. Reconstructed images are also compared for conventional ERT and EET.

6.1 Hardware Requirement

Implementing the EET approach requires a standalone voltage measurement system in addition to a conventional ERT system. An existing tomograph can be used without requiring any modifications. The standalone voltage measurement system is contained within the ad hoc pill and measurements are to be taken for each current injection pattern. This requires a synchronization protocol, which will affect the measurement strategy to include measurements on the ad hoc electrodes. Information on the location of the ad hoc pill and the orientation of the internal electrode pairs are given a separate localization system of the ad hoc pill. For present purposes, position and orientation of the pill is determined manually.

The experimental set-up for the EET system is shown in Figure 6.1. The LCT2 tomograph is used together with a standalone voltage measurement system (SVMS). The SVMS is designed to mimic the features of the anticipated system for the wireless pill. At current stage, the internal electrodes are hardwired to the measurement terminals of the SVMS. The SVMS, vessel and the ad hoc pill are discussed in the following subsections.

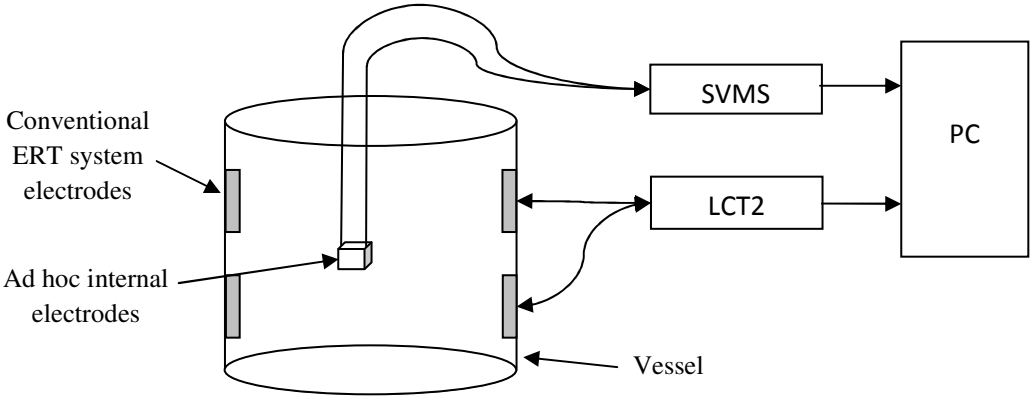

Figure 6.1 Block diagram showing the experimental layout for EET

6.1.1 Standalone Voltage Measurement System

The standalone voltage measurement system (SVMS) was originally designed as a development board for the Functional Electrical Impedance Tomography by Evoked Response (fEITER) project (McCann et. al. 2006). The SVMS is designed to have an isolated ground, which mimics the anticipated system for the wireless pills. The instrumentation circuit, which measures the voltage difference across two electrodes is battery-powered, a feature similar to the instrumentation system contained within a wireless pill. The instrumentation circuit and the data transfer circuit (DAQ) are isolated using opto-isolators. The separation provided by the opto-isolators (~6GΩ||10pF) approximates an isolated pill as the can be considered as open-circuited. This enables data acquisition through cables to the computer with the ground reference for the instrumentation circuit isolated from the common ground.

The instrumentation circuit, as shown in Figure 6.2, consists of two instrumentation amplifiers (AD8222) and an analog-to-digital converter (ADC) driver. The gain of the instrumentation amplifier is set to approximately 10. The second instrumentation

amplifier serves as a low-pass filter. The analog signals from the outputs of the second instrumentation amplifier go through an ADC that is interfaced to a programmable logic device (PLD). The PLD provides control of the ADC, governing the sampling and data transfer. Serial data from the ADC are stored and reshaped into 16-bit parallel data in the PLD. From the PLD, the 16-bit data are transferred to the computer through a digital data acquisition card, via 16 opto-isolators. 5,000,000 samples are captured and stored for each measurement, at a sampling rate of 250k samples/s. The data are stored in binary format, which is then converted into RMS and amplitude values through post-processing done in Labview. The amplitude values are integrated into a frame of measurement.

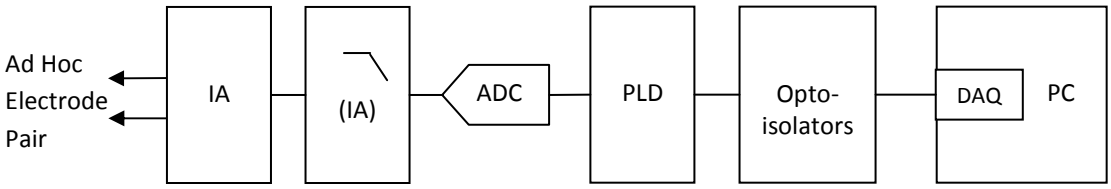

Figure 6.2 Block diagram of the SVMS

The SVMS was calibrated using a Fluke 8845A digital multi-meter (DMM) as a reference. Using the constant-voltage current source provided by the LCT2 instrument, measurements were acquired using the SVMS and compared with measurements obtained using the DMM. Measurements were taken and compared for a range of voltages. The purpose of this calibration was to calibrate the post-processing software, as well as to evaluate the performance of the SVMS. The results are as shown in Figure 6.3 and Table 6.1.

The results indicate that measurements obtained using both systems are in good agreement with the expected values, with the exception for values on the lower end of the scale (~ <8mV). This validates the performance of the SVMS.

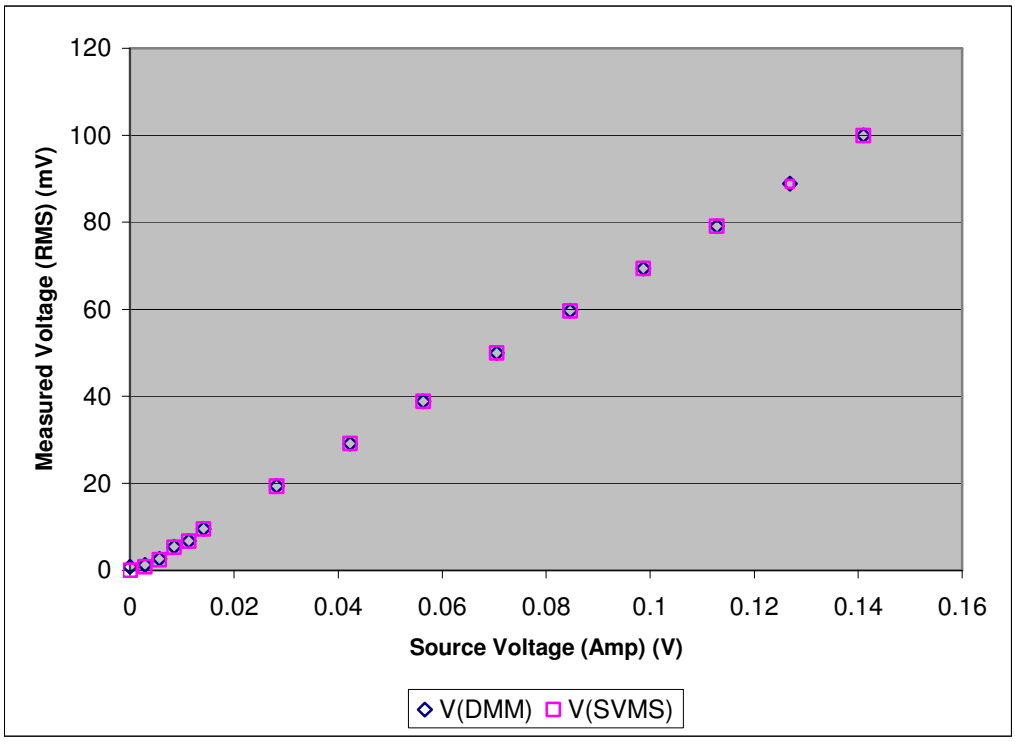

Figure 6.3 Calibration result for the SVMS

Table 6.1: Comparison of measurements taken using the Fluke 8845A DMM and the SVMS

Voltage Source Amplitude (mV)	Corresponding V RMS Value (mV)	Measured V RMS Value (mV)	
		DMM	SVMS
0	0	0.8	0.0
3	2	1.2	0.8
6	4	2.6	2.4
8	6	5.4	5.4
11	8	6.8	6.7
14	10	9.6	9.5
28	20	19.3	19.3
42	30	29.1	29.1
56	40	38.8	38.8
71	50	49.9	49.9
85	60	59.6	59.6
99	70	69.4	69.4
113	80	79.1	79.0
127	90	88.8	88.8
141	100	99.9	99.9

One of the drawbacks of the SVMS is its relatively slow data acquisition time. Each measurement takes approximately 20s and is taken manually, therefore extending the data acquisition time. Another issue is that the SVMS only provides the magnitude of the voltage difference and not the polarity. The polarity of the voltage difference measured is added manually based on prior knowledge of the position and orientation of

the internal electrode pair relative to the current injection electrode pair. This is a feature of the anticipated system for the wireless pill as well. As the ad hoc pills are free to assume any location and orientation within the vessel, the current gradient varies in comparison with a fixed set of wall-mounted electrodes. Therefore the polarity of the measurements should be determined based on knowledge of the position and orientation of the ad hoc pills when the measurements were taken.

6.1.2 Vessel

A cylindrical test vessel was built for laboratory testing of the EET approach. The size of the vessel was chosen such that it is sufficiently large for laboratory-scaled testing of the EET method. This means the vessel should be sufficiently large to accommodate reasonable-sized ad hoc pills in the vessel. The vessel is 34cm in diameter and 55cm in height, and manufactured from Perspex and is shown in Figure 6.4. The vessel is designed to accommodate up to four planes of 16 electrodes per plane. For the present purposes, only two planes of electrodes have been used. The centre of the bottom electrode plane is 10cm from the base of the vessel and the centres of electrode planes are located 10cm apart. The electrodes are 5cm by 3cm in dimensions and are silver-plated. This vessel is referred to as the ‘silver vessel’ here. All the models used in this thesis are based on the dimensions of this vessel.

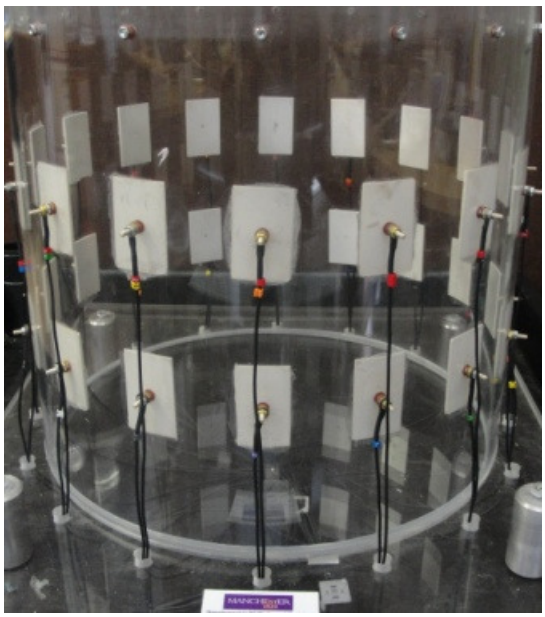

Figure 6.4 Photo of the ‘silver vessel’

The silver vessel was characterized to evaluate the performance of the vessel design. A smaller vessel was used as reference, as the silver vessel is a scaled-up version of the smaller vessel. Details of the smaller vessel are included as the characterisation of the silver vessel is compared to the performance of this vessel. The smaller vessel is 11cm in height and 14cm in diameter, and manufactured from Perspex. The vessel is furnished with two planes of gold-plated electrodes, each plane consisting of 16 electrodes which are 3cm by 1cm. This vessel is referred to as the 'gold vessel'. This vessel has been used extensively previously and has shown to produce reliable results.

A repeatability test was conducted to evaluate the performance of the silver vessel. Ten frames of measurements were taken using the LCT2 tomograph (York et. al. 2005). The adjacent with reciprocity strategy is used. 208 measurements were acquired for each frame of measurement using the two planes of 16 electrodes per plane set-up. Measurements were taken for a homogeneous distribution of tap water (conductivity of ~ 0.10S/m) and each frame of measurements was taken a minute apart. The standard deviations and signal-to-noise ratios (SNR) were calculated for each measurement. The SNRs are calculated as:

$$SNR = 20\log_{10}\frac{V_{mean}}{standard\ deviation} \tag{6.1}$$

The mean and worst SNRs and standard deviations are as shown in Table 6.2. The calculated numbers indicates that the performance, in terms of repeatability is similar with the gold vessel. This suggests the measurements acquired using the silver vessel are comparable to those taken using the gold vessel.

Table 6.2: Comparison of SNR and standard deviation between data sets using the gold and silver vessel

	SNR (dB)		Standard Deviation (V)	
	Mean	Worst	Mean	Worst
Gold Vessel	58.8	47.7	$4x10^{-5}$	$3x10^{-4}$
Silver Vessel	55.8	43.6	$2x10^{-5}$	$1x10^{-4}$

The SNR profiles are plotted and compared with those from the gold vessel in Figure 6.5. The variability of the noise levels associated with the silver vessel is slightly larger

and this is likely to be due to the increase in diameter of the vessel and hence the separation between electrodes. Measurements with the lower SNRs are consistent with measurements acquired where the measuring electrodes are located further away from the current injecting electrodes. This comparison suggests that the scaling-up effect is insignificant and the degradation is minimal in this case.

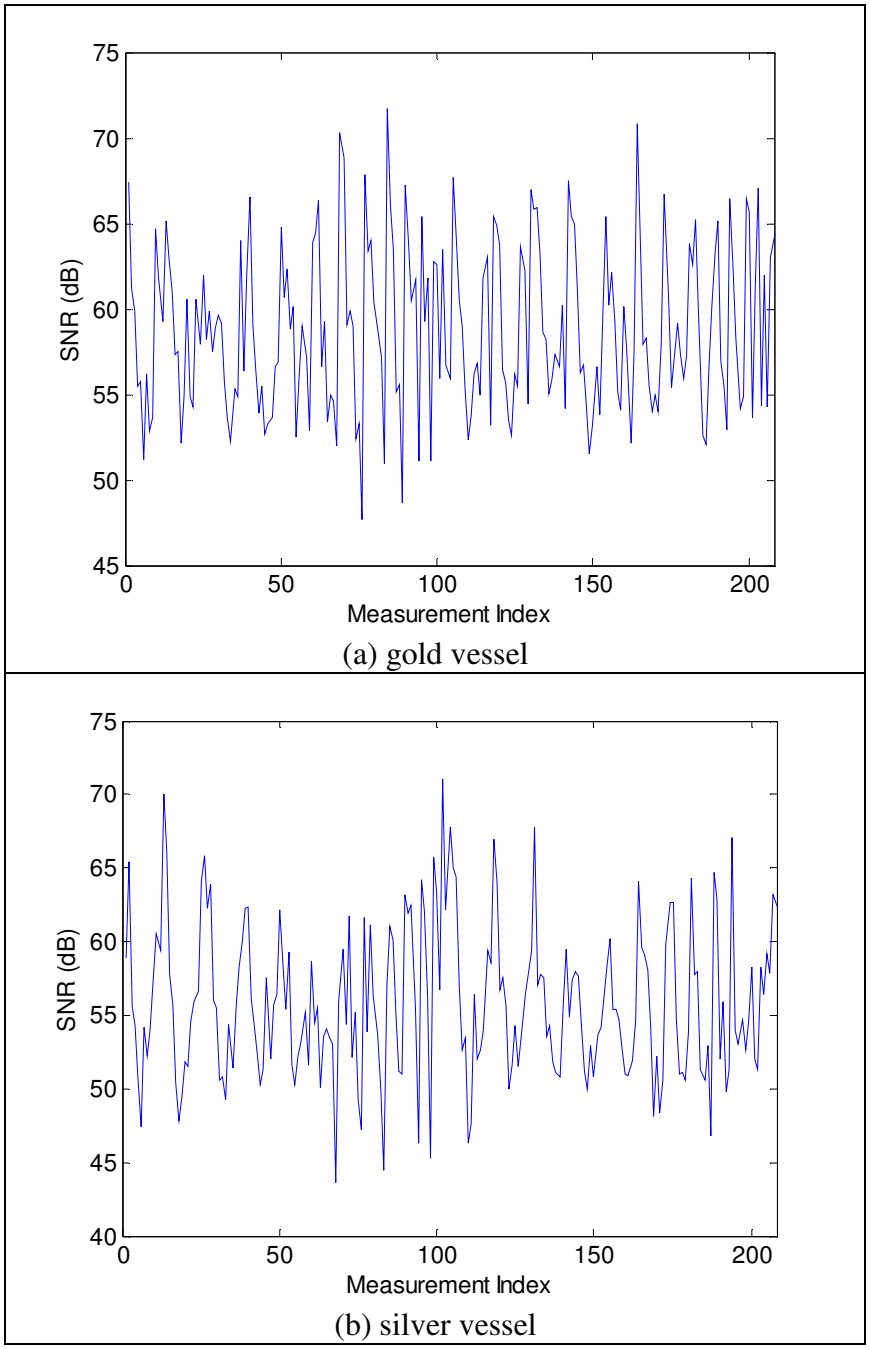

Figure 6.5 Comparison of SNR profile for (a) gold and (b) silver vessels

The measurements acquired are compared to the simulated voltages to evaluate any differences. Simulated voltages are computed using the EIDORS toolkit on a discretized

model. The set-up is similar to that described above. A two plane with 16 electrodes per plane model was used, and voltages were simulated using the adjacent with reciprocity strategy. The measurements acquired are compared and shown in Figure 6.6.

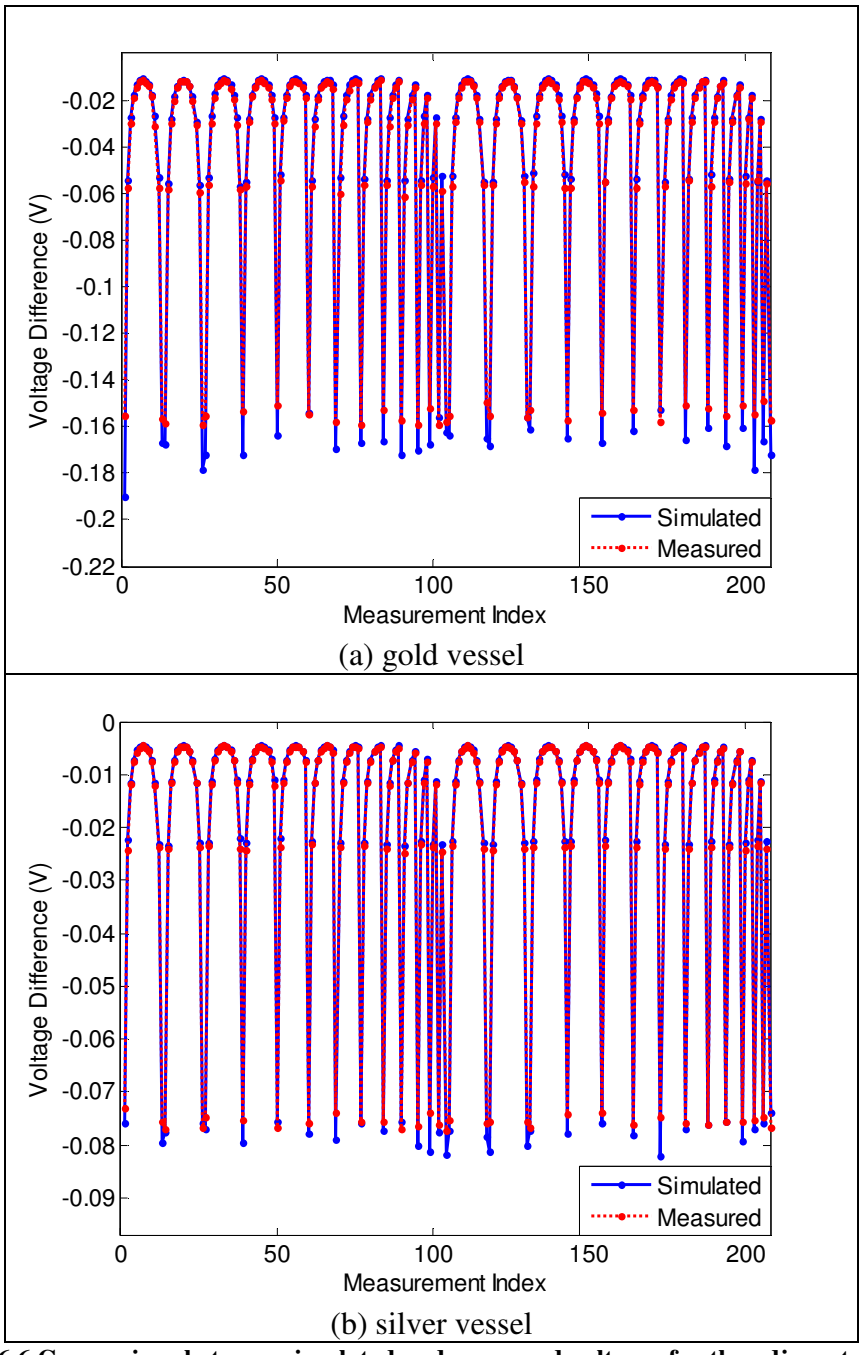

Figure 6.6 Comparison between simulated and measured voltages for the adjacent strategy

Figure 6.6 compares the simulated and measured voltages for both the gold and silver vessel. Both plots indicate that the simulated and measured voltages are well-matched in general. The slight discrepancies are likely to be due to insufficient in the mesh density. In general, the simulated and measured voltages for the silver vessel are better matched

in comparison with those obtained using the gold vessel. This suggests that the performance of the silver vessel is comparable to that of the gold vessel.

6.1.3 Ad Hoc 'Pill'

For the present work, the ad hoc pill is designed as a cube. This enables ease in manufacturing the cubes and simplicity in modelling. It is intended that the pills should be as small as possible. This is to reduce the amount of intrusion to the process and to enable multiple pills to be distributed in the vessel.

An early design of the pill is shown in Figure 6.7. It should be noted that the design of the pill used in this thesis is not intended as a prototype of the wireless and ad hoc pill designed for the WSN4IP project. The pill is manufactured from perspex. Copper plates fully cover two opposite faces of the cube and act as measurement electrodes. The copper plates are replaced regularly such that the surfaces are kept clean and without residue due to electrolysis. The ad hoc pill is fixed onto a stainless steel rod to hold it in place when located within the vessel. At this preliminary stage, the position of the pill is fixed and considered as 'given' information. The rod is approximately 7mm in diameter, which is small in relation to the diameter of the vessel. Therefore, the rod is excluded from the model. Experiments show that this does not affect the measurements taken and the forward voltage and Jacobian matrix calculations, as it can be shown that the simulated and measured voltages are well-matched (an example can be seen in Figure 6.13 in the next section). Coaxial cables, which connect the electrodes to the measurement terminals at the SVMS, are threaded through the stainless steel rod.

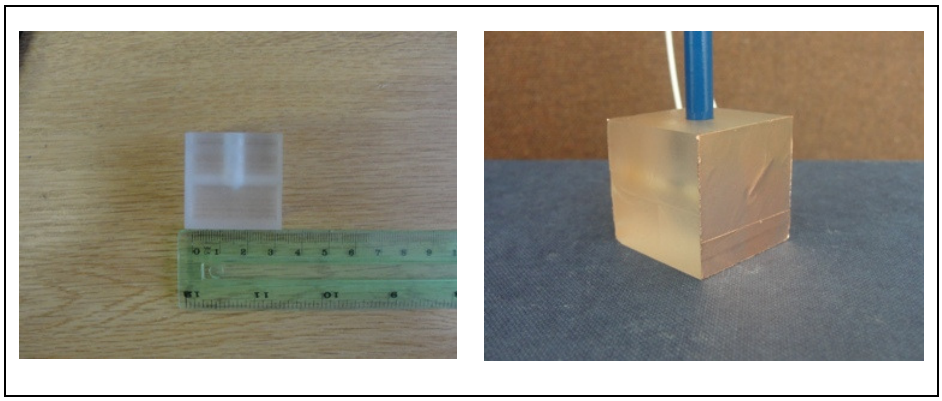

Figure 6.7 Photographs of the ad hoc pill

In subsection 5.4.1, a 3cm cube was used and simulated voltages indicate that measurable voltage difference could be acquired. The dimension was chosen arbitrarily, with the constraint that the dimensions are of a reasonable size to demonstrate the feasibility of the EET approach. To further investigate this factor, this subsection investigates the effect of different pill sizes in order to choose a suitable pill dimension. The size of the cube should be as small as possible in relation to the size of the vessel.

A range of dimensions are considered and compared. Considering the results shown in Section 5.4.1 using a 3cm cube (approximately 9% of the diameter of the vessel), smaller dimensions are considered to investigate whether it is possible to further reduce the size of the pill. The dimensions are reduced to 1cm (approximately 3% of the diameter of the vessel) and 2cm (approximately 6% of the diameter of the vessel). For this investigation, a single plane of 16 electrodes is used with one pill, as shown in Figure 6.8. The pill is located in the centre of the vessel with the electrodes aligned parallel to electrodes 8 and 16 on the wall of the vessel, as shown in Figure 6.8. The centre of the pill is aligned at 0.10cm from the base of the vessel, the same height as the centre of bottom plane of the wall-mounted electrodes. Voltages are simulated for the adjacent current injection strategy, using the EIDORS package.

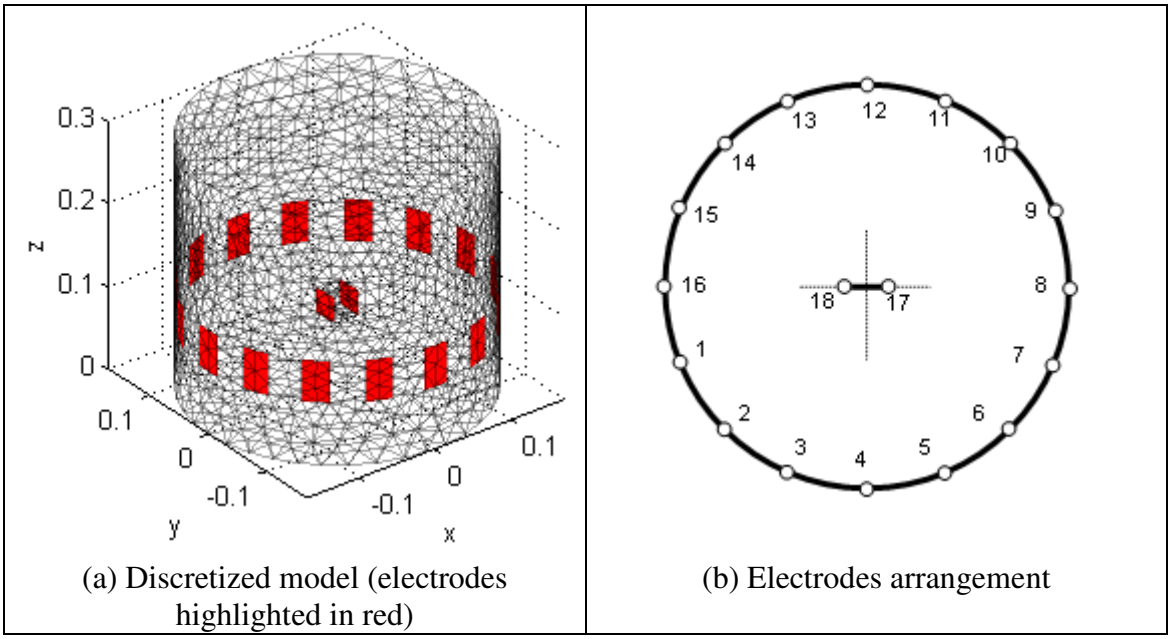

(a) Discretized model (electrodes highlighted in red)

(b) Electrodes arrangement

Figure 6.8 Electrodes arrangement for a 16 electrode model with a pair of internal electrodes

The extended measurements are shown in Figure 6.9. Using the adjacent with reciprocity strategy, there are 16 current injection patterns for 16 boundary electrodes in

a planar arrangement. This results in 16 extended measurements taken on the electrode pair on the pill. The measurement index indicates the voltage difference measured for different current injection patterns. With the increase in the size of the pill, both the separation between electrodes and the area of the electrodes increase. The voltage difference is expected to increase as the separation increases. This is shown in Figure 6.9.

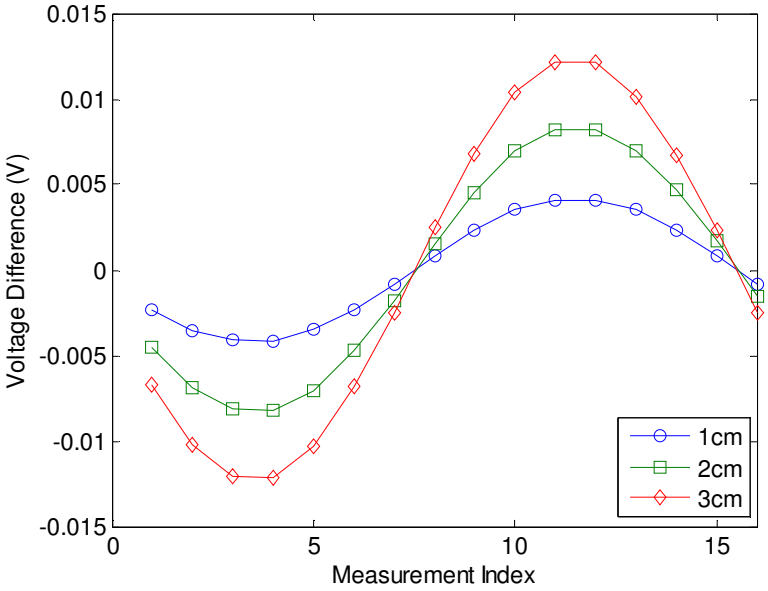

Figure 6.9 Comparison of simulated voltage differences on the ad hoc pill for various pill sizes

The measurement of interest is the smallest magnitude of the voltage differences. The smallest magnitudes of the simulated voltages are as shown in Table 6.3. The smallest voltage difference magnitude for the 1cm pill is approximately 0.8mV. This would pose a challenge to produce consistently accurate measurements using the instrument available. As shown in Table 6.1, the smaller the measured magnitude, the bigger the deviation is from the actual value.

Table 6.3 Smallest simulated voltage difference magnitude for varying pill size

Size of pill	Smallest measured voltage difference magnitude
1cm	0.8mV
2cm	1.6mV
3cm	2.3mV

Experiments were conducted to acquire measurements using the SVMS to evaluate the practicality of acquiring consistently accurate measurements. The arrangement of the

experimental set-up is similar to that shown in Figure 6.8, with the pill located in the centre of the bottom electrode plane. The measurements on the internal electrode pair were acquired using the SVMS while the LCT2 was used as current source through the wall-mounted electrodes. Data were captured using Labview and the RMS values are calculated from the measured amplitudes. The measurements are plotted and shown in Figure 6.10.

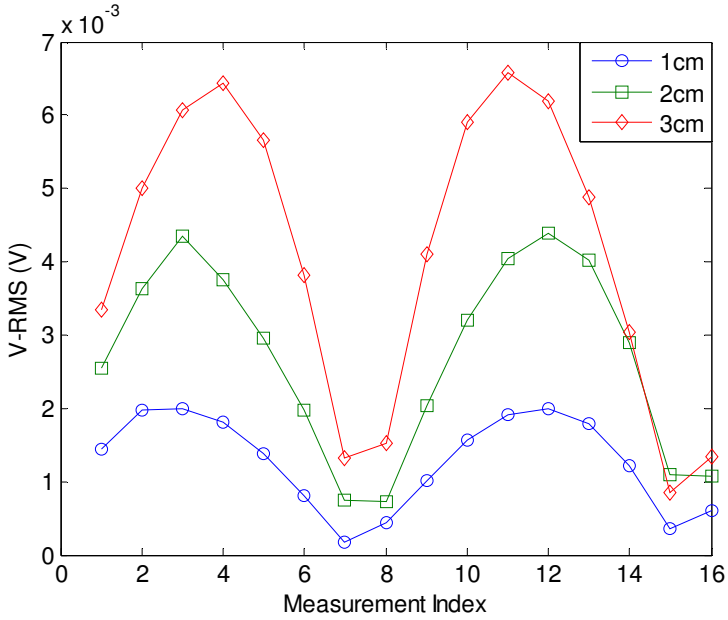

Figure 6.10 Measured voltages on the internal electrode pair for pill size 1cm, 2cm and 3cm

As stated above, the SVMS is only able to provide the voltage difference magnitude. Information on the polarity has to be provided manually through knowledge of the orientation of the pill in relation to the wall-mounted electrodes. From Figure 6.10, the voltage difference magnitudes increase as the size of the pill increases. This is consistent with the simulated result. However, there is a discrepancy between simulated (Figure 6.9) and measured (Figure 6.10) magnitudes. This will be examined later as this investigation is thought to be linked with the difference in grounding for the SVMS used for voltage measurement and the LCT2 instrument. Observing the plots in Figure 6.10, the symmetry could be seen for measurements taken during the first half of the cycle (i.e. measurements 1-8) and the second cycle (i.e. measurements 9-16) with the largest measured voltage difference having similar magnitudes. Any asymmetry may be due to misalignment (i.e. the pill was not aligned perfectly parallel to electrodes 8 and 16).

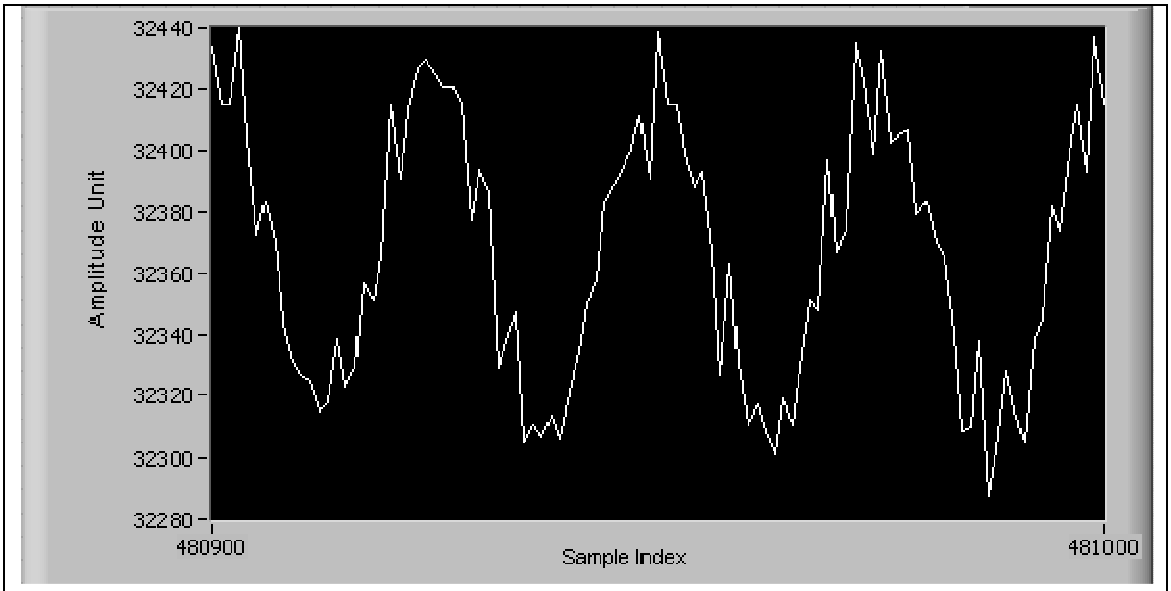

(a) 1cm pill

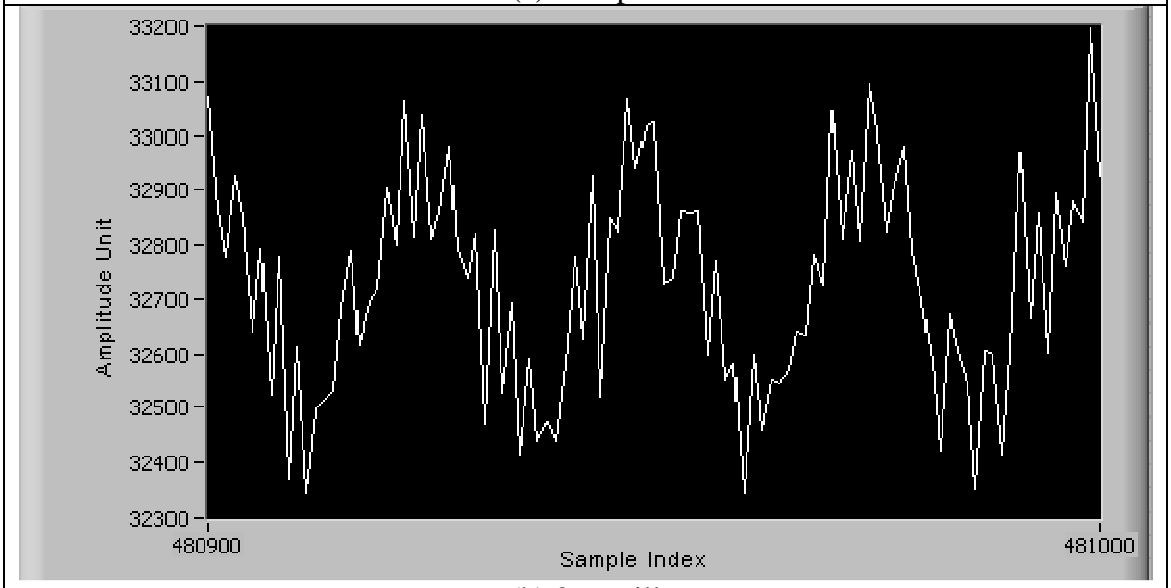

(b) 2cm pill

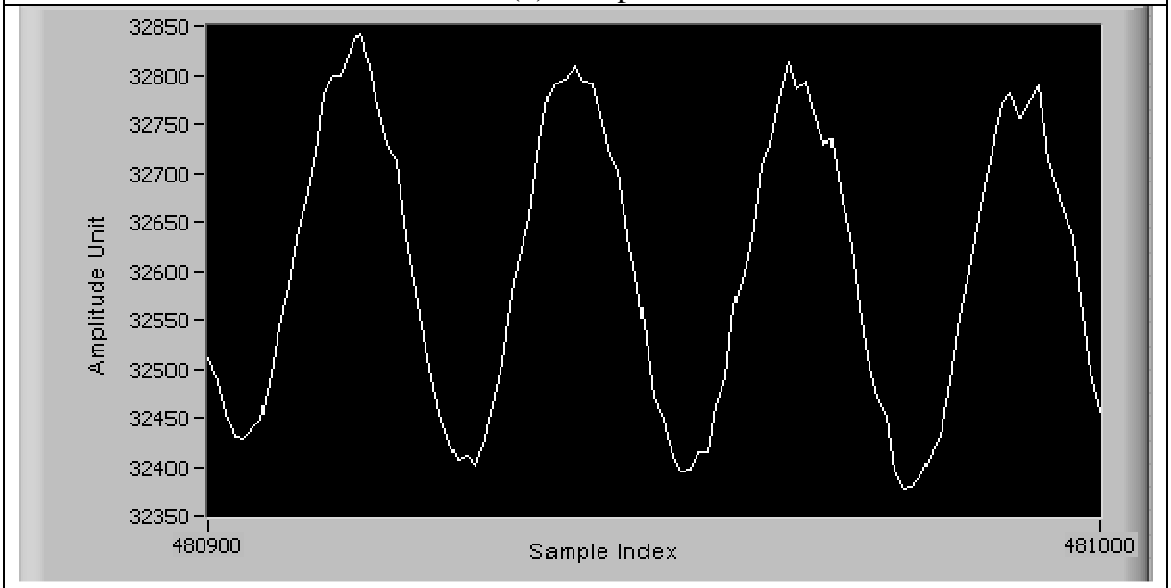

(c) 3cm pill

Figure 6.11 Comparison of raw measurements for the 7th measurement for 1cm, 2cm and 3cm pills

Figure 6.11 shows samples of a full set of measurements acquired using the SVMS and visualized in Labview for measurement 7, the measurement which delivers the smallest magnitude. The plots in the figure show that the measured signal for the smaller pills are noisier in comparison with the measured signal on the 3cm cube. This is recognized as a disadvantage for the smaller-sized cubes as this may lead to unreliable measurements.

A repeatability test was conducted to evaluate the consistency of the measurements. Five sets of measurements were taken and compared. The standard deviation and the SNRs for each measurement were calculated, and the results are as shown in Table 6.4.

Table 6.4 Comparison of SNR and standard deviation for measurements taken using different size pills

Pill size	SNR (dB)		Standard Deviation (V)	
	Mean	Worst	Mean	Worst
1cm	59	31	$5.5\text{x}10^{-6}$	$4.8\text{x}10^{-5}$
2cm	67	26	$2.6\text{x}10^{-5}$	$1.9\text{x}10^{-4}$
3cm	86	72	$2.6\text{x}10^{-7}$	$8.7\text{x}10^{-7}$

Observing the standard deviation, the measurements taken using the 3cm pill are effectively the same. The SNR levels are also high, meaning the measurements are above noise level and reliable. The measurements taken using the 1cm and 2cm pills lack consistency, having higher standard deviations and a large variability in terms of SNRs. The SNRs calculated for each measurement are plotted and shown in Figure 6.12.

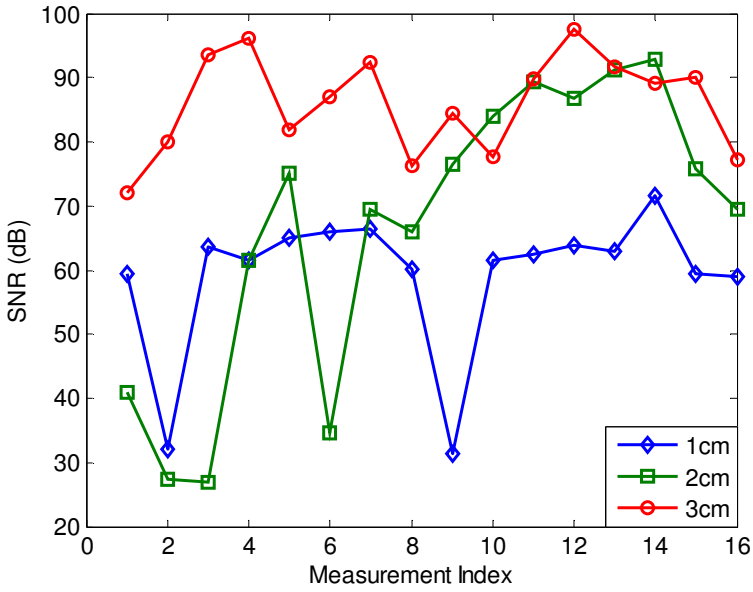

Figure 6.12 Comparison of SNRs for different size pills

The tests suggest that the 3cm pill can provide reliable measurements, while the smaller size pills produce less consistent measurements. Although 3cm (~9% of the 34cm diameter of the vessel) is larger than originally anticipated, it is felt to be reasonable for the present purpose. The 3cm pill will be used in subsequent simulation and experiments in this chapter.

6.2 Modelling of the Extended Electrical Tomography Method

When modelling the EET approach, the ad hoc pills are included in the model. The exact modelling with the inclusion of the ad hoc pills is required, especially for setting up the forward model such that an accurate Jacobian matrix can be computed. The pill is modelled as a void and the faces containing the internal electrodes can be selected manually and defined as electrodes in EIDORS. In reality the inclusion of the pill will have an effect on the electric field. However, the extent of the effect is unknown and requires investigation. Using the set-up as shown in Figure 6.8, the simulated voltage differences are compared for models with and without the inclusion of the pill in Figure 6.13. Voltages were simulated using the EIDORS toolkit, for the adjacent with reciprocity strategy. The voltages are mostly the same in the plots shown in Figure 6.13, with the largest mismatch of the measured magnitudes is recorded at approximately

3.6%. The small amount of mismatch could be caused by difference in meshes. It can be concluded that the inclusion of the pill does not significantly affect the conventional set of voltage measurements.

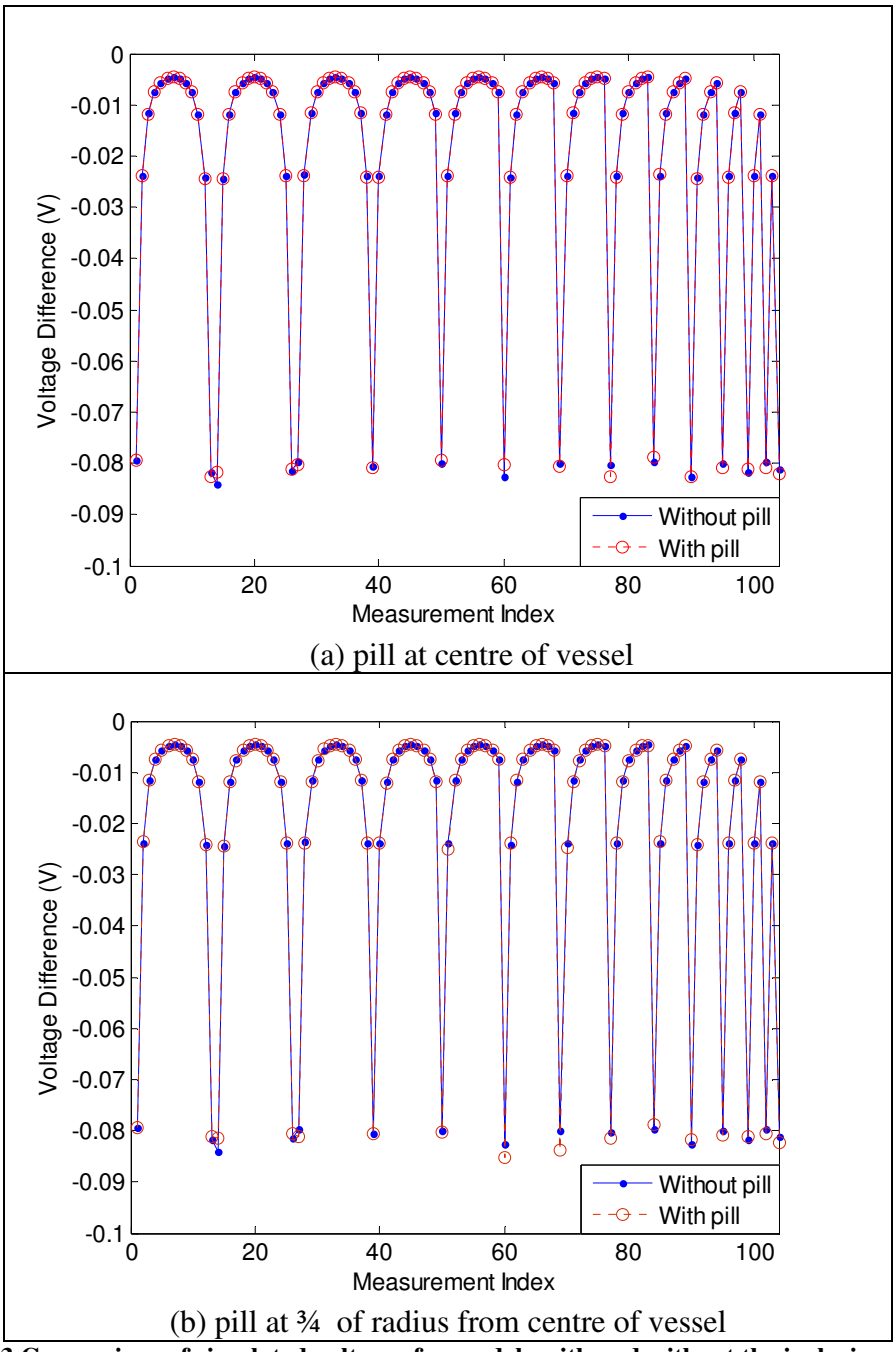

Figure 6.13 Comparison of simulated voltages for models with and without the inclusion of the ad hoc pill for the adjacent with reciprocity strategy for a single plane of 16 electrodes model

Figure 6.13(b) shows the comparison between simulated voltages for the case where the pill is located ¾ of the radius from the centre of the vessel. It can be seen that the voltages are well-matched in this case, similar to the case where the pill is located centrally. The largest mismatch of the measured magnitudes is calculated at

approximately 6.8%, which is higher in comparison to when the pill is located centrally. The difference between voltage difference with and without the inclusion of the ad hoc pill is as shown in Figure 6.14 for both cases. This indicates that the effect of the inclusion of the pill on the voltages is less significant. It is worth noting that the comparisons made only include one pill into the model. When more pills are included, the influence may be more noticeable, as the effect on the current path may be more significant.

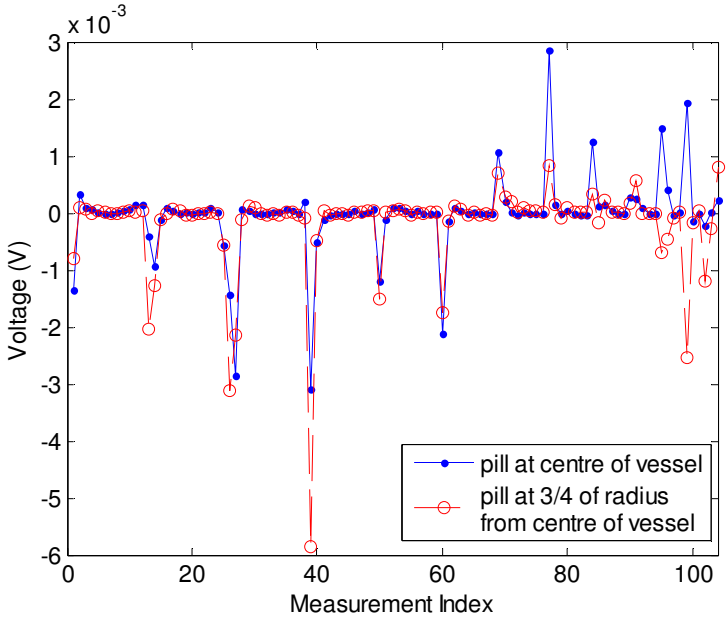

Figure 6.14 Comparison of the difference in simulated voltages for models with and without the inclusion of the ad hoc pill a single plane of 16 electrodes model using the adjacent strategy

One of the issues identified in Subsection 5.1.3 was the difference in grounding between the LCT2 instrument used for current injection and voltage measurement for the wall-mounted electrodes and the SVMS used for voltage measurement for the internal electrode pair. This is likely to cause discrepancies in the predicted voltages and measured voltages. Figure 6.15 compares the simulated voltages and the measured voltages. The measured voltages were acquired using the LCT2 and the SVMS. Polarity of SVMS measurements is determined manually and informed by simulations. The extended measurements acquired using the LCT2 instrument are generally well-matched with simulated voltages. However, the extended measurements acquired using the SVMS, are generally smaller than the simulated voltages. The magnitudes of the voltage difference acquired using the SVMS is generally ~66% of the simulated voltage values. This is thought to be due to the effect of the difference in grounding. In forward modelling, a single reference point is assumed. While this remains true when all

measurements are acquired using the LCT2 instrument, when extended measurements are acquired using the SVMS, there are two ground references. This is likely to be the reason why there is a noticeable difference between measurements acquired using the SVMS and simulated voltages.

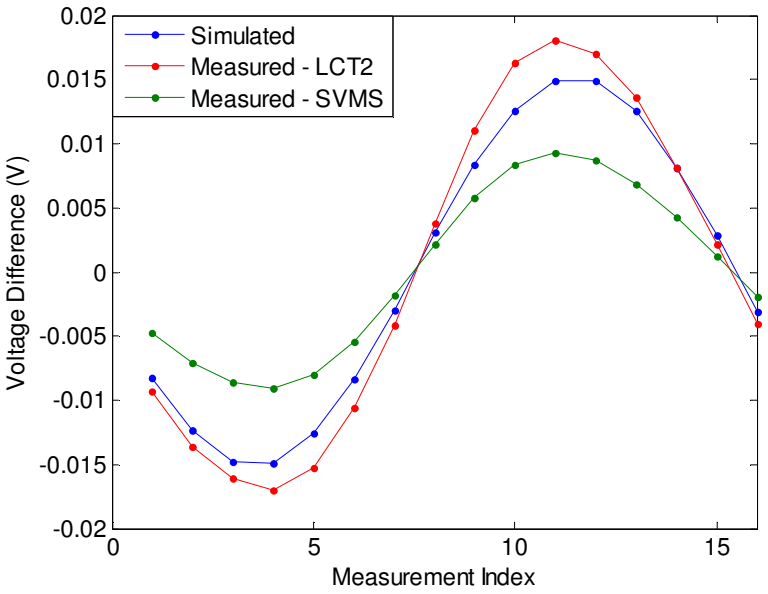

Figure 6.15 Comparison between simulated and measured voltages using the LCT2 and SVMS for a single plane of 16 electrodes arrangement

The stability of the measurements has been investigated for measurements obtained using the LCT2 only and measurements obtained using the LCT2 and the SVMS. Figure 6.16 shows the SVD plots comparing the two sets of measurements. The Fourier Coefficients were compared to observe the number of stable measurements which can be used for reconstruction. The plot in Figure 6.16 indicates that both sets of measurements are equally stable, and are able to provide the same amount of measurements which can be used for image reconstruction. This suggests that the floating reference of the SVMS does not affect the stability of measurements.

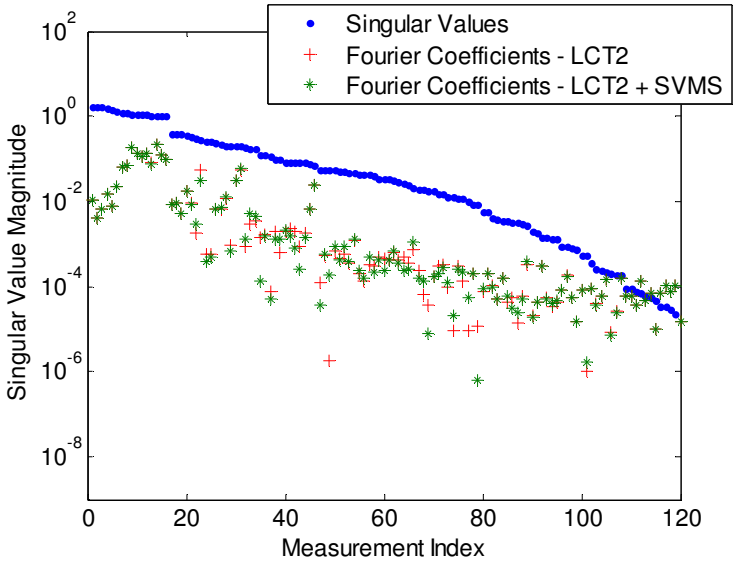

Figure 6.16 Spectral analysis comparing measured voltages using the LCT2 only and the LCT2 with SVMS for EET with one ad hoc pill for the adjacent with reciprocity strategy

6.3 Effect of Varying Position and Orientation of Ad Hoc Pill

As previously mentioned, the idea of EET is that the ad hoc pill is free to assume any location within the vessel. This section investigates the effect of varying position and orientation of the ad hoc pill on the stability of measurements, and image attributes such as sensitivity and spatial resolution. As previously shown in the feasibility study in Section 5.4.1, using the adjacent with reciprocity strategy, for a single plane of 16 electrodes with an internal electrode pair setup, 15 out of 16 extended measurements are stable. It was also shown that improvements are observed in sensitivity and spatial resolution in the vicinity of the ad hoc pill. In this section, the ad hoc pill is relocated to other locations in relation to the wall-mounted electrodes and the resulting effect is investigated.

In this section, a two plane model shown in Figure 6.17 is used. Each plane of electrodes consists of 16 electrodes, with a 3cm pill located in the centre of the vessel. The centre of the pill is 10cm from base, such that it is aligned with the centre of the bottom electrode plane. Using this model, the number of extended measurements increases to 32 measurements for the adjacent current injection protocol.

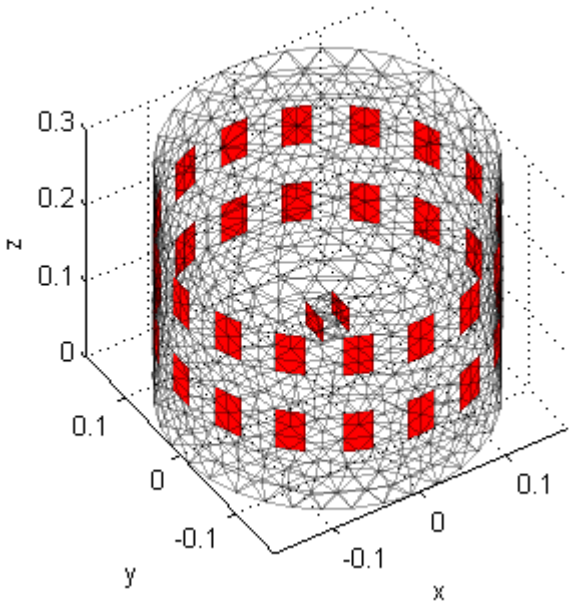

Figure 6.17 Discretized model of a 2 plane of 32 electrodes model with a 3cm ad hoc pill

Figure 6.18 shows that two measurements have singular values magnitude of ~10^{-15}, which is zero to machine precision. This suggests that the measurements are not unique. Knowing that 208 measurements obtained using the adjacent with reciprocity strategy for a 32 electrodes model are unique, it can be deduced that two out of the 32 extended measurements are redundant. Recalling that the results show that one out of 16 extended measurements is redundant for the single plane of 16 electrodes model, this result is consistent with the previous observation shown in the feasibility study in Section 5.4.1.

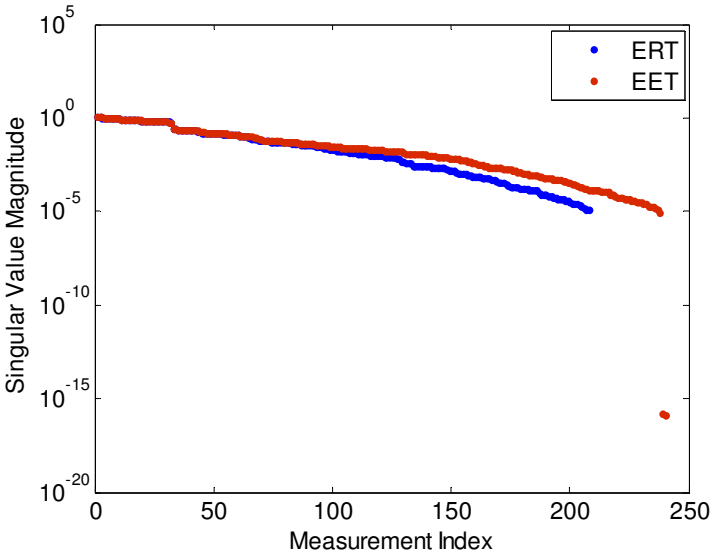

Figure 6.18 Spectral analysis comparing measured voltages using the conventional ERT and EET approach with one ad hoc pill for the adjacent with reciprocity strategy

6.3.1. Varying Position of the Ad Hoc Pill

In this subsection, the position of the ad hoc pill is relocated away from the centre of the electrode plane, along the main axes. The horizontal axes *x* and *y* are as defined in Figure 6.19. The *z*-axis is the vertical axis from the centre of the horizontal plane. Figure 6.19 shows the centre of the pill located at 10cm from the base of the vessel, the same height as the centre of the bottom electrode plane. The 'default' orientation is considered as the internal electrode pair aligned parallel to the wall-mounted electrodes 8 and 16.

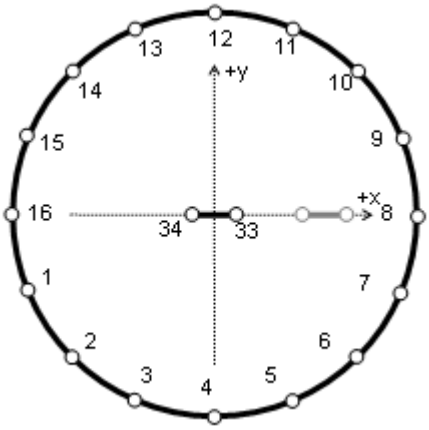

Figure 6.19 The x-y plane at 0.10m height with the pill repositioned along the x-axis

Analysis is done using simulated voltages to evaluate the effect of positioning of the ad hoc pill has on sensitivity and spatial resolution. Figure 6.20 shows the first 16 extended simulated voltage difference measurements, taken when the bottom plane electrodes are used as current injection electrodes with the centre of the ad hoc pill at the centre of is at the centre of the vessel, 2cm, 4cm 6cm, and 8cm away from the centre of the vessel, along the *x*-axis.

Voltages were simulated using EIDORS for the adjacent current injection strategy. As the location of the pill shifts closer to the wall of the vessel along the *x*-axis, an increase in voltage difference measured is observed as the distant between the pill and current source decreases. It can be seen that as the pill is relocated nearer to electrode 8, the magnitudes of the voltage difference for measurements 6 to 9 increases significantly and these measurements are acquired when the current source is closer to the ad hoc pill (electrodes 6 to 9).

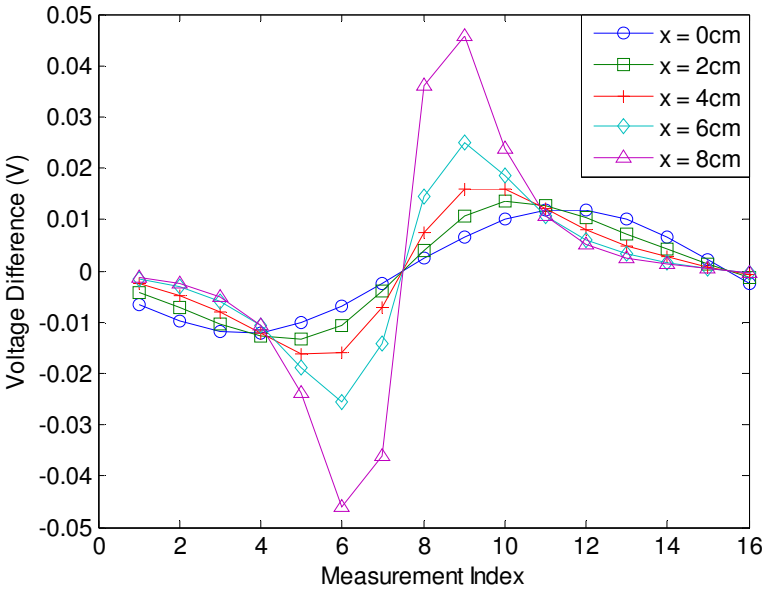

Figure 6.20 Simulated voltages for the adjacent strategy taken at the internal electrode pair with the pill shifted along the x-axis

Figure 6.21 compares the sensitivity variation on a fixed axis on the electrode plane (at height 0.10m from base of electrode) for the pill at different locations on the *x*-axis. As shown in Section 5.4.1, the sensitivity level improves around the vicinity of the ad hoc pill. The same applies to different cases where the centre of the pill is repositioned on the x-axis.

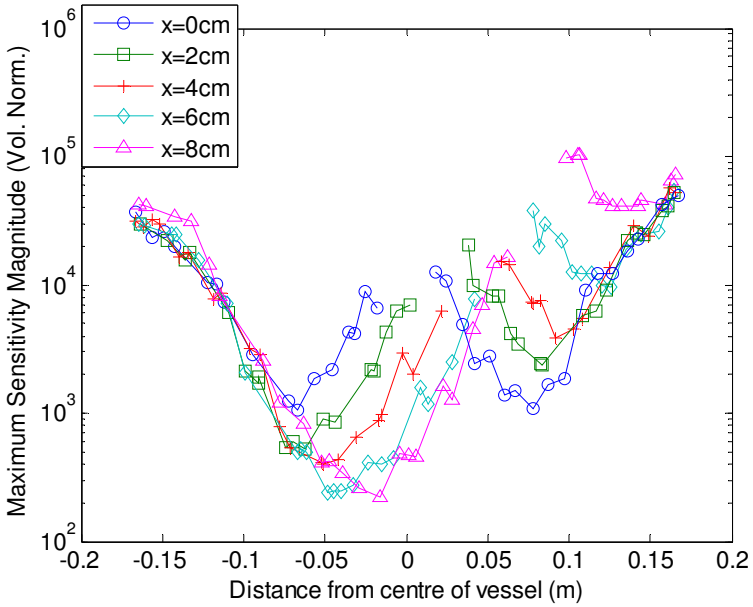

Figure 6.21 Sensitivity analysis for ad hoc pill shifted along the x-axis

As the pill is positioned further away from the centre of the vessel, the sensitivity level in the centre of the vessel starts to decrease, while the sensitivity between the side of the pill nearer to the wall of vessel (the space between electrode 34 and electrode 8 in Figure 6.19) increases. This is especially visible when the pill is located at 8cm (~50% of between the centre and wall of vessel). In terms of improving the overall sensitivity in the central region of the vessel, the pill is most beneficial when located in the centre position as the overall sensitivity level is improved.

Figure 6.22 compares the spatial resolution for the pill at different locations along the x-axis. Similar to the sensitivity analysis the spatial resolution is improved near the vicinity of the pill for the different cases shown. A similar trend as seen in the sensitivity analysis is also observed. The resolution is improved in the area between the side of the pill nearer to the wall and the wall of the vessel (referring to Figure 6.19, the space between electrode 34 and electrode 8) while the resolution reduces on the opposite side of the pill. The resolution is generally better (low percentage of FWHM) when the pill is located centrally.

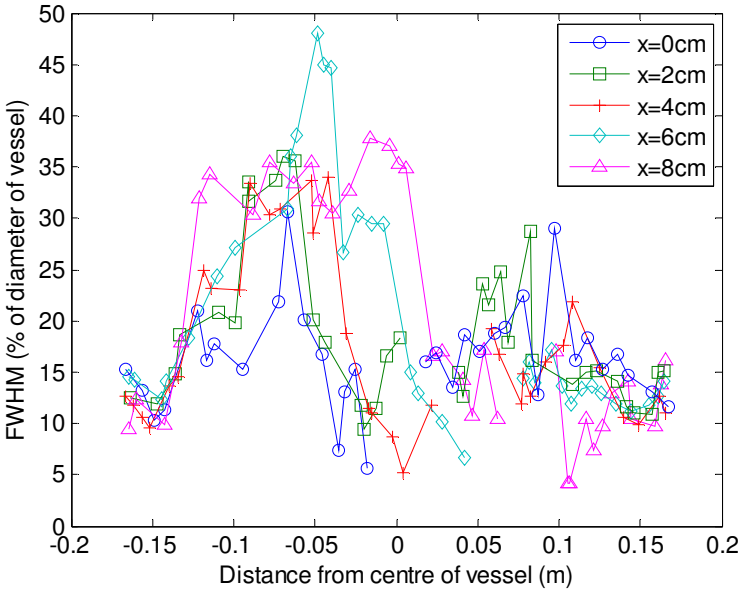

Figure 6.22 Spatial resolution analysis for ad hoc pill shifted along the x-axis

Test distributions were set-up to evaluate the reconstruction performance of the EET setup with a single pill. A 5cm diameter rod is used for the experiment and the arrangement is as shown in Figure 6.23 (a)-(b). The background material is tap water. For test distribution 1, the perspex rod is located approximately equidistant between the

ad hoc pill and the wall of the vessel, with the ad hoc pill located in the centre of the vessel. For test distribution 2, an aluminium rod is located in the centre of the vessel with the ad hoc pill located approximately equidistant between the rod and the wall of the vessel. In this set-up, the centre of the pill is at 10cm from the base of the vessel, aligned with the centre of the bottom electrode plane. Measurements were taken using the LCT2 tomograph for the wall-mounted electrodes and the SVMS for the internal electrode pair.

Reconstructions for the ERT and EET setups are compared. These are computed using different meshes to reflect a real scenario. For the ERT setup (Figure 6.23(c)-(d)), the ad hoc pill is not included in the model, while the ad hoc pill is included in the model in the EET setup (Figure 6.23(e)-(f)). Reconstruction was performed using the Truncated Singular Value Decomposition (TSVD) algorithm on a difference dataset (a homogeneous reference is subtracted from a measurement dataset).

The 3D visualization of reconstructed images is done using MayaVi. Comparing the images in Figure 6.23, the reconstructions using the EET approach do not appear to be better than those using the conventional ERT approach. The iso-surfaces shown are chosen to best represent the shape of the rod for all cases. This choice is made such that the reconstructed images produced using the EET approach can be compared to reconstructed images done using conventional ERT in a fair manner, as well as to observe the effect of the inclusion of the ad hoc sensor on reconstructed images. For test distribution 1, the distortion of the shape of the reconstructed rod which had extended to the wall of the vessel was visibly seen in all reconstructions.

For test distribution 2, similarly the reconstructed images using the EET approach do not show visible difference from the reconstructions done using the ERT approach. This is to be expected as the resolution analysis indicates that the improvement in resolution is not as significant in comparison with when the pill is located in the centre of the vessel. Considering no visible difference was seen in the reconstructions for test distribution 1, similarly no visible difference is observed for reconstructions done for test distribution 2.

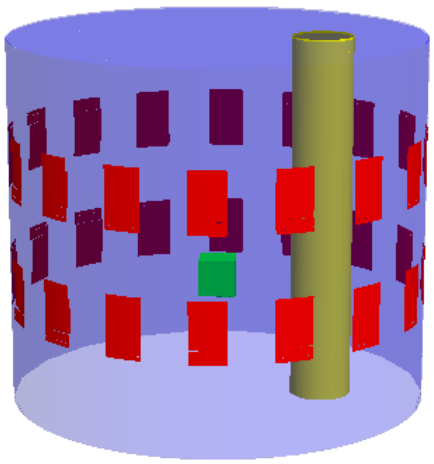

(a) Test distribution 1 (Perspex rod)

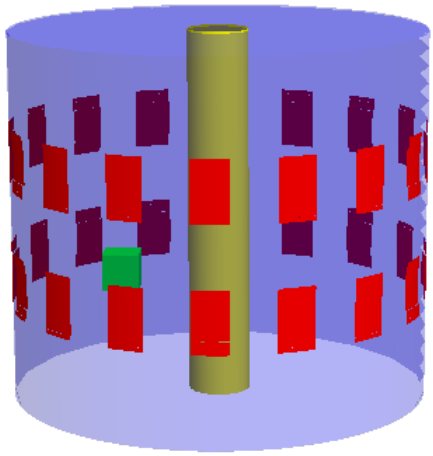

(b) Test distribution 2 (Aluminium rod)

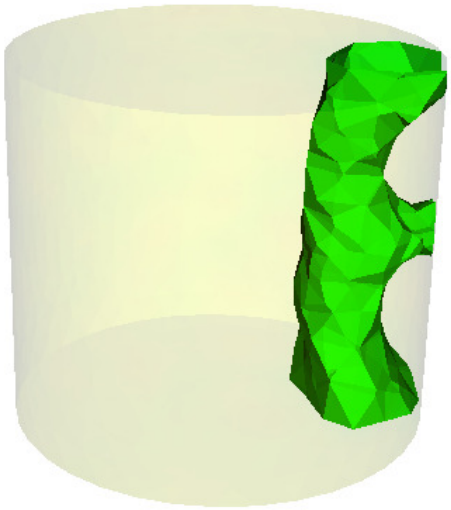

(c) ERT (1)

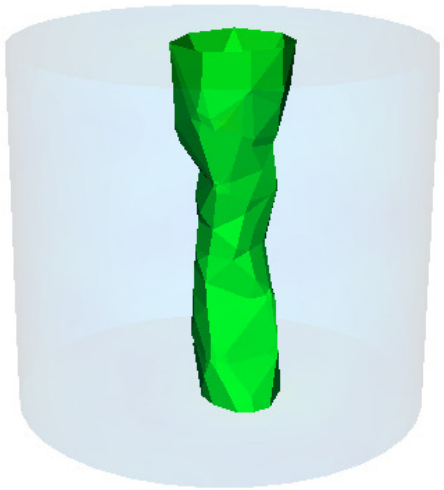

(d) ERT (2)

(e) EET (1)

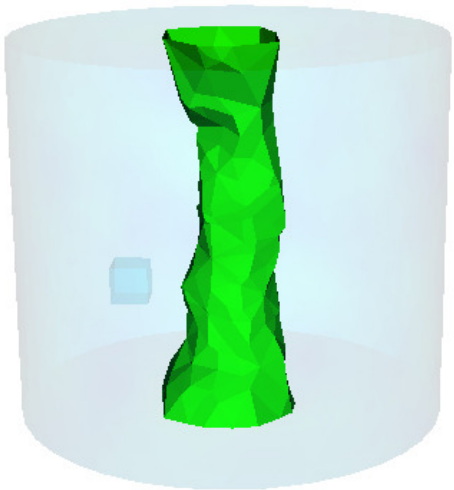

(f) EET (2)

Figure 6.23 Comparison of reconstructions on (a, b) the test distribution using (c, d) conventional ERT and (e, f) the EET approach with ad hoc pill located at the centre and equidistant between centre and the wall of the vessel at z=0.10m

In the comparative studies in the previous sections, the centre of the ad hoc pill is aligned to the centre of the bottom electrode plane. The effect of the ad hoc pill located on an off-electrode plane is investigated. In this comparative study, the centre of the ad hoc pill is relocated to 15cm from the base of the vessel, equidistant between the centre of the top and bottom electrode planes.

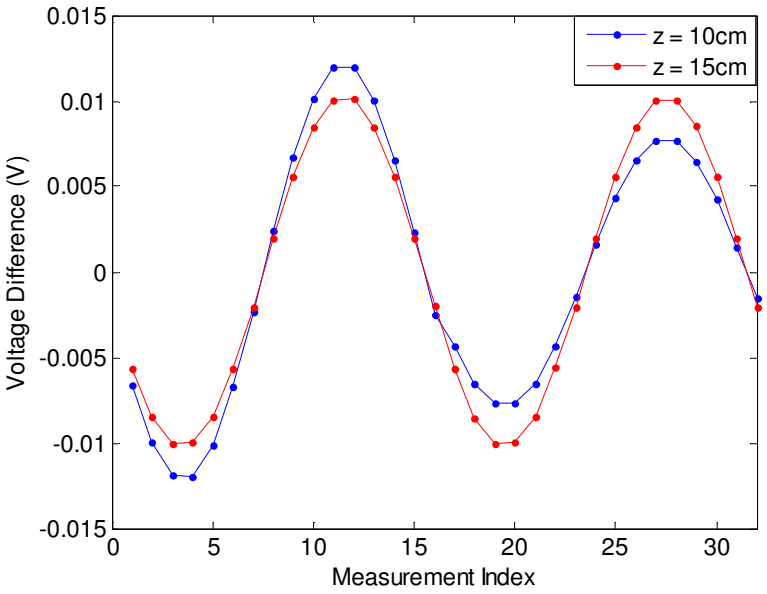

Figure 6.24 Simulated voltages for the adjacent strategy taken at the internal electrode pair with the pill shifted along the z-axis

Figure 6.24 compares the simulated extended voltage difference for measurements taken with the centre of the pill located at 10cm from the base of the vessel and at 15cm from the base of the vessel (equidistant between the two electrode planes). Similar to the previous set-up, the ad hoc pill is located at the centre of the vessel, with the internal electrodes aligned parallel to electrodes 8 and 16 on the wall of the vessel. As expected, with the ad hoc pill located further away from the electrode plane, the magnitudes of the voltage difference decrease. This is also evident when comparing the magnitude for the first 16 measurements for the plot with the pill located at 10cm from the base of the vessel, with the subsequent 16 measurements. Measurements 17-32 were taken with the current injecting sources in the top electrodes plane, which is 10cm above the location of the pill. This results in lower measured voltage difference magnitudes. At equidistant (15cm from base of vessel), the distance of the pill from both planes of electrodes are the same, therefore the measured magnitudes for measurements 1-16 are repeated for measurements 17-32. Similar to previous the comparative study, the sensitivity and spatial resolution analysis uses simulated voltages.

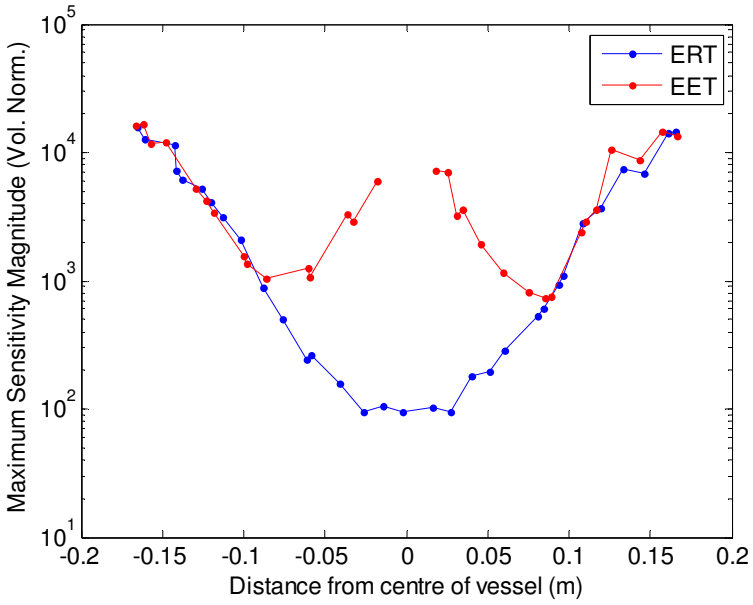

Figure 6.25 Sensitivity variation at z=0.15m for ad hoc pill at z=0.15m from the base of vessel

Figure 6.25 shows the sensitivity variation at height 0.15m from the base of the vessel for a conventional ERT and EET approach with the centre of the pill located at 0.15m from the base of the vessel. Similar to previous comparative studies, an improvement in sensitivity is observed in the vicinity of the ad hoc pill. This suggests that even on an off-electrode plane, the EET approach is able to improve the sensitivity in the vicinity of the pill.

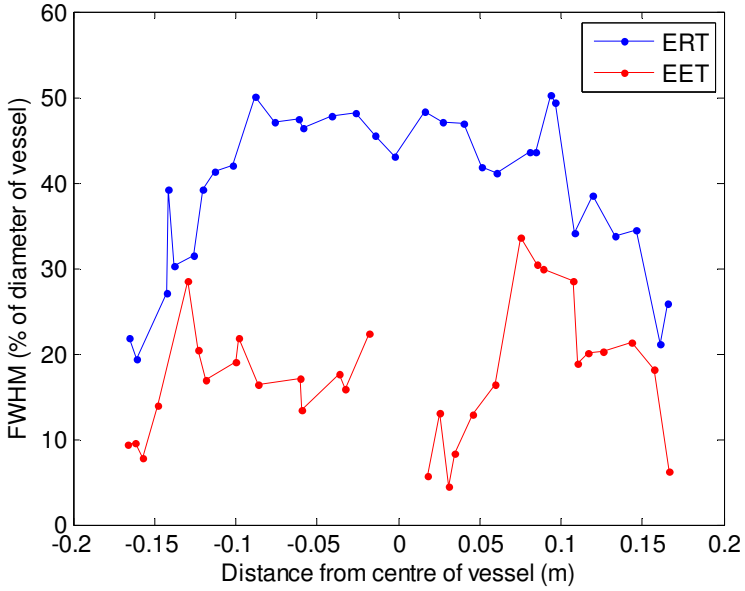

Figure 6.26 Spatial resolution variation at z=0.15m for ad hoc pill at z=0.15m from the base of vessel

The effect of the extended measurements on spatial resolution is as shown in Figure 6.26. Comparison is made between a conventional ERT set-up and for the EET approach. Similarly, an improvement on the spatial resolution can be seen for the EET approach, which was shown in previous comparative studies. In this case, the overall resolution is improved with the inclusion of the extended measurements, but more prominently in the vicinity of the pill. This suggests potential benefit of the EET approach.

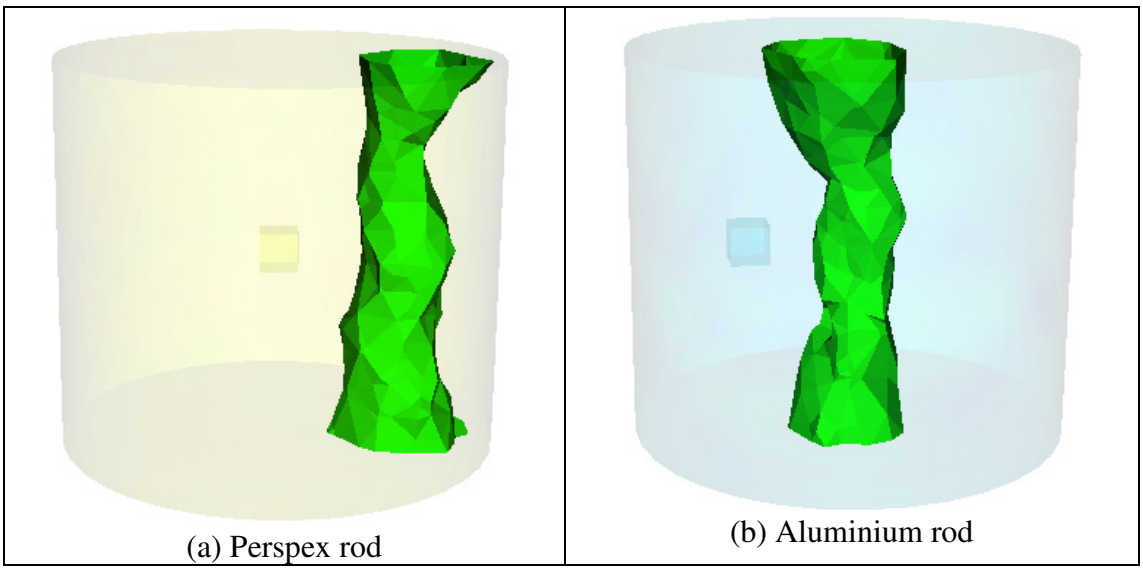

(a) Perspex rod (b) Aluminium rod

Figure 6.27 Reconstructions on test distributions shown in Figure 6.23 (a, b) using the EET approach with the pill located at z=0.15m

Reconstruction was repeated using test distribution 1 and test distribution 2 (Figure 6.23(a) and (b)) with the set-up slightly altered. The only difference is the relocation of the centre of the pill to 0.15m from the base of the vessel. Similarly, measurements for the wall-mounted electrodes were taken using the LCT2 tomograph and measurements for the internal electrode pair were taken using the SVMS. Reconstructions were done using the TSVD algorithm. Comparing the reconstruction shown in Figure 6.27(a) with reconstruction shown in Figure 6.23(c) and (e), it might be deduced that the reconstruction is slightly better in terms of the reconstructed shape. The distortion where the reconstructed shape extends to the wall of the vessel is seen to be improved. The reconstruction for test distribution 2 is similar to those shown in Figure 6.23(d) and (f). The result is consistent with the improvement shown in the spatial resolution analysis (Figure 6.27) with the ad hoc pill located on an off-electrode plane.

Although prior analysis for both sensitivity and resolution indicates visible improvement, this is not consistently reflected in the reconstructed images. In the reconstructed examples shown, images reconstructed using EET are similar in quality to those using conventional ERT. This is perhaps unsurprising considering the small overall increase in the number of unique measurements, despite the fact that resolution analysis suggesting an improvement.

6.3.2 Varying Orientation of the Ad Hoc Pill

As the pill is free to assume any location within the vessel, the orientation of the ad hoc pill is likely to vary as well. In the comparative studies conducted in Section 4.4.1 and 5.3.1, the 'default' orientation of the ad hoc pill is that the internal electrodes are arranged such that they are parallel to electrodes 8 and 16 (referring Figure 6.19). In the following set of simulations, the internal electrode pair is rotated on the horizontal plane to 90^{o} by 22.5^{o} steps, as shown in Figure 6.28.

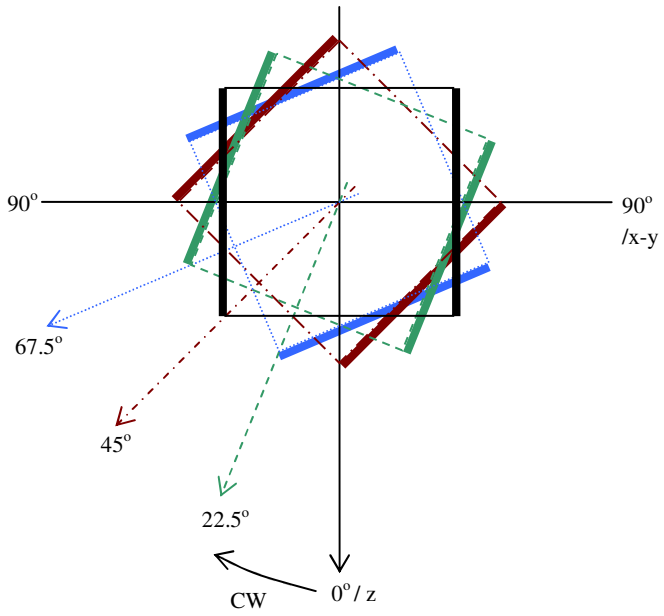

Figure 6.28: The rotation of the internal electrode pair on the horizontal plane in the clockwise direction.

The magnitudes of the simulated voltages taken for when the internal electrodes are at the default position are the largest in comparison to those taken for other orientations. The magnitudes of the voltage differences decrease as the angle increases for clockwise

rotation, as shown in the plots in Figure 6.29. This result is encouraging as it suggests that even when the internal electrodes are positioned at an angle in relation to the wall-mounted electrodes, measurable changes to the voltage differences can be acquired. This also suggests that similar benefits in terms of additional unique measurements, and improvements in sensitivity levels and resolution might be expected.

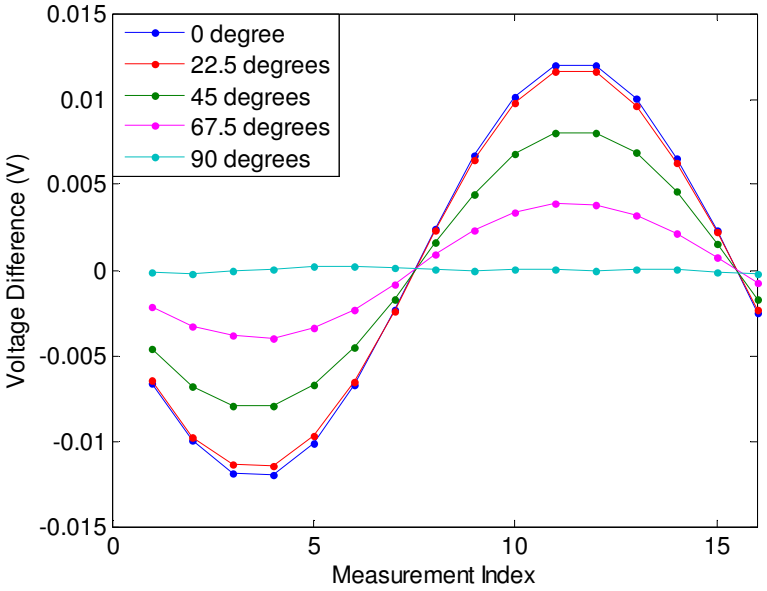

Figure 6.29 Simulated voltages of the internal electrodes pair at different angles when rotated on the horizontal plane for the adjacent strategy

Spectral analysis indicates that the stability of measurements is not degraded. The number of unique measurements remains the same, where 15 out of 16 of the extended measurements are unique. Similar to previous comparative studies, sensitivity analysis, shown in Figure 6.30, shows that there is an improvement in the sensitivity level around the vicinity of the ad hoc pill. This suggests that despite the rotation of the internal electrodes in relation to the wall-mounted electrodes, similar benefit in terms of sensitivity is attainable.

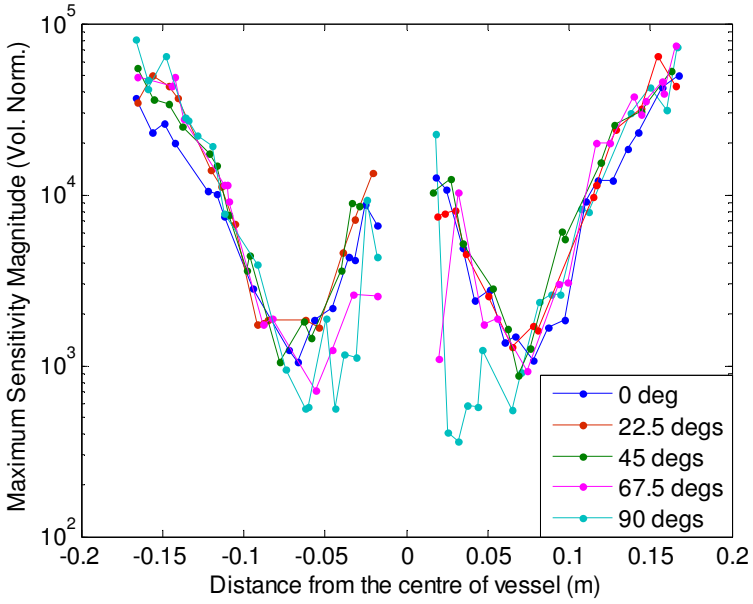

Figure 6.30 Sensitivity variation at z=0.10m for pill at different angles when rotated on the horizontal plane

Figure 6.31 shows the resolution analysis for the pill orientated at different angles in relation to the wall electrodes. It is interesting to note that as the angle between the internal electrodes and the wall-mounted electrodes increases from 0^{o} to 90^{o}, the resolution around the vicinity of the pill degrades. This suggests that the extended measurements are most beneficial when the internal electrodes are aligned parallel or rotated at a smaller angle relative to the wall-mounted electrodes.

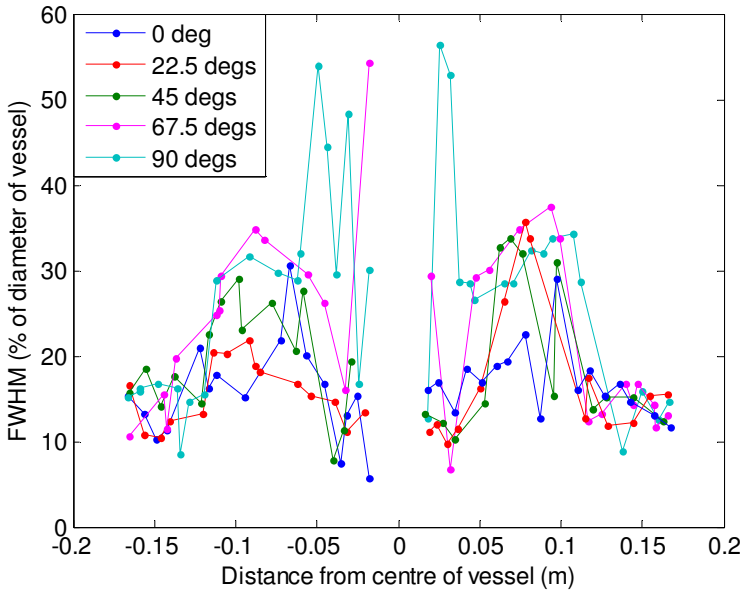

Figure 6.31 Spatial resolution variation at z=0.10m for pill at different angles when rotated on the horizontal plane

Another study considers the rotation of the internal electrodes around the z-axis. Consider the case where the pill is located on the centre of the vessel, this rotation of the internal electrodes is similar to the switching of current injection pairs for the electrode mounted electrodes. For example, rotating the internal electrodes 90^o around the *z*-axis from its default position shown in Figure 6.19 is equivalent to aligning the electrode pair parallel to electrodes 4 and 12. Using the same current injection strategy, essentially a similar set of extended voltage differences is acquired.

A more interesting comparison is to consider relocating the pill along the *x*-axis, similar to the study done in Section 6.3.1 to investigate the effect of the rotation. The pill is shifted along the x-axis at height 0.10m from the base of the vessel with the electrodes maintaining the rotation, as shown in Figure 6.32.

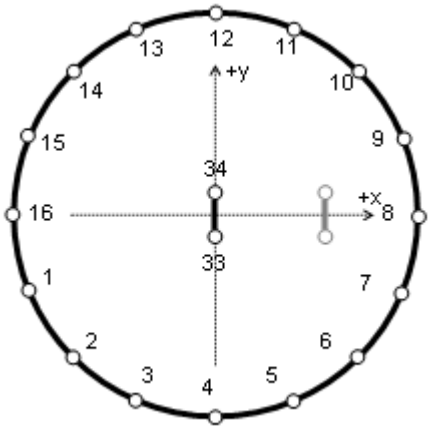

Figure 6.32 The x-y plane at 0.10m height with the pill repositioned along the x-axis with the electrodes rotated 90^o on the z-axis

Figure 6.33 shows the extended measurements for when the centre of the pill is located at the centre of the vessel, 4cm and 8cm from the centre of the vessel with the electrodes aligned parallel with wall-mounted electrodes 4 and 12 shown in Figure 6.31, simulated using the adjacent with reciprocity strategy for a single plane of 16 electrodes arrangement. Similar to the extended measurements shown in Figure 6.20 in Subsection 6.3.1, as the pill is positioned closer to the wall of the vessel, the magnitude measurements 7 and 8 increase as the pill are located closer to the current injection source.

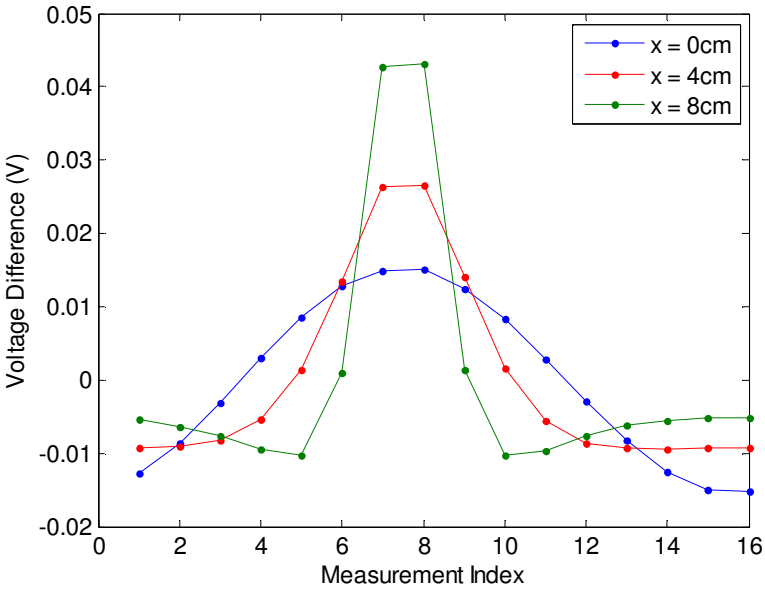

Figure 6.33 Simulated voltages of the internal electrodes pair at different locations on the x-axis when rotated 90° around the z-axis for the adjacent strategy

Spectral analysis indicates that 15 out of 16 extended measurements are unique for this set-up. The analysis also shows that the stability of the measurements is similar with previous cases. In the sensitivity analysis shown in Figure 6.34, a similar trend as in previous sensitivity analyses can be observed. The plots show that the sensitivity levels increase around the vicinity of the ad hoc pill.

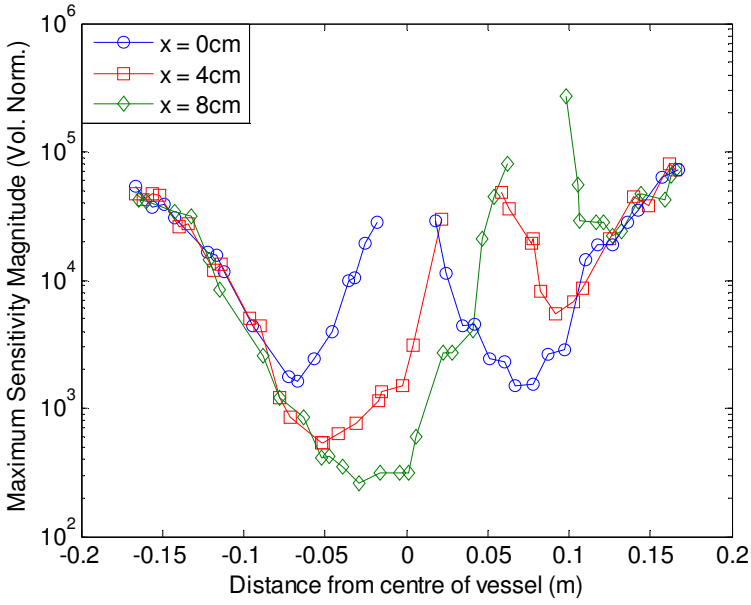

Figure 6.34 Sensitivity variation at z=0.10m for ad hoc pill rotated 90° on the z-axis

The plot for *x*=8cm shows that the sensitivity level is increased significantly between the wall of the electrode and side of the ad hoc pill closest to the wall of the electrode.

This is consistent with the sensitivity variation shown in Figure 6.21 with the internal electrodes aligned parallel with the wall-mounted electrodes 8 and 16. This result suggests that the orientation of the internal electrodes does not compromise the sensitivity levels in the vicinity of the ad hoc pill.

The spectral resolution analysis is shown in Figure 6.35. Similar to previous resolution analyses, the resolutions for elements in close proximity of the ad hoc pill are improved, with the FWHM lowered to a similar percentage to those in the area near the wall of the vessel. This reiterates the observations made in previous analyses. However, in contrast with the resolution analysis shown in Figure 6.22, the resolutions in the region between the wall of the vessel and the side of the pill closest to the wall of the vessel are not improved in this case. This suggests a slight disadvantage with the orientation of the internal electrodes not aligned parallel to the current source.

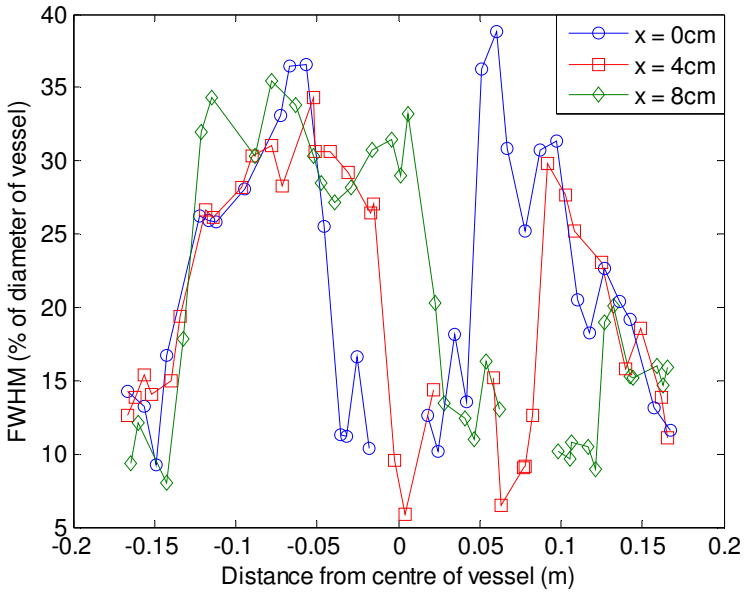

Figure 6.35 Spatial resolution variation at z=0.10m for ad hoc pill rotated 90^{o} on the z-axis

Figure 6.36 shows two reconstructed images for test distributions described previously and shown in Figures 5.23 (a) and (b) using the EET approach with the pill rotated 90^{o} on the z-axis. Similarly, measurements were taken using the LCT2 tomograph for the wall-mounted electrodes and the SVMS for the internal electrode pairs. Image reconstruction was done using the TSVD algorithm. Similar to previous reconstructed images, the reconstructed images using the EET approach are similar to those reconstructed using a conventional ERT set-up as shown in Figures 5.23 (c) and (d).

The reconstructed images are also similar to those reconstructed for when the ad hoc pill is on its 'default' orientation. This suggests that even with a different orientation, the quality of the reconstructed images is comparable.

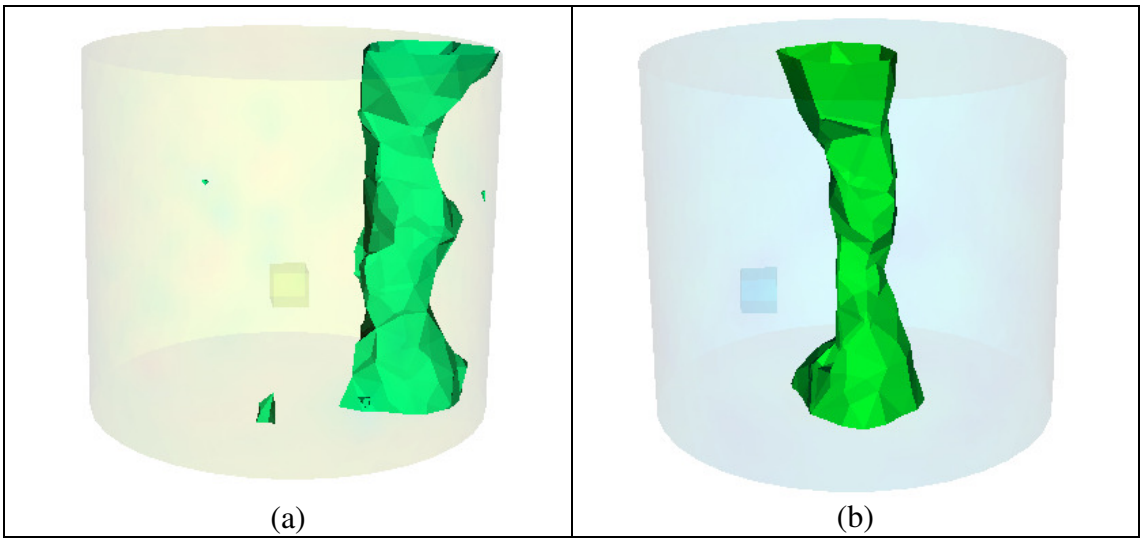

Figure 6.36 Reconstructions for test distributions shown in Figure 6.23 (a,b) using the EET approach with the pill rotated 90^{o} on the z-axis with the pill located at z=0.10m

The results presented are a selection of the available choices in terms of positioning and orientation. The results reiterate the findings from the observations made in the feasibility study in Section 5.4.1, suggesting that regardless of the position and orientation of the internal electrodes, similar benefits in terms of increase in unique measurements, and improvement in sensitivity and resolution can be observed. However, despite the improvement in spatial resolution indicated in the analysis, the reconstructed images show no visible differences from those produced using a conventional ERT setup.

6.4 Effect of Multiple Ad Hoc Pills

In previous comparative studies done throughout this thesis, a single ad hoc pill has been used to examine the feasibility of the EET approach and later, to investigate the performance of EET. While analysis indicates that the EET approach results in improvements in terms of sensitivity and more importantly spatial resolution, the improvement is not reflected in reconstructed images. The improvement shown in the resolution analysis indicates that the improvements are located in areas close to the ad

hoc pill, which may explain why overall improvement of reconstructed images was not visible.

The ultimate goal is to be able to deploy multiple ad hoc pills into the vessel to multiply the impact of having ad hoc localized measurements into a conventional ERT dataset to aid in improving the spatial resolution. There are considerations which require attention when using multiple pills.

One consideration is the degradation to the forward modelling. With more voids, representing the location of the pills, included into the model, the impact on the electric field, and the subsequent computation of the Jacobian matrix should be investigated. With more than one ad hoc pill, the improvements in sensitivity and resolution shown by only having an ad hoc pill could be altered. This section briefly explores the impact of employing two pills on image attributes.

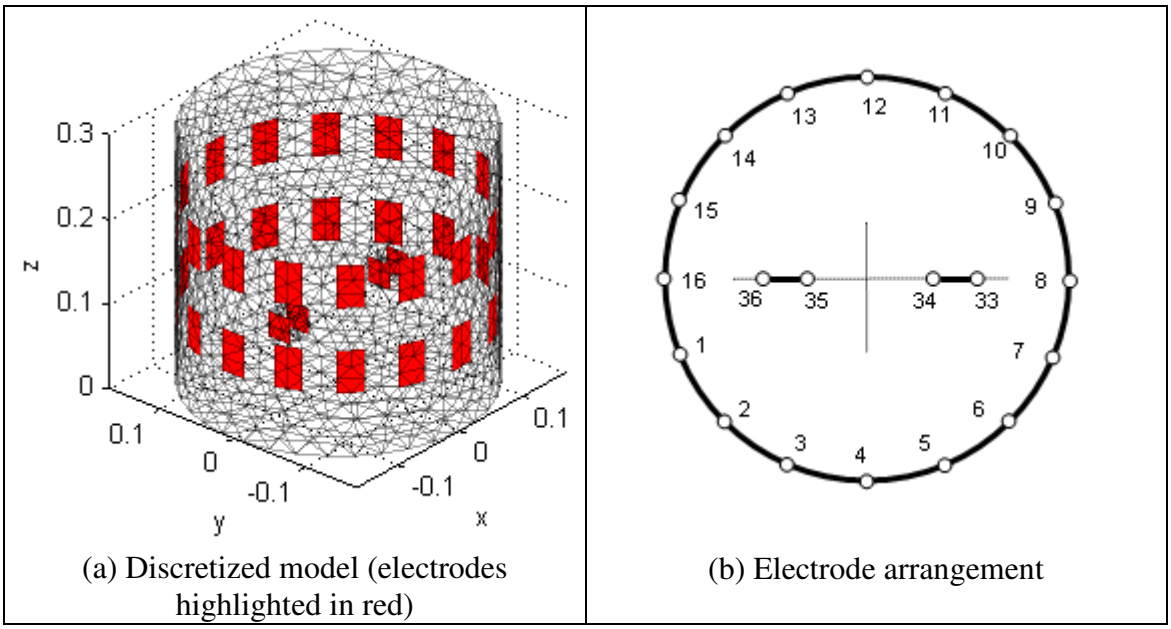

(a) Discretized model (electrodes highlighted in red)

(b) Electrode arrangement

Figure 6.37 Electrodes arrangement for a 32 electrode model with two pairs of internal electrodes

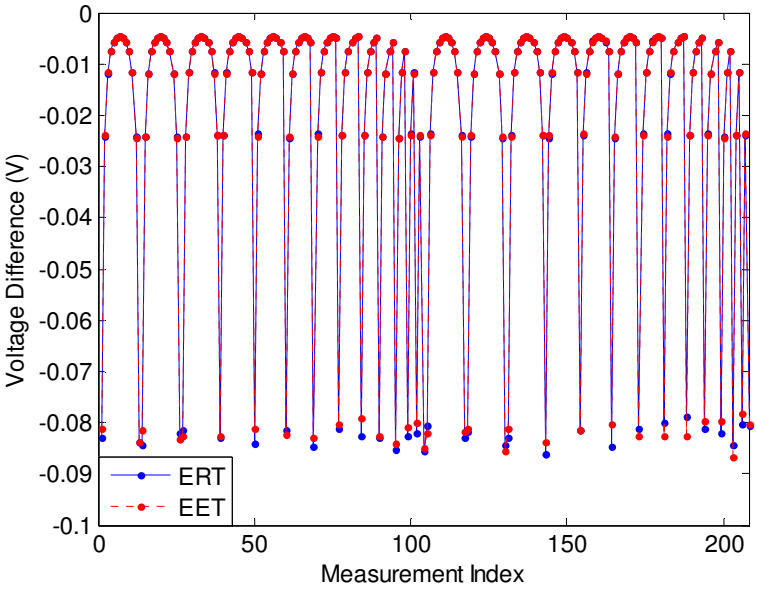

Figure 6.38 Comparison of simulated voltages for models with and without the inclusion of two ad hoc pills for the adjacent with reciprocity strategy for two planes of 16 electrodes model

The model used consists of two 3cm cubes which are located at 8cm from the centre of the vessel, as shown in Figure 6.37(a). The arrangement of the internal electrode pairs is shown in Figure 6.37(b). The centres of the electrodes are at 10cm from the base of the vessel, and aligned parallel to electrodes 8 and 16 on the wall of the vessel. This configuration is similar to the 'default' settings described previously. The simulated voltages for the adjacent with reciprocity strategy using models with and without the inclusion of the two ad hoc pills are shown in Figure 6.38. The voltages for both approaches are well-matched, suggesting that the inclusion of the ad hoc pills does not affect the voltages acquired from the wall-mounted electrodes.

Figure 6.39 shows the spectral analysis for a 32 electrodes model with 2 pairs of internal electrodes in an arrangement as shown in Figure 6.37(a) for the adjacent with reciprocity strategy. For each internal electrode pair, 32 extended measurements are generated for the 32 electrode model using the adjacent strategy. This means 64 extended measurements are acquired using this model. The spectral analysis indicates that 268 out of 272 measurements are unique, as four singular values have magnitudes of ~10^{-15}, which are zero to machine precision. Based on the findings in previous spectral analysis and knowing that 208 measurements taken using the adjacent with reciprocity measurements are unique, it can be deduced that there are two redundant measurements taken on each pill for the 32 current injection patterns.

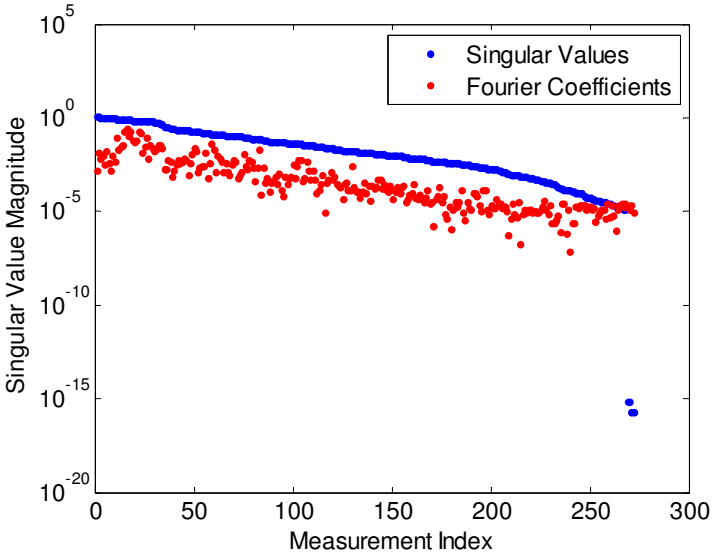

Figure 6.39 Spectral analysis comparing measured voltages using the conventional ERT and EET approach with two ad hoc pills for the adjacent with reciprocity strategy

Figure 6.40 shows the sensitivity variation for the EET approach using two ad hoc pills, in comparison with the EET approach using a single ad hoc pill and conventional ERT set-up. The plot shows that in the area between the two pills, in the centre of the vessel, the sensitivity level is low in comparison with the sensitivity levels near the wall of the vessel, which was observed in previous sensitivity analyses.

It is interesting to note the significant decrease in sensitivity in the centre of the vessel (the area between the ad hoc pills) although the level of sensitivity is slightly higher than the ERT set-up. A possible explanation is that this is because the ad hoc pills are not used as current sources. As discussed in Section 4.2, improvement of sensitivity levels is predominantly influence by current patterns. While using the internal electrodes to acquire voltage difference measurements increases the possibility of detecting changes in conductivity (therefore increasing the sensitivity level), this is insufficient to 'sustain' the improvement in sensitivity level with the presence of non-current driving internal electrodes.

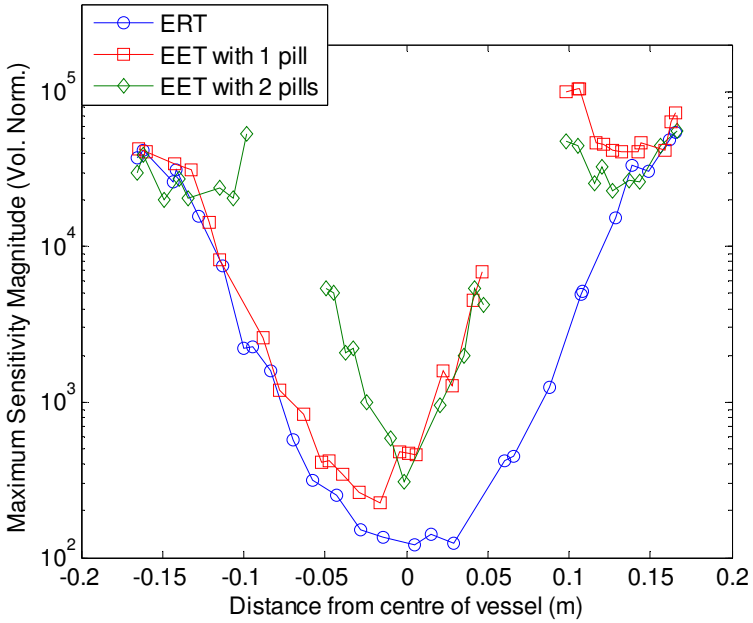

Figure 6.40 Sensitivity variation at z=0.10m comparing conventional ERT and EET with one and two ad hoc pills

The resolution analysis is shown in Figure 6.41. Similar to previous resolution analyses, the resolution near the vicinity of the ad hoc pills are visibly improved. Comparing the resolution between the ad hoc pills, it can be seen that the resolutions are slightly better in comparison with the resolutions for the ERT method, with a lower percentage of FWHM.

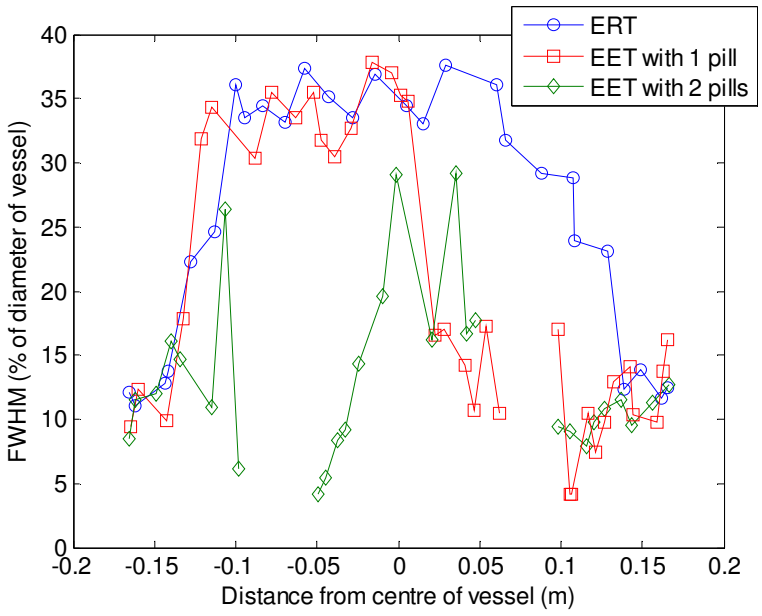

Figure 6.41 Spatial resolution variation at z=0.10m comparing conventional ERT with EET with one and two ad hoc pills

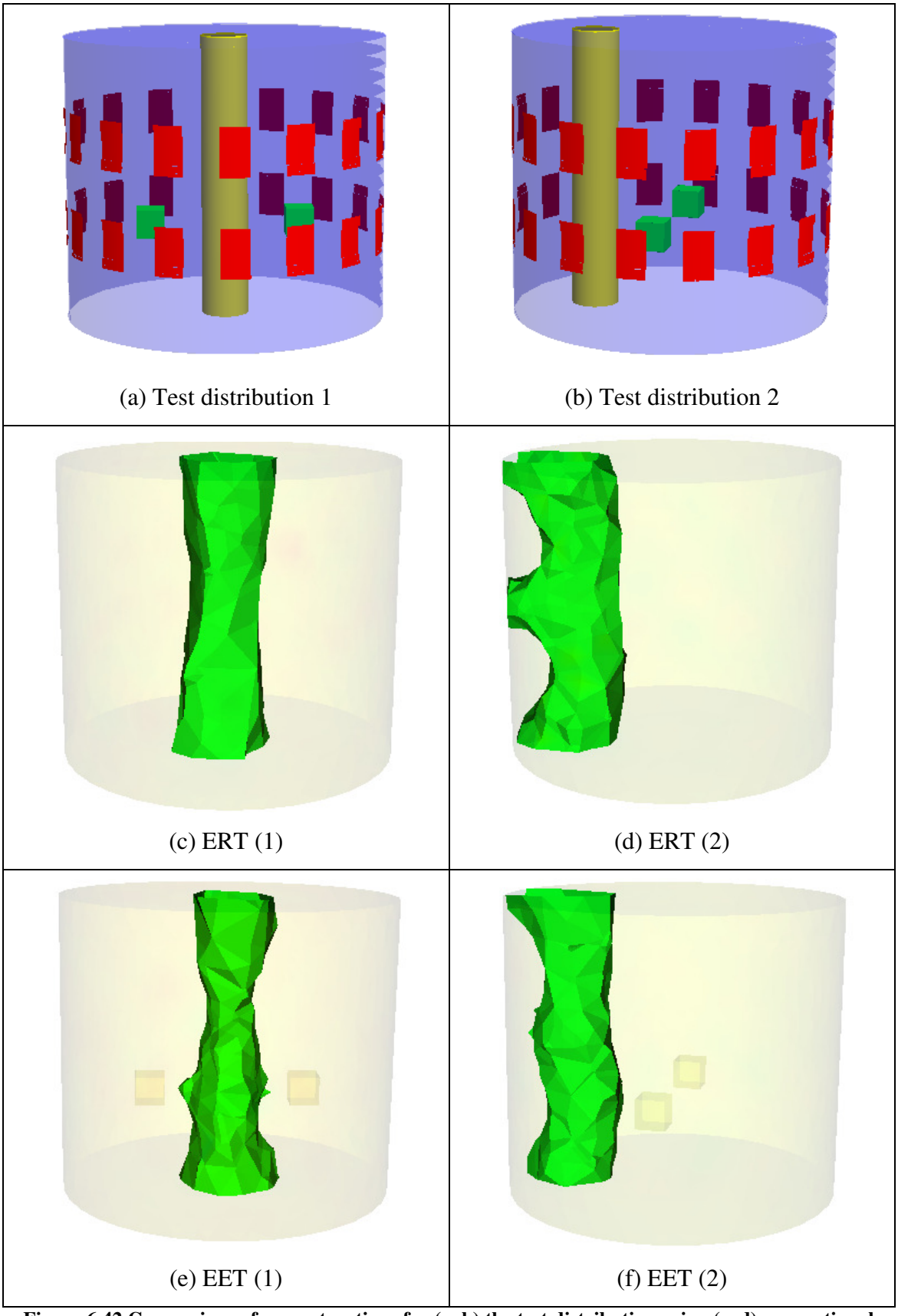

(a) Test distribution 1

(b) Test distribution 2

(c) ERT (1)

(d) ERT (2)

(e) EET (1)

(f) EET (2)

Figure 6.42 Comparison of reconstructions for (a, b) the test distribution using (c, d) conventional ERT and (e, f) the EET approach with two ad hoc pills located 8cm from the centre of the vessel and at height z=0.10m

Figure 6.42 shows reconstructions done using two ad hoc pills in the arrangement as described in Figure 6.37 for two test distributions, shown in Figure 6.42(a) and (b). A single 5cm in diameter Perspex rod is used, with a background of tap water. In the first test distribution, the rod is located in the centre of the vessel, between the two pills. In the second test distribution, the rod is placed approximately equidistant between the centre of the vessel and the wall of the vessel.

Similarly, measurements were acquired using the LCT2 tomograph for the wall-mounted electrodes and the SVMS for the internal electrodes. Reconstructions were done using the TSVD algorithm. The iso-surfaces are chosen to best represent the known shape of the object. Comparing the reconstructed images, for test distribution 1, the reconstructions look similar using both methods (Figures 5.42 (c) and (e)). For test distribution 2, the distorted shape of the reconstructed image extended to the wall of the vessel using the ERT method is slightly improved when using the EET approach.

The results shown in this brief investigation of increasing the number of pills indicate that the improvements in sensitivity and spatial resolution for the EET approach using a single pill is preserved when increasing the number of pills to two. This spectral analysis indicates that extra unique measurements are obtainable with the increase in the number of pills. Improvement in sensitivity and resolution in the vicinity of the ad hoc pills are seen, as it was shown for cases where only one ad hoc pill was used.

6.5 Summary for Application of Extended Electrical Tomography

This chapter aims to investigate different aspects of the EET approach to take a closer look into how measurements on ad hoc pill affect the overall ERT system, such that better understanding on various aspects of the EET approach can be obtained. The effects on the extended measurements and image attributes are also investigated for different cases for various locations and orientations of the ad hoc pill in the vessel.

As the feasibility study in Section 5.4.1 indicates that the EET is able to improve the sensitivity level of the ERT system, as well as improving spatial resolution, it is important that an experimental system is available to verify the simulated results.

Section 6.1 discussed the practical aspects of implementing the EET system are discussed. This includes a standalone voltage measurement system (SVMS), which is a battery-powered voltage measurement system used to acquire voltage difference measurements from the electrodes pair on the ad hoc pill. The system is designed such that it mimics the anticipated system for the wireless pill. The SVMS was tested and calibrated using a DMM, ensuring that the reliability of the measurements. The vessel used for the laboratory experiments of the EET method is described and the characterization of the vessel is detailed.

The design of the ad hoc pill used for the work in this thesis is also described. The pill is designed as a cube in present stage. The shape is chosen considering the ease to manufacture, as well as to eliminate a huge increase in the number of elements when discretizing the model for forward and inverse solving. A suitable dimension in relation to the vessel used is investigated. Although bigger than anticipated, the result of the investigation indicates that a 3cm cube is a suitable dimension used in the 34cm diameter vessel after taking into consideration the reliability of measurements acquired using the SVMS.

Section 6.2 investigates the effect of positioning the ad hoc pill in different locations and orientation within the vessel. The position of the ad hoc pill was strategically rearranged in other locations in the vessel to investigate its effects on the stability of measurements, sensitivity and resolution. The results indicate that similar advantages provided by the EET approach are observed regardless of the location of ad hoc pill in the vessel. The orientation of the internal electrodes has a bigger effect on the sensitivity level and resolution, especially when the internal electrodes are orientated at a bigger angle relative to the wall-mounted electrodes.

Despite the improvements in resolution shown in the analysis, this has not been reflected in reconstructed images. This is likely to be due to relatively small ‘area of influence’ where improvement in resolution is observed in the resolution analysis, and the number of extended measurements acquired is not substantial considering the overall number of measurements in a dataset.

Section 6.3 takes a brief look into using multiple ad hoc pills. Similar analysis and simulations to those for the single pill were conducted. The results show similar characteristics as observed in analyses using one ad hoc pill. The spectral analysis indicates an increase in the number of unique measurements, and shows that the extended measurements acquired are unique. Improvement in sensitivity level and spatial resolution are observed, prominently in the vicinity of the ad hoc pills.

The work presented is a summary of 'proof of concept' for incorporating ad hoc internal electrodes to acquire localized voltage different measurements into a conventional ERT measurement set. The results from both simulations and experiments suggest that the EET approach shows promise in improving spatial resolution of reconstructed images, although visible improvements are not consistently reflected in reconstructed images.

CHAPTER 7
CONCLUSIONS AND FUTURE WORK

7.1 Summary of Findings

The work in this thesis is concerned with improving the spatial resolution of ERT reconstructed images through utilising ad hoc sensors. Spatial resolution is typically poor in the central region of a vessel, further away from the wall-mounted electrodes. This is essentially rooted in the ill-posed nature of the ERT problem. The proposed approaches of utilising ad hoc and wireless sensors described in this thesis break away from a traditional ERT set-up, where the electrodes are conventionally wall-mounted such that the intrusion to the on-going process within the vessel is minimal. By utilising an array of mobile and ad hoc sensors, localized measurements in regions further away from the wall of the vessel can be obtained. This information, which is less accessible using conventional electrode set-ups, potentially contains unique information which could improve the spatial resolution of regions further away from the wall of the vessel.

This thesis explored two approaches, namely the augmented electrical tomography (AET) approach and the extended electrical tomography (EET) approach. The AET approach uses the ad hoc sensors as conductivity probes, while the EET approach utilises the sensors as part of the ERT electrodes system. Feasibility studies were conducted for both approaches, investigating the impact of the ad hoc measurements on the reconstructed images. The EET approach has been explored in more depth, investigating the effect of location and orientation of ad hoc sensors on the stability of

measurements, sensitivity and spatial resolution. This work includes simulations and measurements using a mimic 'wireless' sensor. The effect of using multiple ad hoc sensors was also briefly investigated.

The analysis of performance presented in this thesis adopts a more scientific approach than is normal for ERT. Typically, when evaluating the performance of an ERT setup, results are compared between reconstructed images by visual inspection. This method is subjective and more importantly, no information of the image attributes are extracted in this thesis. Different analysis tools are used to compare the effect of different set-ups on the image attributes of interest. The Singular Value Decomposition (SVD) is used to evaluate the quality of measurements. The quality of measurements, including the number of unique measurements and the stability of the measurements are evaluated for different electrodes set-up. The Discrete Picard Condition (DPC) is applied to evaluate the number of stable or usable measurements out of a full measurement dataset, which can be used for image reconstruction. Sensitivity analysis is used to review the impact of different electrodes set-up or measurements strategies on the maximum sensitivity levels for each voxel in a discretized level, as this indicates the detectability of changes in conductivity. Resolution matrices are used to analyze the spatial resolution of images. Through the analysis, the contributing factor which influences the changes in measurement quality, sensitivity and resolution of images are better understood.

Better understanding on how to improve spatial resolution of reconstructed images
Comparative studies have been conducted to investigate the effect of different measurement strategies and varying number of electrodes has on spatial resolution of ERT reconstructed images. This was done prior to employing ad hoc pills, such that an assessment can be made for existing conventional set-ups to better understand the limitations of set-ups commonly used.

Through comparing different measurement strategies, the analyses suggest that sensitivity is predominantly influenced by current injection pattern. The maximum magnitude of sensitivity changes for each voxel indicates whether a change in conductivity can be detected by the measurements acquired, and therefore is a minimum requirement in order for the change in conductivity to be reconstructed and visualized in a tomogram. Spatial resolution analysis using resolution matrices suggest that resolution

is predominantly influenced by the number of stable and usable voltage measurements acquirable In order to improve the resolution of a reconstructed image, both aspects require improvement. A suitable current injection strategy which provides sufficient 'coverage' to detect the changes in conductivity that take place within the region of interest should be adopted, while a sufficient number of measurements should be acquired in order to reconstruct the changes in conductivity detected.

This comparative study also indicates that there is benefit in undertaking a full 3D measurement strategy. Conventionally, when using multi-plane electrodes system, measurements are only taken for electrodes located on the same plane as the current injecting electrodes. This may compromise the temporal resolution and not all measurements taken are unique. However, there are benefits shown in spatial resolution, especially for off-electrode planes.

An important observation made is that the analyses from the comparative studies suggest that the positioning of the electrodes plays a role in improving the spatial resolution of reconstructed images. The comparative study which compares different number of electrodes on the same electrode plane indicates that while this strategy increases the number of unique measurements, the sensitivity level and spatial resolution in the central region showed no improvement. The comparative study which investigates the difference between a pseudo-3D strategy (each electrode plane are treated independently, therefore measurements are only taken on electrodes on the same electrode plane as the current injecting electrodes) and a full-3D strategy (measurements are taken on all available electrodes which are not used as current injecting electrodes) for a multi-planar electrode system, the results indicate that an improvement can be seen in spatial resolution when the full-3D strategy is applied. The benefit of applying the full-3D strategy is even more evident when reviewing the spatial resolution on an off-electrode plane of the imaged space. This suggests that the position of electrodes plays an important role in effort of improving the spatial resolution of reconstructed images.

Develop methods to incorporate ad hoc sensors into a conventional ERT set-up

Two approaches of utilising ad hoc sensors with a conventional ERT setup are explored in this thesis. The first approach utilises the ad hoc sensors as conductivity probes. Using the localized conductivity measurements, the inverse solutions of the

corresponding voxels where the ad hoc sensors are located can be altered to influence the solutions of the neighbouring voxels. This approach is termed the 'augmented electrical tomography' (AET).

The second approach, known as 'extended electrical tomography' (EET), utilises the ad hoc sensors as part of the electrodes system, hence extending the number of electrodes in the system. Assuming each ad hoc pill is equipped with two electrodes, therefore forming a pair of electrodes, an extra measurement could be acquired. These 'localized voltage difference measurements' are likely to detect changes in conductivities of the material where the ad hoc pills are located, which may not be detected by the voltage measurements acquired by using the wall-mounted electrodes.

Developing the augmented electrical tomography (AET) approach

This approach uses the ad hoc sensors as conductivity probes. Essentially, the conductivity probes measure localized conductivities, which corresponds to the solution which voxels where the ad hoc pills occupy. The localized conductivity values can be substituted into the inverse solution as prior information and used to influence the solution of the neighbouring voxels.

The implementation of the AET approach requires modification to existing inverse solving algorithms. An iterative algorithm is used such that the influence of the localized conductivity values can be incorporated to readjust the solutions of neighbouring voxels. This is a novel approach as the localized conductivity values are used as prior information with the intention to influence the solution of the voxel corresponding to the location where the measurements are acquired, as well as for its neighbouring voxels. In previous published work, the inclusion of information of the conductivity values of materials into a model is intended to reduce the effect of the conductivities of these structures during inverse solving.

The feasibility study conducted indicates that this approach can be implemented with some benefit. Results indicate that the localized conductivity values are capable of readjusting the solutions of the neighbouring voxels, although the area of influence is not large and the readjustments may not be always visibly reflected in reconstructed images. When looking at the raw data, it can be seen that the readjustments are not

always done in a positive manner. In other words, the adjustments made do not always minimize the error to draw the estimated solution closer to the actual solution. The Gauss-Newton algorithm used for inverse solving does not offer the ability to apply more control on how the localized conductivity values incorporated into the inverse solution affects the estimated solution of its neighbouring voxels.

Developing the extended electrical tomography (EET) approach

The EET approach uses the ad hoc sensors as part of the ERT electrodes system, therefore the extending the number of electrodes. Previous published works explored extending the number of electrodes through attaching electrodes on internal structures of a vessel such as baffles and stirrers. The EET approach breaks away from the constraint of fixing electrodes on stationary structures. Voltage difference measurements are taken on a pair of electrodes located on the same ad hoc pill, which is termed as 'internal electrode pair'. The electrodes are only used for voltage difference measurements at current stage, as introducing multiple current sources may cause issues to the stability of the ERT system, especially with the internal current sources having a floating reference ground. Using the internal electrode pairs, localized voltage difference measurements can be acquired in more central regions within a vessel which are less accessible when using wall-mounted electrodes.

The effect of the extended measurements is investigated through evaluating the measurement stability, sensitivity and spatial resolution. Using the adjacent current injection strategy, considering a single plane of 16 electrodes and a pair of internal electrodes, 15 out of 16 acquired extended measurements are unique. The sensitivity analysis shows that the sensitivity levels around the vicinity of the ad hoc pill are improved. With localized voltage difference measurements taken, the changes in conductivity are likely to be measured by the internal electrode pair hence an improvement in detectability. The spatial resolution analysis also indicates an improvement in the area in the vicinity of the internal electrodes. The analyses results suggest benefits in acquiring localized voltage measurements using the ad hoc electrodes.

A feasibility study was also done using the opposite strategy for the same set-up. Similar to the spectral analysis results for the adjacent strategy, the extended

measurements are shown to be unique therefore containing unique information. The sensitivity analysis shows an improvement in the sensitivity levels especially in the vicinity of the internal electrodes. However, it was found that the spectral resolution in regions between the internal electrode and the wall of the vessel is degraded when using the opposite strategy. This suggests that the opposite strategy is not a suitable strategy for this purpose.

Further investigations were done to explore the EET approach. The hardware requirements for implementing the EET approach are identified. Considering the actual wireless ad hoc pill, the measurement system with the required control and communication system is contained within the wireless pill. An important feature is that the systems are self-contained and are battery-powered. Therefore, the measurement system has a separate grounding from the tomographic instrument used to acquire measurements on the wall-mounted electrodes. For this purpose, a standalone voltage measurement system (SVMS) is adopted to acquire voltage different measurements for the internal electrode pair during laboratory experiments. A comparison of measurements acquired using the SVMS is made with simulated measurements and measurements taken using the LCT2 tomograph, which is used data acquisition on the wall-mounted electrodes, to investigate the effect of using two data acquisition systems which are not sharing a common ground. The comparison shows discrepancies between all three voltages, but the difference between the voltages measured using the SVMS and the simulated voltages are more significant. However, spectral analysis indicates that the measurements are stable and are usable for image reconstruction. One of the features of the SVMS is that the system is only able to provide magnitudes of the voltage difference. The polarities of the measurements are to be added manually when incorporated into a conventional measurement set. The polarities are dependent on knowledge of the position and orientation of the internal electrode pair in relative to the current source, therefore this feature mimics the system which is contained within the wireless pill. For this work, the position and orientation of the internal electrodes are known and fixed, therefore the information is considered as ‘prior information’.

Another practical consideration studied was the suitable size of the ad hoc pill. The ultimate goal is to scatter multiple pills in the vessel such that an array of localized measurements could be acquired to enhance the quality of reconstructed images.

Therefore it is desirable to have the ad hoc pills to be as small as possible. Practical consideration is mainly concerned with obtaining a measurable voltage difference reliably. Simulation results indicate that a $1cm^3$ cube produce reasonably measurable voltage difference for the smallest voltage difference magnitude. However, experimental results indicate that the smallest voltage difference magnitude for cubes smaller than $3cm^3$ produce less reliable measurements as the signal measured are seen to be contaminated with noise. The $3cm^3$ cube is chosen to be used for the exploratory work in this thesis, which is approximately 9% of the diameter of the vessel (34cm) used.

Studies indicate that the exact modelling of the ad hoc pill into the discretized model does not affect the predicted voltages acquired using the EIDORS package. The voltages are predicted to match those acquired using the LCT2 tomograph well. The inclusion of the pill, which is modelled as a void, is shown to not affect the predicted voltages even for a case where the pill is located close to the wall of the vessel. This shows that the EET model is comparable to a conventional ERT model.

Further explorations were done to study the effect of different positions and orientations of the internal electrodes in relation to the wall-mounted electrode. Feasibility studies were carried out with the ad hoc pill located in the centre of the vessel with the centre of the pill aligned at the same height as the centre of an electrode plane, and subsequently with the centre of the pill is relocated on a fixed horizontal and vertical axes. The effect of relocating the ad hoc pill was investigated through comparing the sensitivity and spectral resolution. The analyses showed that regardless of the position of the pill in relation to the wall-mounted electrodes, similar improvements in sensitivity and spatial resolution are obtainable. This is consistent with the results shown in the feasibility study. The spectral analysis also indicates that the stability of measurements is not degraded and the number of stable measurements which can be used for image reconstruction is similar for the different cases investigated (moving the internal electrodes nearer to wall of the vessel and moving the ad hoc pill to an off-electrode plane). The results suggest that the localized measurements acquired in any locations in the vessel contribute to improving the spatial resolution of reconstructed images, although the improvement is not visibly shown in reconstructed images.

Orientation of the internal electrodes relative to the wall-mounted electrodes displays a bigger influence on the changes in sensitivity and resolution. While spectral analysis indicates that the number of unique measurements remains the same, the spectral analysis indicates that the improvement in the vicinity of the internal electrodes are not as significant as when the internal electrodes are aligned parallel to the wall-mounted electrodes. The declination of the improvement previously shown in resolution becomes more noticeable as the angle between the internal electrodes and the wall-mounted electrodes increase.

The effect of using multiple pills has been briefly investigated in this thesis. A two ad hoc pill set-up was used. Similar analyses, including spectral, sensitivity and spatial resolution analyses, were conducted. Using the adjacent current injection strategy, it is shown that for each plane of 16 electrodes, only one of the extended measurements is not unique, a similar observation made in previous studies. Therefore for a two planes of 32 electrodes set-up with two pairs of internal electrodes (two ad hoc pills) resulted in 268 unique measurements out of the 272 total measurements acquired. Similarly, an increase in sensitivity in the vicinity of the internal electrodes could be seen in the sensitivity analysis. It is worth noting that the increase in sensitivity level is not sustained for the area between the two ad hoc pills. This is likely to be due to the internal electrodes are not used as current sources, which is shown to play a more substantial role in increasing the sensitivity level. The spatial resolution analysis indicates that an improvement for the voxels in close proximity of the internal electrodes can be seen.

The work presented in this thesis indicates that there are benefits shown in improving the spatial resolution of reconstructed images using ERT when utilising ad hoc pills to acquire localized measurements. Although not clearly reflected in reconstructed images, sensitivity and spatial resolution analyses both suggest improvements especially in the vicinity of the pill. Further more, the results obtained using two ad hoc pills also showed similar improvements. Considering these results, the EET approach shows potential for further work.

7.2 Future Work

Further development of the Augmented Electrical Tomography (AET) approach

The feasibility study indicates that the AET approach could be further pursued. The results obtained assuming a single ad hoc pill is used indicate that the AET approach is feasible. Further exploration requires a better suited reconstruction algorithm. The algorithm should be able to provide more control and flexibility when influencing the voxels in the neighbourhood of the voxel with known conductivity value. A less conventional inverse solving algorithm may be better suited, and incorporation of some level of artificial intelligence might allow for better decisions. The algorithm should be able to choose to keep or discard an adjustment made due to the influence of the known conductivity value, such that the adjustment made should always lead to minimizing the approximation error.

To further investigate the AET approach, the effects of using multiple ad hoc pills needs to be investigated. The feasibility study also omitted including the ad hoc pill into the model. The effect of the inclusion of the pill into the model should be considered and the effects on the forward and inverse models require investigation.

Further development of the Extended Electrical Tomography (EET) approach

The results of the feasibility study and the subsequent studies conducted in this thesis show signs of encouragement for further pursuit of the EET approach. The next step is to increase the number of ad hoc pills. As shown by the results obtained using a single ad hoc pill, it is anticipated that varying the position and orientation of the ad hoc pills would have an impact on how much an improvement could be seen in terms of sensitivity and spatial resolution when using multiple pills. There is also the question of how many ad hoc pills can be used before intrusion of the ad hoc pills begins to degrade the quality of the information obtained.

Beyond the strategy adopted in this iteration of the EET approach, considerations can be made to utilise the ad hoc pills as current sources. This approach is likely to increase the sensitivity within the imaged space. However, this approach is expected to complicate the forward and inverse solving for the ERT problem, as mathematical models for existing computational toolkits (EIDORS, for example) typically use a single reference

point. Using ad hoc pills as current sources would create multiple reference points, since the current sources contained within the ad hoc pills are batteries and resulting in floating references.

Other possible strategies

Similar to wall-mounted electrodes, the function of the internal electrodes can be made interchangeable. Similar to conventional ERT systems, electrodes on the ad hoc pills which are not used as current source during a current injection protocol can be used as voltage measurement electrodes. The functions of the internal electrodes are alternated according to the measurement strategy. This results in an ad hoc ERT system, which allows a complete departure from conventional ERT. Electrodes locations are no longer restricted to being attached on the walls of the vessel, but are allowed to be located anywhere within the vessel. The measurement strategy is expected to be less structured given the mobility of the ad hoc pills to move in the vessel. It is important to ensure that there is only one current source at any given time. A parallel data acquisition protocol may be best suited for this strategy.

Another possible strategy is using the ad hoc sensors to acquire conductivity and voltage difference measurements. Providing that the ad hoc pills can be furnished with both types of sensors, a hybrid of the AET and EET approach is likely to better inform the image reconstruction process. This approach results in extra measurements obtained to improve the under-determined case of the ERT inverse problem through an increase of number of measurements, as well as localized conductivity measurements which improves the estimate of localized conductivity solutions.

AET and EET with Wireless Pills

Relating the work done in this thesis to the WSN4IP project, the ultimate aim is to implement the developed approaches using the ad hoc and wireless pills developed by the WSN4IP project. The ad hoc and wireless pills will be equipped with its localization system and measurement system. A protocol should be established to synchronize voltage measurements with current injection protocols on the wall-mounted electrodes. The ad hoc sensors are mobile within the vessel. Depending on how dynamic the movements of the ad hoc sensors is, a full set of measurements (meaning measurements taken for all current injection patterns in one frame of measurement) may not be

possible. A full set of measurements is not critical and not a requirement as any extended measurements are likely to contain unique information regarding of the position the ad hoc pills are located. However, this should be considered when developing the synchronization protocol.

With the availability of the ad hoc and wireless pill, experiments using dynamic test distributions, such as mixing processes, can be done. This also enables investigations to be done for cases where the ad hoc pill is located on the boundary of the inhomogeneous region.

Better understanding of image reconstruction limitations

The analyses used in this thesis aimed to promote a more objective method to analyse reconstructed images, as well as to obtain information of reconstruction properties, such as sensitivity and spectral resolution. Other techniques should be looked into and developed in order to better understand other reconstruction properties. An interesting one is the 'accuracy' of reconstructed data. One of the influencing factors is the level of discretization of the model. It is an important aspect which is often overlooked and requires more attention. Analysis techniques should be developed to help users make better informed decisions when selection parameters to discretize a model in order to obtain results with better accuracy.

References

Abd-El-Barr M.I., Youssef M.A.M. and Al-Otaibi M.M., 2005a, "Wireless sensor networks – part I: topology and design issues", *Proc. of Canadian Conf. On Electrical and Computer Engineering*, pp. 1165-1168.

Abd-El-Barr M.I., Youssef M.A.M. and Al-Otaibi M.M., 2005b, "Wireless sensor networks – part II: protocols and security issues", *Proc. of Canadian Conf. On Electrical and Computer Engineering*, pp. 69-72.

Barber D.C. and Brown B.H., 1984, "Applied Potential Tomography", *J. Phys. E: Sci. Instrum.,* **17**, pp. 723-733.

Bolton G.T., 2006, "A Review of Linear Electrical Tomography Probes for Monitoring the Behaviour of Multiphase Mixing Processes"*, 12th Euro. Conf. on Mixing, Bologna, Italy*, pp. 27-30.

Boone K.and Holder D., 1996a, "Effect of Skin Impedance on Image Quality and Variability in Electircal Impedance Tomography: A Model Study", *Med. Biol. Eng. Comput.,* **34**, pp. 351-354.

Boone K.G. and Holder D.S., 1996b, "Current Approaches to Analogue Instrumentation Design in Electrical Impedance Tomography", *Physiol. Meas.,* **17**, pp. 229-247.

Borcea L., 2002, "Electrical Impedance Tomography", *Inverse Problems,* **18**, R99-R136.

Borsic A., 2002, “Regularization Methods for Imaging From Electrical Measurements”, *Ph.D Thesis*, Oxford Brookes University.

Brennan M., Holtham P., Khanal M. and Morrison R., 2007, “Comparing ERT Measurements with CFD Predictions for an Industrial Scale Hydrocyclone Classifier”, *Proc. of the 5th World Congress on Industrial Process Tomography*, *Bergen, Norway,* pp. 737-745.

Butler J.E. and Bonnecaze R.T., 1999, “Imaging of Particle Shear Migration with Electrical Impedance Tomography”, *Physics of Fluids*, **11** (8), pp. 1982-1994.

Chaniecki Z., Niedostatkiewicz M. and Sankowski D., 2007, “Graphical Presentation of Transformation of Tomography Data for Gravitation Silo Flow”, *Proc. of the 4th World Congress on Industrial Process Tomography*, pp. 746-754.

Cheney M. and Isaacson D., 1992, “Distinguishability in Impedance Imaging”, *IEEE Trans. Bio. Eng.,* **39**, pp. 852-860.

Cheney M., Isaacson D and Newell J.C., 1999, “Electrical Impedance Tomography”, *SIAM Review*, **41**, pp. 98-101.

Cheng K-S, Isaacson D., Newell J.C. and Gisser D.G., 1989, “Electrode Models for Electric Current Computed Tomography”, *IEEE Trans. Biomed Engr.,* **36**, pp. 918-924.

Cullivan J.C., Wang M., Bolton G., Baker G., Clark W. and Williams R.A., 2005, “Linear EIT for Sedimentation and Sediment Bed Characterization”, *Proc. of 4th World Congress on IPT, Aizu, Japan,* p.p. 910-015.

Davidson J.L., Wright P., Ahsan S.T., Robinson R.L., Pomfrett C.J.D. and McCann H., 2010, "fEITER – a new EIT instrument for functional brain imaging", *Journal of Physics: Conference Series*, **224(1)**, pp. 1-4.

Dickin F.J., Hoyle B.S., Hunt A., Huang S.M., Llyas O., Lenn C., Waterfall R.C., Xie C. G., and Beck M.S., 1992, "Tomographic Imaging of Industrial Process Equipment: Techniques and Applications", *IEE Proc. G Circuits, Devices Syst.,* **139**, pp. 72-82.

Dickin F.J. and Wang M., 1996, "Electrical Resistance Tomography for Process Applications", *Meas. Sci. Technol.,* **7**, pp. 247-260.

Dines K.A. and Lytle R.J., 1981, "Analysis of Electrical Conductivity Imaging", *Geophysics*, **46**, pp. 1025-1036.

Dressler F., Guan Y. and Jiang Z., 2007, "Wireless and Sensor Networks Security (WSNS) A Retrospection," *IEEE Internatonal Conference on Mobile Adhoc and Sensor Systems, 2007,* pp.1-6.

Engl H.W., Hanke M. and Neubauer A., 1996, *Regularization of Inverse Problems*, Kluwer, Dordrecht, Germany.

Fan W. and Wang H., 2010, "Electrode Placement Configuration and Drive Pattern for 3D ERT", *Proc. of the 6th World Congress on Industrial Process Tomography*, *Beijing, China,* pp. 632-641.

Feynman R.P., Leighton R.B. and Sands M., 1977, *The Feynman Lectures on Physics*, 6th ed. Vol. 2, Addison-Wesley, Reading, U.K.

Gisser D.G., Isaacson D. and Newell J.C., 1987, "Current Topics in Impedance Imaging", *Clin. Phys. Physiol, Meas.,* **8**, pp. 39-46.

Gisser D.G., Isaacson D. and Newell J.C., 1988, "Theory and Performance of an Adaptive Current Tomography System", *Clin. Phys. Physiol. Meas.,* **9**, pp. 35-41.

Gnecchi J.A.G., Pineda E.M., Chavez A. G-T., Rojas A. G-T., Gomez, J.C. and Garcia J.C.H., 2007, "Soil Water Infiltration Measurements Using Electrical Impedance Tomography", *Proc. of the 5th World Congress on Industrial Process Tomography*, *Bergen, Norway,* pp. 521-528.

Hansen P.C., 1998, *Rank-Deficient and Discrete Ill-Posed Problems: Numerical Aspects of Linear Inversion,* SIAM, Philadelphia, ISBN 0-89871-403-6.

Heikkinen L.M., Kourunen J., Rastas J., Savolainen T., Vauhkonen P.J., Kaipio J.P. and Vauhkonen M., 2005, "Real Time Three-Dimensional Electrical Impedance Tomography Applied in Multiphase Flow Imaging", *Proc. of 4th World Congress on IPT, Aizu, Japan*, pp. 540-545.

Heikkinen L.M., Leinonen K., Kaipio J.P., Vauhkonen M. and Savolainen T., 2001a, "Electrical Process Tomography with Known Internal Structures and Resistivities." *Inverse Problems*, vol. 9, pp 431-454.

Heikkinen L.M., Vauhkonen M., Savolainen T. and Kaipio J., 2001b, "Modelling of Internal Structures and Electrodes in Electrical Process Tomography", *Meas. Sci. Technol.*, **12**, p.p. 1012-1019.

Heikkinen L.M., Vilhunen T., West R.M. and Vauhkonen M., 2002, "Simultaneous Reconstruction of Electrode Contact Impedances and Internal Electrical Properties: II. Laboratory Experiments", *Meas. Sci. Technol.,* **13**, pp. 1855-1861.

Hoerl A.E., 1962, “Application of Ridge Analysis to Regression Problems”, *Chem Eng. Prog.,* **58**, pp. 54-59.

Holder D. (ed.), 2005, *Electrical Impedance Tomography: Methods, History and Applications,* IOP Publishing, Bristol, ISBN 0-7503-0952-0.

Hua P., Woo J.E., Webster J.G. and Tompkins W.J., 1993, “Using Compound Electrodes in Electrical Impedance Tomography”*, IEEE Trans. Biomed. Eng.*, **40**, pp. 29-34.

Huang C.N., Yu F.M. and Chung H.Y., 2008, “The Scanning Data Collection Strategy for Enhancing the Quality of Electrical Impedance Tomography”, *Instrumentation and Measurement, IEEE Transaction*, **57**(6), pp. 1193-1198.

Ijaz U.Z., Khambampati A.K., Lee J.S., Lim K.Y., Lim M.C. and Kim S., 2006, “Electrical Resistance Imaging of Two-Phase Flow Through Rod Bundles”, *5th Int. Sym. On Meas. Techniques for Multiphase Flows, Macau, China,* pp. 1051-1056.

Isaacson D., 1986, “Distinguishability of Conductivities by Electric Current Computed Tomography”, *IEEE Trans. Med. Imaging*, **MI-5** (2), pp. 91-95.

Ismail K., Wang M. and Hoyle B.S., 2010, “A Novel Zigzag EIT Sensor for Multiphase Pipeline Flows”, *Proc. of the 6th World Congress on Industrial Process Tomography*, *Beijing, China*, pp.573-582.

Jiang P., Ren H, Zhang L., Wang Z. and Xue A., 2006, “Reliable Application of Wireless Sensor Networks in Industrial Process Control,” *The 6th World Congress on Intelligent Control and Automation, 2006*, pp. 99-103.

Jin H., Tong Z., Yang S., Wang M. and Williams R.A., 2007, "Profiles of Gas Holdup in a Gas Liquid Countercurrent Bubble Column Using Electrical Resistance Tomography", *Proc. of the 5th World Congress on Industrial Process Tomography*, *Bergen, Norway,* pp. 390-396.

Johnson M., Healy M., van de Ven P., Hayes M.J., Nelson J., Newe T. and Lewis E., 2009, "A Comparative Review of Wireless Sensor Network Mote Technologies," *IEEE Sensors,* pp. 1439-1442.

Kaminoyama M., Nishi K., Misumi R. and Taguchi S., 2005, "Dispersion States of Floating and Sedimenting Particles in a Stirred Vessel Using Tomography Measurements", *Proc. of the 4th World Congress on Industrial Process Tomography*, pp. 922-927.

Kaminoyama M., Nishi K., Misumi R. and Tagawa A., 2007, "Measurement of Liquid-Liquid Dispersion Phenomena in a Stirred Vessel using Electrical Resistance Tomography", *Proc. of the 5th World Congress on Industrial Process Tomography*, *Bergen, Norway,* pp. 321-326.

Kim K., Kang S., Kim M., Kim S., Lee Y. and Vauhkonen M., 2002, "Dynamic Image Reconstruction in Electrical Impedance Tomography with Known Internal Structures", *IEEE Trans. Mag.,* **38** (2), p.p. 1301-1304.

Kolehmainen V., Vauhkonen, M., Karjalainen P.A. and Kaipio J.P., 1997, "Assessment of Errors in Static Electrical Impedance Tomography with Adjacent and Trigonometric Current Patterns," *Physiol. Meas.,* vol. 18, pp. 289-303.

Kourunen J., Heikkinen L.M., Vauhkonen M., Kayhko R., Matula J. and Kayhko J., 2007, "Imaging of Mixing of Two Miscible Liquids using Electrical Impedance Tomography", *Proc. of the 5th World Congress on Industrial Process Tomography*, *Bergen, Norway*, pp. 803-809.

Kuorilehto M., Hannikainen M. and Hamalainen T.D., 2005, “A survey of application distribution in wireless sensor networks,” *EURASIP Journal on Wireless Communications and Networking*, vol. 5, pp. 774-788.

LaBrecque D.J. Ramirez A.L., Daily W.D., Binley A.M. and Schima S.A., 1996, “ERT Monitoring of Environmental Remediation Processe”s, *Meas. Sci. Technol.,* **7**, pp. 375-383.

Lee Q.F. and Bennington C.P.J., 2007, “Investigation of Liquor Flow in a Model Kraft Batch Digester”, *Proc. of the 5th World Congress on Industrial Process Tomography*, *Bergen, Norway,* pp. 414-422.

Lionheart W.R.B., 2004, “EIT Reconstruction Algorithms: Pitfalls, Challenges and Recent Developments”, *Physiol. Meas.,* **25**, pp. 125-142.

Lionheart W., Polydorides N. and Borsic A., 2005, “Part 1: The Reconstruction Problem.” In: Holder D. (ed) *Electrical Impedance Tomography: Methods, History and Applications,* Bristol, pp. 3-64.

Lucas G.P., Cory J., Waterfall R.C., Loh W.W. and Dickin F.J., 1999, “Measurement of the Solids Volume Fraction and Velocity Distributions in Solids-Liquid Flows using Dual-Plane Electrical Resistance Tomography”, *Flow Measurement and Instrumentation*, **10** (4), pp. 249-258.

Lyon G.M., 1997, “A Study of Stirred Vessel Mixing Using Electrical Resistance Tomography”, *Ph.D Thesis*, University of Manchester.

Lyon G.M. and Oakley J.P., 1993, "A Simulation Study of Sensitivity in Stirred Vessel Electrical Impedance Tomography" In: Beck M.S. (ed) *Tomography Techniques for Process Design and Operation*, Southampton, pp. 137-146.

McCann H, Polydorides N., Murrieta-Lee J.C., Ge K., Beatty P. and Pomfrett C.J.D., 2006, "Sub-Second Functional Imaging by Electrical Impedance Tomography", *28th Annual Intl. Conf. of the IEEE Engineering in Medicine and Biology Society*, pp. 4269-4272.

Meng G., Jaworski A.J. and Kimber C.S., 2006, "A Multi-Electrode Capacitance Probe for Phase Detection in Oil-Water Separation Processes: Design, Modelling and Validation", *Meas. Sci. Technol.,* **17**, pp. 881-894.

Menke W., 1989, *Geophysical Data Analysis: Discrete Inverse Theory Rev. Ed.,* Academic Press, San Diego, ISBN: 0-12-490921-3.

Metherall P., Barber D.C., Smallwood R.H. and Brown B.H., 1996, "Three-Dimensional Electrical Impedance Tomography", *Nature*, **380**, p.p. 509-512.

Molinari M., Cox S.J., Blott B.H. and Daniell G.J., 2001, "Adaptive Mesh Refinement Techniques for Electrical Impedance Tomography", *Physiol. Meas.,* **22**, pp 91-96.

Murphy S.C. and York T.A., 2006, "Electrical Impedance Tomography with Non-Stationary Electrodes", *Meas. Sci. Technol.,* **17** (11), pp. 3042-3052.

Murphy S.C., Stanley S.J., Rhodes D. and York T.A., 2007, "Electrical Impedance Tomography Imaging of Solid-Liquid Suspensions Using Vertically Deployable Sensor Electrode Arrays", *Proc. of the 5th World Congress on Industrial Process Tomography*, *Bergen, Norway,* pp. 487-494.

Murphy S.C. and York T.A., 2007, "Design of an Impeller Mounted Electrode Array", *Proc. of 5th World Congress on Industrial Process Tomography*, *Bergen, Norway,* pp. 94-101.

Murphy S.C., 2008, "Ad Hoc Electrode Arrangements for Electrical Tomography", *Ph.D Thesis*, University of Manchester.

Normi V., Lehikoinen A., Voutilainen A., Saren M. and Vauhkonen M., 2010, "Measuring Non-Dissolved Gas Content in A Pulp Flow Using Real-Time 3D Tomography", *Proc. of the 6th World Congress on Industrial Process Tomography*, *Beijing, China,* pp. 149-158.

Parkinson G., Boon M., Davis J.G. and Sloan R., 2009, "3D Positioning Using Spherical Location Algorithms for Networked Wireless Sensors Deployed in Grain," *2009 IEEE MTT-S International Microwave Symposium Digest*, pp. 1417-1420.

Parkinson G., Crutchley D., Green P.M., Antonio M., Boon M., Green P.N., Green P.R., Sloan R. and York T., 2010, "Environmental Monitoring in Grain," *2010 IEEE International Instrumentation & Measurement Technology Conference (I2MTC)*, pp. 939-943.

Paulson K., Breckon W. and Pidcock M.K., 1992, "Electrode Modelling in Electrical Impedance Tomography", *SIAM J. Appl. Math.,* **52** (4), pp. 1012-1022.

Phillips D.L., 1962, "A Technique for the Numerical Solution of Certain Integral Equations of the First Kind", *J. Assoc. Comput. Mach.,* **9**, pp. 84-97.

Pinheiro P.A.T., Loh W.W., and Dickin F.J., 1998, "Optimal Sized Electrodes for Electrical Resistance Tomography", *Electron Lett.,* **34**, pp. 69-70.

Polydorides N., 2002, “Image Reconstruction for Soft Field Tomography”, *Ph.D Thesis*, UMIST.

Polydorides N. and Lionheart W.R.B., 2002, “A Matlab Toolkit for Three-Dimensional Electrical Impedance Tomography: A Contribution to the Electrical Impedance and Diffuse Optical Reconstruction Software Project”, *Meas. Sci. Technol.,* **13**, pp. 1871-1883.

Polydorides N. and McCann H., 2002, “Electrode Configurations for Improved Spatial Resolution in Electrical Impedance Tomography”, *Meas. Sci. Technol.,* **13**, pp. 1862-1870.

Primrose K. and Qiu C., 1999, “Performance and Application Studies of an Electrical Resistance Tomography System”, *Proc. of 1st World Congress on Industrial Process Tomography, Buxton, U.K.,* pp. 133-139.

Ramskill N.P. and Wang M., 2010, “Measurement and Recognition of Gas-Liquid Multiphase Horizontal Flow Regimes using Electrical Resistance Tomography”, *Proc. of the 6th World Congress on Industrial Process Tomography*, *Beijing, China,* pp. 159-167.

Romanowski A., Grudzien K., Banasiak R., Williams R.A. and Sankowski D., 2007, “Hopper Flow Measurement Data Visualization: Developments Towards 3D”, *Proc. of the 5th World Congress on Industrial Process Tomography, Bergen, Norway*, p.p. 986-993.

Ricard F., Brechtelsbauer C., Xu X.Y. and Lawrence C.J., 2005, “Monitoring of Multiplhase Pharmaceutical Processes Using Electrical Resistance Tomography”, *Chemical Engineering Research and Design*, **83** (A7), pp. 794-805.

Sasaki Y., 1992, "Resolution of Resistivity Tomography Inferred From Numerical Simulation", *Geophysical Prospecting*, **40**, pp. 453-463.

Schlaberg H.I., Qiu C., Podd F.J.W., Jia X., Primrose K. and Bolton G.T., 2007, "Design and Appraisal of the M3000 Multimodal Tomography System", *Proc. of the 5th World Congress on Industrial Process Tomography, Bergen, Norway*, p.p. 652-659.

Schoberl J., 2008, Netgen: Automatic Mesh Generator, http://www.hpfem.jku.at/netgen

Seager A.D., Barber D.C. and Brown B.H., 1987, "Theoretical Limits to Sensitivity and Resolution in Impedance Imaging", *Clin. Phys. Physiol. Meas.,* **8**, pp. 13-31.

Shao F.G. and Liu X.H., 2006, "Using Tomographic Techniques to Monitor Moisture Distribution of Grain in Barn", *Journal of Northeastern University (Natural Science),* **27** (2), pp. 134-137.

Sharifi M and Young B., 2010, "The Potential Utilisation of Electrical Resistance Tomography (ERT) in Milk Powder Processing for Monitoring and Control", *Proc. of the 6th World Congress on Industrial Process Tomography*, *Beijing, China,* pp. 1-14.

Shi X., Dong X., Shuai W., You F., Fu F. and Liu R., 2006, "Pseudo-Polar Drive Patterns for Brain Electrical Impedance Tomography", *Physiol. Meas.,* **27**, pp. 1071-1080.

Somersalo E., Cheney M. and Isaacson D., 1992, "Existence and Uniqueness for Electrode Models for Electric Current Computed Tomography", *SIAM J. Appl. Math.,* **52**, pp. 1023-1040.

Steele P.H., Cooper J.E., Mitchell B.K., Boden C. and Lionheart W.R.B., 2007, "EIT Detection of Juvenile and Knot Wood in Southern Pine Logs", *Proc. of the 5th World Congress on Industrial Process Tomography*, *Bergen, Norway,* pp. 431-438.

Stephenson D.R., 2008, "Choices and Implications in Three-Dimensional Electrical Impedance Tomography", *Ph.D Thesis,* University of Manchester.

Stephenson D.R., Davidson J.L., Lionheart W.R.B., Grieve B.D. and York T., 2005, "Comparison of 3D Image Reconstruction Techniques using Real Electrical Impedance Measurement Data", *Proc. of 4th World Congress on IPT, Aizu, Japan*, pp. 643-650.

Sudhakaran H., Randall E.W., Ramdhani U. and Rawatlal R., 2010, "Application of Electrical Resistance Tomography in Evaluating the Influence of Nozzle Design on the Gas Hold-up Distribution in Boiling Bubble Column Reactors", *Proc. of the 6th World Congress on Industrial Process Tomography*, *Beijing, China,* pp. 179-195.

Sun D-M and He B., 2006, "Review of Key Management Mechanisms in Wireless Sensor Networks," *Acta Automatica Sinica*, Vol. 32 No. 6, pp. 900-906.

Tarantola A., 1987, *Inverse Prolem Theory,* Elsevier.

Tikhonov A.N., 1963, "Solution of Incorrectly Formulated Problems and the Regularization Method", English Translation of *Dokl Akad Nauk SSSR* ***151***, pp. 501-504.

Vauhkonen P.J., Vauhkonen M., Savolainen T. and Kaipio J.P., 1999, "Three-Dimensional Electrical Impedance Tomography Based on the Complete Electrode Model", *IEEE Trans. Biomed. Eng.,* **46**, pp. 1150-1160.

Vauhkonen M., Lionheart W.R.B., Heikkinen L.M., Vauhkonen P.J. and Kaipio J.P., 2001, "A Matlab Package for the EIDORS Project to Reconstruct Two-Dimensional EIT Images", *Physiol. Meas.,* **22**, pp. 107-111.

Vilhunen T., Kaipio J.P., Vauhkonen P.J., Savolainen T. and Vaukonen M., 2002, "Simultaneous Reconstruction of Electrode Contact Impedances and Internal Electrical Properties: I. Theory", *Meas. Sci. Technol.,* **13**, pp. 1848-1854.

Vigoureux J.M. and Courjon D., 1992, "Detection of Nonradiative Fields in Light of the Heisenberg Uncertainty Principle and the Raleigh Criterion", *Applied Optics*, **31**(16), pp. 3170-3177.

Vogel C., 2001, *Computational Methods for Inverse Problems*, SIAM, Philadelphia, U.S.A.

Wang M., Dickin F.J. and Williams R.A., 1994, "Electrical Resistance Tomography of Metal Walled Vessels and Pipelines", *Elec. Letters,* **30**, pp. 771-773.

Wang M., Jones T.F. and Williams R.A., 2003, "Visualization of Asymmetric Solids Distribution in Horizontal Swirling Flows using Electrical Resistance Tomography", *Chemical Engineering Research and Design*, **81**, pp. 854-861.

Warsito W., Marashdeh Q., Fan L-S, 2007, "Electrical Capacitance Volume Tomography", *Sensors Journal, IEEE,* **7**(4), pp. 525-535.

Webster J.G. (ed.), 1990, *Electrical Impedance Tomography*, IOP: Bristol.

Wheeler J.L., Wang W. and Tang M., 2002, "A Comparison of Methods for Measurement of Spatial Resolution in Two-Dimensional Circular EIT Images", *Physiol. Meas.,* **23**, pp. 169-175.

Williams R.A. and Beck M.S., 1995, *Process Tomography, Principles, Techniques and Applications*, Butterworth-Heinemann, Oxford, ISBN 0-7506-0744-0.

Wilkinson A.J., Randall E.W., Long T.M. and Collins A., 2006, "The Design of an ERT System for 3D Data Acquisition and a Quantitative Evaluation of its Performance", *Meas. Sci. Technol.,* **17**, pp. 2088-2096.

Woo E.J., Hua P., Webster J.G. and Tompkins W.J, 1994, "Finite-Element Method in Electrical Impedance Tomography", *Med. & Biol. Eng. & Comput.,* **32**, pp. 530-536.

Wu L, 2003, "A Parameter Choice Method for Tikhonov Regularization", *Elec. Trans on Numerical Analysis,* **16**, pp. 107-128.

Yick J., Mukherjee B. and Ghosal D., 2008, "Wireless Sensor Network Survey," *Computer Networks,* Vol. 52 No. 12, pp. 2292-2330.

York T.A, 2005, "Electrical Tomography for Industrial Applications" In: Holder D. (ed) *Electrical Impedance Tomography: Methods, History and Applications,* Bristol, pp. 295-347.

York T.A., Murphy S., Burnett-Thompson A. and Grieve B., 2005, "An Accessible Electrical Impedance Imaging System", *Proc. of 4th World Congress on Industrial Process Tomography*, *Aizu, Japan,* pp. 100-105.

York T., Davidson J., Flanagan M. and Kowalski A., 2007, "ERT for Charactirisation of Physical Stability in Liquid Composition", *Proc. of the 5th World Congress on Industrial Process Tomography*, *Bergen, Norway,* pp. 439-446.